NTNU

Norwegian University of
Science and Technology

Experimental and Numerical Study of Fluid Displacement in Subsea Pipe Sections

Hanne Gjerstad Folde

Petroleum Geoscience and Engineering
Submission date: June 2017
Supervisor: Milan Stanko, IGP

Norwegian University of Science and Technology
Department of Geoscience and Petroleum

Abstract

The objective of the thesis is to study displacement operations in offshore petroleum industry. Typically MEG or Methanol is circulated through parts of the subsea production systems to lower their hydrocarbon content. This is often done at the beginning of a prolonged production shut-in, to avoid formation of hydrates or to minimize the emissions of chemicals to the environment when a component is to be replaced.

Experimental and numerical analyses have been conducted on a previously built pipe system formed like a U-shaped jumper. Through the project it has been investigated necessary displacing time required to achieve target hydrocarbon concentration in the domain, optimal displacement rate for efficiently removal of hydrocarbons, and how these variables depend on different fluids and their properties. The investigation was performed through measuring the volume fraction in the domain of the displacing fluid by draining the jumper, after the fluid had been flooding in the system for a certain time. The system was filled and displaced with both water and Exxsol D60. The experimental results have been used as validation for the accuracy of the models made in the transient multiphase flow commercial simulator LedaFlow®. A sensitivity analysis was performed, considering density, viscosity, interfacial tension, different fluids and geometry.

The experimental results showed small changes in the amounts displaced between 2 and 3 volumes. For the displacement to be considered successful, a criterion of a volume fraction for the displacing fluid higher than 95 % was set. For oil displacing water, a flow rate of 28.16 m^3/h was required. For water displacing oil, 20.77 m^3/h was sufficient. LedaFlow predicted the volume fractions well, deviating from the experimental points with an average of 5.5 % for oil displacing water and 5.7 % for water displacing oil. The sensitivity analysis showed significant changes in the displaced amounts, when changing the density of the displaced fluid. For a density a bit higher than the displacing fluid, the amount was decreasing exponentially as the density increased. Changes in viscosities for both the displacing fluid and the fluid to be displaced had little effect, unless the viscosity of the displacing fluid was highly increased. It was observed a linear relationship between changes in interfacial tension and obtained volume fraction. Simulations with methanol displacing oil predicted higher amounts displaced than when oil displaced water. With gas included as a fluid to be displaced

in the system, the displaced amounts were reduced. With a dead-leg included in the geometry, it showed no visible effects in the simulation.

Experimental data and observations have been obtained. The results of the numerical models in LedaFlow are in good agreement with the experimental data.

Sammendrag

Formålet med denne oppgaven er å studere fortrengingsoperasjoner i offshore petroleumsindustri. Typisk blir MEG eller metanol sirkulert gjennom deler av undersjøiske produksjonssystemer for å redusere innholdet av hydrokarboner. Dette gjøres ofte i starten av en midlertidig stenging av produksjonen. Dette er for å hindre dannelse av hydrater eller for å minimere utslipp av kjemikaler til omgivelsene dersom en komponent skal erstattes.

Eksperimenter og numeriske analyser har blitt utført for et tidligere bygget U-formet rørsystem, som skal illustrere en jumper-geometri. Gjennom prosjektet har det blitt undersøkt nødvendig fortrengningstid for å oppnå ønsket hydrokarbonkonsentrasjon i domenet, optimal rate for effektiv fjerning av hydrokarboner, og hvordan disse variablene avhenger av forskjellige fluider og fluidenes egenskaper. Studien har blitt utført gjennom å måle volumfraksjonen i domenet til det fortrengende fluidet ved å drenere systemet, etter at fluidet har strømmet for en gitt tid. Systemet ble fullt med og fortrengt, av både vann og Exxsol D60. De eksperimentelle resultatene har blitt brukt som validering for nøyaktigheten av modellen laget i den transiente flerfase strømningssimulatoren LedaFlow®. Sensitivitetsanalyser har blitt utført for tetthet, viskositet, grenseflatespenning, ulike fluider og geometri.

De eksperimentelle resultatene viste små endringer i fortrengt mengde mellom 2 og 3 volumer. For å betrakte fortrengningsprosessen som suksessfull, ble det satt et kriterium på at volumfraksjonen til det fortrengende fluidet skulle være høyere enn 95 %. Når olje fortrengte vann, krevdes en strømningsrate på 28,16 m^3/h. For vann som fortrengte olje, var 20,77 m^3/h tilstrekkelig. LedaFlow gav gode prediksjoner av volumfraksjonene, som hadde et gjennomsnittlig avvik fra de eksperimentelle verdiene på 5,5 % for olje som fortrenger vann, og 5,7 % for vann som fortrenger olje. Sensitivitetsanalysene viste signifikante endringer i fortrengt mengde, når endringer ble gjort i tettheten til fluidet som skulle fortrenges. Fra en tetthet bare litt høyere enn tettheten til fortrengningsfluidet, førte en økning i tetthet til en eksponentiell reduksjon i fortrengningseffektiviteten. Endringer i viskositet for både fluidet som skulle fortrenge og det som skulle bli fortrengt hadde liten effekt, med mindre viskositeten til det fortrengende fluidet ble veldig forhøyet. Det ble observert et lineært forhold mellom endringer i grenseflatespenning og oppnådd volumfraksjon. Simuleringer med metanol som fortrenger olje anslo høyere fortrengt mengde enn for olje som fortrenger

vann. Med gass inkludert i systemet, ble den fortrengte mengden redusert. Når et blindrør ble inkludert i geometrien, viste dette ingen tydelige effekter i simuleringen.

Det har blitt anskaffet eksperimentelle data og observasjoner. Resultatene av de numeriske modellene i LedaFlow er i bra samsvar med de eksperimentelle dataene.

Preface

This Master's thesis is written as part of the course "TPG4920 – Petroleum Engineering, Master's Thesis", spring 2017 at the Department of Geoscience and Petroleum at the Norwegian University of Science and Technology. The thesis is written as the final part of a five years Integrated Master's Programme in Petroleum Engineering, with specialization in Production. The work is a continuation of my specialization project "Experimental and Numerical Analysis of Fluid Displacement in Complex Pipe Systems" written fall 2016, and of the work done by Jon Arne Opstvedt in his thesis, "Experiments and Numeric Simulation on Displacement and Flushing of Hydrocarbon Fluid in Subsea Systems", spring 2016.

Through the last year, I have learned a lot from my experimental work and the creation of the numerical models. I appreciate this knowledge and will bring it with me further, when I am now finishing my studies at NTNU.

I would like to thank Associate Professor Milan Stanko for supervising this thesis and contributing with important guidance. When I had a question or a problem, your door was always open and you gave me support and helped me finding a solution. I am also very grateful for the financial support to buy the pumps from OneSubsea that has been essential for making the experiments possible, and the good inputs and time offered from Dr. Anna Elisabet Borgund on different matters of the thesis.

Moreover, I would like to thank Senior Engineer Noralf Vedvik for always helping me with the system in the lab, when I needed an additional hand or an advice. This also applies to Senior Engineer Steffen Wærnes Moen for contributing with the system and the electronics when needed. Furthermore, I want to thank Åge Sivertsen for helping me with meters for measuring the volume fractions in the system. Engineer Håkon Myhren and Engineer Terje Bjerkan do also have my gratitude for helping me make parts that I needed, and offering me help if I needed for doing maintenance on the system. I also want to thank Ole Jørgen Nydal from EPT at NTNU for the permission to use an academic license of LedaFlow. In addition, I will thank Dr. Wouter Dijkhuizen in the Energy division in Kongsberg Digital for contributing with useful inputs regarding my simulations in LedaFlow, and not at least Kongsberg for offering academic licences of LedaFlow to NTNU.

Finally, I would like to thank my fellow students for making these 5 years in Trondheim knowledgeable and enjoyable. And not at least my family, for always believing in me and supporting me through my education.

Trondheim
June 2017

Hanne Gjerstad Folde

Table of Contents

List of Figures

List of Equations

List of Tables

Nomenclature

Latin Letters

A Area [m^2]

C Capacitance [F = As/V]

D Diameter [m]

f Frequency [Hz]

I Current [A]

m Mass [g]

$\dot{m}$ Mass flow rate [kg/s]

p Pressure [atm]

Q Flow rate [m^3/s] / [kg/s] / [L/min]

R Resistivity [Ω]

t Time [s] / thickness [mm]

T Time period [1/Hz] / Temperature [°C]

U Voltage [V]

v Velocity [m/s]

V Volume [m^3] / [L] / [cm^3]

WC Water Cut [-]

Z Impedance [Ω]

Greek Letters

ρ Density [kg/m^3] / [g/cm^3]

α Volume fraction [-]

ε Absolute roughness [m] / Permittivity [F/m] / Error [-]

μ Viscosity [Pa s]

σ Interfacial tension [N/m]

Subscripts

disp	Displacement
exp	Experimental
fin	Final
g	Gas
hom	Homogeneous standard free-surface model
i	Internal
inhom	Inhomogeneous mixture model
Leda	LedaFlow model
m	Methanol
num	Numerical
o	Oil
s	Superficial
stab	Stabilizing
tot	Total
w	Water

Abbreviations

1D	One dimension
3D	Three dimensions
CFL	Courant-Friedrichs-Lewy
CAD	Computer-aided design
FPSO	Floating Production, Storage and Offloading
CFD	Computational Fluid Dynamic
P&ID	Piping and Instrumentation Diagram
MEG	Monoethylene glycol
NTNU	Norwegian University of Science and Technology
PVT	Pressure-Volume-Temperature
PVC	Polyvinyl chloride

1 Introduction

The challenges that are faced in the petroleum industry today are increasing in complexity, resulting in a need for solutions that are more efficient and economical. This especially applies to the offshore production, where the companies are drilling in deeper environments with lower temperatures. According to Thomas (2010) this means that subsea technology will continue to become more important for developments in the oil industry. Subsea equipment plays a significant role, and it is crucial to handle both the equipment and the fluids in the systems correctly.

When temporarily shutting down the production of oil and gas from a well, there may still be hydrocarbons and water in the pipelines. Due to safety, environmental and economic reasons, removal of these fluids should be considered.

One option for removing the fluids is through displacement with a displacing fluid. The analysis of fluid displacement is an important field to study in the petroleum industry. This is to avoid hydrate formation in pipelines or contaminant emissions to the environment. It is common for subsea equipment to consist of complex pipe geometries. The removal of fluids in these subsea structures is not straight forward, due to uncertainties regarding displacement volumes and rates in these structures. Often are pipelines displaced for a longer time period than necessary, which is costly. In the petroleum industry MEG or methanol is commonly used as displacement fluid (Opstvedt, 2016).

The displacement process is conducted by injecting another fluid into the system at a certain rate with the objective of displacing the original fluid. The system is circulated for a given time period that should be sufficient to remove the unwanted fluid.

Due to the uncertainties regarding the displacement process, petroleum companies often perform the displacement in a very conservative manner. Some of the uncertainties are:

- For how long should one displace?
- What is the optimal displacement rate?
- How do these variables vary with different displacement fluids?

When displacing for a longer time period than necessary, the displacement process becomes both time-consuming and costly. Therefore, it would be advantageous knowing the optimal

displacement rate, and how this variable together with time would vary for different fluids. Numerical models for simulating these processes and experimental data for validation, are therefore of interest to the industry.

There has been conducted some work on the liquid-liquid flow in pipes. Brauner (2003) analyzed and studied flow patterns and pressure drops in liquid-liquid flow. However, this study is more directed at the steady-state flow conditions in long pipes. The research at liquid displacing liquid is more limited, but one can mention Schumann et al. (2014) who did a study on the displacement process through experiments for low flow rates with simple pipe geometries. An investigation of diesel oil displacing water to avoid water accumulation in low spots was conducted by Xu et al. (2011). It was executed experiments with an inclined downhill pipe, then a horizontal pipe followed by an uphill inclined pipe. Water was injected into the system, and then flowed with diesel oil at low rates to see the displacement effect of the water. Cagney et al. (2006) looked into the effect of methanol injection and gas purging to remove and inhibit water in a jumper. Dellecase et al. (2013) also studied using methanol and MEG to remove water from the geometry of a jumper.

In 2013 at NTNU Kazemihatami (2013) did his Master's thesis at NTNU on displacement of viscous oil in an M-shaped jumper using water. In the Master's thesis of Opstvedt (2016), both water displaced by oil and oil displaced by water were investigated in a U-shaped jumper at the Department of Geoscience and Petroleum at NTNU.

2 Objectives and Tasks

The topic of this Master's thesis is "Experimental and Numerical Study of Fluid Displacement in Subsea Pipe Segments". The purpose is to investigate the efficiency of one fluid displacing another fluid depending on displacement time and velocity, where the focus will mainly be on the study of liquid-liquid displacement in complex pipe geometries.

The study will be performed through experimental research and numerical simulations. Experiments will be carried out in a previously built pipe system representing a U-shaped jumper. The jumper is located at the laboratory hall at the Department of Geoscience and Petroleum at NTNU. Tap water and the synthetic oil Exxsol D60 will be used as fluids.

To obtain realistic simulation models for calculating the displacement efficiency, the transient multiphase flow commercial simulator LedaFlow® will be used. The model will be validated against results obtained through experiments. Furthermore, additional models will be created to study the effects of varying fluid properties, different fluids and a change in the geometry.

The objectives of the project are as follows:

1. Contribute in the repair and upgrade of the experimental rig: installation of new pumps and manifold for oil and water, detection and fix of leakages, general maintenance and installation of new flow meter.
2. Contribute in the development of a volume fraction meter to automate the process of measuring volume fraction in the pipe. Documentation of the operating principles, perform calibration and quantify its performance.
3. Run displacement experiments, both oil displacing water, and water displacing oil.
4. Make a three phase transient 1D numerical model using the commercial simulator LedaFlow, simulating the displacement process considering:
    a. a U-shaped jumper
    b. varying fluid properties
    c. methanol as displacing fluid
    d. gas included in the system
    e. a dead-leg included in the geometry
5. Validate the model simulating the U-shaped jumper against experimental results.

The thesis is a continuation of the work conducted by the author in the specialization project, "Experimental and Numerical Analysis of Fluid Displacement in Complex Pipe Systems", fall 2016 at NTNU. The experimental setup that will be used, was mainly built by Opstvedt (2016) as a part of his Master's thesis spring 2016. This work is part of the activity group on subsea engineering between OneSubsea and NTNU-IGP.

3 Theory and Background

This theory chapter is based on subsea systems and fluid displacement, impedance for measuring volume fractions and numerical analysis by using LedaFlow.

3.1 Subsea Systems and Fluid Displacement

3.1.1 Subsea Systems and Jumpers

The offshore industry is continuously looking for new hydrocarbon reservoirs, resulting in a need of new technology as the trend is moving towards operations at deeper and deeper sea levels. Deeper sea levels mean that it becomes more challenging to produce, and high requirements for the subsea equipment become necessary. Locating as many components as possible of the hydrocarbon facilities directly on the seabed seems to be both an economic and a practical solution (Offshore, 2016).

The subsea system consists of many elements, designed to function below sea level. The equipment has different functions and shapes. Low seabed temperatures make especially subsea trees, manifolds, jumpers, flowlines and risers at particular risk of developing hydrates because of rapid cool-down time upon shut-in and the problem of isolating them efficiently (Dellecase et al., 2013). Flow assurance is therefore an important subject to consider during field development and as part of the production cycle.

The main objective of a jumper is to connect subsea structures. According to Technip (2014) a jumper is a short pipe that can be either flexible or rigid, and which is used for connecting flowlines to subsea structures located closely to one another. For example, a jumper is frequently placed between satellite wells that are located at a distance from the manifolds (FMCTechnologies, 2016). It could also connect structures like PLEM or PLETS and Riser Bases (FMCTechnologies, 2016). A problem with the jumper design is that it includes low-spot areas where the water may easily accumulate, increasing the risk of forming hydrates (Dellecase et al., 2013). An illustration of a jumper structure with its low spot areas is presented in Figure 3.1 (FMCTechnologies, 2016).

Figure 3.1: Jumper geometry with its low spot areas

3.1.2 Fluid Displacement in Subsea Pipe Structures

Fluid displacement is a process where something is pushing the fluid out of the way, and taking its area. Liquid-liquid displacement is a fluid displacement where one liquid is replaced by another liquid. This kind of displacement is of interest for subsea pipe structures. Different geometric systems will have various challenges related to this process. Different fluids may replace one another in various manners.

One of the reasons for executing displacement is to avoid the formation of gas hydrates in the pipelines when the petroleum fluids start to cool down after the production is temporarily shut down. The formation of gas hydrates is a huge problem in the oil industry. A picture of a hydrate plug inside a pipeline is given in Figure 3.2 (Giavarini and Hester, 2011). A gas hydrate is a solid substance that consists of natural gas molecules surrounded by water molecules (Kvenvolden, 1988). It has a crystalline form that is similar of an ice-like structure (Max et al., 2006). An illustration of a hydrate structure with a methane molecule in the middle, surrounded by water molecules, is illustrated in Figure 3.2 (Sain, 2008).

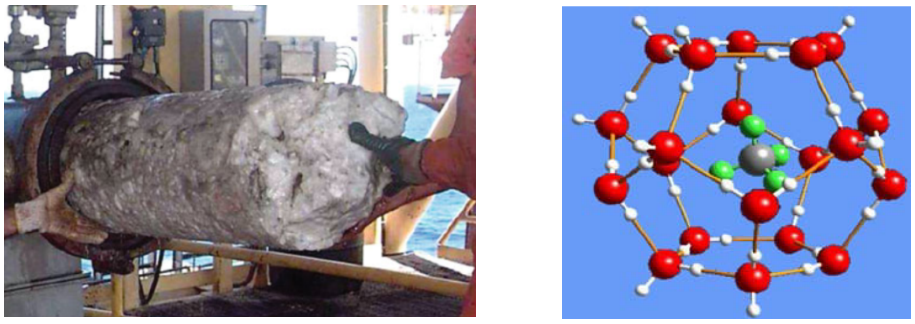

Figure 3.2: Left: Hydrate plug forming inside a pipeline,
Right: Hydrate structure

The hydrates are formed at low temperatures and high pressures when gases are combined with water (Max et al., 2006). These are conditions that are often reached in an operation for retrieving oil and gas subsea. The temperatures in the sea water at the depth where the piping systems are located are low, and the pressures in the fluids coming out of the reservoirs are high. Problems occur for hydrocarbon production when the solids are building up inside the pipelines and leading to a blockage (Giavarini and Hester, 2011). The plugs are difficult to remove as depressurizing may happen to only one side, resulting in the pressure gradient across the plug turning it into a high-speed projectile (Giavarini and Hester, 2011). If using heating, this may access a pressure buildup and then a pipeline explosion since one volume of hydrate contains 160 volumes of gas (Giavarini and Hester, 2011). By replacing the fluids necessary to form hydrates, this is less likely to happen.

A second reason for doing displacement in subsea systems is to reduce the amount of contaminant emissions when performing subsea operations like corrective- or preventative-maintenance, replacing components and abandonment, which may require both disconnection and lifting of the equipment (Opstvedt, 2016). In addition to hydrocarbons having a bad impact on the environment, it is costly for the oil companies since they have to pay fines if there is a leakage of unwanted chemicals into the sea. The rules and regulations regarding harmful liquids are getting stricter as a consequence of accidents and increased environmental focus (Opstvedt, 2016). The Norwegian Environment Agency, or Miljødirektoratet, is a government agency under the Ministry of Climate and Environment. The main tasks of the agency are reducing greenhouse gas emissions, manage Norwegian nature and prevent pollution (NorwegianEnvironmentAgency, 2017). According to Miljødirektoratet (2015) the operator of a field is responsible for finding measures that allow a reduction in the use of chemicals by choosing other materials or solutions for optimal dosage. The emissions from the petroleum industry to the sea in Norway in 2015 were 33.75 ton of oil (Miljødirektoratet, 2017a) and 183029989.54 m^3 of water containing oil (Miljødirektoratet, 2017b). It is therefore of interest to look at methods for removal of these fluids, before they are leaked to the environment.

Flow assurance in form of displacement is integrated in the industry. At the Cascade and Chinook offshore field outside of Brazil, all of the trees, jumpers, manifolds, flowlines and risers are insulated. The operators at the FPSO then have time to displace all of the produced

fluids with diesel in case of shut-in, before problems arise (Offshore, 2016). Methanol will also be injected to keep hydrates from forming in the wellbore, trees and the well jumpers (Offshore, 2016). Methanol is classified as a chemical in the green category, by The Norwegian Environment Agency, and is easily degradable in the sea (Øren and Christensen, 2016). Spilling methanol into the sea is preferred compared to crude oil, even though it should be avoided if possible.

Due to uncertainties regarding the displacement properties of a fluid in a geometry, subsea structures are often displaced for a longer time period than necessary. This takes time, costs money and results in use of unnecessary displacement fluids. Experimental research is therefore of great interest to be able to better understand how the fluids are behaving in the pipelines.

3.1.3 Multiphase Flow

A general definition of multiphase flow is simultaneous passage in a system of a stream composed of two or more phases. A multiphase flow may consist of three different phases; solids, liquids and gases. Liquids are relatively incompressible, but have an interface that is deformable in contact with other phases. Liquid-liquid flow is one of the most common two-phase flows that exists. It includes emulsion flows of oil and water in pipelines. Among usual three-phase flows one can find gas-liquid-liquid, where oil, water and natural gas are common. In typical offshore oil and gas developments, these multiphase flows are standard in wells, flowlines and risers, and in the transportation of fluids from the wells to the platforms or facilities at shore. (Falcone et al., 2009)

When discussing the “flow regime” or the “flow pattern” of a flow, one is referring to the behaviour and shape of the interfaces between phases in the multiphase mixture (Falcone et al., 2009). Different forces and mechanisms are occurring within the multiphase fluid at the same time, and how these forces balance decides upon the flow pattern. According to (Falcone et al., 2009) the flow pattern of a multiphase flow in a conduit is determined by factors listed below:

- Phase properties, fractions and velocities
- Operating temperature and pressure
- Conduit diameter, roughness, shape and inclination

- Presence of any upstream or downstream pipe work (bends, valves, junctions)
- Types of flow; transient, pseudo steady state or steady state

Most research has been conducted on two-phase flows with gas and liquid. For liquid-liquid flow, the flow regimes are more complex. Vertical flow patterns for oil-water flow are illustrated in Figure 3.3, and horizontal flow in Figure 3.4. Oil and water have different densities, and the flow patterns are highly affected by the densities. This is seen by studying Figure 3.4, where the left picture has a density ratio for oil-water of 0.83 and the other near 1.0. (Falcone et al., 2009)

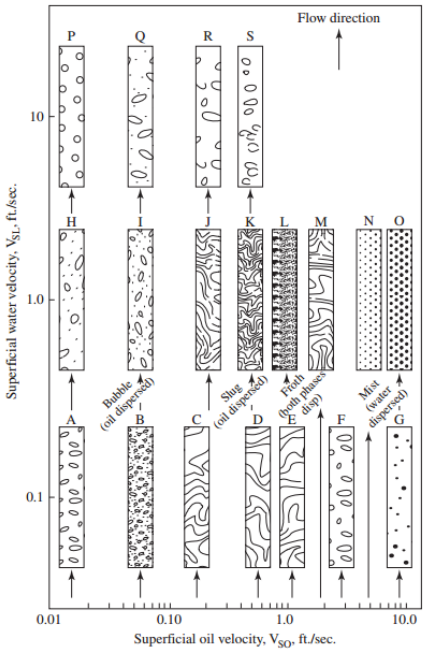

Figure 3.3: Flow patterns in vertical oil-water flow

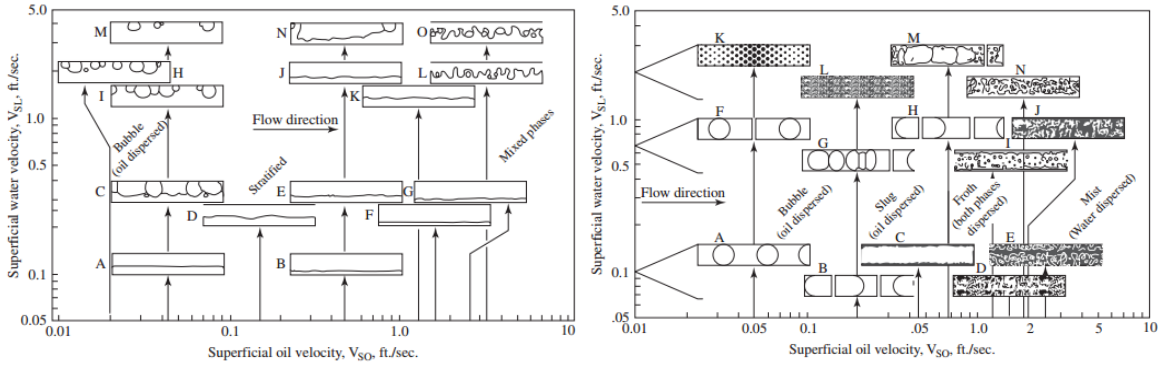

Figure 3.4: Flow patterns for horizontal oil-water flow

Left: oil-water density ratio: 0.83, Right: oil-water density ratio: near 1.0

In a horizontal pipeline, where oil and water flow together at low rates, gravitational forces will dominate over turbulent forces, resulting in the water phase separating into its own layer in a stratified flow regime. An increase in flow rate will result in an increase in the turbulence energy, making the water gradually becoming more dispersed in the oil phase. (Cai et al., 2012, p. 334)

According to Kannan et al. (2016) the wetting properties of a liquid with respect to the wall, become important for conduits with small diameters. It has been reported that the most wetting liquid forms a film on the wall, while the other liquid flows through the passage as droplets, plugs or continuous flow.

3.1.4 Previously Work on Displacement at NTNU

Both Kazemihatami (2013) and Opstvedt (2016) wrote their Master's theses about displacement in jumper geometries at the Norwegian University of Science and Technology in Trondheim. A description of their work and main findings will be presented in this section.

3.1.4.1 Work by Milad Kazemihatemi

Kazemihatami (2013) wrote his Master's thesis at the Department of Energy and Process Engineering on the subject of displacement in an M-shaped jumper. The experimental activities were to investigate displacement of viscous oil in pipes by using a small scale of a jumper with an M-form, illustrated in Figure 3.5. In total, 56 experiments were conducted where measurements were taken of different oil and water flows in horizontal and inclined pipelines. The results showed that the front of the shape of the propagation interface is changing along the pipe, and that the minimum superficial velocity of water in order to remove all the residual oil in the jumper was 0.38 m/s.

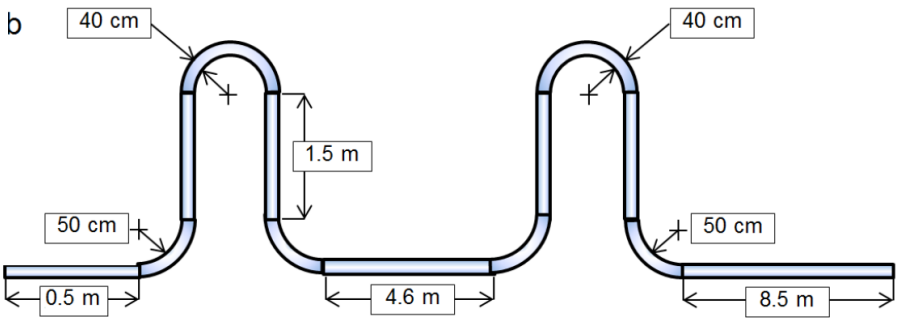

Figure 3.5: Illustration of the M-jumper used in the experiments of Kazemihatami (2013)

3.1.4.2 Work by Jon Arne Opstvedt

Opstvedt (2016) analysed how the shape of the displacement front, flow pattern and phase hold up evolve with varying displacement velocities for a U-shaped jumper setup. The original experimental facility built by Opstvedt (2016) is illustrated in Figure 3.6.

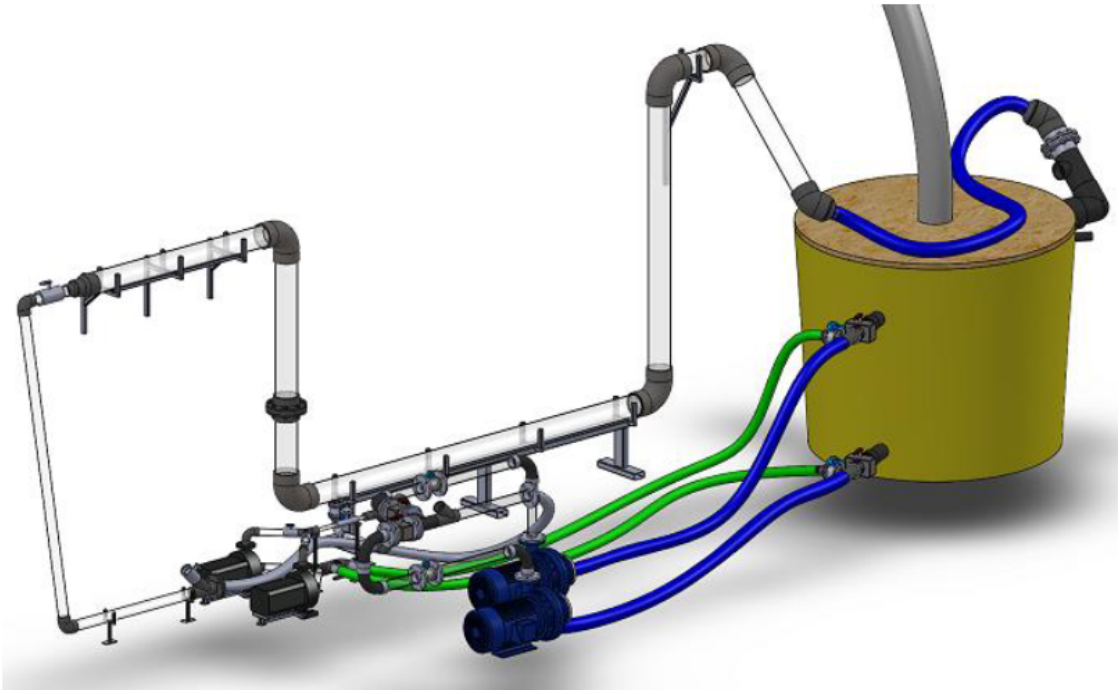

Figure 3.6: CAD model of the experiment rig built by Opstvedt (2016)

16 experiments were conducted using two different geometries. Both water-oil displacement and oil-water displacement were studied for 4 different flow rates. The displacement efficiency is defined as the volume fraction of the displacing fluid at a given time. The volume fraction α of a fluid *i*, is calculated using Equation 3.1. V_i is the total volume of fluid *i* in the domain, and V_{tot} is the total volume in the domain.

Equation 3.1: Volume fraction of a fluid *i*

$$\alpha_i = \frac{V_i}{V_{tot}}$$

Opstvedt (2016) found that the displacement efficiency is dependent on the establishment of a displacement front, which was not clearly observed until flow rates above 20 m^3/h. The highest displacement efficiency was seen for water-oil displacement, even though it was severely reduced after one displacement volume. Oil-water displacement showed better

displacement efficiency after one volume, but with lower sweep due to reduced front height. The numerical simulations conducted in ANSYS CFX had more problems predicting the displacement for low velocities.

The experimental results that Opstvedt (2016) obtained from his experiments are presented in the tables below. Table 3.1 contains the results of oil displacing water through the top inlet, and Table 3.2 the results of water displacing oil.

Table 3.1: Experimental results from oil displacing water through top inlet

Superficial Velocity v_s [m/s] (± 0.009 m/s)	**Rate Q [m^3/h] (± 0.6 m^3/h)**	**Remaining water volume for oil displacing water (top inlet) [L] (± 0.01 L) Displacement Volumes**		
		1	**2**	**3**
0.09	6	59	56	54
0.15	10	56	44	41.5
0.30	20	49	22.2	16.2
0.45	30	23.42	4.65	1.72

Table 3.2: Experimental results from water displacing oil through top inlet

Superficial Velocity v_s [m/s] (± 0.009 m/s)	**Rate Q [m^3/h] (± 0.6 m^3/h)**	**Remaining oil volume for water displacing oil (top inlet) [L] (± 0.01 L) Displacement Volumes**		
		1	**2**	**3**
0.09	6	29.5	29	29
0.15	10	21	17	16
0.30	20	12.8	4	3.3
0.45	30	1.32	0.35	0.28

3.2 Impedance for Measuring Volume Fractions

Volume fraction is a parameter that is typically measured when studying multiphase flow experimentally. It allows for characterizing the distribution of the phases inside the pipe and it is often used to validate models. According to Zhai et al. (2012) it is necessary to determine the individual phase flow rates of oil and water in a two-phase flow to better optimize the oil production performance. In case of studying fluid displacement in pipelines, it is essential to know which fractions that are obtained after flowing for a certain time. The principle of impedance may be used for the purpose of finding volume fractions in pipes.

Electrical impedance Z is the ratio between voltage U and current I in an alternating current circuit, and is measured in ohm (Sandstad, 2015). The relation is given in Equation 3.4.

Equation 3.2: Impedance

$$Z = \frac{U}{I}$$

It might be considered a complex quantity, where the absolute value gives the ratio between the effective values of voltage and current, and the phase angle the phase difference between them (Sandstad, 2015).

3.2.1 Fundamental Principles of an Impedance Probe

The impedance probe may be used as a tool for measuring the volume fraction of a multiphase flow. The principle is based on the fact that electrical impedance varies with concentration and distribution of phases. One advantage by using this technique is that it gives a virtually instantaneous response. Thus, it is suitable for experiments with rapidly changing conditions. (Falcone et al., 2009)

The meter is working by measuring impedance between electrodes that are placed either in the flow or at the wall of the channel. This determines whether the impedance is governed by conductance or capacitance as the dominating factor. One may often experience variance in the liquid conductivity due to changes in temperature. Therefore, to operate at high enough frequencies to ensure domination by capacitance is essential. According to Falcone et al. (2009) it is preferable to place the electrodes in the tube wall, due to less interference with the

flow. Some methods of mounting electrodes in the tube wall for impedance measurements are presented in Figure 3.7. Falcone et al. (2009)

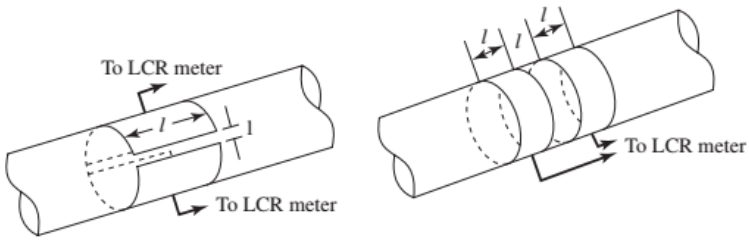

Figure 3.7: Wall mounted electrodes for impedance measurements
(Left: Strip type) (Right: Ring type)

One problem with the impedance method for measuring the volume fraction is that it might be highly sensitive to the flow pattern within the channel. Another main difficulty is the composition of an oil-water mixture. Oil exhibits dialectical properties, while water is a conductor. If the mixture is dominated by oil, it will behave as a capacitor. If water is the dominant phase in the mixture, it will behave as a conductor. If the flow switches from either water-continuous to oil-continuous or the other way around, a change should be done in the impedance measuring technique. (Falcone et al., 2009)

Figure 3.8 is showing the geometry of a ring conductance probe that has four stainless steel ring-shaped electrodes, axially separated and flush-mounted on the inside of the wall of the flow pipe. E is representing exciting electrodes while H represents measuring electrodes. The measuring electrodes are giving fluctuating signals that are correlated with the phase volume fraction. (Zhai et al., 2012)

Merilo et al. (1977) proposed an alternative electrode system with 6 electrodes mounted as a part of the tube wall, and in this way eliminating the disturbance to the flow. The three pairs of electrodes are forming parallel plates uniformly spaced around the circumference as may be visualized in Figure 3.9 (Merilo et al., 1977).

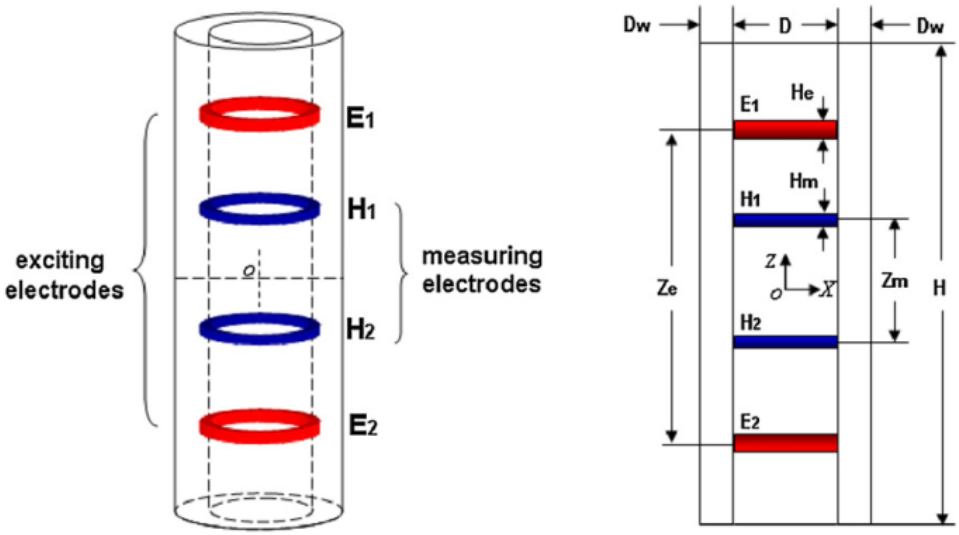

Figure 3.8: Geometry and parameter definition of the ring conductance probe

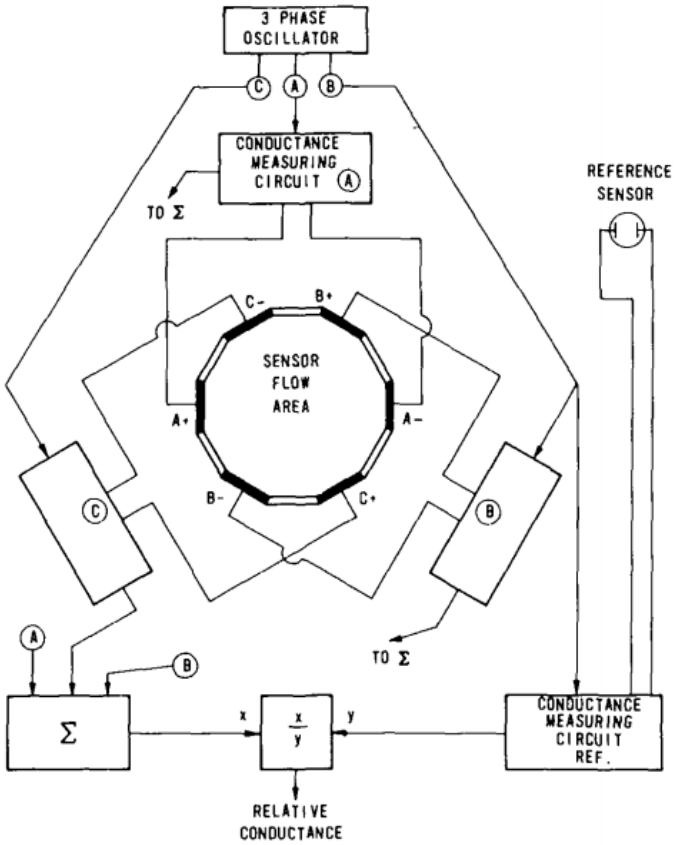

Figure 3.9: Schematic diagram of the conductance monitor

The three pairs get energy from oscillators which make the electric field vector rotating as illustrated in Figure 3.10 (Falcone et al., 2009). An average is taken of the fractions from the pairs, due to a suggestion that this should give a more valid mean void fraction (Falcone et al., 2009). A reference sensor may be placed in a location where it only sees single phase liquid, and may be used to compensate for changes in the conductivity of the liquid due to variations from temperature and concentration of impurities (Merilo et al., 1977).

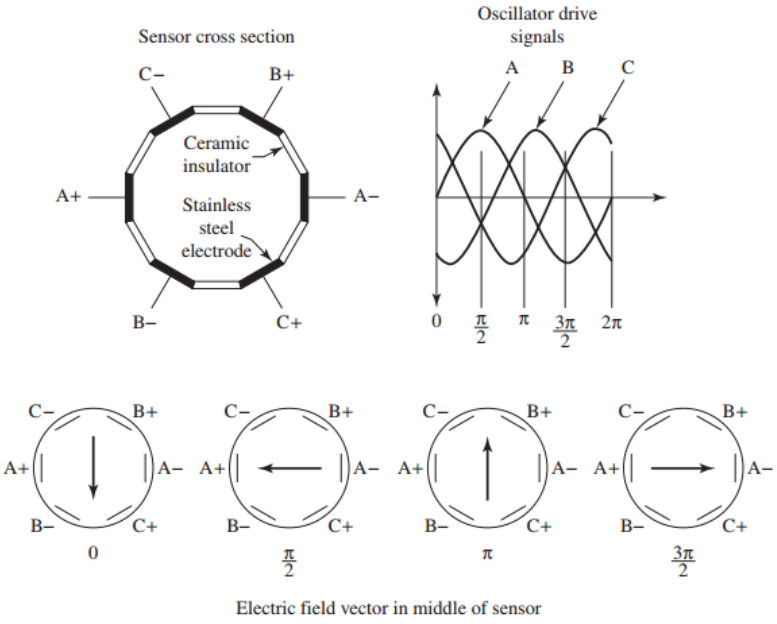

Figure 3.10: Rotating field electrode system

3.2.2 Volume Fraction Meter Developed by Åge Sivertsen at NTNU

An electronic device for measuring electrical parameters in liquids using the impedance principle has been developed at the Department of Geoscience and Petroleum at NTNU by Sivertsen (2002). The device is measuring impedance and is governed by capacitance between two isolated electrodes placed on the outside of a flow channel.

The method was originally developed for measuring volume fractions in core samples. However, due to the meter having the possibility of placing electrodes on the outside wall of the channels, the meter have the potential of measuring volume fractions in pipelines (Sivertsen, 2002). Since the meter is compact and can be placed near the electrodes, this should minimize the problem of electromagnetic noise. The electrode plates will work as a condenser, which is illustrated in Figure 3.11 (Sivertsen, 2002). Between the plates one has an

isolating medium, which is called dielectric. According to Falcone et al. (2009) this means that the meters should work best for an oil continuous flow, due to oil exhibiting dielectric properties and water is a conductor. Two plates of copper are used as electrodes and placed on the pipe wall. Between these two electrodes are current, voltage and the phase angle between the current and the voltage measured (Sivertsen, 2002). Larger electrodes will give more accurate readings, as long as contact between them is avoided, as this will result in shorting.

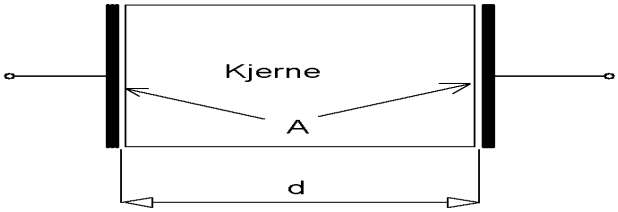

Figure 3.11: Sketch of a condenser with plates

According to Sivertsen (2002), the ohmic losses resulting from a large phase angle, will be higher when the water content is big. The losses should decrease when the water content decreases. Every material has a resistance, and when electric current flows through a material, losses will occur due to this resistance. Since the unit of resistance is called ohm, the losses are called ohmic losses. They will continue to decrease as the water fraction decreases for some time, until they reach a value that behaves like a resonance point and the losses stay at this point until the water fraction is very low. Then the losses will continue to decrease again. The method is therefore assumed to be working best for high oil fractions.

The capacitance C is given by Equation 3.3. The permittivity or dielectric constant ε is from the dielectric of the plate condenser, and is depending on material and medium. A dielectric constant for a certain material is giving the signal velocity through the material where low permittivity causes high velocity. Different rocks have a dielectric constant varying between 3 and 40, oil between 2 and 5 and water approximately 80. ε_0 is the permittivity of vacuum, and is given as $8.85 \cdot 10^{-12}$ F/m. (Sivertsen, 2002) The K for a plate condenser is given in Equation 3.4, where A is the area and D is the diameter.

Equation 3.3: Capacitance

$$C = \varepsilon_0 \, \varepsilon \, K$$

Equation 3.4: K for a plate condenser

$$K = \frac{A}{D}$$

The principle behind the electronics for the volume fraction meter is shown in Figure 3.12 (Sivertsen, 2002).

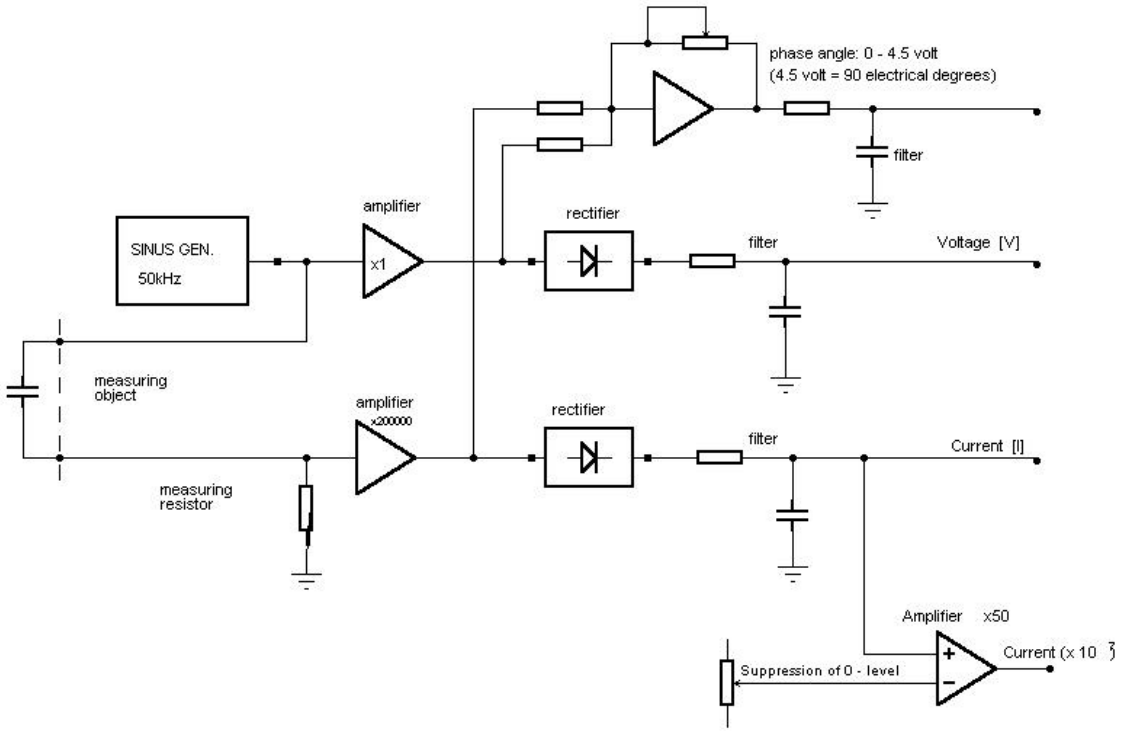

Figure 3.12: Principe scheme for the electronic

First, a sinus generator is sending signals to the electrodes. The sinus generator is used to obtain alternating current, in order to avoid polarization. The signals are amplified, to achieve desired voltage of approximately 5-6 volt. The measuring object, or the electrodes, is connected to the meter trough a BNC-contact. The current through the measuring object is then measured, through a resistance. The voltage is measured directly over the measuring object. Both these signals are sent through a rectifier and a filter, before they are read. Before the signals are rectified, they may be sent to a comparator for measuring the phase angle. In a condenser where there are no losses, the phase angle will be 90 electrical degrees, which means that the current is 90 degrees ahead of the voltage (Sivertsen, 2002). If the signal has a frequency f, is the time period T = 1/f. 90 degrees equals a time difference of 1/(4f). A wiring diagram of the meter developed by Sivertsen (2002) can be seen in Figure D.1 in 0.

The volume fraction is obtained by calculations of the voltage across the measuring electrodes, the current through the electrodes, and the phase angle between the current and the voltage.

The impedance Z is found by dividing the voltage by the current, and is given by Equation 3.2.

3.3 Numerical Analysis

When using a numerical computer tool for analyzing multiphase flow, the user has several options. One may choose between the 1D simulator tools LedaFlow by KONGSBERG and OLGA by Schlumberger, or the 3D computational fluid dynamic tool ANSYS CFX. LedaFlow is a transient multiphase flow simulator, based on multiphase physics from large scale experiments and gathered field data. OLGA is also based on experimental data and intended for large scale problems. The CFD software is governed by physical laws, and applied through averaged Navier-Stokes equations along with models for phase interaction and turbulence (Opstvedt, 2016). In the present work, LedaFlow will be explored as a tool for simulating displacement, and compared to the models made in CFX by (Opstvedt, 2016).

3.3.1 The LedaFlow Software

LedaFlow is a computer program developed by SINTEF that were guided and supported by TOTAL and ConocoPhilips. KONGSBERG did the commercializing and have developed it further. LedaFlow Engineering 1D can be used for solving multiphase hydrodynamic problems with oil, gas and water in a pipeline in a one dimensional system. How the fluid behaves in other directions when looking at a fully three dimensional problem, is approximated by using closures derived from laboratory experiments and from an understanding of physics that applies for flow in a circular pipe. (KONGSBERG, 2016a).

According to KONGSBERG (2015a) the software has been validated against comprehensive data sets to ensure that the models become as representative as possible. Focus on the design has been to build an intuitive user interface to ensure improved productivity.

Two models are included in LedaFlow; the Point model and the 1D model. The Point model is used for “one point” of all the three flow cases; single, 2-phase and 3 phase to solve steady state equations. It is assumed that there exists a thermodynamic equilibrium, which means no

compositional effects are taken into account when the fluid distribution is computed. The mixture temperature is giving the foundation of the temperature distribution. In the Point model a fast and steady state solution with exact mass conversation is reached, and is the basis of the steady-state pre-processor for 1D transient code. The other model, 1D model, is used for transient situations for the same three flow cases. In the field approach from LedaFlow there is included a detailed modelling of water and oil dispersions and gas bubbles in liquid phase, where there exists a mass equation for each field. The fields are visualized in Figure 3.13. The equations for enthalpy and energy are solved for continuous phases. In this model, heat transfer and complex networks with manifolds, wells, valves, controllers, etc. are included. (KONGSBERG, 2016b)

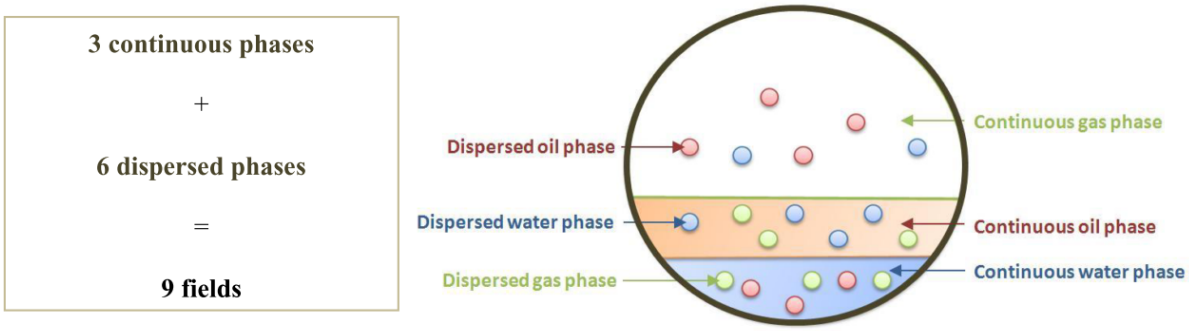

Figure 3.13: The fields used in the 1D model in LedaFlow

The simulation speed in LedaFlow is mainly limited by the size of the calculation time step that can be performed. Another important limitation is the number of calculations that may be resolved at each time step. One may directly relate this to the number of mesh cells resolved. The time steps in multiphase transient simulators are limited by the Courant-Friedrichs-Lewy method, which makes sure that no phase has the possibility to traverse a mesh cell in less than a time step. This means that the velocity of a fluid through the shortest cell will decide upon the maximum calculation time step, and therefore it is useful to keep the length of the smallest cell as big as possible. (KONGSBERG, 2015b)

There are four methods available to generate mesh automatically in LedaFlow, and these are presented in Table 3.3 (KONGSBERG, 2015b). The required properties for the creation of the mesh are listed, as well as the properties of the resulting generated mesh.

Table 3.3: Options for mesh construction in LedaFlow

Mesh Construction Types	Required Properties for Creation	Properties of Generated Mesh
Least squares	Min number cells between locked points[1] Min cell length Max expansion factor	Number of cells in each individual section (pipe between locked points) equal or superior to the total number of cells provided All cells inferior or equal to maximum cell length provided Expansion factor for any consecutive cells inferior or equal to maximum provide
Uniform	Total number of cells	As uniform as possible and close to total number provided (slightly inhomogeneous due to locked points)
DeltaX/D	Ratio of cell length and diameter	As uniform on portions of the pipe where diameter is constant with a cell length approximately equal to the one provided (slightly inhomogeneous due to locked points)
Horizontal/ Vertical	Max vertical cell length Max horizontal cell length Vertical angle	Split the pipe into vertical and horizontal zones If the inclination angle of mesh cell is greater than specified vertical angle, it is in the vertical zone Cell lengths as close as possible to the value provided

[1] A locked point in LedaFlow is a point in the mesh construction that has been fixed to an exact location in the profile. This is included to make sure that angles in the profile are included.

4 Methodology

The methodology chapter is divided into two parts. The first part is presenting the setup and procedures for the experiments. The second part is about the creation of numerical models in the software LedaFlow.

4.1 The Experimental Study

4.1.1 Experiment Rig

The main part of the experimental setup is the same as built by Opstvedt (2016) and illustrated in Figure 3.6. The setup consists of a U-shaped jumper, pumps, separator and connections. A visual picture of the jumper showing the geometry and the measures is given in Figure 4.1. The measures are from Opstvedt (2016). The jumper consists of a horizontal inlet, a vertical pipe, a horizontal bottom pipe and a second vertical pipe. Afterwards, the fluid is directed through an outlet back to the separator.

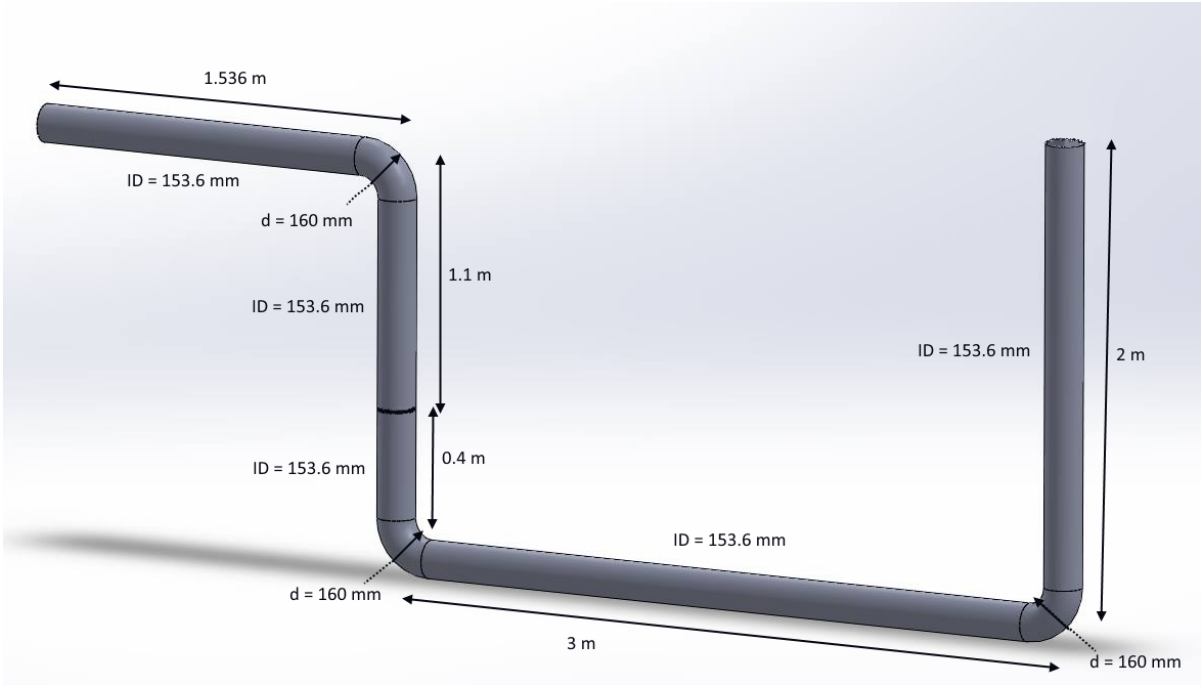

Figure 4.1: The measures of the U-formed jumper based on Opstvedt (2016)
(Drawing without dimensions: Espen Hestdahl)

Opstvedt (2016) designed the system to work with two different geometries. The first geometry is the regular one, by using the first horizontal pipeline at the top as the inlet. Then

the whole volume of the jumper is investigated. The other geometry is made through inserting a blind flange in the first riser, as shown in Figure 4.2 (Opstvedt, 2016).

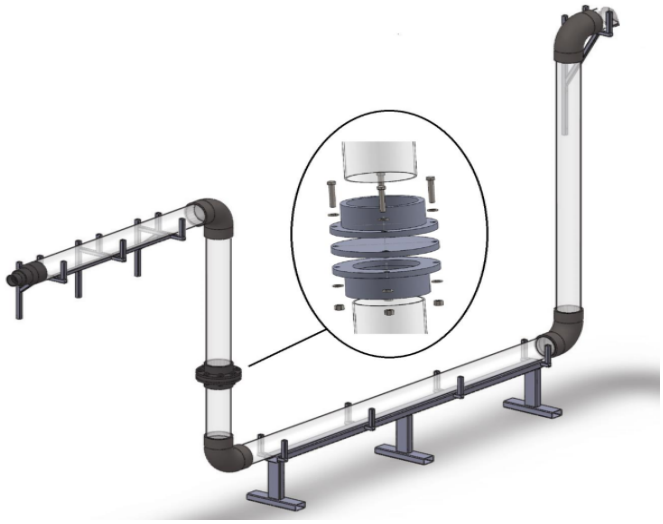

Figure 4.2: Blind flange in the first riser

For the second geometry an extra inlet is built, shown as the bottom inlet in Figure 4.3 (Opstvedt, 2016). When the first riser is cut off, this gives the possibility of studying displacement in a closed off section. Due to time limitations, this has not been prioritized for experiments in present work, but will be recommended further investigation.

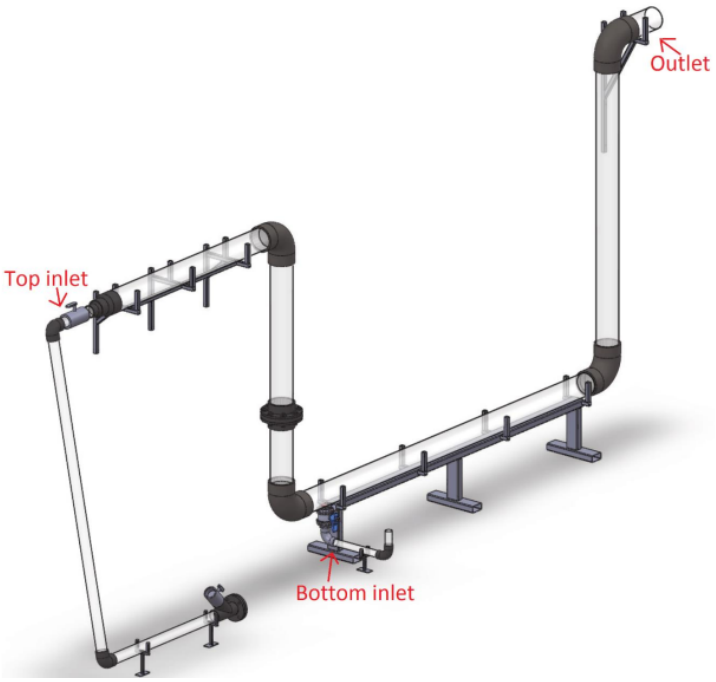

Figure 4.3: Top inlet, bottom inlet and outlet of the jumper

A list of the parts used for building the U-jumper is presented in Table 4.1 (Opstvedt, 2016). Transparent PVC pipe is used for the system to allow for observations of the flow pattern.

Table 4.1: Parts list for the U-jumper

Part	Location	Description	Quantity
Pipe	Inlet section	160x3.2 mm	1.536 m
	Top of first riser	160x3.2 mm	1.1 m
	Bottom of first riser	160x3.2 mm	0.4 m
	Bottom section	160x3.2 mm	3 m
	Second riser	160x3.2 mm	2 m
	Outlet section	160x3.2 mm	0.3 m
Bend	Inlet – First riser	160 mm x 90°	1
	First riser – Bottom section	160 mm x 90°	1
	Bottom section – Second riser	160 mm x 90°	1
	Second riser – Outlet	160 mm x 90°	1
Sleeve	First riser	ID 160 mm	2
Flange	First riser	ID 160 mm	2
Bind flange	First riser	OD 220 mm	1
Bolts	Flange	M16x120	4
Nuts	Flange	M16x10	4
Discs	Flange	M16	8

Due to poor pump performance, new pumps and a new flowmeter have been acquired. In addition to the new pumps and the new flowmeter, some major changes were conducted to the other facilities that are sharing the separator with the displacement rig. It was requested that all of the pumps should have the possibility of being used for the three different experiment facilities, both in pairs or separately. This required a flexible system for the pumps. A manifold was designed by Senior Engineer Noralf Vedvik at NTNU to combine the pumps, and the design of the system is shown in Figure 4.4.

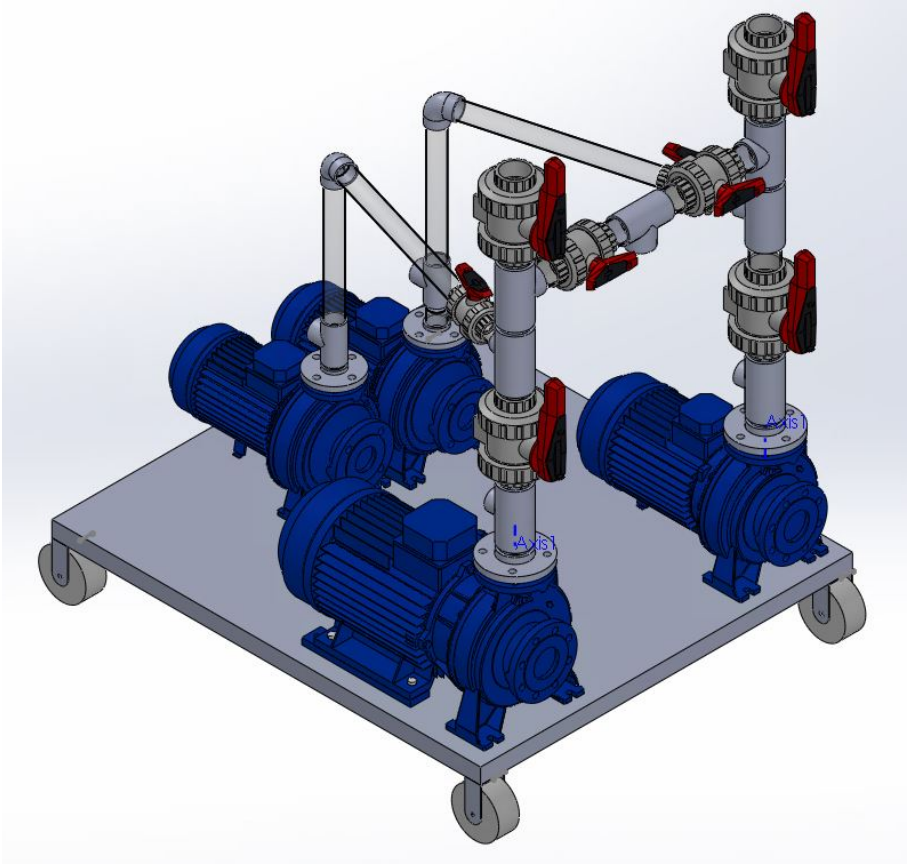

Figure 4.4: Manifold for pumps (Drawing by Espen Hestdahl)

An overview of the system as it looks today may be seen in the P&ID in Figure 4.5. The piping and instrumentation diagram includes pipelines, valves, pumps and instrumentation in the system. The flowmeter is marked as a box with an F, the pressure sensors as “PT” and the temperature sensors as “TT”.

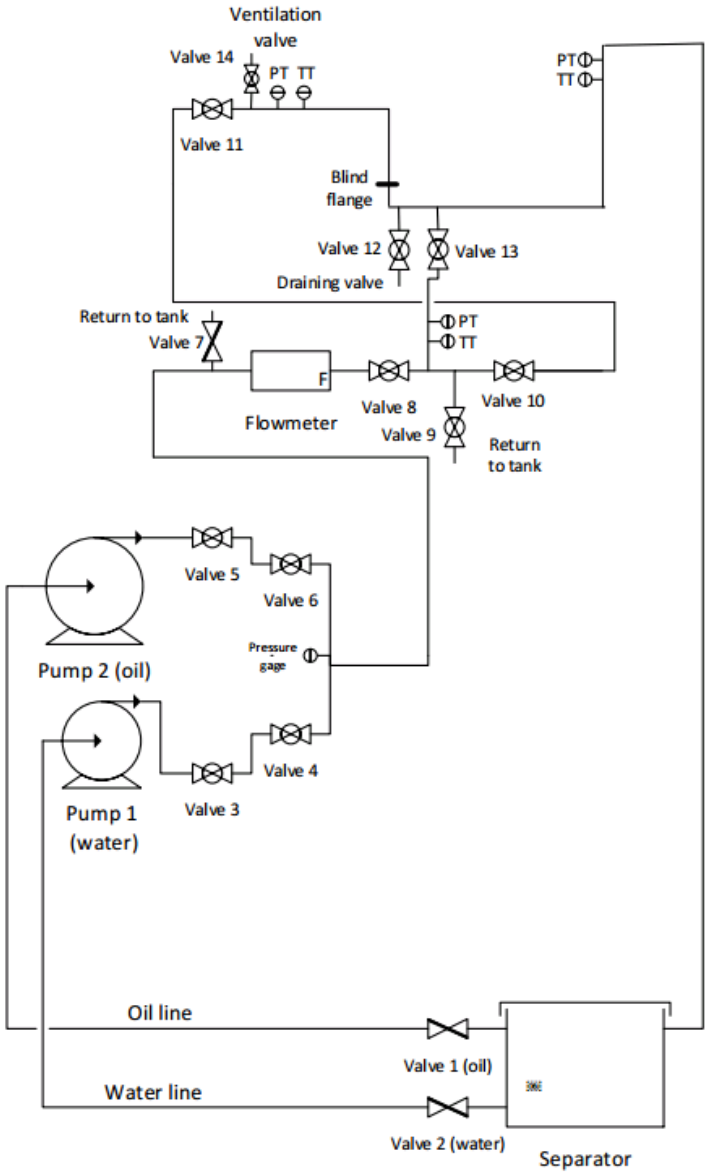

Figure 4.5: P&ID of the system

The picture in Figure 4.6 is showing the pump manifold to the left. Four pumps are connected together. The two pumps in the back are the new pumps for the displacement rig, funded by OneSubsea. A hose is connecting the manifold to the displacement rig, which is seen in the right part of the picture. One may also see the flowmeter and indicator in the lower horizontal section of the picture.

Figure 4.6: Pump manifold and connection to the displacement rig

Figure 4.7 is showing the riser leading to the top inlet of the U-jumper.

Figure 4.7: Top inlet of the displacement rig

The U-jumper used for the experiments is photographed in Figure 4.8. The second riser continues out of the picture, and then the flow is lead back to the separator.

Figure 4.8: The U-jumper used for experiments

4.1.2 Pumps

The two pumps that will be used for the displacement facility are of the type standardized centrifugal pumps F40/200A from Pedrollo. These are new pumps that were funded by OneSubsea last fall, due to poor pump performance by the old ones. The datasheet and specifications of the pumps can be found in section D-1 in Appendix D.

4.1.3 Flowmeter

In addition, IGP has funded a Nixon Turbin Flowmeter of the type NT48-2" that has the range of 0(110) – 1100 LPM for water. The accuracy of the meter is ± 0.5 %. The output is induced sinus pulses of 70-800 mV.

A F110P-AP-HD-OT-BP-ZC Fluidwell Process Indicator was also ordered. This has a transmitter and a display for showing the flow rate and total flow. The k-factor of the indicator is separate for the total flow and the flow rate. An average k-factor from

experimental tests was given by the producer as 46.53579 pulses/L, with linearity over a full range of 0.473608 %. The output for AP is 4-20 mA passive and for OT a pulse transistor.

4.1.4 Sensors

The temperature sensors and the pressure sensors were calibrated during fall 2016 as a part of the specialization project “Experimental and Numerical Analysis of Fluid Displacement in Complex Pipe Systems”.

4.1.4.1 Temperature sensors

The rig has 3 temperature sensors for measuring the temperature in the system. One is placed at the top inlet, one at the bottom inlet and one at the outlet. The sensors are of the type PT100 RTD, resistance temperature detector. They are chosen due to being field proven and able to measure in the desired temperature range 20 °C ± 10 °C. The measured resistance R_x will increase by an increase in temperature T. At 0 °C the sensor has a resistance R_0 of 100 Ω. The temperature-resistance relationship is given by the “Callendar-van Dusen”-equation in Equation 4.1 (Opstvedt, 2016).

Equation 4.1: "Callendar-van Dusen"-equation

$$R_x = R_0(1 + A\,T + B\,T^2 + C(T - 100)\,T^3)$$

A, B and C are constants. When solving Equation 4.1 for temperature one obtain Equation 4.2 which for $t_{measured} > 0$ will have C = 0. For a PT100 element are A = $3.9083 \cdot 10^{-3}$ °C^{-1} and B = $-5.775 \cdot 10^{-7}$ °C^{-1} (Opstvedt, 2016).

Equation 4.2: The "Callendar-van Dusen"-equation solved for temperature

$$T = \frac{-R_0\,A + \sqrt{R_0^2\,A^2 - 4\,R_0\,B\,(R_0 - R_x)}}{2\,R_0\,B}$$

4.1.4.2 Pressure Sensors

There are 3 pressure sensors in the system, placed at the same locations as the temperature sensors. The type is from the UNIK 5000 pressure sensing platform, more precisely the PTX 5072-tc-al-ca-h1-pa. This is a piezo resistive pressure transducer where an output signal of 4-20 mA is proportional to the pressure applied. According to GeneralElectricCompany

(2014) the sensors are a good solution for reliable, accurate and economical measurements in a long term.

4.1.4.3 Volume Fraction Meter

One of the purposes by running experiments is to see how well one fluid is able to displace another fluid in the jumper. This requires measurements of the volume fractions in the system. An accurate method is manually draining the pipes. However, since this is time-consuming, a more automatic method has been inquired. This other possibility is using a volume fraction meter developed by Sivertsen (2002). The principles behind this method are explained in the theory section, 3.2.2.

The electrodes are fastened in two pairs at the pipe wall as displayed in Figure 4.9. To the left it is shown a picture of electrode pair 1 and meter 1, which is placed in the beginning of the lower horizontal section. The picture in the middle is showing how the electrodes are fastened on the pipe wall from the side. One is placed at the bottom and one at the top. The picture to the right is showing electrode pair 2 and meter 2, placed close to the end of the lower horizontal section. It also includes the connection from the electrodes to the meter, which has one cable for getting power and has one for sending the signals to the computer.

It is important to place the electronic part and the electrodes as close as possible in order to avoid noise.

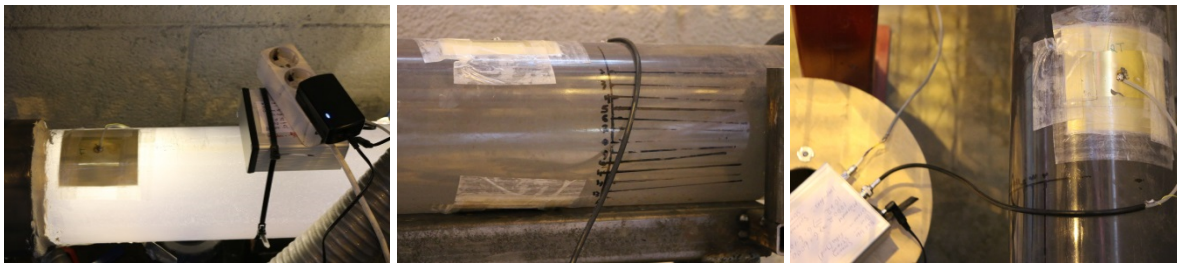

Figure 4.9: Electrodes placed at the pipe wall
(Left: Electrode pair 1 and Meter 1, Middle: Electrodes fastened at top and bottom,
Right: Electrode pair 2 and Meter 2)

In advance, it was anticipated that the meter would work best for low water fraction (Sivertsen, 2002). It is important to calibrate the meters before use, as this will give an

indication of which interval the meter should be used for. It is also important to check the results manually for the first tests executed, before one trusts the meters.

4.1.4.3.1 Calibration of the Volume Fraction Meters

A calibration was executed for the volume fraction meters upfront the experiments. It was conducted by using a closed container with a known volume. The meter was calibrated against the liquids that will be used in the experiments for better accuracy. The container was filled with known volumes of each fluid so that the fractions are known. Figure 4.10 is showing it filled with 100 % water and Figure 4.11 with 50-50 % water and Exxsol D60.

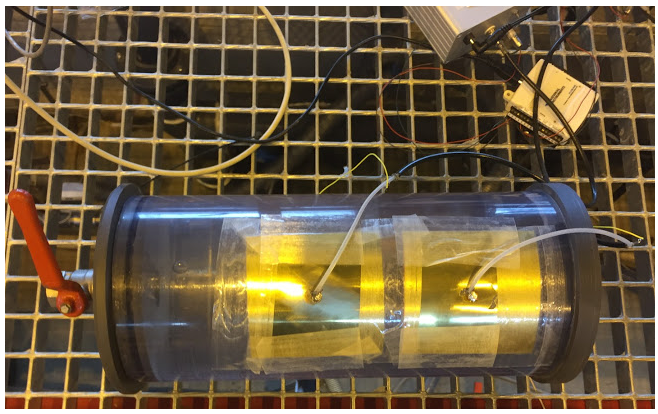

Figure 4.10: Calibration cylinder for volume fraction meters filled with 100 % water

Figure 4.11: Calibration cylinder filled with 50-50 % Exxsol D60 and water

The process was repeated for different volume fractions. LabVIEW is calculating the impedance from the input voltage signal and the current signal, using Equation 3.2 and multiplying with 60000 due to a measuring resistance of 10 kΩ being used. The measured impedance values with their uncertainties within a confidence level of 95 %, are displayed in

Table 4.2. Meter 1 appears to be more stable than meter 2, due to the lower uncertainties.

Table 4.2: Impedance from calibration measurements

Water Fraction α_w [-]	Impedance Z [Ω]	
	Meter 1	Meter 2
100 %	202478 ± 14	212191 ± 16
75 %	244107 ± 46	240422 ± 604
50 %	249149 ± 6	269982 ± 59
25 %	253745 ± 17	266107 ± 169
10 %	252625 ± 28	269216 ± 71
0 %	257316 ± 28	273091 ± 59

These points are used for making the calibration curves that relates impedance and volume fraction. The curves are presented in Figure 4.12.

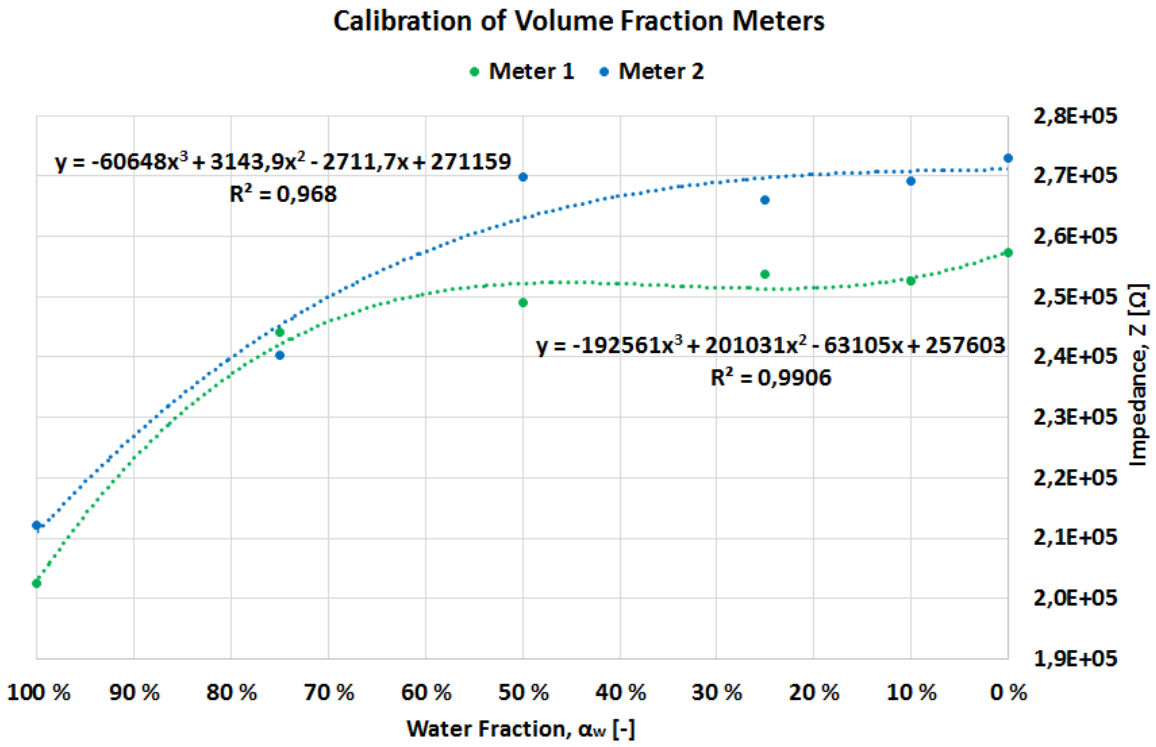

Figure 4.12: Calibration curves for the volume fraction meters

Figure 4.12 is showing the impedance measured for water fractions of 0 %, 10 %, 25 %, 50 %, 75 % and 100 %. The trend is similar for both meters. The change in impedance is highest where the water is dominating, which is unexpected when looking at the studies of Sivertsen (2002) and what is written about oil-water flow by Falcone et al. (2009). It should have been measured additional points in the area where the water fraction is highest, but the focus area during the calibration was where it is lowest due to the expectations. One reason for these calibration results might be that the measured resistance by the meter was too high for the corresponding current signal. Third degrees equations have been fitted to match the data points. For the first meter, the equation is corresponding well to the data points with R^2 = 0.9906. For the second meter R^2 = 0.968. From the plot in Figure 4.12, one may conclude that for water fraction below approximately 70 %, the change in impedance is too small to be used for determining volume fractions.

The water fractions α_w in the experiment pipe may be found using the impedance *Z* from the volume fraction meters and solving Equation 4.3 and Equation 4.4, within an interval of the water fraction of 70-100 %. These equations will be used when testing the volume fraction meters during the experiments.

Equation 4.3: Relation between impedance and water fraction for meter 1 (WF: 70-100 %)

$$Z_{meter1} = -192561\ {\alpha_w}^3 + 201031\ {\alpha_w}^2 - 63105\ \alpha_w + 257603$$

Equation 4.4: Relation between impedance and water fraction for meter 2 (WF: 70-100 %)

$$Z_{meter2} = -60648\ {\alpha_w}^3 + 3144\ {\alpha_w}^2 - 1712\ \alpha_w + 271159$$

4.1.5 Computer Program, LabVIEW

A LabVIEW VI has been created to record the measured data in the system. The VI is saving the data to a chosen file. It is logging the flow rate, the impedance from the volume fraction meters, the temperature and the pressure in the system. The front panel of the program is visualized in Figure 4.13 and the block diagram in Figure 4.14.

Unfortunately, the flow meter indicator was unable to send signals to the computer, has been sent to the producer for testing. However, the flow rate was visible on the indicator during the experiments, and the flow rates were recorded using a video camera.

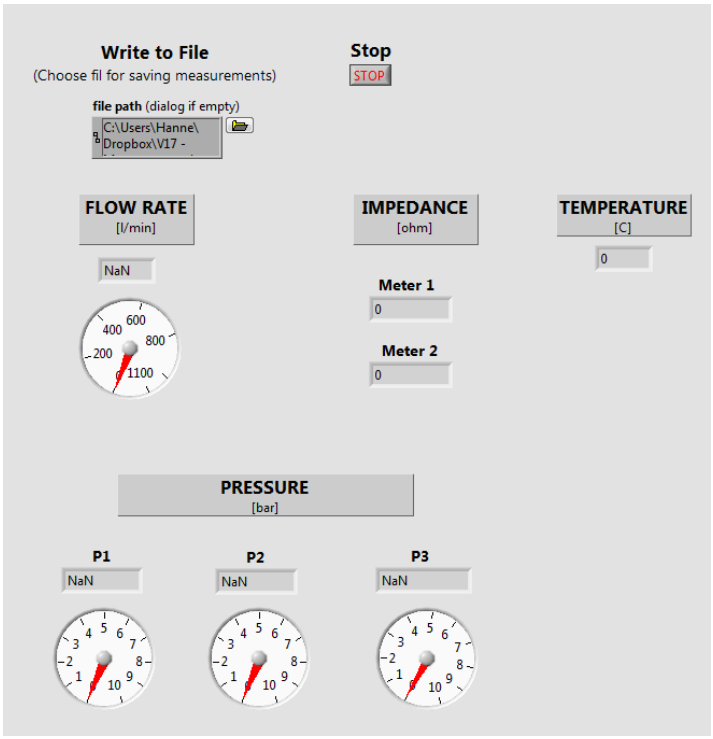

Figure 4.13: LabVIEW Virtual Instrumentation front panel

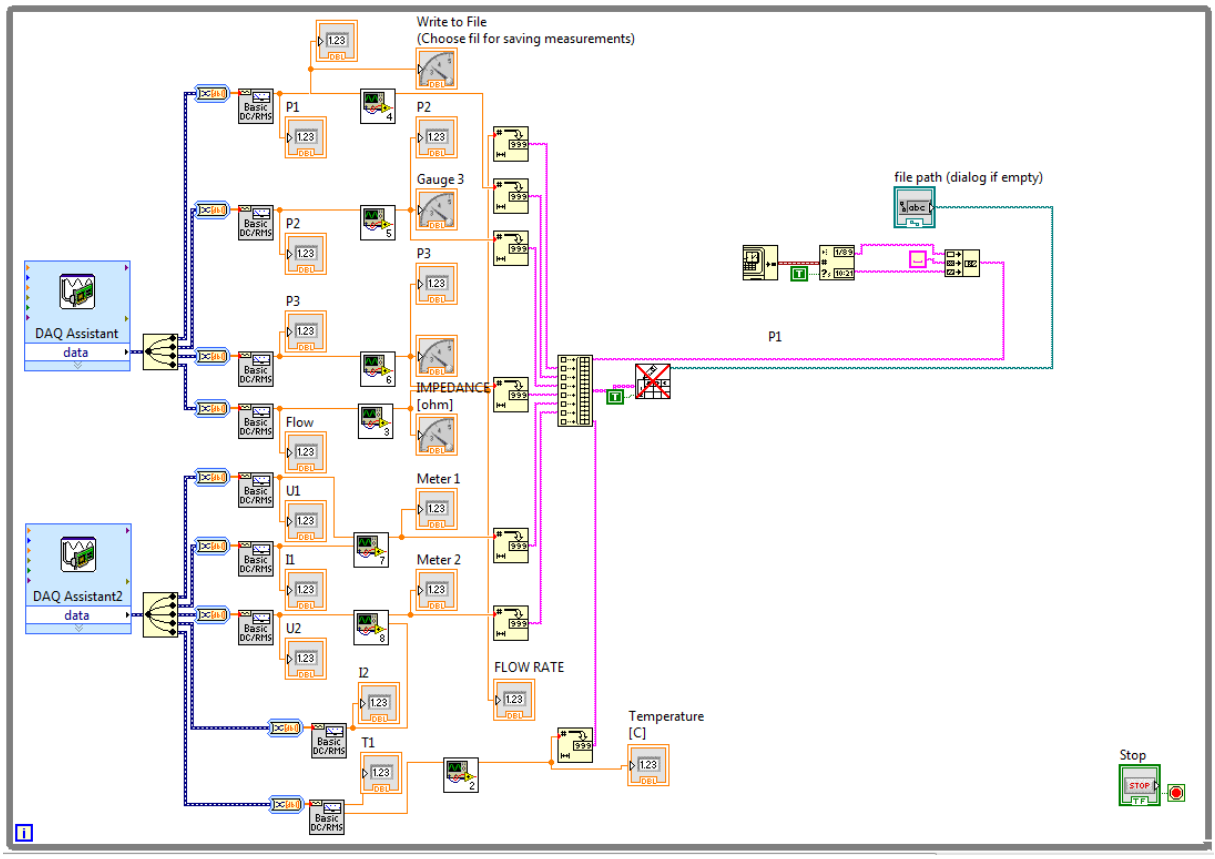

Figure 4.14: LabVIEW Virtual Instrumentation block diagram

4.1.6 Fluids

The purpose of the experiments is to run liquid-liquid displacement in a pipe, to simulate removal of hydrocarbon and water in a subsea pipe system. A system consisting of two phases, both liquids, have been evaluated. In the industry would Methanol or MEG be common options for displacing fluids in pipe. However, methanol is not allowed in the experiment facility (Opstvedt, 2016) and MEG is expensive. It was therefore chosen to use oil and water.

For oil it was used synthetic oil, Exxsol D60, from ExxonMobil Chemicals, which is widely used for experimental work. To use Exxsol D60 was decided by Opstvedt (2016). Crude oil would have been preferred to make the situation as realistic as possible. However, its toxicity and the fact that is not sold through regular channels made it difficult. From ExxonMobil (2005) one can see that the viscosity at 25 °C is 1.43 mPa s. Due to high temperatures, real crude oils might actually exhibit viscosities similar to the Exxsol D60.

The plan in the beginning of the project was to run experiments using saltwater, as this was required for the separation rig sharing the same fluid tank. Therefore, measurements of PVT-properties have been taken of saltwater (3.5 wt-% NaCl) and Exxsol D60. However, a delay in the build-up of the other facility made it unnecessary to use saltwater after all. Due to the bad effect of saltwater on the pumps leading to reduced operation time, it was decided to use regular tap water instead. Even though the properties of tap water may vary some from placeto place, the properties of the water under for the experiments should stay consistent for the testing period. Due to time limitations, it was chosen to process further using PVT-properties for water from other references in the numerical models. The interfacial tension between water and Exxsol D60 has been measured to 36 mN/m in 2016 by SINTEF, using a Pendant Drop measurement method with a Teclis Tracker tensionmeter from Teclis Instruments (Fossen, 2016).

To be able to distinguish between the transparent liquids, Exxsol D60 and water, the oil was dyed with “Oil Red O” color powder. The Oil Red O color powder does not affect the surface tension of the oil (Chen et al., 2016).

Earlier is has been a problem with bacteria forming in the tank containing oil and water, creating Diesel bugs. Diesel bugs are small microorganisms that live in water and are eating

diesel. They leave behind a slippery, dark mass that clogs filters, damages tanks, pipes and motor systems (MaritimConsultants, 2017). Before filling the tank again with water and oil, it was properly cleaned to remove the microorganisms. An agent, called Bio-Protect 2, was added to the oil and water mixture to avoid them and keep the interface between the fluids clean. The agent is produced by Maritim Consultants AS (MaritimConsultants, 2017).

4.1.7 Experimental Procedure

This subchapter is providing an overview of the experimental procedure for measuring fluid displacement in the U-shaped pipe system. Prior to the experiments, the total drainable volume in the U-jumper was measured, and further used to decide upon displacement times. An overview of the planned experiments is given in Figure 4.15.

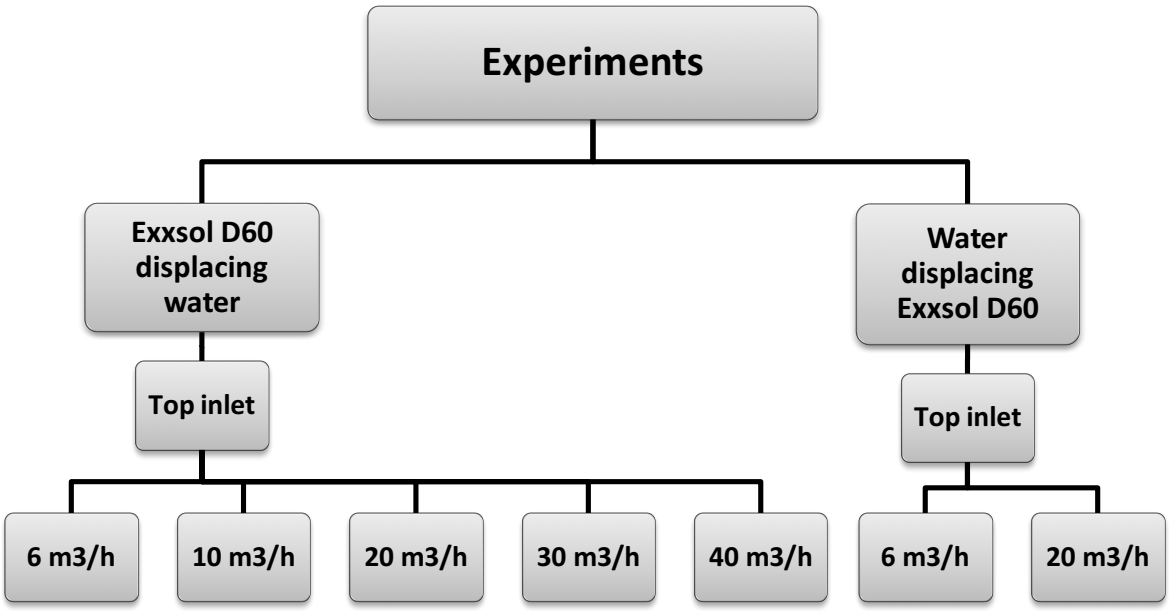

Figure 4.15: Planned displacement experiments

The experiments were conducted by first establishing the initial conditions. They are established by filling the system with the fluid to be displaced. A low flow rate was used for filling the system, so the fluid would flow calmly, and make it easier to remove the air using the ventilation valve, valve 14 in Figure 4.5, at the top of the horizontal inlet pipe. Then, the flow rate was increased to remove air bubbles in the jumper and rests of the other fluid if present.

Next, valve 4 or valve 6 in the P&ID in Figure 4.5, depending of which fluid that was to be displaced, was closed at the same time as the pump was stopped. This is done to sustain the pressure in the system and keep the fluid in place. Further, the pump of the displacing fluid was set to a specific frequency, which was held constant during the experiment. The frequencies for the different rates can be seen in Table 4.3. In addition, due to logging problems specified in 4.1.4.3, a camera was used for filming the flow rate. The videos were later used to write down the rates.

Table 4.3: Pump frequencies used for the experiments

Flow Rate Q		**Pump Frequency** f
[m^3/h]	**[L/min]**	**[Hz]**
6	100	10.50
10	166.7	13.50
20	333.3	24.50
30	500	34.00
40	666.7	44.40

The pump was then started at the same time as the valve to the pump with the displacing fluid, valve 4 or valve 6, was opened. The time was taken from when the displacing fluid reached the entrance of the horizontal inlet pipe. After flooding for a given time, presented in Table 4.4, the system was shut down by closing valve 4 or 6 and valve 8 in Figure 4.5, in addition to stopping the pump. Since all of these things were done manually, there are some uncertainties regarding the displacement time. This uncertainty for time is set to ± 2 s. The fluids in the system got some time for separation, before the system was drained using valve 12, see Figure 4.5.

Table 4.4: Displacement times

	Rate Q [m³/h]	Displacement Time t_{disp} [s]				
oil displacing water	6	35	70	105	209	314
	10	23	45	63	125	188
	20	11	20	31	63	94
	30	9	14	21	42	64
	40	6	13	16	31	48
water displacing oil	6	37	72	106	209	314
	20	11	21	32	63	95

The system was drained into 15 L transparent buckets from Jula, shown in Figure 4.16. The bucket has a measurement scale from 1 to 12 L, with steps of 0.1 L. The measurement readings had an uncertainty of ± 0.1 L. The transparency made it simple to distinguish between red colored Exxsol D60 and water.

Figure 4.16: Bucket used for volume measurements

The total volume fractions of the fluids in the system were calculated using Equation 3.1.

4.2 Numerical Simulations in LedaFlow

As a part of this Master's thesis, simulations have been created in the transient multiphase flow commercial simulator LedaFlow®. The simulations are executed to study different displacement rates, displacement times and displacement fluids.

An overview of conducted simulations is listed below:

- Reproducing the current experimental points
- Reproducing the experimental points of Opstvedt (2016)
- Sensitivity analysis considering changes in
    - Density
    - Viscosity
    - Interfacial tension
    - Displacing fluid (methanol)
    - Fluid to be displaced (gas – methane)
    - Geometry (dead-leg)

Appendix G contains instructions for how to build a simple model in LedaFlow.

4.2.1 Experiments of Liquid-Liquid Displacement in U-Jumper

This model has been created to simulate the performed experiments. The experimental data will be used for validating the model.

4.2.1.1 Creating a Case

A default case of 3-phases is chosen to be able to run the model with both oil and water. By setting the gas fraction in the system equal to 0, the gas phase is not included.

4.2.1.2 Case Settings

Important settings for the case are PVT-properties, numerical settings and output settings. The choosing of PVT-properties will be discussed firstly. For the numerical simulations in this thesis, it is chosen constant PVT-properties for a given reference pressure and temperature. Required PVT-properties are density, viscosity, compressibility, thermal conductivity, heat capacity and surface tension. No specification of equation of state is needed.

Depending on the fluid type and flow rate, the pressure in the system will vary some. However, the pressure variation is low. The separator is an open system with atmospheric pressure, and this is used as a simplification of the system. The author would like to refer to the specialization project written fall 2016 at the topic “Experimental and Numerical Analysis of Fluid Displacement in Complex Pipe Systems”, where a single phase model for analyzing

the pressure in the system was made. It has been noticed small variations in the temperature in the laboratory hall, but based on observations before conducting experiments, an average temperature value of 17 °C was assumed. PVT-properties for a temperature of 17 °C and atmospheric pressure will therefore be used for the simulations.

It is especially difficult to find PVT properties for Exxsol D60 at 17 °C, and therefore experiments were executed in the core analysis lab at IGP. As mentioned in chapter 4.1.6 it was originally intended to use saltwater. Since the PVT-measurements were conducted with that intention, they were measured for saltwater with 3.5 wt-% NaCl and Exxsol D60. However, the results are still included for future use.

First, the densities ρ of the fluids were measured using a pycnometer. A pycnometer is a container with a known volume V, illustrated in Figure 4.17. The mass m of the container is measured, first without any liquid, then with liquid.

Figure 4.17: Pycnometer for density measurements

The densities are calculated using Equation 4.5.

Equation 4.5: Density using a pycnometer

$$\rho = \frac{m_{filled} - m_{empty}}{V}$$

The measured and calculated values are found in Table 4.5. The masses were only measured once, and should have been measured at least three times, to make a proper assumption about the uncertainties. Unfortunately, the prioritized work with making the experimental facility ready took a lot of time. The density of the Exxsol D60 has therefore been compared to the

values reported from ExxonMobil (2005) which says that at 15 °C the density should be between 774.0 kg/m^3 and 809.0 kg/m^3, with a typical value of 792 kg/m^3. As the temperature of 17 °C is somewhat higher than the testing temperature for ExxonMobil, it seems likely that the density of Exxsol D60 is lower, with a reasonable value of 786 kg/m^3.

Table 4.5: Pycnometer measurements and results

Description	T [°C]	V [cm^3]	m_{empty} [g]	m_{filled} [g]	ρ [g/cm^3]
Exxsol D60 27.01.17	17 °C	52.722	30.99	72.45	0.786
Saltwater 3.5 wt-% NaCl 27.01.17	17 °C	52.693	31.292	85.164	1.022

The viscosities were measured using a Rheometer of type MCR 302, illustrated in Figure 4.18 (AntonPaar, 2017). The apparatus did the measurements at a constant temperature of 17 °C and atmospheric pressure.

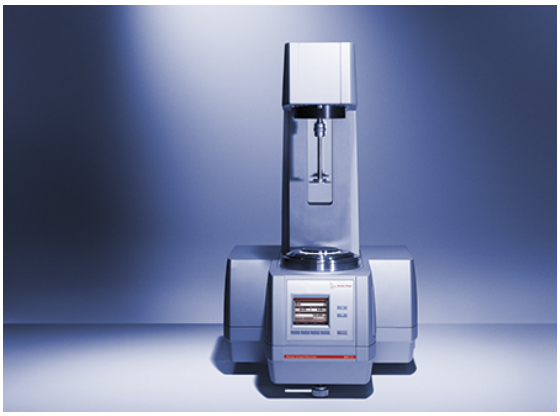

Figure 4.18: Rheometer MCR 302

The results of the viscosity from the measurements are presented in Table 4.6. One measurement was made for saltwater and two for Exxsol D60. Again, at least three measurements should have been taken. The resulting values are 0.00107 Pa s for saltwater, and 0.00156 Pa s ± 0.00010 Pa s for Exxsol D60 within a confidence interval of 95 %.

Table 4.6: Results from viscosity measurements

Fluid	Measurement Number	Viscosity μ [Pa s]
Saltwater	1	**0.00107**
Exxsol D60	1	0.00149
	2	0.00163
	Average	**0.00156 ± 0.00010**

As LedaFlow requires the interfacial tension, measurements were made of saltwater and Exxsol D60. An apparatus from KRÜSS was chosen, which is using the pedant drop principle. 20 measurements were taken, resulting in an interfacial tension of 27.313 mN/m ± 0.841 mN/m, within a confidence interval of 95 %. Due to the change from saltwater to tap water, the interfacial tension measured by SINTEF presented in section 4.1.6 was used instead.

The PVT properties used for the model in LedaFlow are summarized in

Table 4**.7**. The rest of the PVT-properties were either found online or reported by (Opstvedt, 2016).

Table 4.7: PVT properties for the numerical simulation

Property	Water	Oil (Exxsol D60)
Density [kg/m^3]	998.9 (TheEngineeringToolbox, 2017b) (17 °C)	786 (17 °C)
Viscosity [Pa-s]	0.001095 (TheEngineeringToolbox, 2017a) (17 °C)	0.00156 (17 °C)
Compressibility [kg/m^3/bar]	0.0391 (Default value from LedaFlow) (25 °C)	0.0391 (Default value from LedaFlow) (25 °C)
Conductivity [W/m-K]	0.6069 (Opstvedt, 2016)	0.136 (Opstvedt, 2016) (25 °C)

Heat capacity [J/kg-K]	4183.8 (TheEngineeringToolbox, 2017b) (17 °C)	1760 (Opstvedt, 2016) (25 °C)
Molar mass [g/mol]	18.02 (Opstvedt, 2016)	158 (Opstvedt, 2016)
Property	**Water – Exxsol D60**	
Interfacial Tension [N/m]	0.036 (Fossen, 2016)	

In addition, the numerical and output settings have to be specified. The settings are presented in Table 4.8. Smaller time steps are chosen for the first time period, due to the most rapidly changes happening here. This is also reflected in the output settings, where the logging is happening more rapidly for the first 250 seconds. When the system starts to stabilize, the changes in data will be smaller, needing fewer data. The CFL is the Courant-Friedrichs-Levy number, specified to ensure that the time step is low enough in relation to the grid cell length and the phase velocities.

Table 4.8: Numerical settings and output settings

Simulation time 3600 s			
	Numerical settings		**Output settings**
Time [s]	**Maximum time step [s]**	**CFL**	**Logger [s]**
0	0.05	0.3	0.05
250	0.5	0.4	1
350	100	0.8	10

4.2.1.3 Network

The network for this model is simplified to one pipeline, illustrated in Figure 4.19. Simulations have been executed for both oil displacing water, and water displacing oil. The pipeline is initially filled with the fluid to be displaced. For boundary nodes, it is chosen constant rate upstream the system, and constant pressure downstream.

Figure 4.19: Network for model simulating experimental data in LedaFlow

Simulations are run according to conducted experiments. The test matrix in Figure 4.15 presents an overview of the planned experiments. The real flow rates were found from analyzing the measured rates during the experiments. LedaFlow requires mass flow rates $\dot{m}$, which are converted from volume flow rates Q using density ρ as given in Equation 4.6.

Equation 4.6: Mass flow rate

$$\dot{m} = Q \cdot \rho$$

The simulated flow rates are presented in Table 4.9.

Table 4.9: Flow rates for simulations of performed experiments

Exxsol D60 displacing water			**Water displacing Exxsol D60**		
$Q_{planned}$ [m^3/h]	$Q_{measured}$ [m^3/h]	$\dot{m}_o$ [kg/s]	$Q_{planned}$ [m^3/h]	$Q_{measured}$ [m^3/h]	$\dot{m}_w$ [kg/s]
6	4.589	1.002	6	6.190	1.718
10	8.925	1.949			
20	19.730	4.308			
30	28.164	6.149	20	20.769	5.763
40	37.743	8.241			

4.2.1.4 Pipe

In the pipe settings are the profile and geometry of the pipe, as well as the mesh constructed. The profile is created in a Cartesian coordinate system. The profile of the jumper is two dimensional, using *X* and *Z*. The measures are initially based on the thesis of Opstvedt (2016) with some adjustments to fit the measured drainable volume of 165.98 L. The lengths of the bends are included in the model. The profile of the jumper is presented in Table 4.10. The calculated length *L* from LedaFlow is included. However, it should be noticed that after all of the experiments were conducted, the average measured total volume was 165.0 L ± 0.3 L. Due the model already having been made in LedaFlow and simulations run, it was

decided to keep the first measured volume. The difference is small, and it is therefore not believed to have had a significant effect on the results.

Table 4.10: Profile of the jumper in LedaFlow

X **[m]**	***Y*** **[m]**	***Z*** **[m]**	***L*** **[m]**
0	0	1.81	0
1.536	0	1.81	1.536
1.696	0	1.71	1.725
1.696	0	0.16	3.275
1.856	0	0	3.501
4.856	0	0	6.501
5.016	0	0.16	6.727
5.016	0	2.16	8.727
5.14	0	2.24	8.875

In Figure 4.20 a picture showing the profile of the system is given. It is built as one unit, starting with liquid flowing from the left into the horizontal inlet, moving down the first riser, next the lower horizontal zone, and then up the second riser and moving towards the separator.

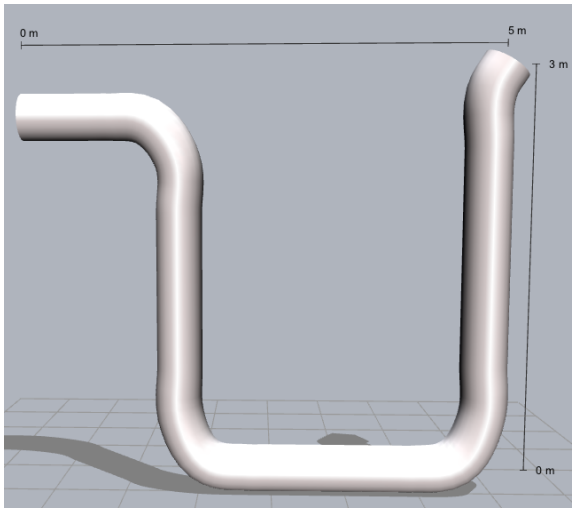

Figure 4.20: Profile of U-form used for the numerical model of performed experiments

Table 4.11 contains the geometry of the model. It is providing the internal diameter, which is varying based whether it is a bend or regular transparent PVC pipe, for the calculated length of the profile *L*. The absolute roughness for a PVC pipe is given as ε = 0.0015 mm (SulzerPumpesLtd). In addition, the thickness of the pipe is specified as *t* = 32 mm.

Table 4.11: Geometry of the U-jumper

Calculated length of pipe for profile *L* [m]	**Internal diameter D*i* [mm]**
0	153.6
1.536	160.0
1.725	153.6
3.275	160.0
3.501	153.6
6.501	160.0
6.727	153.6
8.727	160.0
8.875	160.0

The properties of the PVC-pipe are presented in Table 4.12.

Table 4.12: Properties of the PVC pipe

Property	**Symbol**	**Value**	**Reference**
Density	ρ_{PVC}	1400 kg/m^3	(TheEngineeringToolbox, 2016f)
Heat capacity	c_p	1005 J/(kg °C)	(TheEngineeringToolbox, 2016c)
Conductivity	k	0.19 W/(m K)	(TheEngineeringToolbox, 2016d)
Emissivity	ε	0.92	(TheEngineeringToolbox, 2016a)
Youngs modulus	E	3.25 GPa	(TheEngineeringToolbox, 2016b)
Viscosity	μ_{PVC}	0 Pa-s	(PVC is solid)
Thermal expansion coefficient	α	0 1/C	(TheEngineeringToolbox, 2016e)

A numerical solution is a solution to a problem that is defined through a mesh and boundary conditions. The "converged" solution is therefore depending on the mesh and the boundary conditions to be accurate. Three conditions must be fulfilled for a steady state simulation, for it to be converging. The criteria are; residual RMS error values need an acceptable value, monitored points that are of interest should have reached a steady solution and the domain should have imbalances less than 1 %. (Coputational Fluid Dynamics blog (CFD), 2013)

To determine which mesh construction to use, all the four different options described in Table 3.3 in 3.3.1 were tested, and then compared to the experimental data obtained. For the specific displacement times, the error between the experimental value and the numerical value was calculated. These errors were then averaged and compared for the different methods, and are presented in Table 4.13. From the table one may see that the uniform mesh type has the lowest error. It also has the highest running time, the largest file size, and the highest number of mesh points. This might explain the low error. The deltaX/D method is having a ratio of 2 between the cell length and diameter, and still giving a high error. This construction is therefore not considered in use. Even though reducing the length of the mesh cells for the other methods might have made their errors closer to the uniform method, the differences are small and within a tolerance of 3 %. It was therefore decided to use the uniform mesh construction.

Table 4.13: Results from determining which mesh type to use

Mesh Type	Properties	Average error	Running time [s]	File size [MB]
Least squares	Min number cells between locked points: 1 Min cell length: 0.25 m Max expansion factor: 2	5.6 %	20	105
Uniform	Total number of cells: 40	5.4 %	32	120
DeltaX/D	Ratio, cell length and diameter: 2	5.6 %	27	93
Horizontal/ Vertical	Max vertical cell length: 0.25 m Max horizontal cell length: 0.25 m Vertical angle: 60°	5.6 %	17	108

A method frequently used for determining required number of mesh points in a numerical model, is to monitor the variation of a certain property for different numbers of mesh cells (Coputational Fluid Dynamics blog (CFD), 2013). For high enough number of mesh points, the value of the variable usually “stabilizes”, which means that it is converging towards a value. Then a mesh size is frequently chosen such as the value of the variable has a deviation less than X % from the converged value. In this study a value of 3 % was used.

For this case it was chosen to follow the overall water fraction of the total volume of the jumper. This property is reported as a function of number of mesh points in Figure 4.21. One may see from the plot that there are small variations in the water fractions when the number of mesh cells is changed. The trend of the three first points is behaving strangely, compared to the trend of the other values, and not like one would have expected. This is most likely due to the ratio of the cell lengths between locked points being too big, as was given as a warning from LedaFlow. The maximum reported value is approximately 62.3 % and the lowest 61.8 %. If the real value is close to 62.1 %, this means that the other values are deviating with 0.3 % and 0.5 % respectively. This is within the tolerance of 3 %, and therefore one may conclude that it is irrelevant how many points that are chosen for the model. The approximation with 50 mesh cells is therefore chosen.

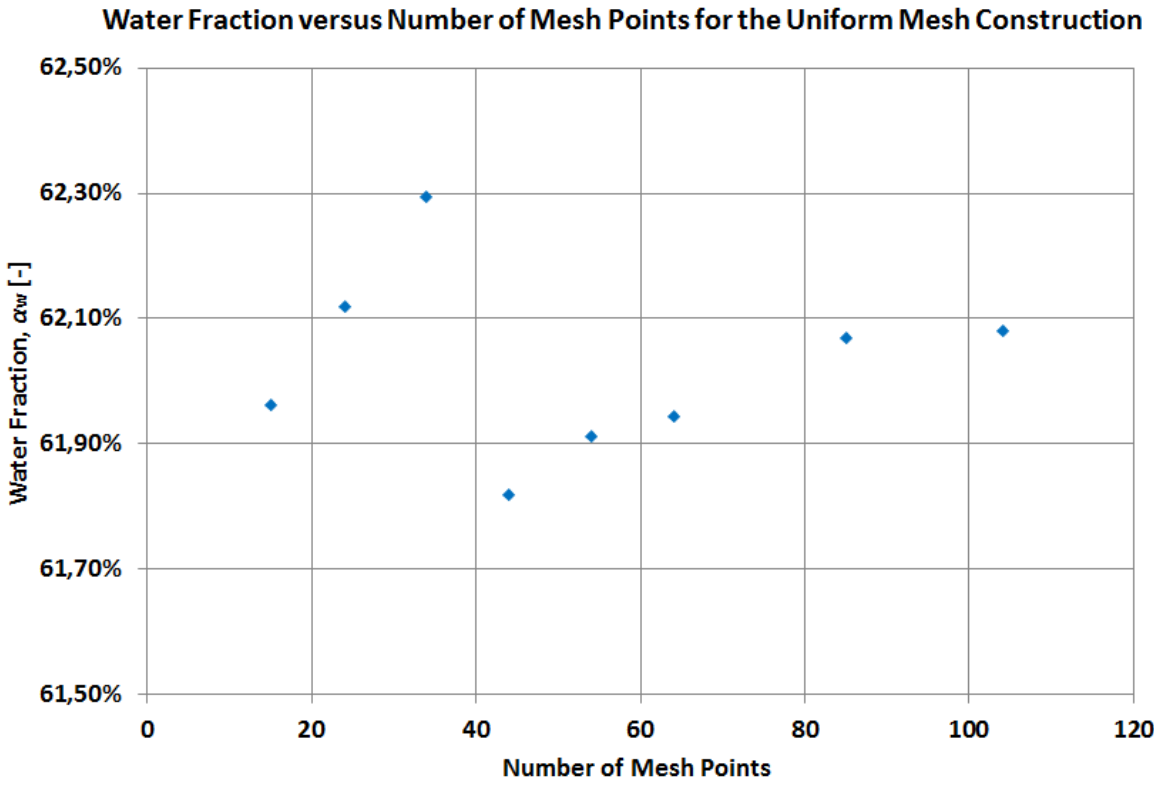

Figure 4.21: Water fraction as a function of the number of mesh points using the uniform mesh construction

Figure 4.22 contains a picture showing mesh points along the profile of the jumper. The locked points are marked with a black circle. The lengths of the mesh cells may be seen in Table H.1 in Appendix H.

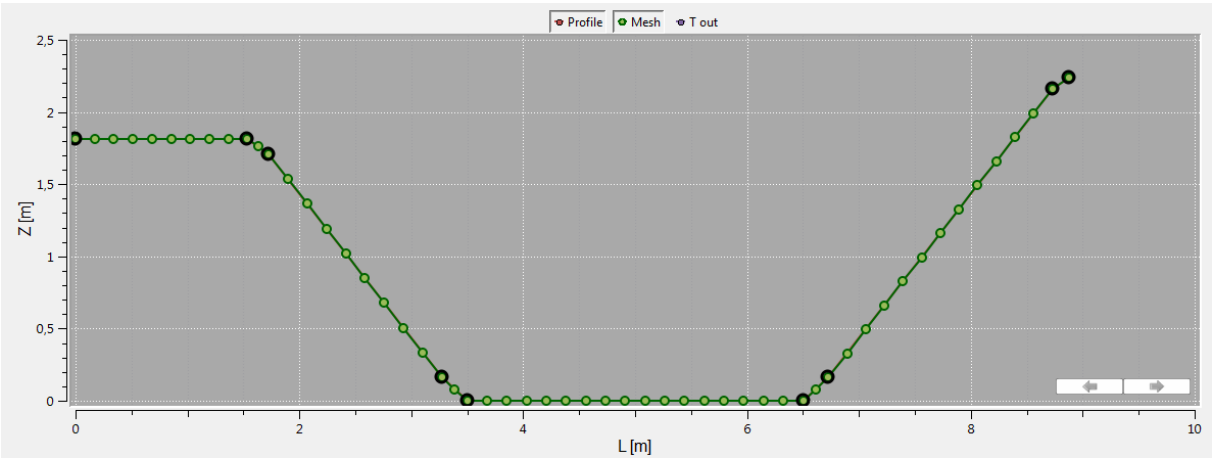

Figure 4.22: Uniform mesh construction with 54 cells

Based on the numerical settings presented in this subchapter, a model has been created to simulate the displacement process in the U-shaped jumper discussed. The results from the model and the experiments will be compared and discussed in section 5.3.

4.2.2 Reproducing the Results of Opstvedt (2016)

As mentioned in the section about previously work, this thesis is a continuation of the work done spring 2016 by Opstvedt. A model in LedaFlow has been created to simulate those results, and to compare the model from LedaFlow with the two models made in ANSYS CFX.

For this case as well, a 3-phases model is chosen in LedaFlow, where the gas phase is put equal to 0. Opstvedt (2016) also run experiments using tap water and Exxsol D60. The PVT-properties reported by Opstvedt (2016) in his thesis are presented in Table 4.14. They are given for a reference temperature of 25 °C and a reference pressure of 1 atm.

Table 4.14: PVT-Properties for simulating experiments from Opstvedt (2016)

Property	**Water (Tap Water)**	**Oil (Exxsol D60)**
Density [kg/m^3]	997 (Opstvedt, 2016) (25 °C)	792 (Opstvedt, 2016) (25 °C)
Viscosity [Pa-s]	0.0008899 (Opstvedt, 2016) (25 °C)	0.0012989 (Opstvedt, 2016) (25 °C)
Compressibility [kg/m^3/bar]	0.0391 (Default value from LedaFlow) (25 °C)	0.0391 (Default value from LedaFlow) (25 °C)
Conductivity [W/m-K]	0.6069 (Opstvedt, 2016) (25 °C)	0.136 (Opstvedt, 2016) (25 °C)
Heat capacity [J/kg-K]	4181.7 (Opstvedt, 2016) (25 °C)	1760 (Opstvedt, 2016) (25 °C)
Molar mass [g/mol]	18.02 (Opstvedt, 2016)	158 (Opstvedt, 2016)
Property	**Water – Exxsol D60**	
Interfacial Tension [N/m]	0.036 (Fossen, 2016)	

The numerical settings and the output settings are the same as for the model created in section 4.2.1, and are presented in Table 4.8. This includes the network as well, presented in Figure 4.19.

Initially, the pipe system was filled entirely with the fluid to be displaced. For boundary nodes, it was chosen constant rate upstream the system, and constant pressure downstream the system. The experiments were run for the flow rates, 6, 10, 20 and 30 m^3/h, for both oil displacing water, and water displacing oil. The converted mass flow rates used in LedaFlow are provided in Table 4.15.

Table 4.15: Flow rates for simulating results of Opstvedt (2016)

Volume Flow Rate Q **[m^3/h]**	**Water Mass Flow Rate** $\dot{m}_w$ **[kg/s]**	**Oil Mass Flow Rate** $\dot{m}_o$ **[kg/s]**
6	1.32	1.662
10	2.20	2.769
20	3.30	5.539
30	6.60	8.308

The profile of the network is given in Table 4.10. The total volume measured and used is not specified in the thesis of Opstvedt (2016). The first average volume measured by the author is decided used. The internal diameter of the pipe is 153.6 mm, and the PVC pipe has a thickness of 32 mm. The absolute roughness is 0.0015 mm (SulzerPumpesLtd). The rest of the properties for the PVC pipe are presented in Table 4.12.

In addition, the uniform mesh construction is used with a total cell number of 54. The mesh may be visualized in Figure 4.22.

The results from this model will be presented in subchapter 5.4, and be compared to the experimental and numerical data of Opstvedt (2016).

4.2.3 Simulations for Sensitivity Analyses

4.2.3.1 Effects of Changing PVT-Properties of Water and Oil

To see how changes in PVT-properties affect the displacement efficiency is important. Crude oils typically have a big variation in properties such as viscosity, interfacial tension and density. A model has been created to study these variables, using water and diesel oil.

The PVT-properties for the comparison case are listed in Table 4.16. Changes will be conducted to PVT-properties, in form of water density, water viscosity, oil viscosity and the interfacial tension between water and oil. All of the cases will be simulated with diesel oil displacing an initially water filled pipe system, with a flow rate of 6 m^3/h.

Table 4.16: PVT-properties for the "general" case

Property	Water	Oil (Diesel)
Density [kg/m^3]	998.3 (The Engineering Toolbox) (20 °C)	834 (Kolev and SpringerLink, 2007) (20 °C)
Viscosity [Pa-s]	0.001002 (The Engineering Toolbox) (20 °C)	0.002 (Environment Canada) (20 °C)
Compressibility [kg/m^3/bar]	0.0391 (Default value from LedaFlow) (25 °C)	0.0391 (Default value from LedaFlow) (25 °C)
Conductivity [W/m-K]	0.6069 (Opstvedt, 2016) (20 °C)	0.126 (Kolev and SpringerLink, 2007) (20 °C)
Heat capacity [J/kg-K]	4182 (The Engineering Toolbox) (20 °C)	2810 (Kolev and SpringerLink, 2007) (20 °C)
Molar mass [g/mol]	18.02 (Opstvedt, 2016)	170 (Kolev and SpringerLink, 2007)

The interfacial tension between the diesel oil and fresh water is $\sigma = 29.4\ \mathrm{mN/m}$ at 15 °C. (Environment Canada). The constituents of diesel are given in Table I.1 in Appendix I. In addition, there might be small amounts of other constituents like sulfur and ash (Kolev and SpringerLink, 2007). However, since the constituents are different for different geographical origination sources, one may obtain various properties in different locations.

The changed PVT-properties are presented in Table 4.17. It was decided to both increase and decrease the property with 10 % and 40 %. Oils in the reserves may be more viscous than diesel oil, and therefore it was added a case with high viscous oil. This is based on the viscosity of 0.1 Pa s for the NexBase oil (Kjølaas).

Table 4.17: Values of the changed PVT-properties

Water Density	**Density** ρ **[kg/m^3]**
+ 10 %	1098.13
+ 40 %	1397.62
- 10 %	898.47
- 40 %	598.98
Water Viscosity	**Viscosity** μ **[Pa-s]**
+ 10 %	0.0011022
+ 40 %	0.0014028
- 10 %	0.0009018
- 40 %	0.0006012
Oil Viscosity	**Viscosity** μ **[Pa-s]**
+ 10 %	0.0022
+ 40 %	0.0028
- 10 %	0.0018
- 40 %	0.0012
High viscous – NexBase	0.1000
Interfacial Tension – Oil-Water	**Interfacial Tension** σ **[N/m]**
+ 10 %	0.03234
+ 40 %	0.04116
- 10 %	0.02646
- 40 %	0.01764

The rest of the case settings, both the numerical settings and the output settings are presented in Table 4.18.

Table 4.18: Numerical settings and output settings

Simulation time 3600 s			
	Numerical settings		Output settings
Time [s]	Maximum time step [s]	CFL	Logger [s]
0	0.05	0.3	0.05
250	0.5	0.4	1
300	100	0.8	10

The network for this case consists of three elements; a horizontal inlet pipe, a U-jumper and a horizontal outlet pipe. An illustration of the network is given in Figure 4.23. It differs some from the models presented in the previous subchapters. This is due to the model being made before the experiments were conducted, and it is based on the model made in the specialization project by the author. The boundary nodes chosen are constant flow rate upstream, and constant pressure downstream the system.

Figure 4.23: Network for case studying changes in PVT-properties

The profile of the pipe system is presented in Table 4.19, and an illustration from LedaFlow in Figure 4.24. The pipes are connected in junction points, shown as links in the figure.

Table 4.19: Profile for case studying changes in PVT-properties

	X **[m]**	***Y*** **[m]**	***Z*** **[m]**	***L*** **[m]**
Horizontal Inlet	0	0	1.31	0
	1.536	0	1.31	1.536
U-Jumper	1.536	0	1.31	0
	1.536	0	0	1.31
	4.536	0	0	4.31
	4.536	0	1.8	6.11
Horizontal Outlet	4.536	0	1.8	0
	4.836	0	1.8	0.3

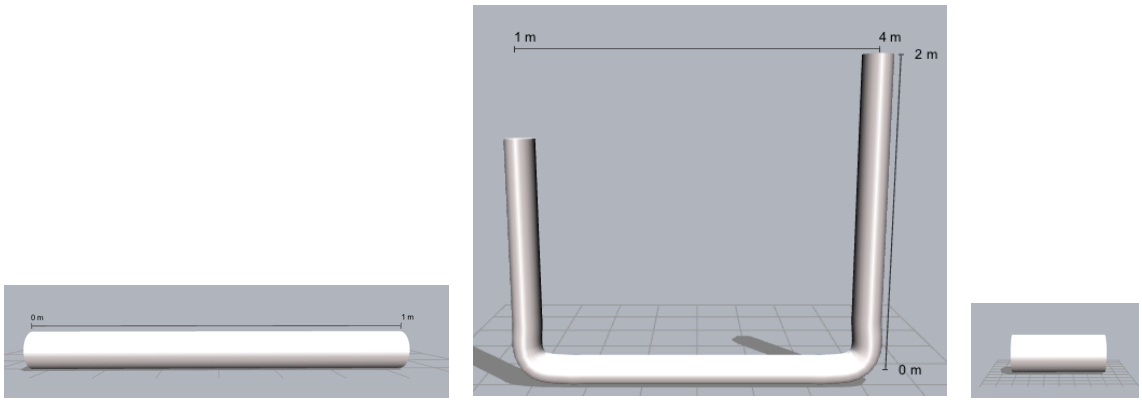

Figure 4.24: Profile of the system from LedaFlow

The internal diameter is 153.6 mm, and the PVC pipe has a thickness of 32 mm. The absolute roughness is 0.0015 mm (SulzerPumpesLtd). The other properties for the PVC pipes are presented in Table 4.12.

It is chosen uniform mesh construction for this model as well. The mesh constructions are shown in Figure 4.25. The horizontal inlet pipe has 9 cells, the jumper has 33 cells and the horizontal outlet pipe has 2 cells. The lengths of the cells may be found in Table H.2 in Appendix H.

Horizontal inlet pipe, 9 cells

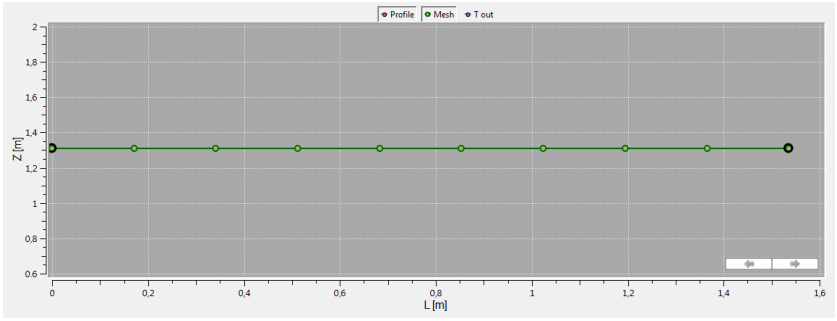

U-Jumper, 33 cells

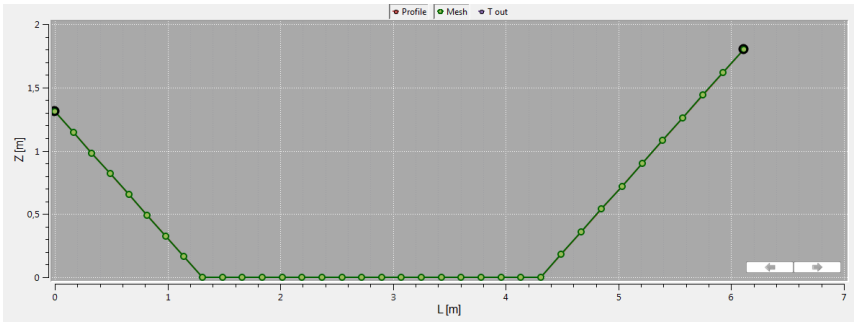

Horizontal outlet pipe, 2 cells

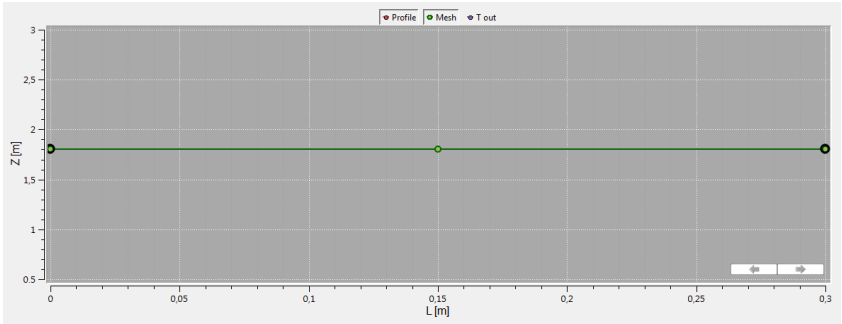

Figure 4.25: Uniform mesh construction of the three pipe elements

The results of the simulations will be presented in section 5.5.1.

4.2.3.2 Methanol Displacing Oil

A more common situation for offshore displacement is using methanol as the displacing fluid. A model has been constructed with the pipe system filled with diesel oil, and then the oil is removed by methanol. The PVT-properties for methanol and diesel oil, with a reference pressure of 1 bar and a reference temperature of 20 °C, are presented in Table 4.20. The surface tension at 20 °C is given as 22.6 mN/m (MethanolInstitute, 2017).

Table 4.20: PVT-Properties for simulating methanol displacing oil

Property	Methanol	Oil (Diesel)
Density [kg/m^3]	796 (Liu et al., 2011)	834 (Kolev and SpringerLink, 2007) (20 °C)
Viscosity [Pa-s]	0.0007 (Liu et al., 2011) (20 °C)	0.002 (Environment Canada) (20 °C)
Compressibility [kg/m^3/bar]	0.0391 (Default value from LedaFlow) (25 °C)	0.0391 (Default value from LedaFlow) (25 °C)
Conductivity [W/m-K]	0.200 (MethanolInstitute, 2017) (35 °C)	0.126 (Kolev and SpringerLink, 2007) (20 °C)
Heat capacity [J/kg-K]	2531 (MethanolInstitute, 2017) (25 °C)	2810 (Kolev and SpringerLink, 2007) (20 °C)
Molar mass [g/mol]	32.042 (PubChem_Compound_Database, 2017)	170 (Kolev and SpringerLink, 2007)

The rest of the case settings for the model are the same as for the model in 4.2.1, may be found in Table 4.8. This also applies to the network, seen in Figure 4.19. The flow rates are given in Table 4.21.

Table 4.21: Flow rates for methanol

Methanol	
Volume Flow Rate $\dot{Q}$ [m^3/h]	**Mass Flow Rate $\dot{m}$ [kg/s]**
2	0.4422
6	1.327
10	2.211
20	4.422
30	6.633
40	8.844

The profile and the geometry of the pipe are found in Table 4.10 and Table 4.11, and the mesh construction in Figure 4.22.

4.2.3.3 System with Gas Included

This simulation case is looking at how the U-formed system is affected by initially including gas in the system, making it consist of three-phases. The gas properties are based on methane. The other fluids are water and diesel oil. A reference pressure is p_{ref} = 170 bar and a reference temperature is T_{ref} = 70°C. The PVT-properties for the fluids are presented in Table 4.22.

Table 4.22: PVT-Properties for the simulations where gas is included

Property	Water	Oil (Diesel)	Gas (Methane)
Density [kg/m^3]	985.1 (Wischnewski, 2017b)	834 (Kolev and SpringerLink, 2007) (20 °C)	104.5 (Wischnewski, 2017a)
Viscosity [Pa-s]	$4.0818 \cdot 10^{-4}$ (Wischnewski, 2017b)	0.002 (Environment Canada) (20 °C)	$1.708685 \cdot 10^{-5}$ (Wischnewski, 2017a)
Compressibility [kg/m^3/bar]	0.0391 (Default value from LedaFlow) (25 °C)	0.0391 (Default value from LedaFlow) (25 °C)	0.8 (Default value from LedaFlow) (25 °C)
Conductivity [W/m-K]	0.6714307 (Wischnewski, 2017b)	0.126 (Kolev and SpringerLink, 2007) (20 °C)	0.035 (TheEngineeringToolbox_A, 2017) (25 °C, 1 atm)
Heat capacity [J/kg-K]	4152.8 (Wischnewski, 2017b)	2810 (Kolev and SpringerLink, 2007) (20 °C)	3078.87 (Wischnewski, 2017a)
Molar mass [g/mol]	18.02 (Opstvedt, 2016)	170 (Kolev and SpringerLink, 2007)	16.0

This model is based on the model in section 4.2.1. The numerical settings and the output settings are found in Table 4.8. The network is seen in Figure 4.19. Initially the system is filled with 40 % water, 30 % oil and 30 % gas. Then it is flowed with oil. The flow rates may be found in Table 4.23.

Table 4.23: Flow rates for diesel oil

Oil (Diesel)	
Volume Flow Rate Q **[m³/h]**	**Mass Flow Rate** $\dot{m}$ **[kg/s]**
2	0.4633
6	1.39
10	2.317
20	4.633
30	6.95
40	9.267

The profile is found in Table 4.10, the geometry in Table 4.11 and the mesh construction in Figure 4.22.

4.2.3.4 Including a Dead-Leg in the Simulation

Finally, it was run a simulation where a dead-leg, formed as an L, was included in the network of the jumper. The L is located in the Y-Z plane.

A case of 3 phases was chosen here as well, with the purpose of only studying liquid-liquid flow. It will be used diesel oil and water. The same PVT-properties are used as for the case in section 4.2.3.1, listed in Table 4.16. The numerical and output settings are as presented in Table 4.8.

The network consists of 3 pipes and is illustrated in Figure 4.26. Part one is the first half of the jumper, including the horizontal inlet. Then the pipes are meeting in a junction point. The flow can go either into a dead-leg which has a closed valve at the end, or to the other part of the U-jumper that includes the horizontal outlet. The boundary nodes are constant rate upwards, and constant pressure downwards.

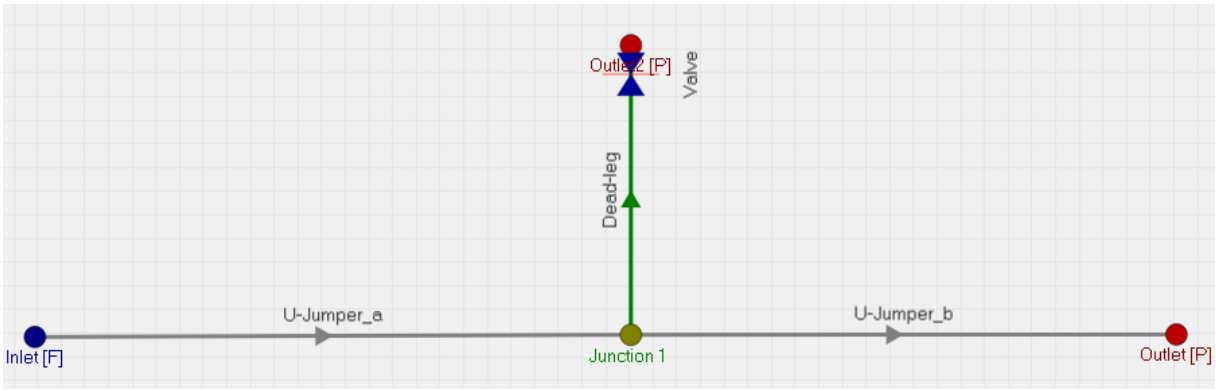

Figure 4.26: Network for simulation including a dead-leg

Two situations will be studied, one where the system is initially filled with water and flowed with oil, and one where it is filled with oil and flowed with water. Both cases will be run for 3 flow rates, listen in Table 4.24. The valve at the outlet of the dead-leg will stay closed during the simulations.

Table 4.24: Flow rates for water and diesel oil

Volume Flow Rate Q **[m^3/h]**	**Water Mass Flow Rate** $\dot{m}_w$ **[kg/s]**	**Oil (Diesel) Mass Flow Rate** $\dot{m}_o$ **[kg/s]**
6	1.664	1.39
20	5.546	4.633
40	11.09	9.267

Table 4.25 contains the profile of the system with the dead-leg included.

Table 4.25: Profile for the system including a dead-leg

	X **[m]**	Y **[m]**	Z **[m]**	L **[m]**
U-Jumper_a	0	0	1.31	0
	1.536	0	1.31	1.536
	1.536	0	0	2.846
	2.936	0	0	4.246

	X [m]	*Y* [m]	*Z* [m]	*L* [m]
Dead-Leg	2.936	0	0	0
	2.936	0.5	0	1.31
	2.936	0.5	0.5	4.31
U-Jumper_b	2.936	0	0	0
	4.536	0	0	1.600
	4.536	0	1.8	3.400
	4.536	0	1.8	4.700

Based on the profile presented in Table 4.25, the system is illustrated in Figure 4.27.

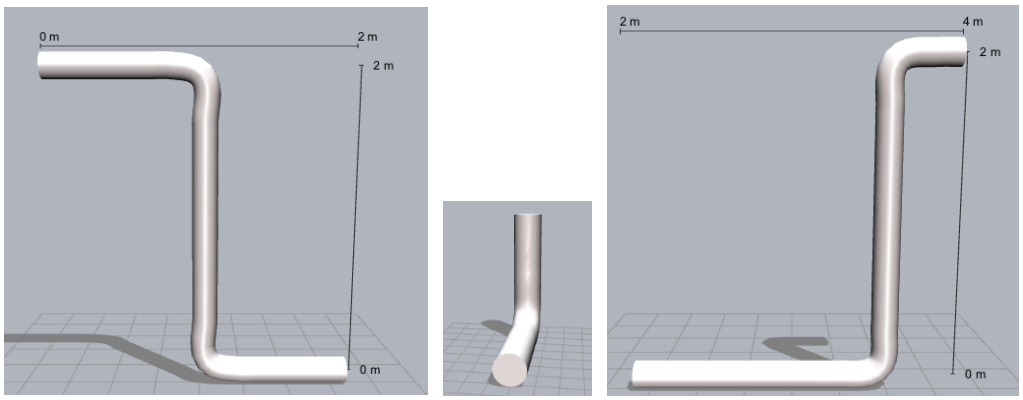

Figure 4.27: Jumper including a dead-leg (From left: U-jumper_a, dead-leg, U-jumper_b)

The internal diameter is still kept as 153.6 mm, with a thickness of the PVC pipe of 32 mm. The absolute roughness is 0.0015 mm (SulzerPumpesLtd), and the rest of the properties for the PVC pipes are given in Table 4.12.

Uniform mesh construction is chosen, and presented in Figure 4.28. The lengths of the cells may be found in Table H.3 in Appendix H.

U-jumper_a, 25 cells

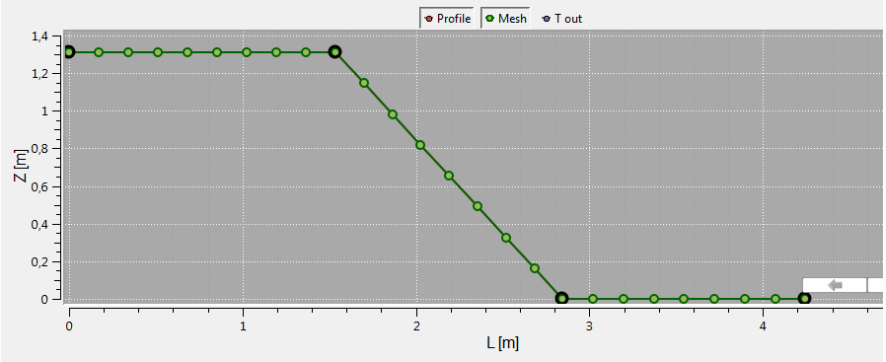

Dead-leg, 6 cells

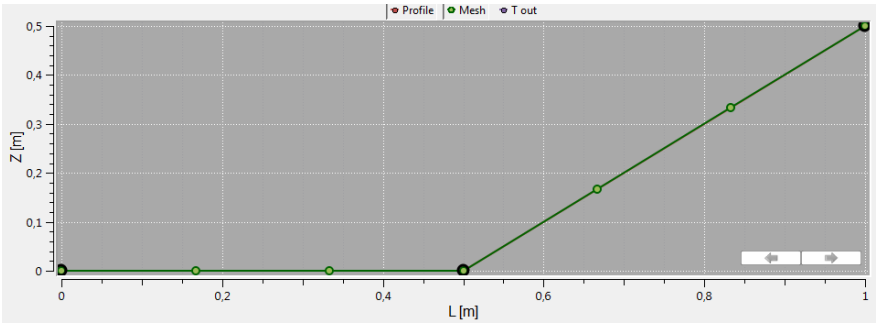

U-jumper_b, 21 cells

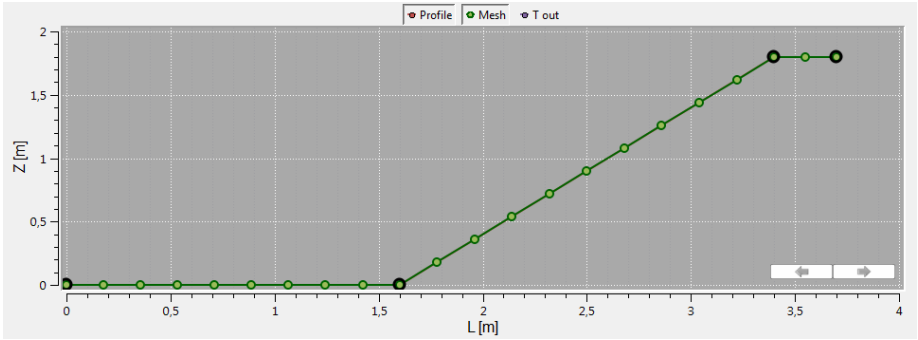

Figure 4.28: Uniform mesh construction for system including a dead-leg

The results from the simulations are presented in section 5.5.4.

5 Results

5.1 Experiments of Liquid-Liquid Displacement in U-Jumper

Experiments have been conducted in the U-shaped jumper, with the setup as described in section 4.1. Tests have been run for both oil displacing water, and water displacing oil.

The temperatures were measured during the experiments. An average gave a temperature of 18.3 °C ± 0.2 °C, within a confidence interval of 95 %.

5.1.1 Oil Displacing Water

The results from the experiments where oil is displacing water are displayed in Table 5.1. The table is presenting oil volume fractions, for different displacement times, for different flow rates. The volume fractions were calculated using Equation 3.1, looking at the volume of the displacement fluid relative to the total volume, in the domain. The table also gives how many displaced jumper volumes the times correspond to, based on an average of the measured total volume of 165.0 L.

Table 5.1: Results from experiments where water is displaced by oil

Pump Frequency f **[Hz]**	**Flow Rate** Q **[m³/h]**	**Time** t **[s] ± 2 s**	**Volumes Displaced** V_{disp} **[-]**	**Oil Volume Fraction** α_o **[-]**
10.50	4.59 ± 0.42	35	0.3	24.3 % ± 0.3 %
		70	0.5	47.8 % ± 0.4 %
		105	0.8	60.7 % ± 0.4 %
		209	1.6	66.8 % ± 0.4 %
		314	2.4	68.3 % ± 0.4 %
13.50	8.93 ± 0.44	23	0.3	29.3 % ± 0.3 %
		45	0.7	56.7 % ± 0.4 %
		63	0.9	69.7 % ± 0.4 %
		125	1.9	76.5 % ± 0.3 %
		188	2.8	77.0 % ± 0.3 %

Pump Frequency f [Hz]	Flow Rate Q [m^3/h]	Time t [s] ± 2 s	Volumes Displaced V_{disp} [-]	Oil Volume Fraction α_o [-]
24.50	19.73 ± 0.70	11	0.4	39.8 % ± 0.4 %
		20	0.7	67.9 % ± 0.3 %
		31	1.0	83.4 % ± 0.3 %
		63	2.1	92.1 % ± 0.1 %
		94	3.1	93.0 % ± 0.1 %
34.00	28.16 ± 1.03	9	0.4	39.2 % ± 0.4 %
		14	0.7	67.1 % ± 0.4 %
		21	1.0	89.9 % ± 0.2 %
		42	2.0	98.0 % ± 0.1 %
		64	3.0	99.1 % ± 0.1 %
44.40	37.74 ± 1.2	6	0.4	43.2 % ± 0.4 %
		13	0.8	72.5 % ± 0.3 %
		16	1.0	93.8 % ± 0.1 %
		31	2.0	99.6 % ± 0.1 %
		48	3.1	99.5 % ± 0.1 %

In addition, the results are plotted in Figure 5.1. The figure is showing the oil volume fractions as a function of time, for the different rates. The experimental values are illustrated with diamonds. The plus symbols close to the diamonds are representing the ± uncertainties. They are based on the time being measured manually and the uncertainties in the volume readings. All data related to one rate are plotted in the same colour. Observing the plot, one can see that the volume fractions for the different flow rates are following the same trend. In the beginning, the volume fraction is increasing fast and close to linearly. This is most likely due to a piston-like displacement until the front is reaching the end of the domain. After approximately one volume has been displaced, point 3, the volume fraction is starting to stabilize, and a curved behaviour is seen. This is most likely due to penetration of one phase into the other. The differences between the two last points, approximately 2 and 3 volumes displaced, are quite small. It seems like there is little effect of displacing for further additional volumes.

Figure 5.1 shows that the displacement efficiency for oil is increasing when the flow rate is increased. The displacement efficiency is defined as the volume fraction of the displacing fluid at a given time. It seems like the higher flow rates with their increased pressures in the system, are forcing a better displacement.

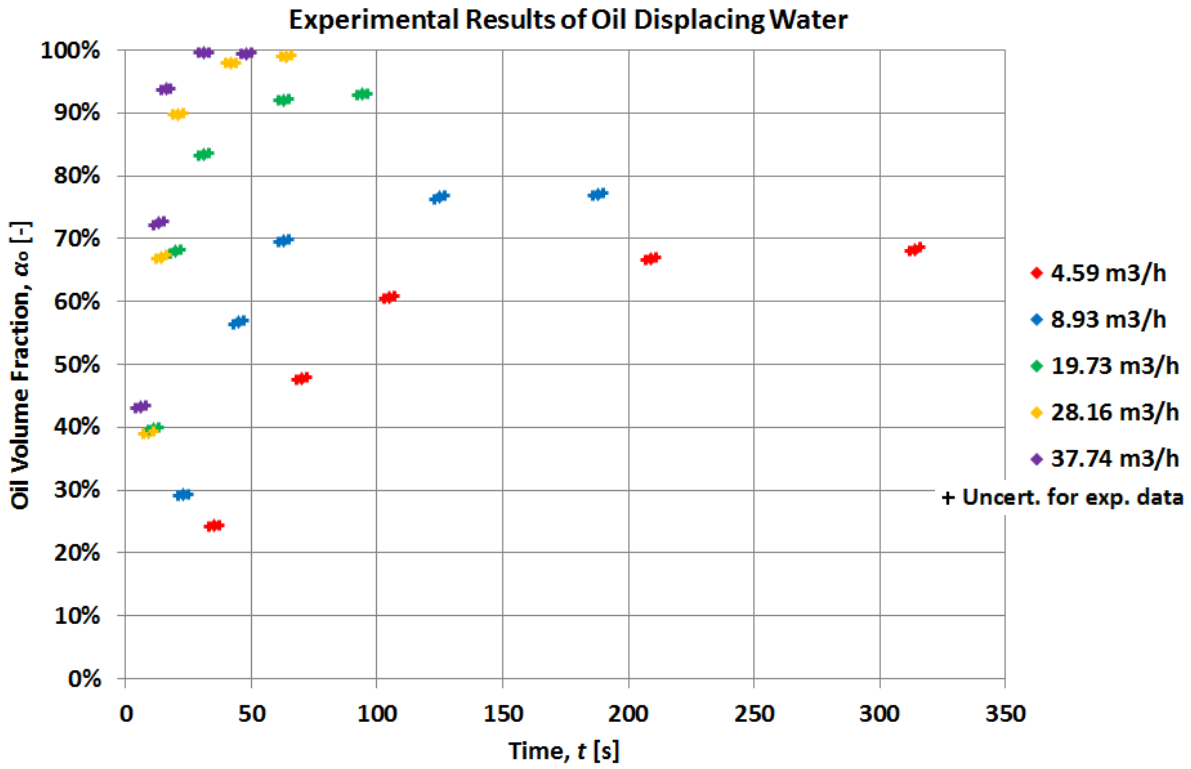

Figure 5.1: Experimental results of oil displacing water

The water amount in the pipe required for hydrates to form is unknown. Calculations would have had to be made, and this is not studied further in this thesis. It is assumed that a volume fraction of the displacing fluid of 95 % is sufficient for the process to be considered successful. From the experimental results of oil displacing water, it is observed that to reach the criterion, the flow rate 28.16 m3/h ± 1.03 m3/h is required. The rate results in an oil volume fraction of 98.0 % ± 0.1 %, after 2.0 volumes displaced.

Figure 5.12 in section 5.3.3 and Figure F.1 to Figure F.4 in Appendix F are containing pictures of the system at different times during the displacement experiments. Videos of the tests are attached digitally. Pictures are included for all the times at which the volume fractions were measured. It was observed during the experiments that the oil was easily displacing the water in the horizontal inlet pipe and the first riser. When the front reached the

lower horizontal section, the removal depended on the flow rate. For the lowest flow rate 4.59 m^3/h, it was observed that the front was only moving in the upper part of the pipe. The oil displaced the water in this area, and continued with displacing the second riser. The remaining amount of water in the horizontal section seemed to be stabilized after approximately one volume was displaced. An almost clear interface between the oil and the water was observed. For the middle rate 19.73 m3/h, the front moved a larger part of the water at the bottom, still moving in the upper part of the pipe. A wavy interface between the liquids was seen. For the highest tested rate 37.74 m3/h, the front moved the whole cross section of water in the bottom pipe. No interface was seen clearly here, as the water visible for the eye was displaced by the oil.

5.1.2 Water Displacing Oil

The results of the experiments where water is displacing oil are given in Table 5.2, and plotted in Figure 5.2. Both are presenting the water volume fractions as functions of time for different flowrates. In the plot are the uncertainties included as plus signs close to the diamonds for the experimental results. How many jumper volumes that have been displaced for a given time, based on the average total volume 165.0 L, are included.

Table 5.2: Results from experiments where oil is displaced by water

Pump Frequency f **[Hz]**	**Flow Rate** Q **[m^3/h]**	**Time** t **[s] ± 2 s**	**Volumes Displaced** V_{disp} **[-]**	**Oil Volume Fraction** α_o **[-]**
10.50	6.19 ± 0.23	37	0.4	37.4 % ± 0.4 %
		72	0.8	74.4 % ± 0.3 %
		106	1.1	86.4 % ± 0.2 %
		209	2.2	86.2 % ± 0.2 %
		314	3.3	87.3 % ± 0.2 %
24.50	20.77 ± 0.67	11	0.4	42.3 % ± 0.4 %
		21	0.7	68.0 % ± 0.3 %
		32	1.1	91.8 % ± 0.2 %
		63	2.2	98.3 % ± 0.1 %
		95	3.3	98.6 % ± 0.1 %

The same trend for the displacement efficiency is observed for water displacing oil in Figure 5.2, as for oil displacing water. In the beginning, the water volume fraction is increasing rapidly and linearly. After 1.1 volumes have been displaced is the increase in water fraction slowing down, and the system starts to stabilize as 2.2 and 3.3 volumes are displaced. In addition, higher flow rates give higher volume fractions of the displacing fluid. This is consistent with the findings of Opstvedt (2016).

The same pump frequencies were used for both the water pump and the oil pump. The analysis of the flow rates shows that the rates obtained for water displacing oil, are higher than for oil displacing water in the jumper. The analysis of the flow rates is further discussed in section 5.1.3.

It should be noticed, that it seems like the displacement ability for a water flow rate to displace the oil in the system, is higher than for an oil rate displacing water in the system. This might be due to differences in flow rate, density or viscosities.

For the rate 6.190 m^3/h, one may observe that the displacement efficiency after 2.2 volumes is 0.25 % lower than after 1.1 volumes. However, the difference is small, and is most likely due to inaccuracies in the volume readings.

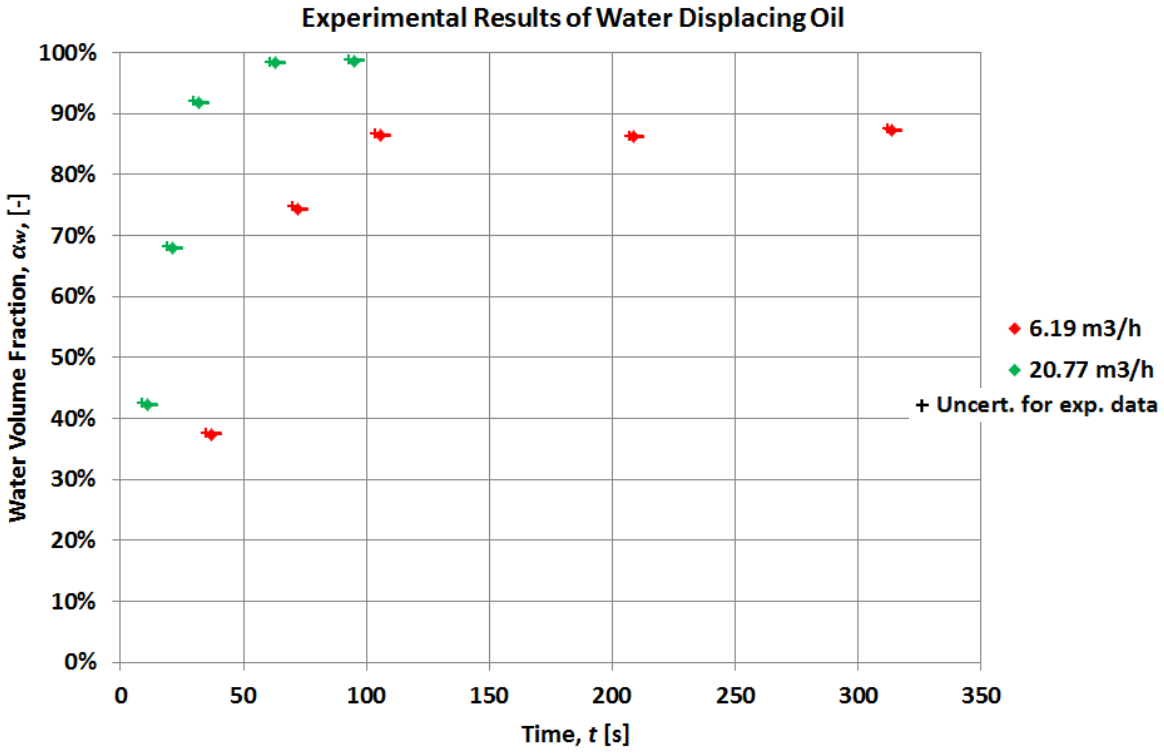

Figure 5.2: Experimental results of water displacing oil

From the experimental results of water displacing oil, it is observed that for the displacing fluid to reach a volume fraction of 95 %, the flow rate 20.77 m3/h ± 0.67 m3/h is required. The rate results in a volume fraction of 98.6 % ± 0.1 %, after 2.2 volumes displaced.

During the experiments, it was observed that the water entering was moving down in the system, leading to an accumulation of oil at the top. When the front reached the bottom section, it was moving in the lower part of the pipe, dragging the oil with the water. With time, all of the oil in the lower horizontal pipe was displaced. This is observed in the pictures in Figure F.5 and Figure F.6 in Appendix F, and can be seen in the videos in the digital appendix. The displacement of oil carries on well in the second riser. The water struggles with removing the oil from the first horizontal pipe and the first riser. Only small oil droplets are removed. With time, the water is able to remove more and more of the oil in those sections, but not all even within the testing period of the highest flow rate tested.

5.1.3 Analysis of the Flow Rate

Figure 5.3 shows the flow rates with time during the experiments for oil displacing water, and Figure 5.4 for water displacing oil. Each plot contains one flow rate. The set of "points" in the plot, match the different measurements executed for finding the volume fraction in the system. The data in "Point 1" correspond to the first measured volume fraction points in Figure 5.1 and Figure 5.2. Constant pump frequencies were used

.

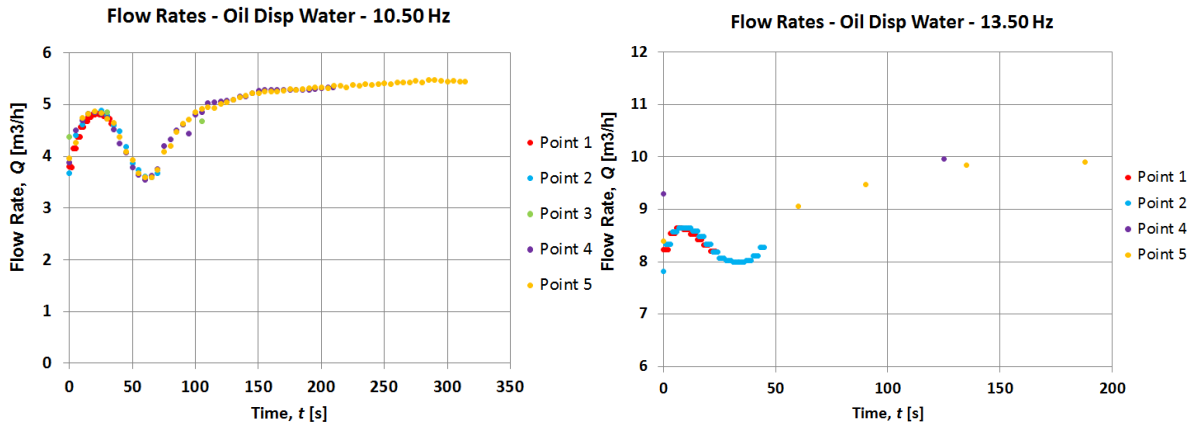

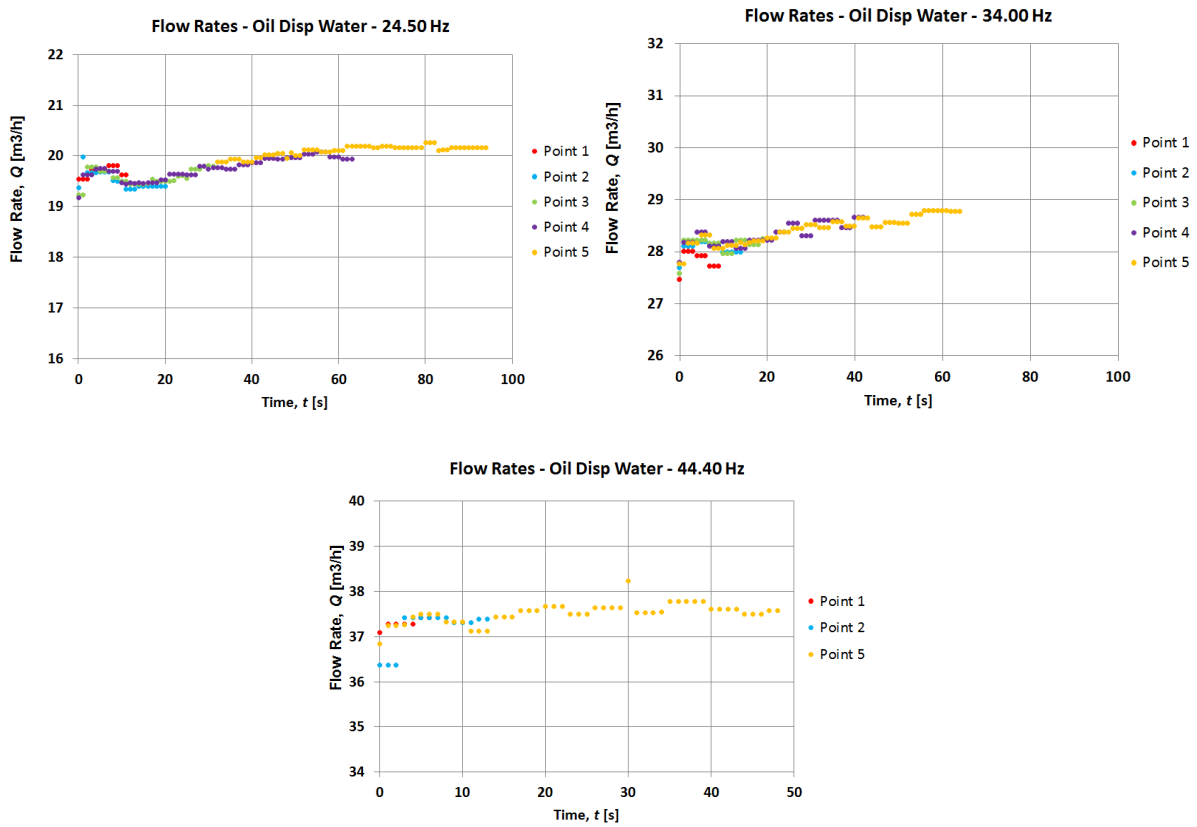

Figure 5.3: Measured flow rates for oil displacing water at different pump frequencies

Looking at the plots in Figure 5.3 one can see that the rates are varying. The alternations are largest in the beginning, and then seem to stabilize as time goes. The variation in flow rate is highest for the lowest rates. The rates are first increasing to a top, and then decreasing to a bottom, before it increases and reaches a stable value.

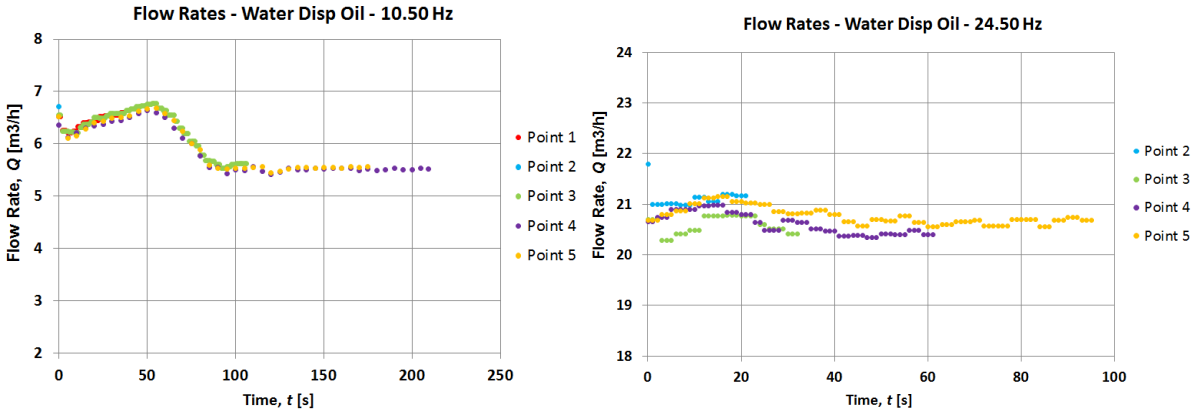

Figure 5.4: Measured flow rates for water displacing oil at different pump frequencies

The plots in Figure 5.4 are also showing alternations in the flow rate, particularly in the beginning. However, the rates are slowly increasing some, before they are reduced to a value where it seems to be stabilizing.

The plots show that the flow rates during the experiments are not constant. Based on these data, average rates were calculated. The variations arise due to different fluids having various properties, resulting in different hydrostatic pressures and friction losses in the system.

5.2 Volume Fraction Meters

This subchapter presents the findings of the tests of the volume fraction meters, constructed by Åge Sivertsen as explained in section 3.2.2. The meters were connected to the pipe and the computer. When the pipe was filled with liquid, it showed errors in the readings. Sivertsen was unavailable several weeks during the semester, and this made it difficult to progress further with the troubleshooting. Due to time limitations at this stage, it was decided to run experiments measuring the volume fraction manually.

The signals from the meters were read by LabVIEW and then converted to impedance values. The meters were calibrated as described in section 4.1.4.3.1. This resulted in Equation 4.3 and Equation 4.4, for determining the volume fractions in the pipe. Based on the calibration, the equations seemed reliable for a water fraction interval between 70 % and 100 %.

Towards the end of running experiments, it was detected that wrong cables were used for connecting the meters and the DAQ device. The current signal and the voltage signal were not isolated properly. The cables were replaced, and the meters were tested during the last four experiments, where water was displacing oil at the flow rates 6.19 m^3/h and 20.77 m^3/h.

Figure 5.5 is showing the results of the first test conducted with the volume fraction meters from Sivertsen, for water flowing at 6.19 m^3/h. The water was flooding for 106 seconds, and then stopped. The manually measured water fraction was 86.40 %. Unfortunately, there is an uncertainty of one minute for when the water was reaching the first pair of electrodes, due to the time stamp of the camera. An interval for when the water has had to reach electrode pair 1, is shown by two black stippled lines in the figure. The time for when the water reached electrode pair 2 is also unknown. However, due to the known velocity of the flow, it it being more than a few seconds later is unlikely.

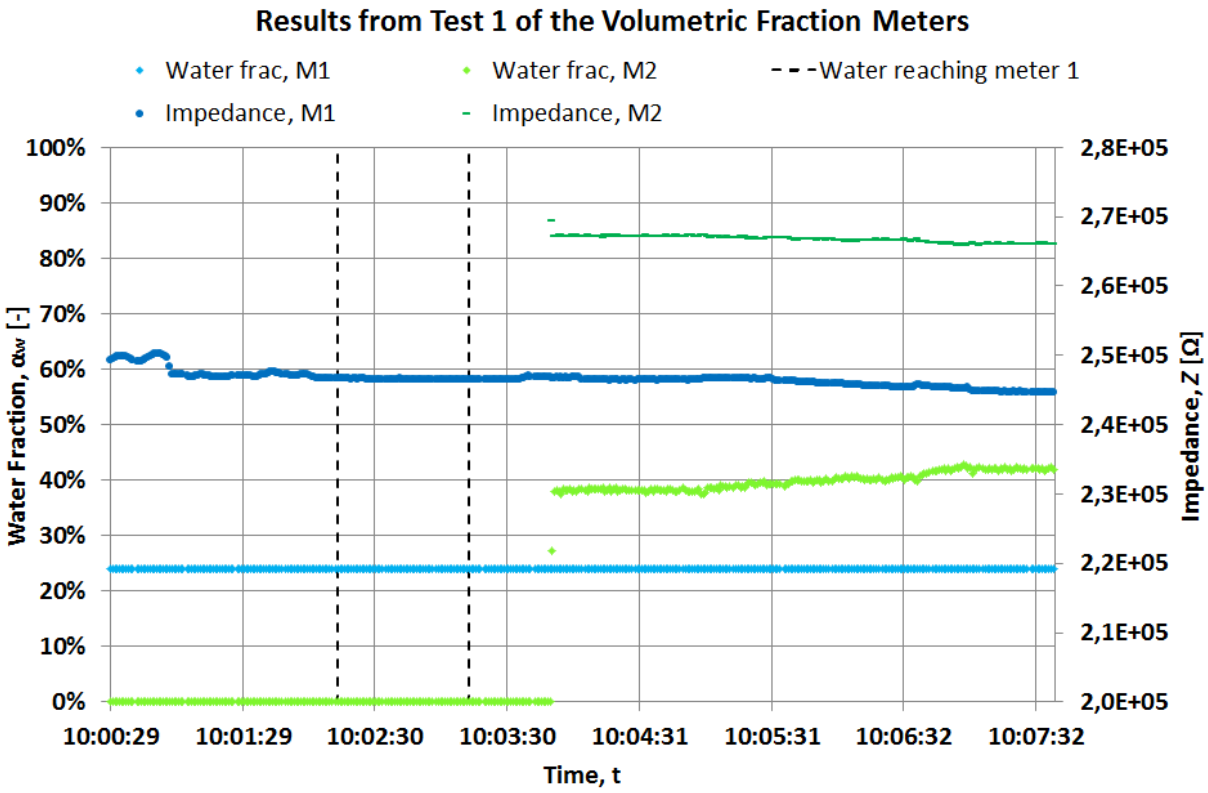

Figure 5.5: Results from the volume fraction meters - test 1, 6 m3/h (106 s)

The first volume fraction meter is showing a constant water fraction of 24 % both before and after the water reaches the electrode pair, seen in Figure 5.5. Firstly, there is not detected any significant changes in the impedance as a result of water entering the system. Secondly, the displayed water fraction is far from the value manually found and is not within the interval the meter was calibrated for, of a water fraction between 70 % and 100 %. The second meter is showing an impedance value higher than the calibrated interval for a long time, resulting in 0% water fraction. Then, after the system is filled with water, it might be responding to this. The impedance value is lowered and it is showing a water fraction of approximately 40-43 %. Again, the fraction is too low when comparing to the experimental value. It is difficult to say whether this happens exactly when the water is reaching the area between the electrodes or not, but based on the time line it seems to be happening afterwards.

The plots from the other tests are presented in Figure B.1, Figure B.2 and Figure B.3 in Appendix B. The results of these tests are similar to the ones presented in Figure 5.5, and are not in agreement with the calibrated values.

A reason for this might be that since the resistance of the load measured was very high, a higher resistance for the current signal was required. Some changes were conducted by Sivertsen before the meters were taken into use. However, the resistance of the load became big, higher than 500 kΩ, and then the properties of the meters were no longer sufficient. The operation range was unfortunately not known before testing, which would have made it easier to optimize the meters in advance.

Another way of obtaining volume fractions is by direct contact with the fluids in the pipe, applying the conductance principle as described in 3.2.1. Sivertsen has in addition built a meter, meter 3, with the possibility of measuring by using physical contact with the fluid. A picture of the meter is presented in Figure 5.6. However, as this requires making holes in the pipe, it was decided to use the meter with the capacitance principle, as this is possible as well. A qualitative test was executed to see if any significant observations were made, when the pipe was either water filled or oil filled.

Figure 5.6: Meter 3 for measuring volume fraction

Of course, it should have been conducted a calibration of this meter as well, before testing. However, these tests found place towards the end of the project, and calibration was considered too time-consuming. The tests were therefore executed qualitatively, mostly to see if the meter has a potential of being used for future experiments. For the tests, it was chosen a constant pump frequency of 34.00 Hz for both pumps.

The meter in Figure 5.6 was placed next to the DAQ device and the computer. Coax cables were used for reaching the electrode pairs fastened on the pipe. The first pair was connected to port B, and the second to port C. Only voltage signals were sent from the meter to LabVIEW, where it was converted to impedance.

A formula for impedance *Z* using meter 3 is given in Equation 5.1. The voltage *U* is received from the meter. The constant *c* is depending on the resistance chosen by the user.

Equation 5.1: Impedance from meter 3

$$Z_{meter\ 3} = \frac{c}{U}$$

For the tests conducted, it was chosen an area of resistance from 2000 Ω to 100 000 Ω, resulting in the constant *c* = 20 000. The tests were performed by first filling the system with water. Then oil is entering the system, and the time for when the oil is reaching the electrode pair, is marked with a stippled red line in the diagrams. Next, water is sent into the system, and the time for when water is reaching the electrode pair, is marked with a stippled blue line. The process is repeated until oil has filled the system three times, and then water is entering one last time. In total, 2 tests were executed. During the first test, only the signal from the first pairs of electrodes was read by the computer. In the second test, signals from both pairs of the electrodes were working. The results are presented in Figure 5.7 for electrode pair number 1 for the first test, Figure 5.8 for pair 1 for the second test, and Figure 5.9 for pair 2 from the second test. The plots are displaying impedance versus time.

When oil is entering the system with the given frequency, this corresponds to the rate 28.16 m^3/h according to the results in section 5.1.1. After displacing for approximately one minute, the oil volume fraction of the whole jumper is 99.1 %. The water accumulates in the lower horizontal pipe, leading to a higher water fraction between the electrodes. The volume of the lower horizontal pipe is 55.6 L, and after 64 seconds it was measured 1.5 L at the bottom of the system, resulting in a water fraction of 2.8 %. This gives an indication of how much oil that is between the electrode pairs after some displacement time. When water was entering the system, it was quickly able to displace all of the oil in this area.

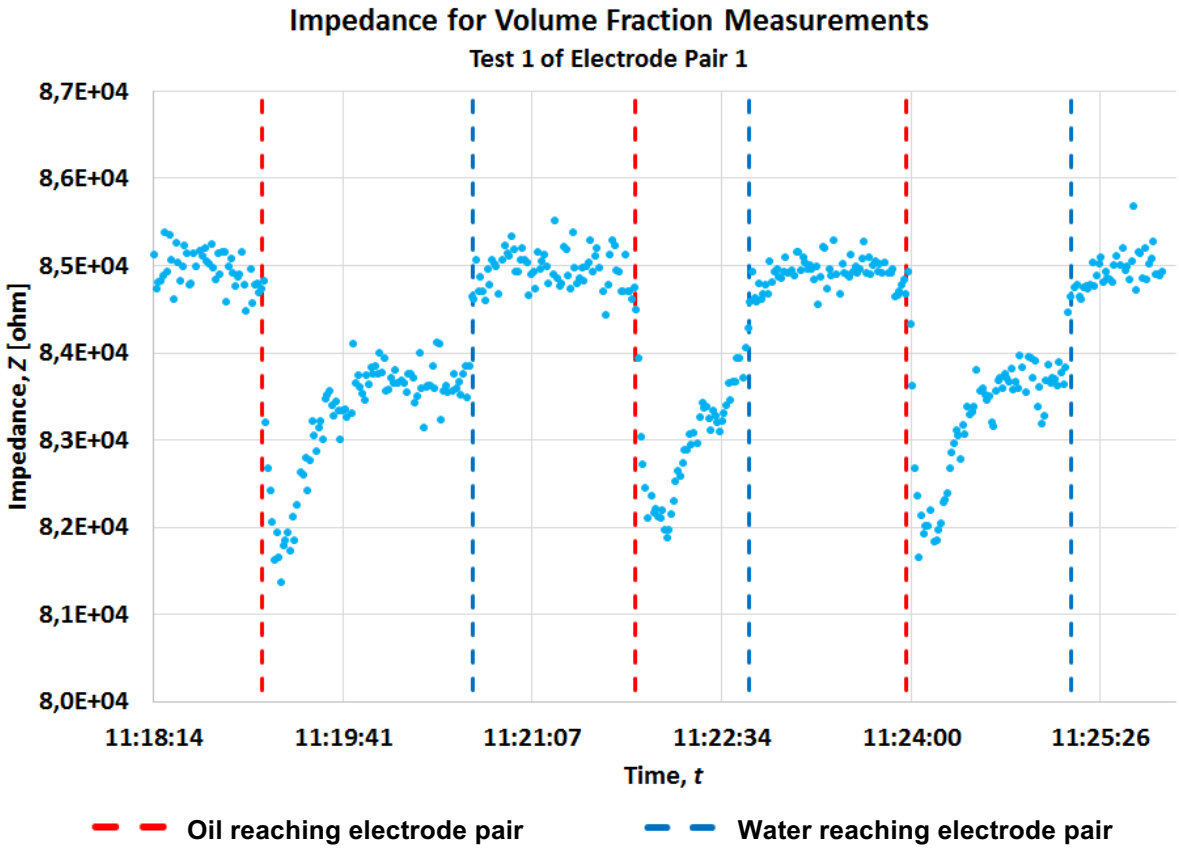

Figure 5.7: Results from test 1 for electrode pair 1 (beginning of lower horizontal section)

The plot in Figure 5.7 is showing changes in the impedance measurements as oil and water in turns are reaching the electrode pairs. One may see that for the water measurements, the impedance is close to constant, with an average of 84957 Ω ± 23 Ω. For the oil measurements, the average is 83205 Ω ± 95 Ω. In addition, the standard deviation is studied as this gives a better indication of the variation in the dataset. For the water measurements it is 194 Ω, which is quite low compared to 705 Ω for the oil measurements. This agrees with the trend in the plot, where one may observe that the variations in the impedance are higher for the measurements where oil is filled in the pipe. It is observed that immediately when oil is filling the area between the electrodes, the impedance is decreased rapidly. Then, very soon it is starting to increase again. It does so for some time before it seems like it might be stabilizing. It would have been interesting to see how it progresses for a longer time period. The difference in the average impedance values for approximately 100 % water and 97 % oil is 1752 Ω.

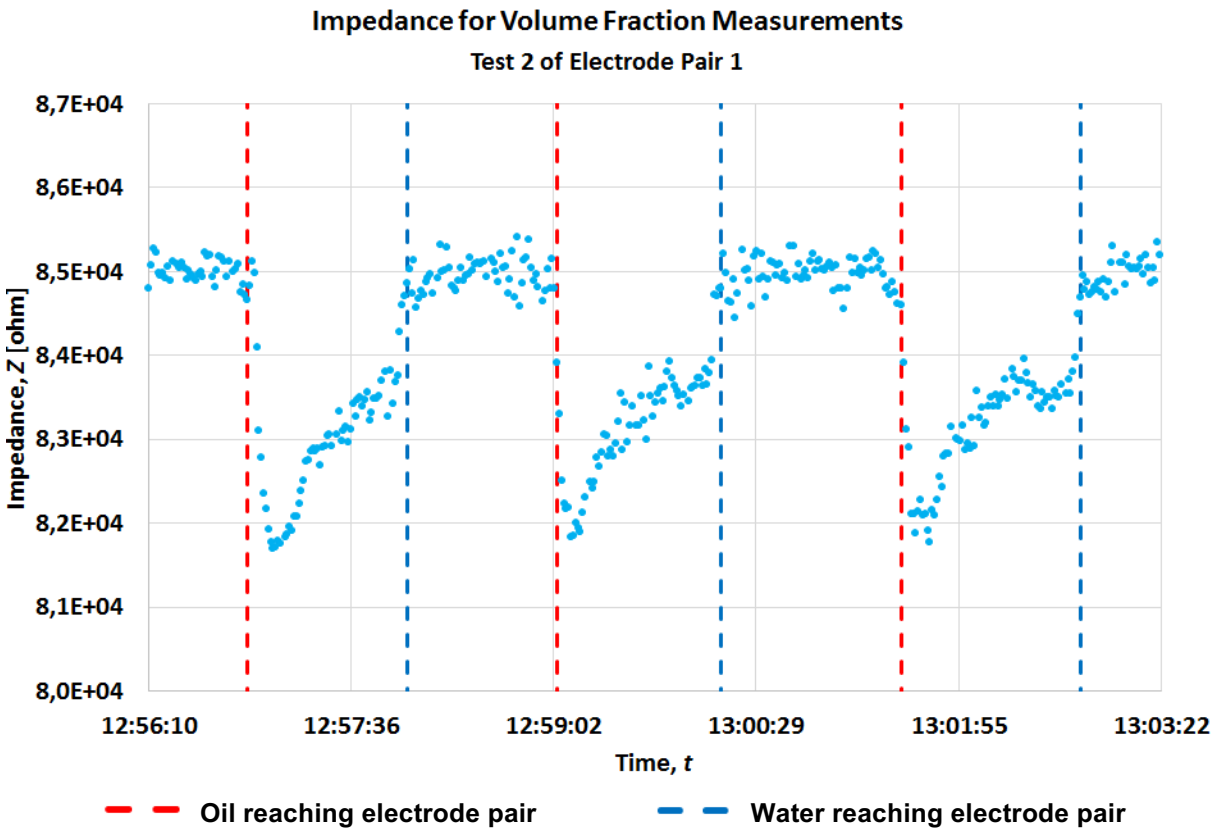

Figure 5.8: Results from test 2 for electrode pair 1 (beginning of lower horizontal section)

The trend of the measurements for pair 1 from test 2, is the same as for test 1. This is found by comparing the plot in Figure 5.8 with the plot in Figure 5.7. For water the average is 84891 Ω ± 34 Ω, with a standard deviation of 319 Ω. For oil it is 83168 Ω ± 100 Ω, with a standard deviation of 733 Ω. The difference between the water average and the oil average is 1723 Ω, very close to 1752 Ω. The difference is 66 Ω between the averaged water values from the two tests, and 37 Ω for the oil values.

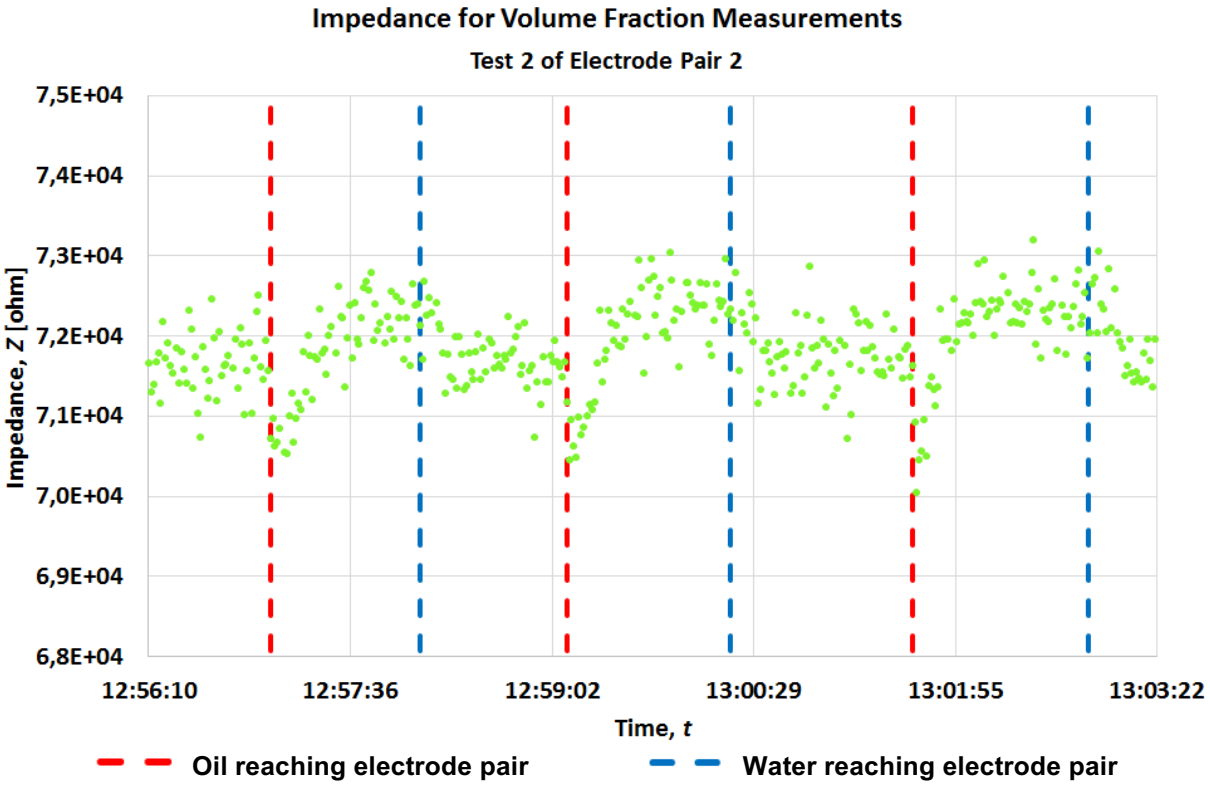

Figure 5.9: Results from test 2 for electrode pair 2 (end of lower horizontal section)

Figure 5.9 contains the results from electrode pair 2, placed towards the end of the horizontal bottom section. The impedance result for water is 71739 Ω ± 38 Ω, with a standard deviation of 362. The result for oil is 71986 Ω ± 87 Ω, with a standard deviation of 627 Ω.

One may observe that the average values measured for oil and water for this electrode pair are very close. The difference is only 0.3 %, and makes it difficult to distinguish between whether the pipe is oil filled or water filled. It is observed a trend in the plot that when oil is reaching the electrode pair, the impedance is slowly increasing, and when water is reaching the electrode pair, it is slowly decreasing again.

A reason why these results are much closer than for the other pair, might be the different sizes of the electrodes fastened to the pipe. In addition, the second electrode set is placed further away from the measuring device, and does therefore require a longer cable. This might increase the noise of the signal. It was realized after conducting the tests, that the meter should have been placed nearer the electrode pairs to minimize the electrical noise and make the readings more accurate.

A problem using only two pairs of electrodes for measuring volume fractions is that the pipeline is U-shaped with vertical pipes, a horizontal inlet and a horizontal outlet at the top. Since oil is less dense than water, it will flow to the top areas of the system. The volume flow meters placed in the lower horizontal section will therefore not capture these areas. If the system has a high oil volume fraction, a clear interface will be seen in the lower pipe, and one could to assume that the rest is filled with oil. However, if the oil fraction is low, one may measure only water in the pipe, while there is oil lying in other parts of the system. In addition, it is observed a small slope in the lower horizontal section. This results in more of the water gathering where electrode pair 1 is placed, and less where electrode pair 2 is.

Using the meter for measuring volume fractions, is of great interest as it would reduce the amount of time necessary for running an experiment. The two last tests showed that the first pair of electrodes is giving results that have potential to indicate the volume fraction in the pipeline. It is therefore recommended to continue working with the meter, run calibration of the equipment, and test it again. It would be recommended trying to use the conductivity principle, by making holes in the pipe to let the electrodes gain physical contact with the fluids.

5.3 Simulations of the Performed Displacement Experiments

A model was created in LedaFlow to simulate the experimental results presented in section 5.1.

The average measured temperature is 18.3 ± 0.2 °C. This means that the prediction of 17 °C was close, but too low. The difference in temperature is approximately 5 %. It might have small effects on the PVT-properties used for the numerical simulations, but should not be very significant.

5.3.1 Oil Displacing Water

Figure 5.10 is showing the oil volume fractions as functions of time, for the five different flow rates tested. Despite that there are some variations in the flow rate, it is used a constant number based on the average of the measured rates. The figure contains data from both experiments and simulations. In the plot, the experimental data is labeled with an E, and the numerical with an N. The uncertainties of the experimental data are included in form of plus signs with the respective colors of the flowrates.

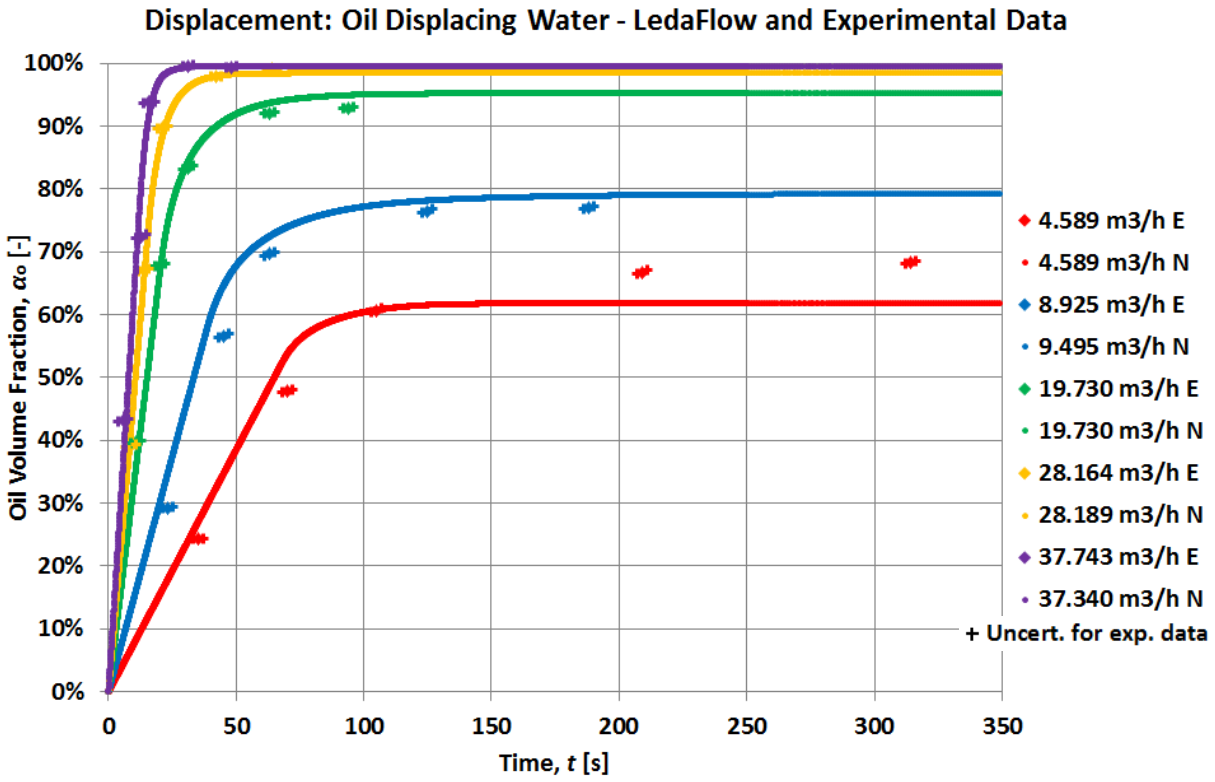

Figure 5.10: Numerical and experimental results for oil displacing water

Looking at the plot in Figure 5.10, one can see that the numerical models follow the same trend as the experimental data. The oil volume fraction is increasing linearly in the beginning, then curving some before it is stabilizing. It is visible from the plot, that the volume fractions predicted are closer to the experimental data when the rates are increasing.

In addition, the numerical and the experimental oil volume fractions are given in Table 5.3. The errors of the numerical model relative to the experimental data are included.

Table 5.3: Experimental and numerical oil volume fractions, including the error

Flow Rate Q [m^3/h]	**Time** t [s]	**Experimental Oil Volume Fraction** $\alpha_{o,exp}$ [-]	**Numerical Oil Volume Fraction** $\alpha_{o,num}$ [-]	**Absolute Error** ε [-]	**Absolute Difference** [-]
4.589	35	24.3 %	27.0 %	10.9 %	2.6 %
	70	47.8 %	53.8 %	12.5 %	6.0 %
	105	60.7 %	60.8 %	0.1 %	0.1 %
	209	66.8 %	61.9 %	7.4 %	4.9 %
	314	68.3 %	61.9 %	9.4 %	6.4 %
8.925	23	29.3 %	34.5 %	17.7 %	5.2 %
	45	56.7 %	64.6 %	14.1 %	8.0 %
	63	69.7 %	72.5 %	4.0 %	2.8 %
	125	76.5 %	78.2 %	2.1 %	1.6 %
	188	77.0 %	78.9 %	2.5 %	1.9 %
19.730	11	39.8 %	36.4 %	8.5 %	3.4 %
	20	67.9 %	66.2 %	2.5 %	1.7 %
	31	83.4 %	84.3 %	1.0 %	0.9 %
	63	92.1 %	93.7 %	1.8 %	1.6 %
	94	93.0 %	95.0 %	2.2 %	2.0 %
28.164	9	39.2 %	42.5 %	8.5 %	3.3 %
	14	67.1 %	66.1 %	1.4 %	1.0 %
	21	89.9 %	88.2 %	1.8 %	1.6 %
	42	98.0 %	98.0 %	0.0 %	0.0 %
	64	99.1 %	98.4 %	0.6 %	0.6 %
37.743	6	43.2 %	37.9 %	12.2 %	5.3 %
	13	72.5 %	81.7 %	12.8 %	9.3 %
	16	93.8 %	92.0 %	2.0 %	1.8 %
	31	99.6 %	99.4 %	0.2 %	0.2 %
	48	99.5 %	99.6 %	0.2 %	0.2 %
Average				**5.5 %**	

The model in LedaFlow is able to predict the final experimental measured oil volume fractions very well. With exception of the lowest flow rate 4.589 m^3/h with an error of 9.4 %, the rest of the flow rates have errors decreasing from 2.5 % to 0.2 %, as the rates increase. LedaFlow is better at predicting final displacement efficiency for higher flow rates.

The average error for the model compared to the experimental data is 5.5 %. By studying Table 5.3, one may see that the largest deviation between the experimental and numerical values are in the beginning, in the transient region. With exception of 8.925 m^3/h, the errors have a maximum of approximately 12 %. When entering the zones where the changes are smaller, the errors are rapidly reduced.

5.3.2 Water Displacing Oil

The results from water displacing oil are presented in Figure 5.11 and Table 5.4. The figure and the table are presenting the water volume fractions as a function of time for two different flow rates. In the plot, the experimental data are labeled with an E, and the numerical with an N. The uncertainties of the experimental data are included in form of plus signs in the respective colors of the flowrates.

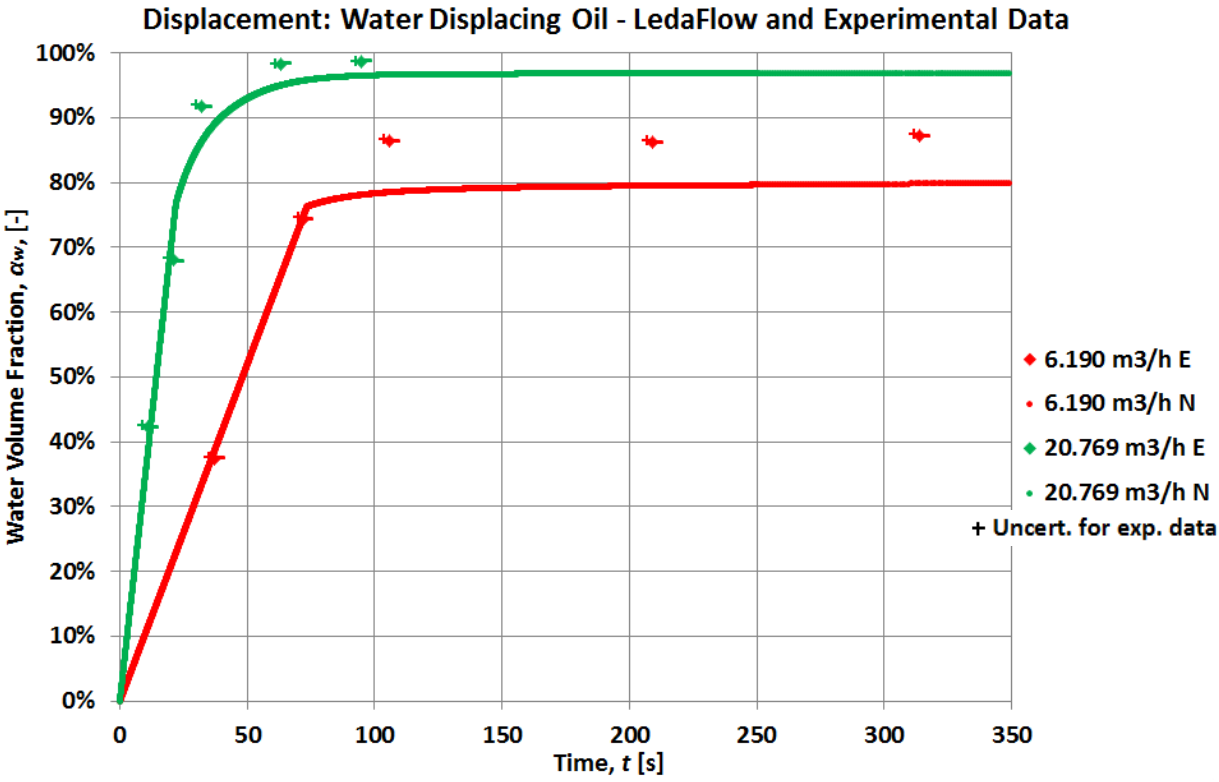

Figure 5.11: Numerical and experimental results for water displacing oil

From studying Figure 5.11, one can see that the model for water displacing oil seems to be deviating more from the experimental points in the stabilizing zones, compared to model for oil displacing water. In the transient regions, the results are within the uncertainties of the experimental data. The accuracy of the predicted final volume fraction is increasing for higher flow rates.

In the plot, it seems like LedaFlow rapidly exhibits a trend from linear to curved, visible for 6 m^3/h, after approximately one volume has been displaced. This is strange, but one suggestion is that the model is changing from a piston-like displacement, and that the oil starts to penetrate the water. It is observed from the animated solutions in LedaFlow that the behavior occurs when the displacing front is reaching the end of the domain.

Table 5.4: Experimental and numerical water volume fractions, including the error

Flow Rate Q **[m^3/h]**	**Time** t **[s]**	**Experimental Oil Volume Fraction** $\alpha_{o,exp}$ **[-]**	**Numerical Oil Volume Fraction** $\alpha_{o,num}$ **[-]**	**Absolute Error** ε **[-]**	**Absolute Difference [-]**
6.190	37	37.4 %	38.4 %	2.7 %	1.0 %
	72	74.4 %	74.8 %	0.5 %	0.4 %
	106	86.4 %	78.5 %	9.1 %	7.9 %
	209	86.2 %	79.5 %	7.7 %	6.7 %
	314	87.3 %	79.8 %	8.5 %	7.4 %
20.769	11	42.3 %	38.3 %	9.5 %	4.0 %
	21	68.0 %	73.1 %	7.6 %	5.1 %
	32	91.8 %	86.3 %	6.0 %	5.5 %
	63	98.3 %	95.0 %	3.3 %	3.3 %
	95	98.6 %	96.5 %	2.2 %	2.2 %
Average				**5.7 %**	

The lowest reported error in Table 5.4 is 0.5 %, and the highest 9.5 %. The averaged error for water displacing oil is 5.7 %. This shows that both models in LedaFlow are giving predictions with similar accuracy of the displacement efficiency, when comparing over a time period.

5.3.3 Snapshots of Performed Experiments and LedaFlow Simulations

As mentioned in section 5.1, it has been taken videos of the experiments as they were running. Figure 5.12 contains snapshots of oil displacing water at 4.589 m^3/h. Pictures for the other flow rates tested, are found in Figure F.1 to Figure F.6 in Appendix F. The videos are included as digital attachments. LedaFlow provides a visual model showing how the fluids are flowing in the system. Snapshots have been taken of the animations as well, and are presented together with the experimental pictures. From evaluating the pictures, one can see that the solutions in LedaFlow follow similar trends that were observed during the experimental research.

4.589 m^3/h: Exxsol D60 displacing Water (f = 10.50 Hz)

35 s

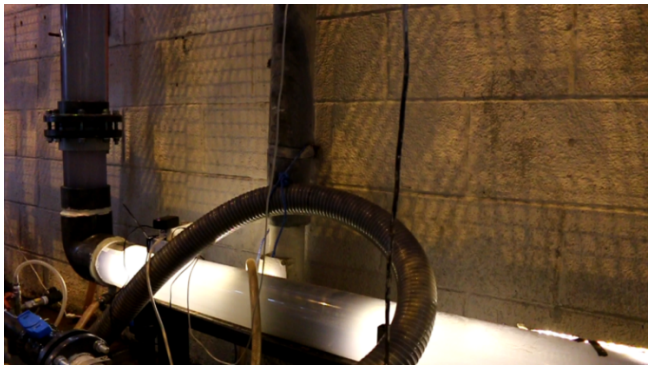

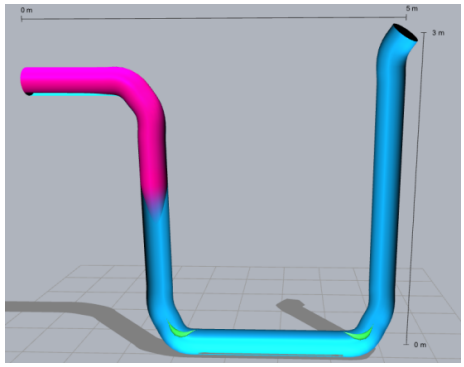

70 s

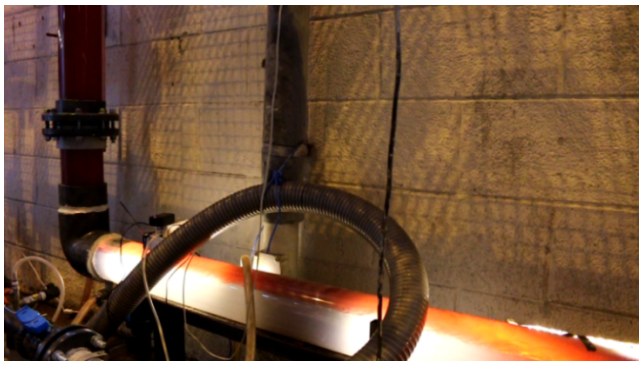

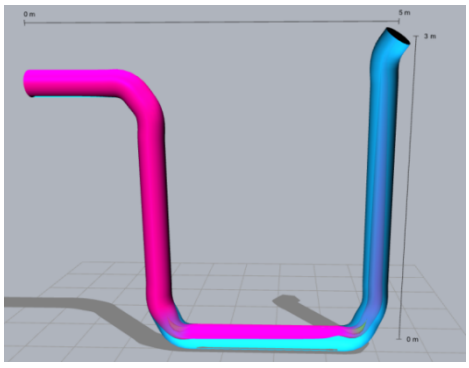

105 s

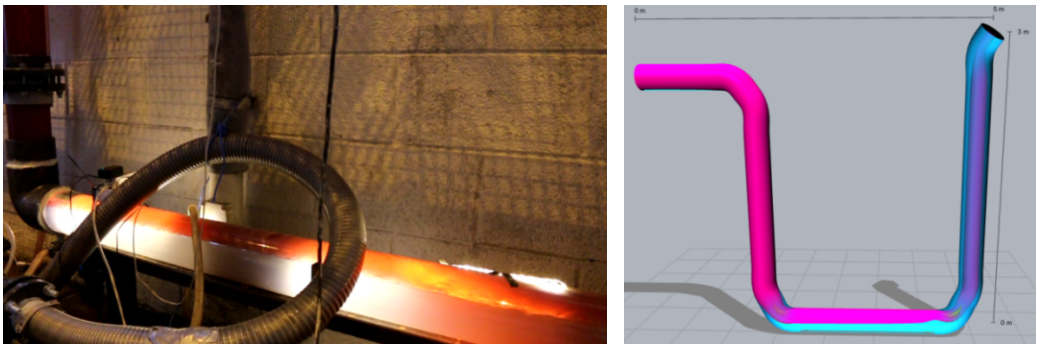

209 s

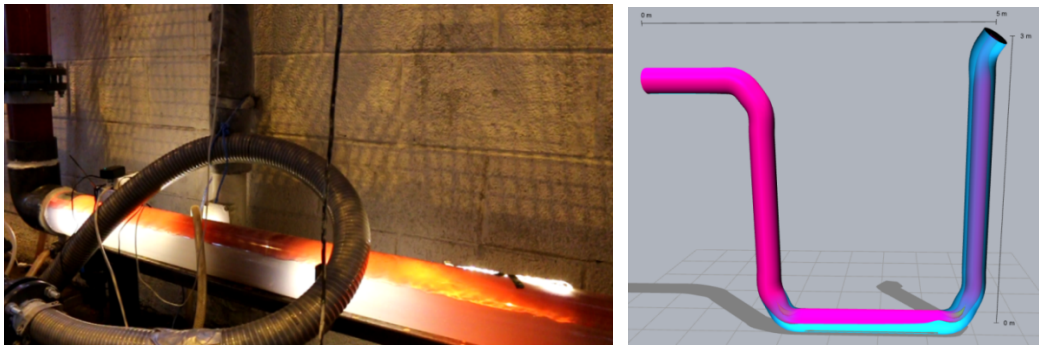

314 s

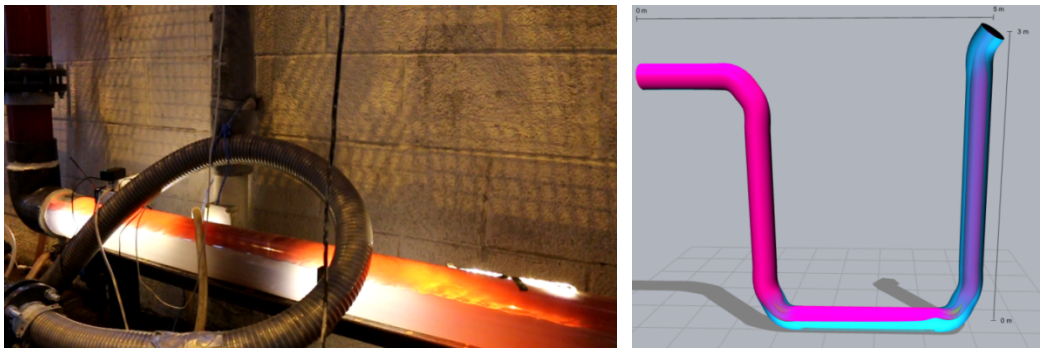

356 s

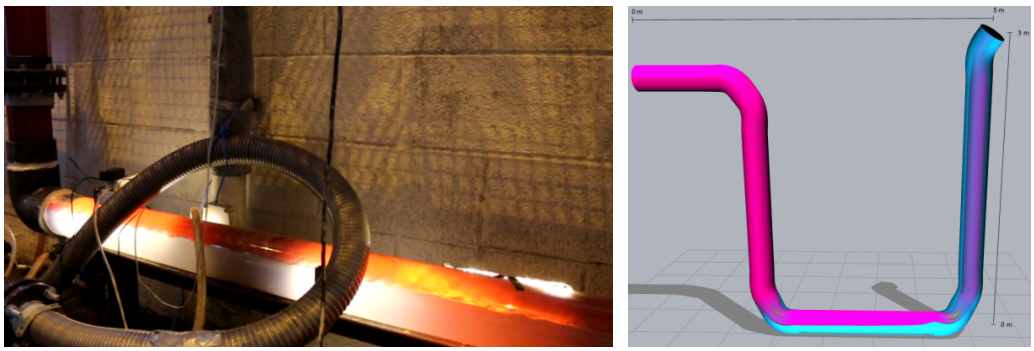

Figure 5.12: Pictures of experiment and LedaFlow model for oil displacing water at different times, 4.859 m^3/h

5.4 Reproducing the Results of Opstvedt (2016)

The results from Opstvedt (2016) are presented graphically in the figures in section 5.4.1 and section 5.4.2, together with the numerical results from the model in LedaFlow performed by the author. The figures give the volume fractions of the displacing fluids versus time for different flow rates. Every rate is plotted in an own figure. As described in section 3.1.4.2, Opstvedt (2016) executed experiments in the U-shaped pipe system presented in section 4.1.1. These results are marked with blue diamond points. Plus signs are included in the same colour, for marking the uncertainties of the experimental data. In addition, Opstvedt (2016) created two numerical models in ANSYS CFX. The first was a homogeneous standard free-surface model. These results are marked with red squares. The other was an inhomogeneous mixture model, where the results are marked with yellow squares. Opstvedt (2016) reported the results for one, two and three volumes displaced, represented in the plots by point 1, 2 and 3. A Shear Stress Transport model was used for modelling turbulence in both models. The results from LedaFlow are illustrated with continuous lines in the plots.

5.4.1 Oil Displacing Water

The following plots in Figure 5.13 to Figure 5.16 are comparing the results of Opstvedt (2016) to the results from LedaFlow, for oil displacing water. Results from flow rates of 6 m^3/h, 10 m^3/h, 20 m^3/h and 30 m^3/h are studied.

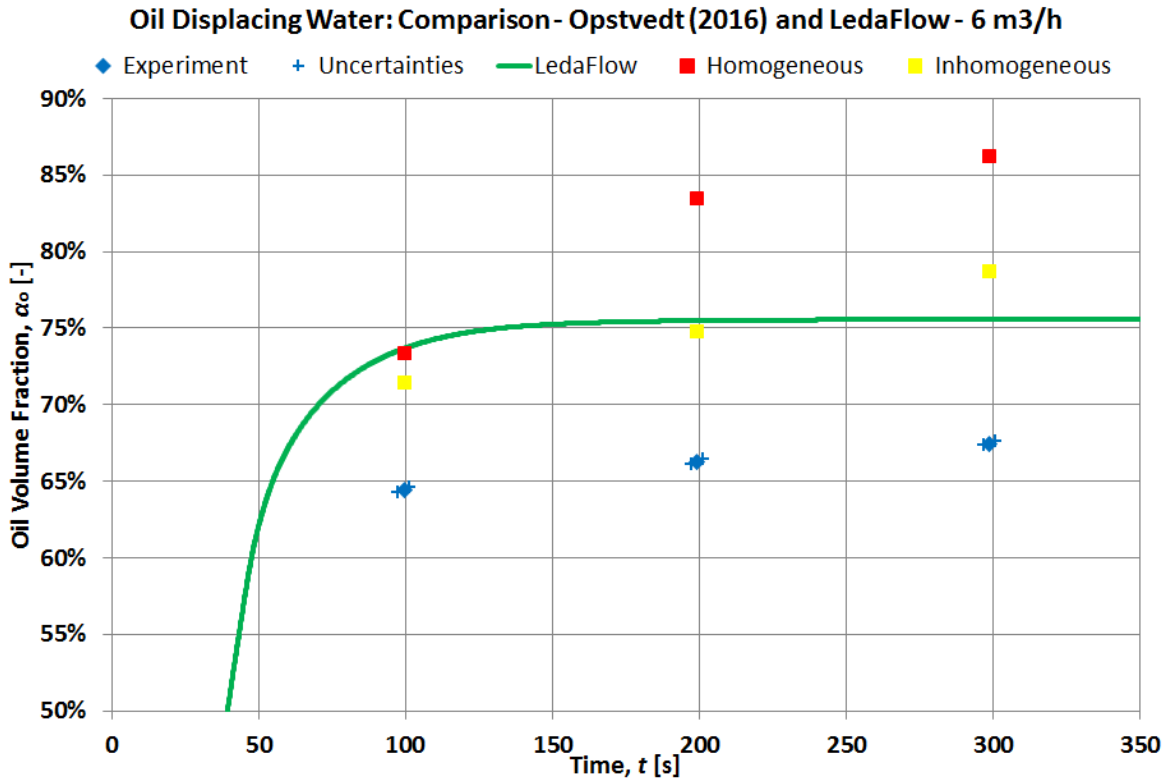

Figure 5.13: Comparison of Opstvedt and LedaFlow, oil displacing water, 6 m^3/h

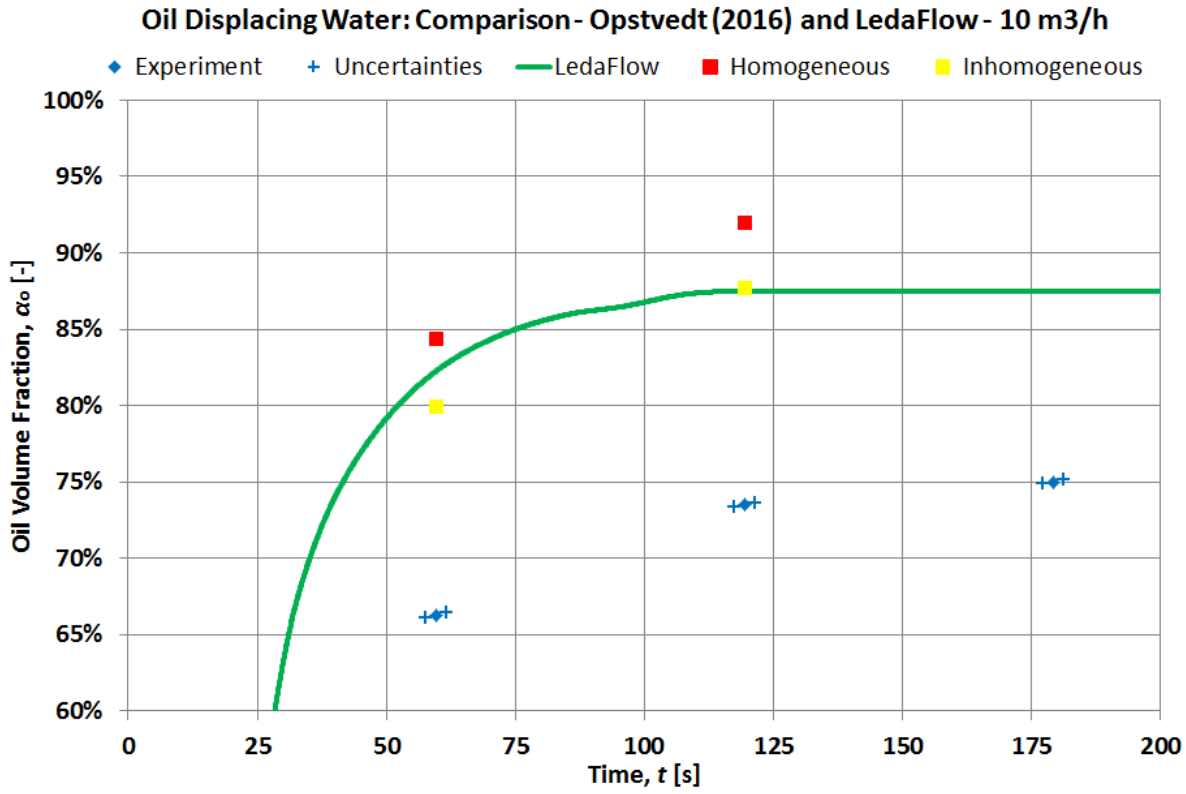

Figure 5.14: Comparison of Opstvedt and LedaFlow, oil displacing water, 10 m^3/h

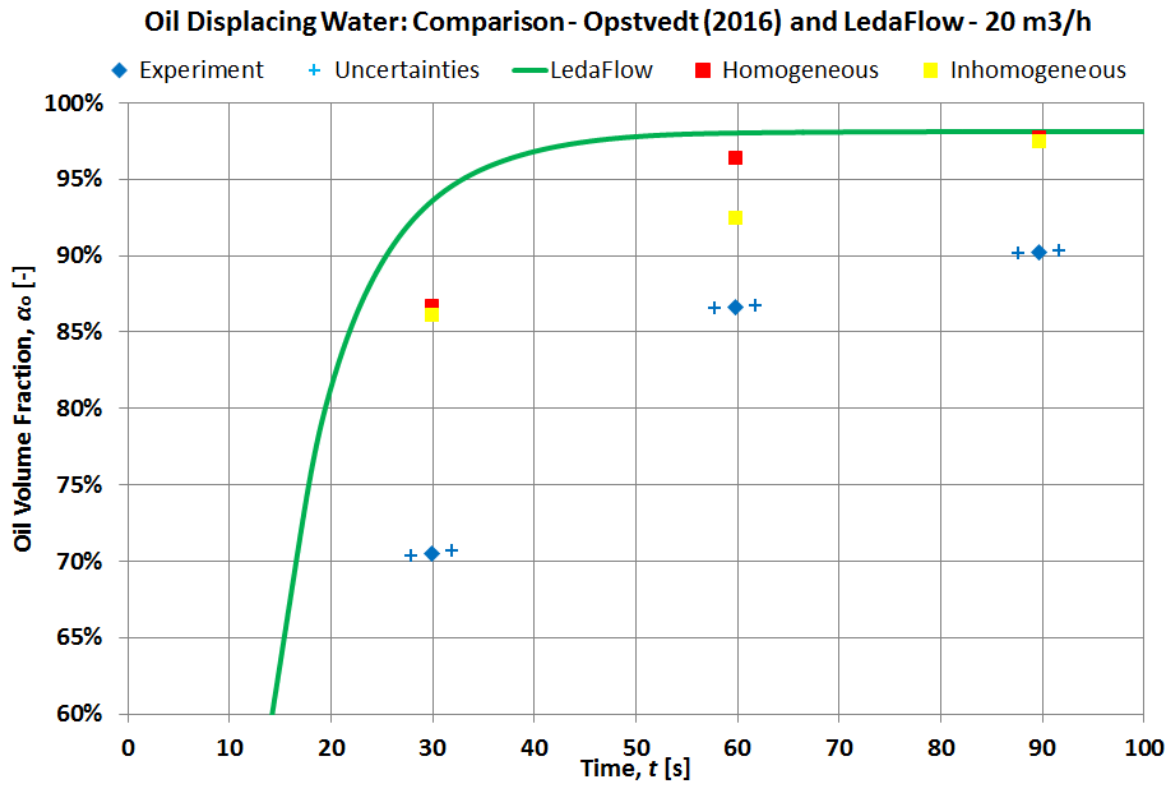

Figure 5.15: Comparison of Opstvedt and LedaFlow, oil displacing water, 20 m^3/h

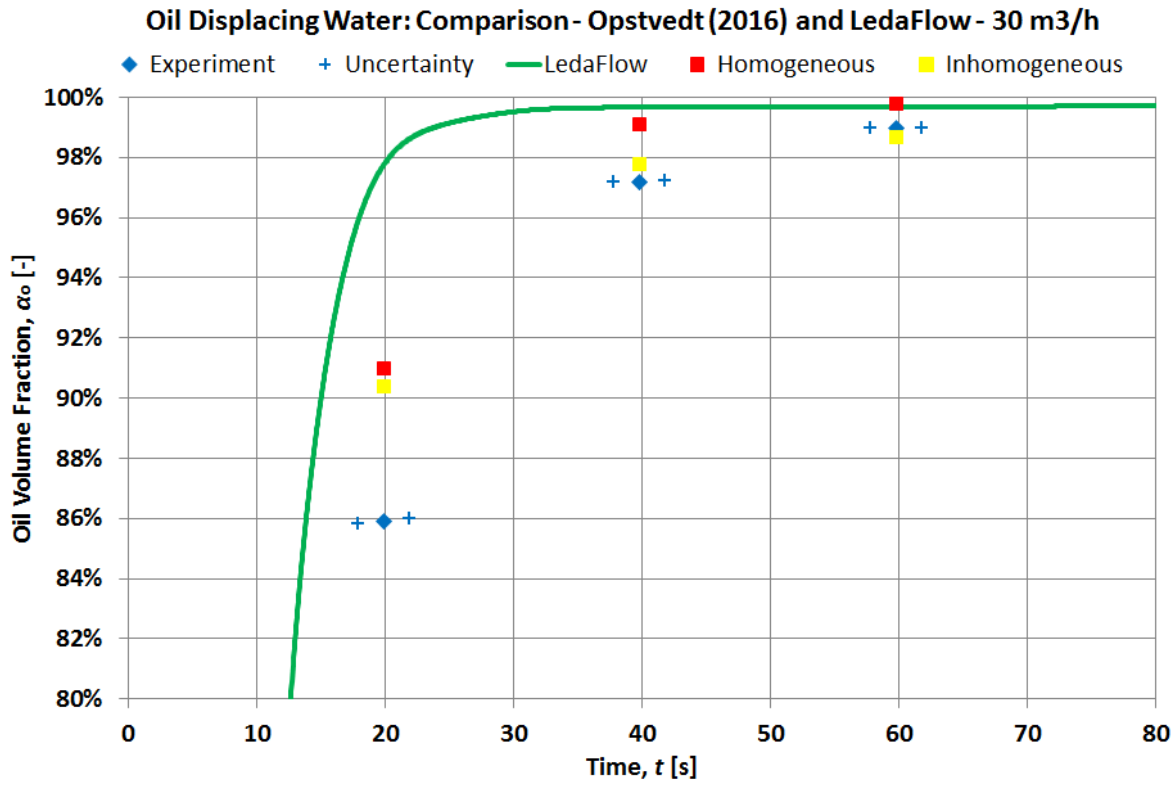

Figure 5.16: Comparison of Opstvedt and LedaFlow, oil displacing water, 30 m^3/h

A general observation from the plots in Figure 5.13 to Figure 5.16, is that the numerical models often are over predicting the oil volume fractions, when oil is displacing water. In the plots, it is shown that the results of inhomogeneous mixture model in most of the cases are closest to the experimental data. Studying Figure 5.13 and Figure 5.14, one may see that the model from LedaFlow is closer than the homogeneous standard free-surface model. For the two highest rates, in Figure 5.15 and Figure 5.16, the homogeneous model is closer to the experimental points than the LedaFlow model.

Table 5.5 is presenting the oil volume fractions in the jumper after 1, 2 and 3 volumes displaced. It includes the results of the experiments of Opstvedt (2016), the homogeneous model, the inhomogeneous model and the model in LedaFlow. The errors of the numerical fractions relatively to the experimental fractions have been calculated.

Table 5.5: Comparison of the results from Opstvedt and LedaFlow – oil disp. water

Rate Q [m^3/h]	**Vol. Disp V_{disp} [-]**	**Exp. water fraction $\alpha_{w,exp}$ [-]**	**Homog. water fraction $\alpha_{w,hom}$ [-]**	**Abs. error ε [-]**	**Inhomo. water fraction $\alpha_{w,inhom}$ [-]**	**Abs. error ε [-]**	**LedaFl. water fraction $\alpha_{w,Leda}$ [-]**	**Abs. error ε [-]**
6	1	64.5 %	73.4 %	13.8 %	71.4 %	10.8 %	73.7 %	14.3 %
	2	66.3 %	83.5 %	26.0 %	74.8 %	12.9 %	75.5 %	13.9 %
	3	67.47 %	86.2 %	27.8 %	78.7 %	16.7 %	75.6 %	12.0 %
10	1	66.3 %	84.4 %	27.3 %	79.9 %	20.6 %	82.3 %	24.2 %
	2	73.5 %	92.0 %	25.2 %	87.7 %	19.3 %	87.5 %	19.1 %
	3	75.0 %					87.5 %	16.7 %
20	1	70.5 %	86.7 %	23.0 %	86.1 %	22.2 %	93.6 %	32.7 %
	2	86.6 %	96.4 %	11.3 %	92.5 %	6.7 %	98.0 %	8.7 %
	3	90.2 %	97.8 %	8.3 %	97.5 %	8.0 %	98.1 %	13.8 %
30	1	85.9 %	91.0 %	5.9 %	90.4 %	5.2 %	97.8 %	2.5 %
	2	97.2 %	99.1 %	1.9 %	97.8 %	0.6 %	99.7 %	0.7 %
	3	99.0 %	99.8 %	0.8 %	98.7 %	0.3 %	99.7 %	1.3 %
Average				**15.6 %**		**11.2 %**		**14.3 %**

From the averaged errors calculated in Table 5.5, one can see that the inhomogeneous mixture model is closest to the experimental data, with an averaged error of 11.2 %. Then, the model in LedaFlow follows, with an averaged error of 14.3 %. The homogeneous model has the highest averaged error, of 15.6 %. One can see that LedaFlow is closer in its prediction of the volume fraction after 3 volumes have been displaced, than the inhomogeneous model from ANSYS CFX. Neither the homogeneous nor the inhomogeneous model is able to predict the volume fraction after displacing for 3 volumes with 10 m^3/h. This is done by LedaFlow.

5.4.2 Water Displacing Oil

The following plots in Figure 5.17 to Figure 5.20, are comparing the results of Opstvedt (2016) and LedaFlow, for water displacing oil.

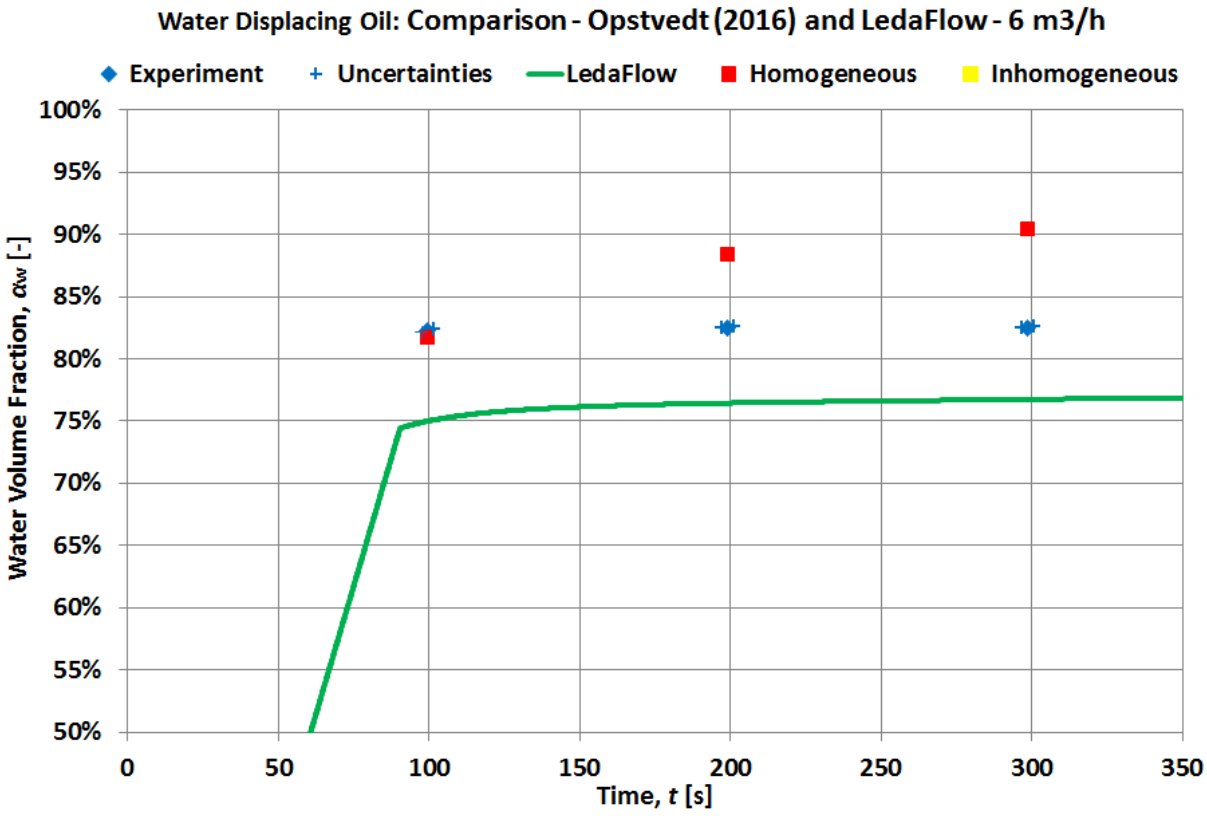

Figure 5.17: Comparison of Opstvedt and LedaFlow, water displacing oil, 6 m3/h

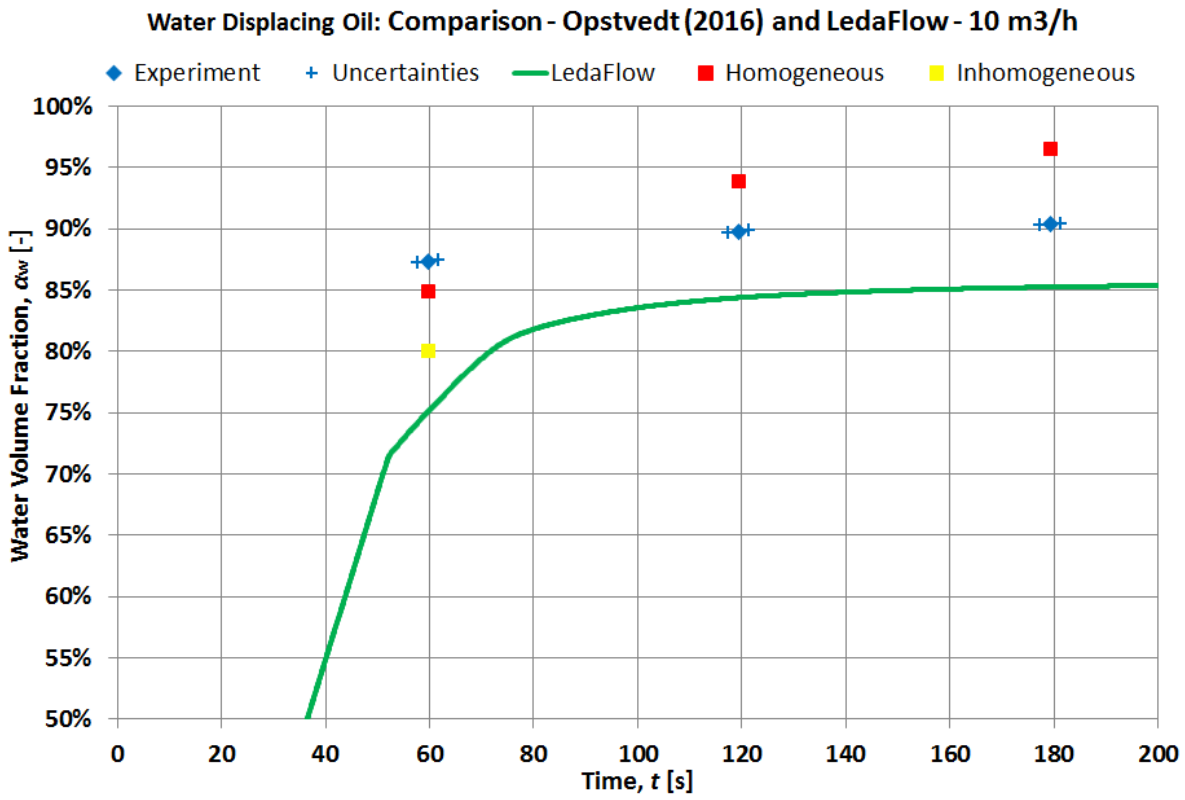

Figure 5.18: Comparison of Opstvedt and LedaFlow, water displacing oil, 10 m3/h

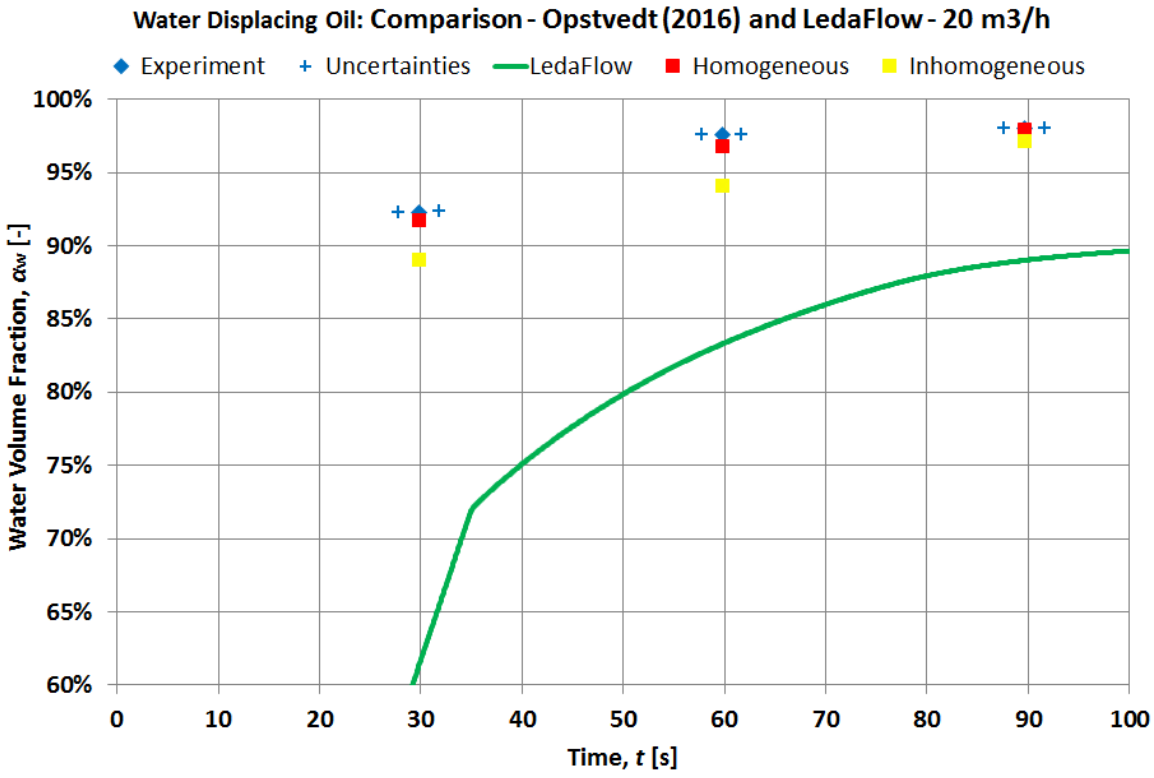

Figure 5.19: Comparison of Opstvedt and LedaFlow, water displacing oil, 20 m3/h

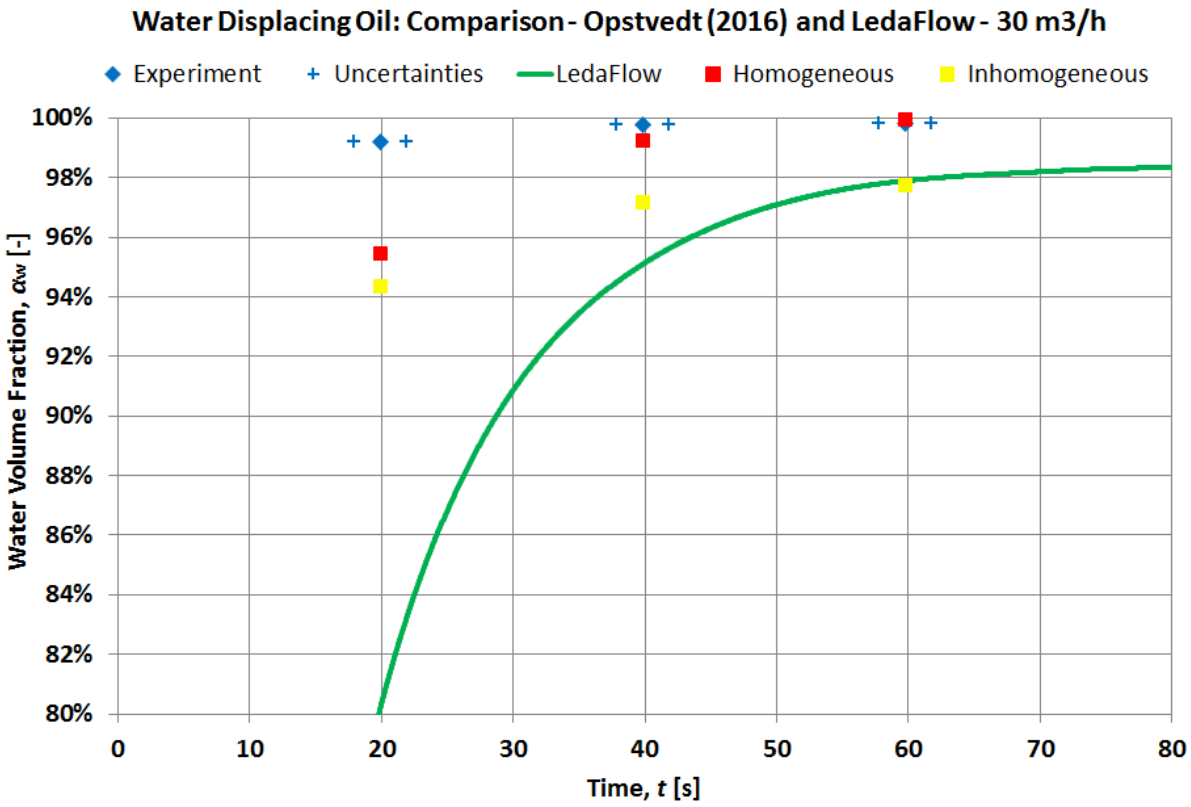

Figure 5.20: Comparison of Opstvedt and LedaFlow, water displacing oil, 30 m3/h

For the plots in Figure 5.17 to Figure 5.20 are the numerical models both under and over predicting the water volume fractions, as water is displacing oil. Under predictions are most common, and especially for the model from LedaFlow.

The inhomogeneous model from ANSYS CFX is missing all the data points for the lowest flow rate, and point 2 and 3 for the second flow rate, seen in Figure 5.17 and Figure 5.18. The homogeneous model in Figure 5.17 corresponds well with the first experimental points, but with time the deviation is increasing. For rate 20 m^3/h in Figure 5.19, are the results of the homogeneous model close to the experimental data. The LedaFlow model is far from the experimental values. In Figure 5.20 is the homogeneous model still closest to the experimental points. An observation made is that the gap between the experimental values and the LedaFlow values is smaller than in Figure 5.19.

Table 5.6: Comparison of the results from Opstvedt and LedaFlow – water disp. oil

Rate Q [m^3/h]	Vol. Disp V_{disp} [-]	Exp. water fraction $\alpha_{w,exp}$ [-]	Homog. water fraction $\alpha_{w,hom}$ [-]	Abs. error ε [-]	Inhomo. water fraction $\alpha_{w,inhom}$ [-]	Abs. error ε [-]	LedaFl. water fraction $\alpha_{w,Leda}$ [-]	Abs. error ε [-]
6	1	82.2 %	81.8 %	0.6 %			75.0 %	8.8 %
	2	82.5 %	88.4 %	7.1 %			76.4 %	7.4 %
	3	82.5 %	90.4 %	9.6 %			76.7 %	7.0 %
10	1	87.4 %	84.9 %	2.8 %	80.1 %	8.3 %	75.1 %	14.0 %
	2	89.8 %	93.9 %	4.6 %			84.4 %	6.0 %
	3	90.4 %	96.5 %	6.8 %			85.2 %	5.7 %
20	1	92.3 %	91.7 %	0.6 %	89.1 %	3.5 %	61.3 %	33.4 %
	2	97.6 %	96.8 %	0.8 %	94.1 %	3.5 %	83.3 %	14.6 %
	3	98.0 %	98.0 %	0.0 %	97.2 %	0.9 %	89.0 %	9.2 %
30	1	99.2 %	95.4 %	3.8 %	94.4 %	4.9 %	80.2 %	19.2 %
	2	99.8 %	99.3 %	0.5 %	97.2 %	2.6 %	95.1 %	4.7 %
	3	99.8 %	100.0 %	0.1 %	97.8 %	2.1 %	97.9 %	1.9 %
Average				**3.1 %**		**3.7 %**		**11.0 %**

Table 5.6 shows that the homogeneous standard free-surface model, is the best at predicting water displacing oil in the jumper. The averaged error is 3.1 %, compared to 4.1 % for the inhomogeneous model, and 11.0 % for the LedaFlow model. However, one should be aware that almost half of the desired data points are not obtained through the inhomogeneous model.

From the discussion of the comparison of the results from Opstvedt (2016) and LedaFlow one may conclude that the models from ANSYS CFX are better at predicting the displacement in the jumper system studied. For oil displacing water, the inhomogeneous model is best, and for water displacing oil, the homogeneous model is best. This agrees with the conclusion of Opstvedt (2016).

However, the model in LedaFlow is based on properties and measurements presented in the work of Opstvedt (2016). The averaged errors between the model in LedaFlow and the experimental data are 14.3 % for oil displacing water, and 11.0 % for water displacing oil. They deviate from the reported errors of respectively 5.5 % and 5.7 % obtained by the author for this project. This might be due to uncertainties regarding the experiments conducted by Opstvedt (2016). Only the remaining liquid in the system is reported, and not the total measured volume. The volume in the LedaFlow model was therefore based on the volume measured by the author. In addition, the temperatures were not reported, which might have an effect on the PVT-properties.

5.5 A Sensitivity Analysis based on Numerical Results

Simulations have been run with the purpose of conducting a sensitivity analysis of the displacement process.

5.5.1 Effects of Changing PVT-Properties for Water and Oil

It is interesting to see how varying the PVT-properties affect the volume fractions of the displacing fluids. Simulations have been run in the same U-formed system, initially filled with water, and then displaced with oil at 6 m^3/h. The changes in the properties are summarized in Table 4.17.

5.5.1.1 Changing the Water Density

Figure 5.21 is showing final oil volume fraction versus water density, after LedaFlow has run a simulation of oil displacing water for 3600 seconds. Each point has a label indicating its change relative to the original case.

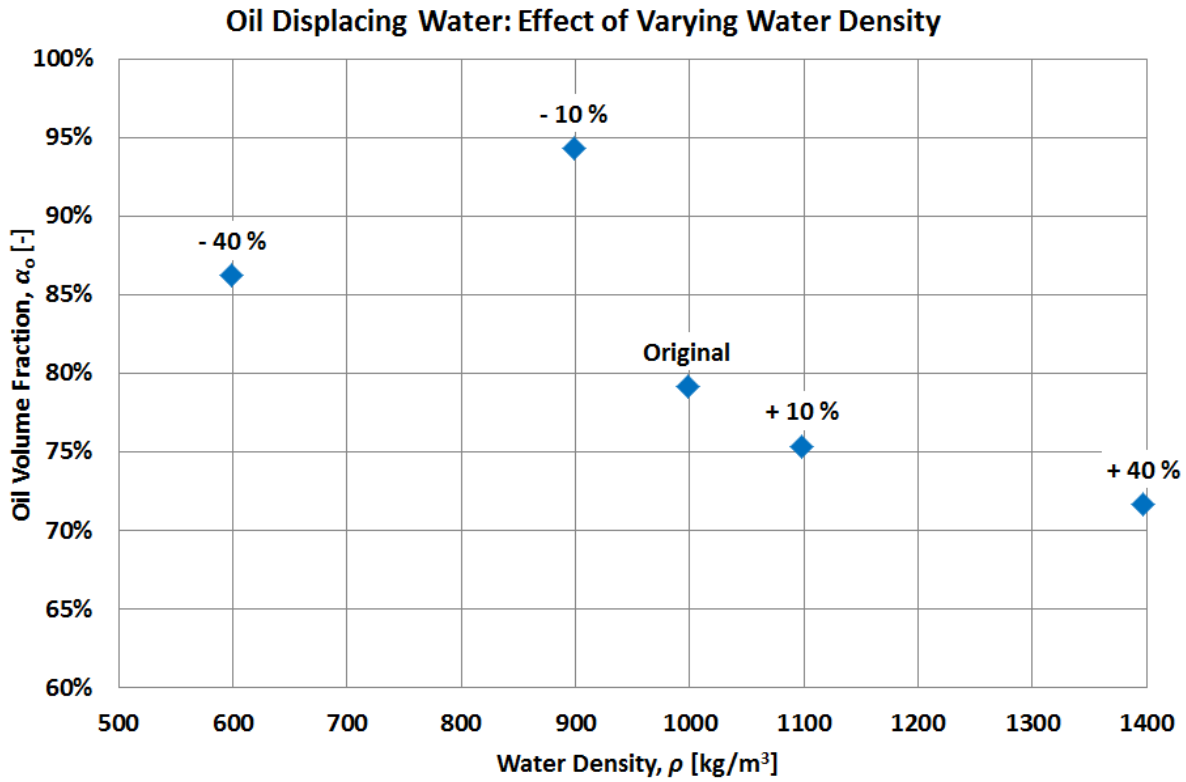

Figure 5.21: Final oil volume fraction versus water densities for oil displacing water

The displacement efficiency is defined as the volume fraction of the displacing fluid. The trend in Figure 5.21 is showing that for water densities higher than the density of the displacing oil, the displacement efficiency is decreasing exponentially as the water density is increased. The point labeled -40 % is not following this trend. This is probably due to the water density of this point being lower than the density of the displacing oil.

The numerical results indicate that it is better to displace with a fluid that is only a little less dense than the fluid to be displaced, so that the densities are close. The plot in Figure 5.21 has the potential of being used for designing a more efficient displacement fluid, which is optimized based on the properties of the fluid to be displaced.

5.5.1.2 Changing the Water Viscosity

The results from the LedaFlow simulations were water viscosity is changed, are presented in Figure 5.22. The plot is showing oil volume fraction versus time for 1200 seconds.

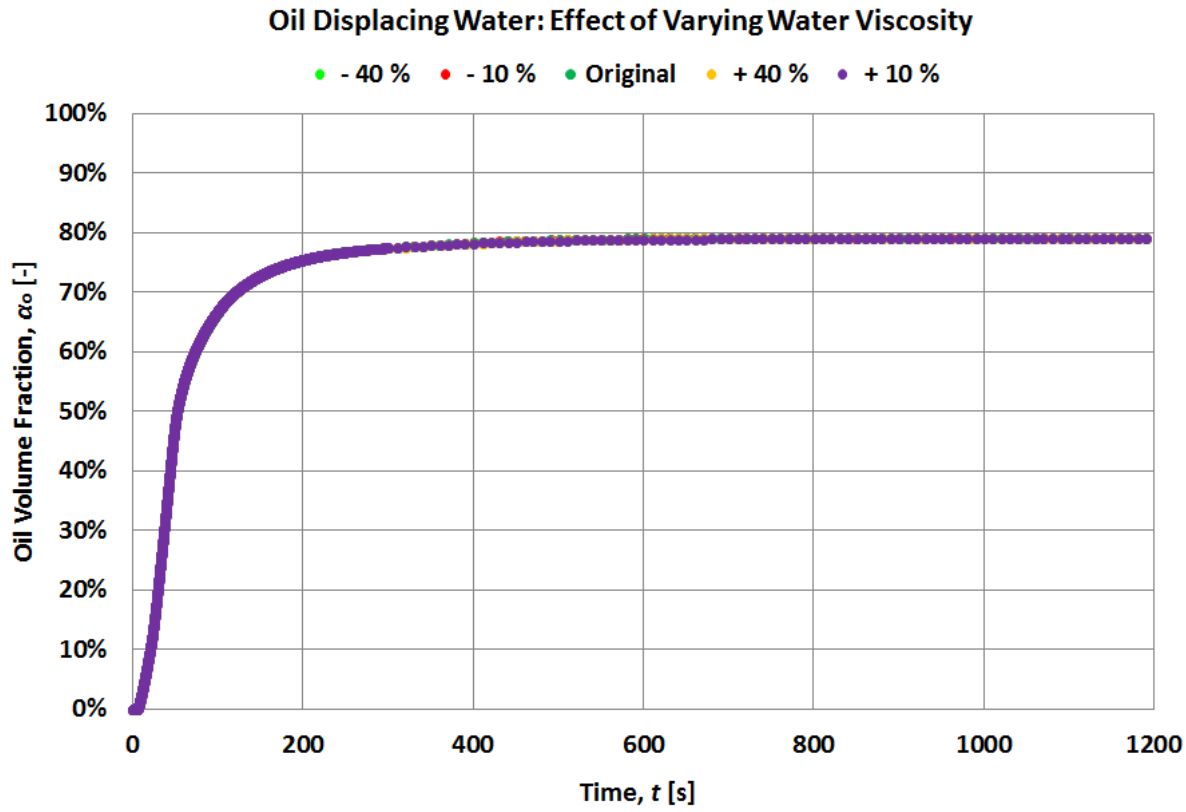

Figure 5.22: Oil volume fractions versus time for varying water viscosities

From the plot in Figure 5.22, one can see that varying the water viscosity in an interval of -40 % to +40% of the original value, shows no significant changes in the oil volume fractions.

5.5.1.3 Changing the Oil Viscosity

Figure 5.23 shows the results of changing oil viscosity in the model in LedaFlow. The oil volume fraction is plotted as a function of time for 1200 seconds, due to the rest of the simulation time showing no further changes in oil volume fractions.

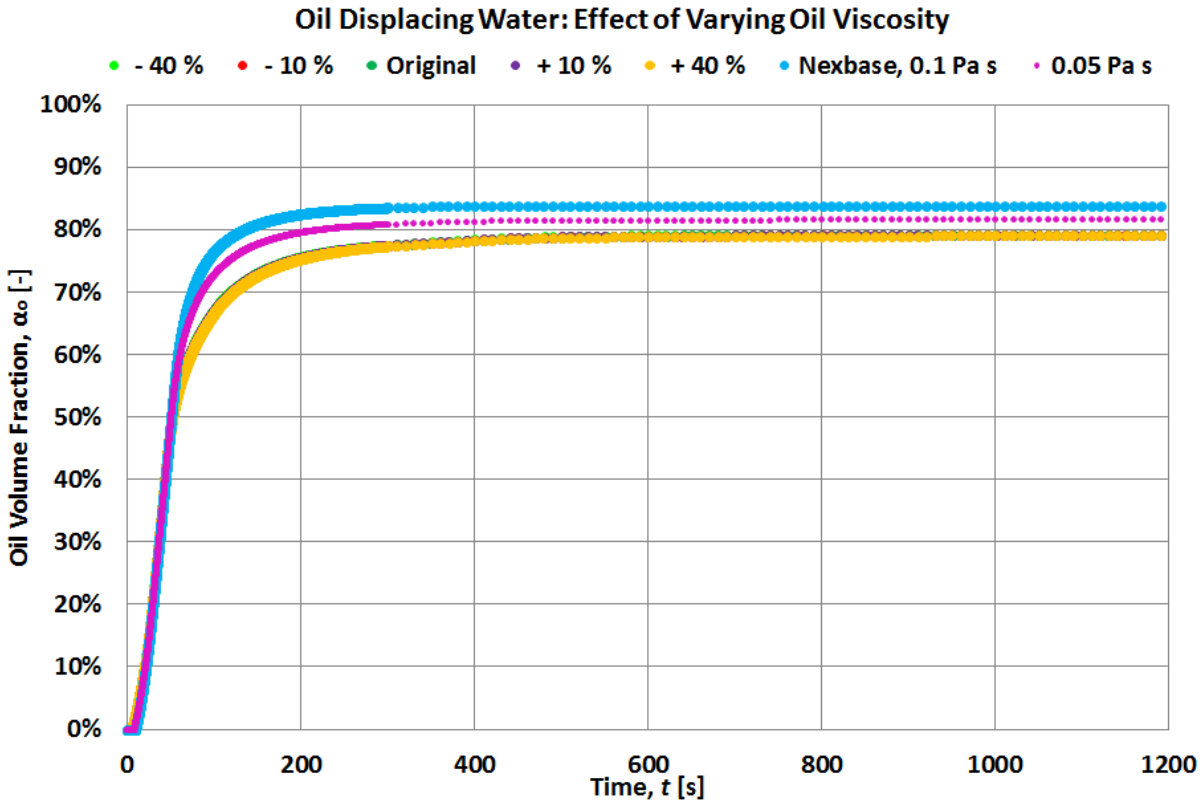

Figure 5.23: Oil volume fractions versus time for varying oil viscosities

Figure 5.23 shows that changing the oil viscosity for an interval of -40% to +40%, is not having any significant changes on the oil volume fraction from the original case. However, a simulation was run using a higher viscosity, corresponding to NexBase oil with 0.1 Pa s. The viscosity is 50 times higher than the viscosity of the original case. This resulted in an oil volume fraction of 84 %, which is an increase of 6.3 %. In the original case, the viscosity of the displacing fluid is 2 times higher than for water, and with 0.1 Pa s it is 100 times higher. An extra simulation was run using an oil viscosity of 0.05 Pa s, backed by interest in how this viscosity behaves compared to the others. As expected, the curve lies in between the original viscosity and the Nexbase viscosity. This indicates that the displacement efficiency, will increase if the displacing fluid is more viscous than the fluid to be displaced.

5.5.1.4 Changing the Interfacial Tension

Figure 5.24 shows final oil volume fraction versus interfacial tensions after LedaFlow has run simulations for 3600 seconds, where oil is displacing water. Each point has a label indicating the change relative to the original case.

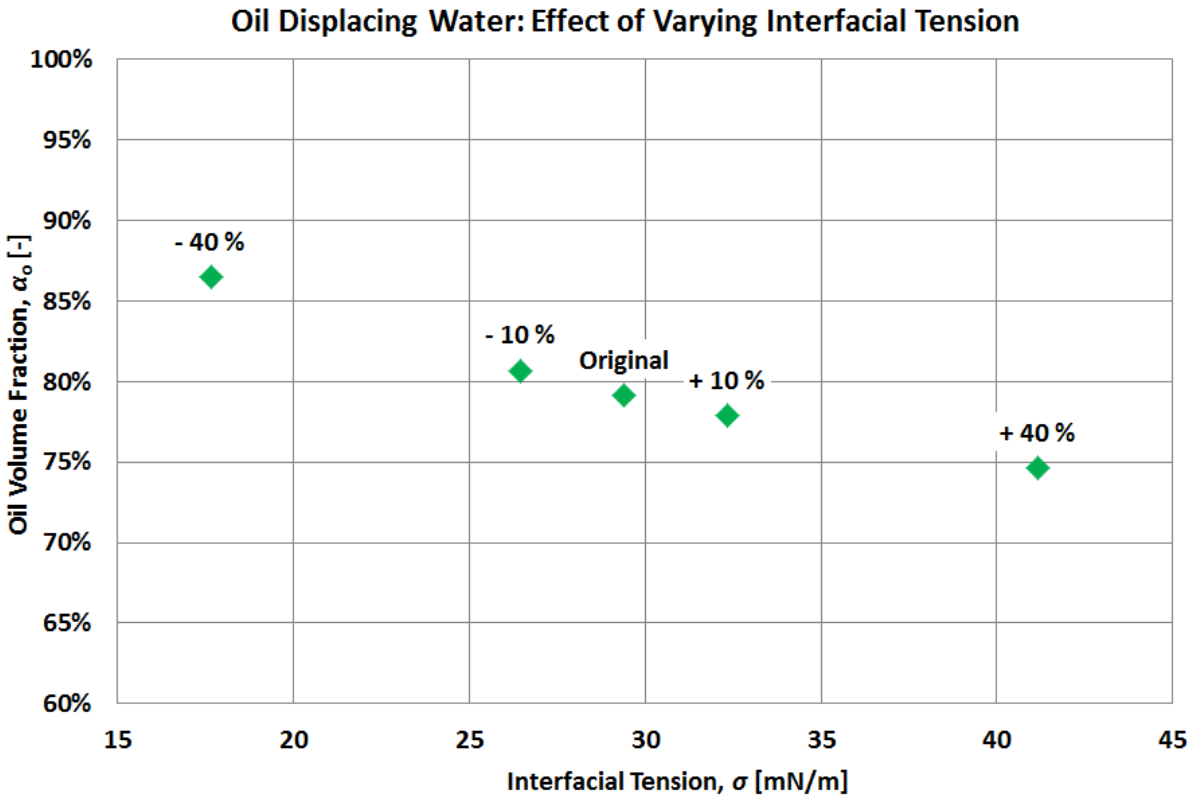

Figure 5.24: Final oil volume fraction versus interfacial tensions for oil displacing water

The plot in Figure 5.24, reveals a linear trend for the oil volume fractions of varying interfacial tensions. An increase in interfacial tension is reducing the displacement efficiency, and hence reducing the tension is increasing the efficiency. This suggests that if one is able to reduce the interfacial tension between the liquids, a more successful removal will be obtained.

One should be aware that the conclusions regarding changes in PVT-properties, only are based on simulations in LedaFlow, and that experimental data are required for validation.

5.5.2 Methanol Displacing Oil

Due to methanol often being used as displacement fluid in the industry, it is interesting to see how it is modelled in LedaFlow, compared to oil displacing water. The results of the simulations where methanol is displacing oil, are presented in Figure 5.25. The methanol volume fractions versus time are plotted for different rates. After the simulation has reached 600 seconds, the changes in the methanol volume fraction for the rest of the simulation time are negligible.

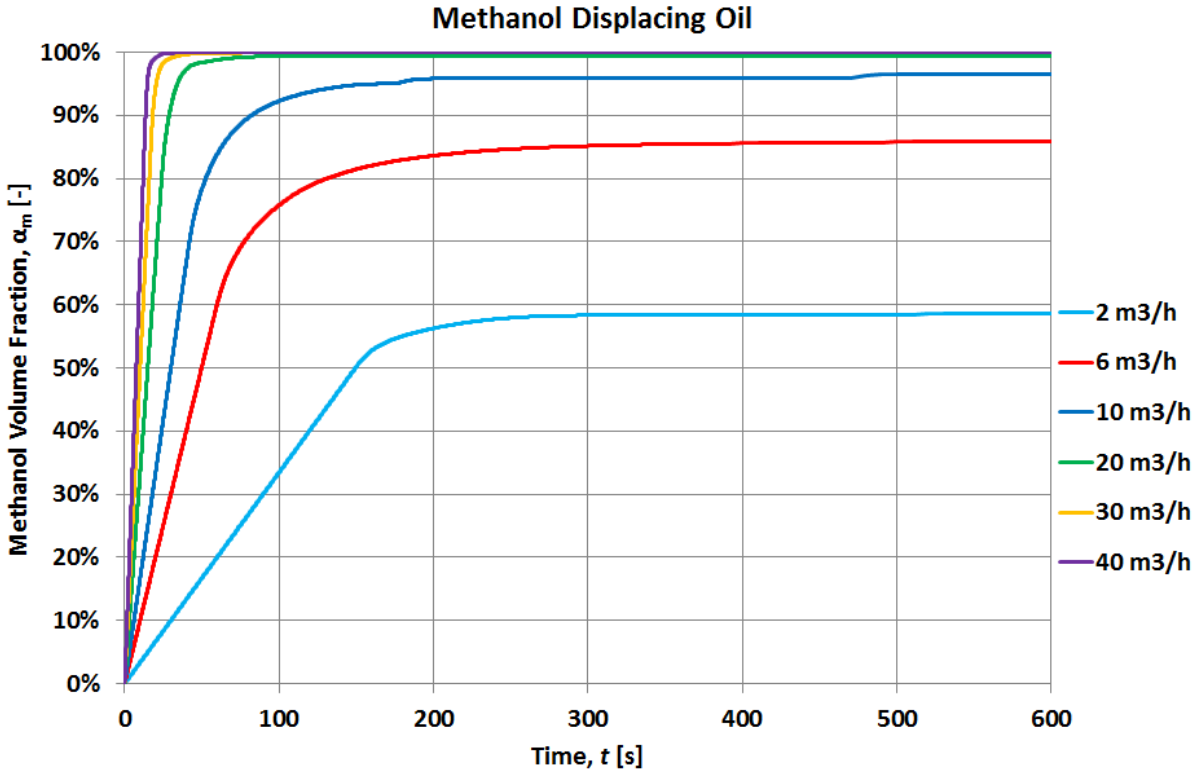

Figure 5.25: Simulation results for methanol displacing oil

The trend of methanol displacing oil in Figure 5.25 is similar to the other simulations where oil is displacing water, displayed in Figure 5.10. The displacement efficiency, given by the methanol volume fraction at a certain time, is increasing as the flow rates are increasing. In the beginning the methanol volume fraction is increasing rapidly and linearly. After approximately one volume displaced, it is starting to stabilize. The plot shows that there are small differences in the displacement efficiencies when displacing at 20 m^3/h or higher.

Table 5.7 is presenting the final methanol volume fractions for the different flow rates, after LedaFlow has run a simulation for 3600 seconds. It is also studied when the displacement process seems to be stabilizing. The criterion is set for when the volume fraction is not changing more than 0.1 % within a time interval of 1 s. It is presented how many volumes displaced, this stabilizing time corresponds to. In addition, simulations are run for oil displacing water at the same flow rates, to be able to compare the two processes. The oil volume fractions are given for the times where the methanol volume fraction is stabilizing.

Table 5.7: Volume fractions for methanol displacing water

Rate Q [m^3/h]	Final Methanol Volume Fraction $\alpha_{m,fin}$ [-]	Stabilizing Time t_{stab} [s]	Volumes Displaced when Stabilizing V_{disp} [-]	Methanol Volume Fraction when Stabilizing $\alpha_{m,stab}$ [-]	Oil Volume Fraction When Met. is Stabilizing $\alpha_{m,stab}$ [-]	Oil Volume Fraction Final $\alpha_{m,fin}$ [-]
2.0	58.7 %	177	0.6	54.8 %	51.4 %	52.3 %
6.0	86.2 %	120	1.2	78.8 %	71.4 %	72.7 %
10.0	96.5 %	88	1.5	90.9 %	82.6 %	85.5 %
20.0	99.7 %	42	1.4	97.7 %	93.1 %	97.4 %
30.0	100.0 %	27	1.3	98.7 %	97.5 %	99.6 %
40.0	100.0 %	22	1.5	99.5 %	99.3 %	99.8 %
12.0	97.7 %	74	1.5	94.1 %		
15.0	98.8 %	58	1.5	96.7 %		

Looking at Table 5.7, one can see that if displacing for one hour, even the low rate of 10 m^3/h will reach the criterion of 95 %, with a methanol fraction of 96.5 %. It will require displacing for some time, and other rates were therefore investigated for the optimal rate.

If one studies the methanol fractions for the time when displacement is stabilizing according to the criterion specified, it is observed that 20 m^3/h is reaching a methanol fraction of 97.7 % after 1.4 volumes displaced.

Further investigation was made to find an optimal rate, and two more simulations were run for 12.0 m^3/h and 15.0 m^3/h. The simulations resulted in volumes fractions of 94.1 % and 96.7 % respectively, at their given displacement times. By linear interpolation between these rates, it is found that 13.0 m^3/h will result in a volume fraction of 95.0 %, after approximately displacing for 1.5 volumes.

One of the reasons for simulating methanol displacing oil, was to see how LedaFlow predicts the displacement compared to oil displacing water. From Table 5.7, one can see that the volume fractions of the displacing fluid when oil is displacing water are lower, than for methanol displacing oil at the stabilization time. It was calculated averages of the volume

fractions, showing 86.7 % for methanol and 82.6 % for oil. According to simulations run in LedaFlow, the displacement efficiency is lower when using oil for displacing water, than methanol for displacing oil. A reason for testing displacement with oil displacing water in the lab was to try to illustrate methanol displacing oil. From the results in LedaFlow, one may assume that the experiments with oil and water are an under prediction of the displacement efficiency, that would have been obtained for methanol displacing oil.

5.5.3 System with Gas Included

A model was made to simulate the jumper initially filled with 40 % water, 30 % oil and 30 % gas. For gas, it was used properties of methane. Oil is the displacing fluid. The resulting oil volume fractions with time in the system, for different oil flowing rates, are presented in Figure 5.26.

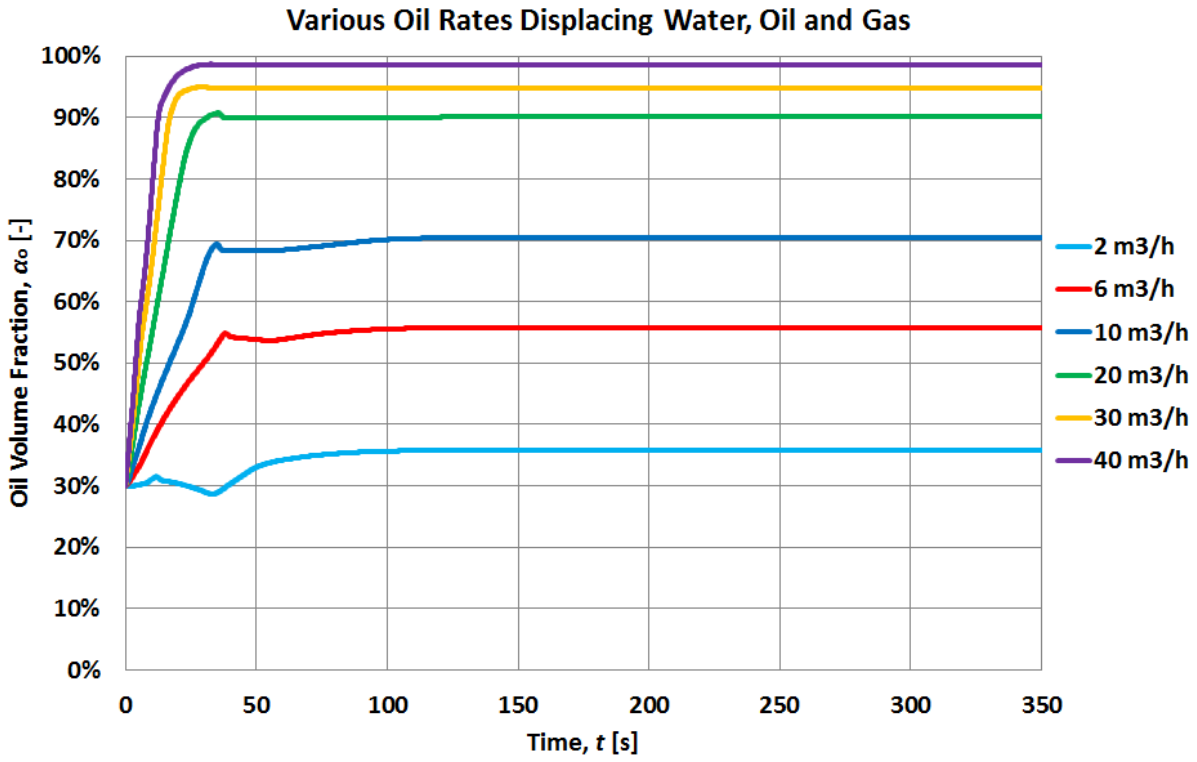

Figure 5.26: Simulations of oil is displacing water (40 %), oil (30 %) and gas (30 %)

It is visible from Figure 5.26 that the displacement efficiency is increasing with increased flow rate. The displacement efficiency refers to the total oil volume fraction in jumper, relative to the total volume including gas, water and oil.

Table 5.8 is presenting the volume fractions for the different fluids in the system, oil, water and gas, after oil has been flowing at various rates for 3600 seconds.

Table 5.8: Obtained volume fractions for simulation case where gas is included

Flow Rate Q **[m^3/h]**	**Oil Volume Fraction** α_o **[-]**	**Water Volume Fraction** α_w **[-]**	**Gas Volume Fraction** α_g **[-]**
2	35.8 %	47.7 %	16.5 %
6	55.8 %	28.6 %	15.6 %
10	70.5 %	14.7 %	14.8 %
20	90.2 %	2.3 %	7.5 %
30	94.8 %	0.4 %	4.8 %
40	98.5 %	0.2 %	1.3 %

From studying Table 5.8 one can see that for 2 m^3/h, the obtained oil volume fraction is only 35.8 %, compared to 98.5 % for the highest flow rate 40 m^3/h. By displacing at 30 m^3/h, a volume fraction of 94.8 % is obtained which is close to the criterion of 95 %. It appears to be critical to displace with high flow rates, when gas is included in the system.

For methanol displacing oil, the final volume fraction obtained was 100.0 %, and for oil displacing water it was 99.8 %, when flowing at 40 m^3/h. For 6 m^3/h it was 86.23 % for methanol displacing oil, and 72.7 % for oil displacing water, compared to 55.8 % when oil is displacing water, oil and gas. These results show that when gas is included in the system, the displacement process for the jumper becomes less efficient. Experimental data should be obtained for validation of the results.

The volume fractions of gas and water in Table 5.8 show that for low rates, it is easier to remove gas than water, while it for higher rates is hardest to remove gas.

Figure 5.27 and Figure 5.28 are showing volume fractions for oil, water and gas in the pipe, as a function of time. The oil fraction is shown with a red line, water with a blue and gas with a green. The first figure is presenting 6 m^3/h, and the second is presenting 40 m^3/h.

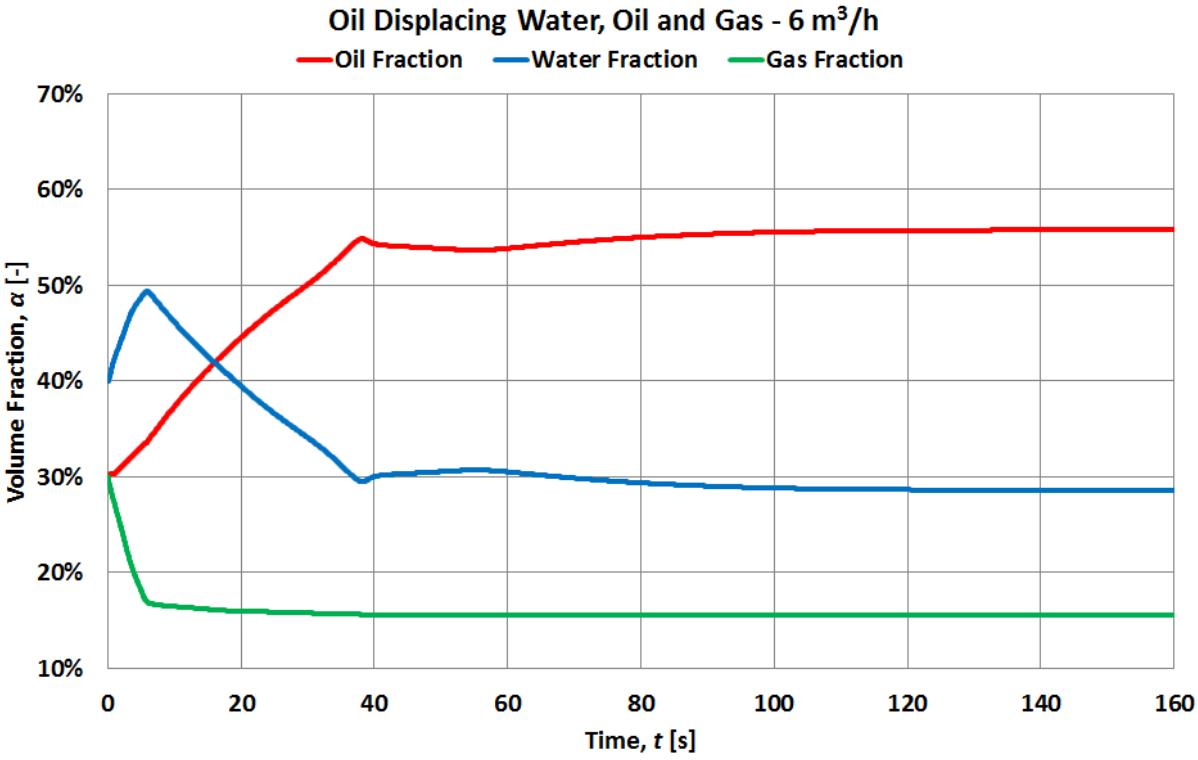

Figure 5.27: Volumes fractions versus time as oil displaces water, oil and gas at 6 m^3/h

Figure 5.27 shows that when oil is entering the system, the water fraction is increasing as the gas fraction is decreasing. When most of the gas is removed, the water fraction starts to decrease. Only a small part of the fluids are removed, and at the end there are still a lot of water and gas left in the system.

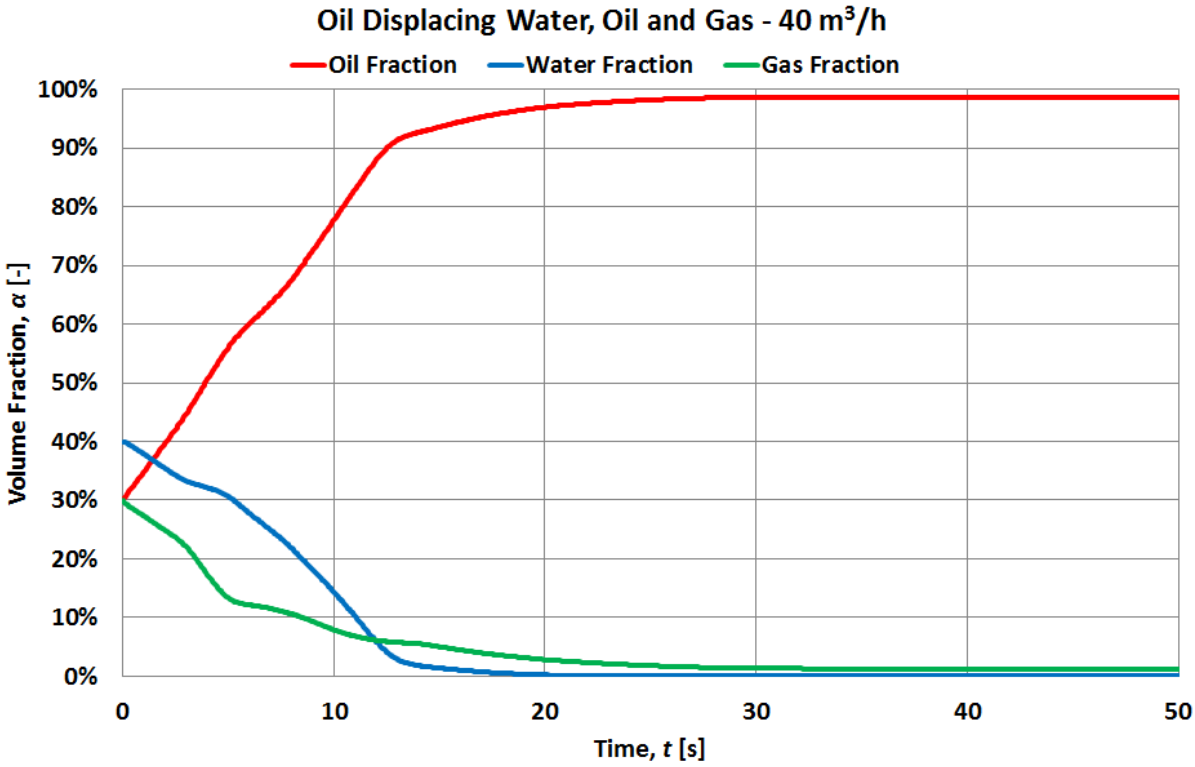

Figure 5.28: Volumes fractions versus time as oil displaces water, oil and gas at 40 m^3/h

Figure 5.28 shows another trend than observed in Figure 5.27. As oil is entering the system, both the water fraction and the gas fraction are starting to decrease. The slope of the gas fraction is less steep, compared to the slope of the water fraction. The water is removed more efficient than the gas is.

5.5.4 Including a Dead-Leg in the Simulation

An extra L-pipe illustrating a dead-leg was added in the lower horizontal section of the U-pipe, trying to simulate how the volume fraction in a dead-leg is changing when the system is displaced.

The results of the system initially filled with water, and then displaced by oil, are presented as oil volume fraction versus time for the different flowrates, in Figure 5.29.

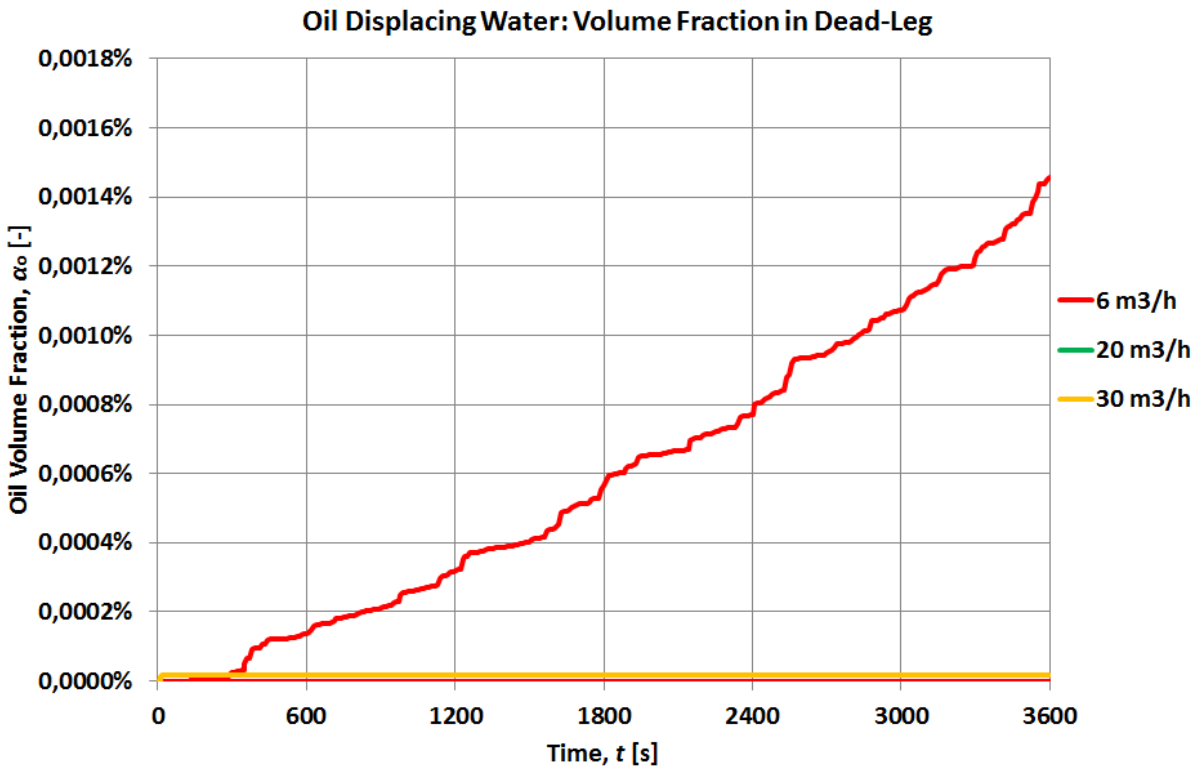

Figure 5.29: Oil volume fraction in the dead-leg versus time for oil displacing water

By studying Figure 5.29, one can see that LedaFlow predicts the oil fractions at all times and for all rates in the dead-leg to be 0 %. The range of the oil volume fraction in the plot is from 0.0000 % to 0.0018 %, and only for 6 m^3/h, is there observed a very small change.

Figure 5.30 is presenting the water volume fraction versus time in the dead-leg for different flow rates, when water is displacing oil.

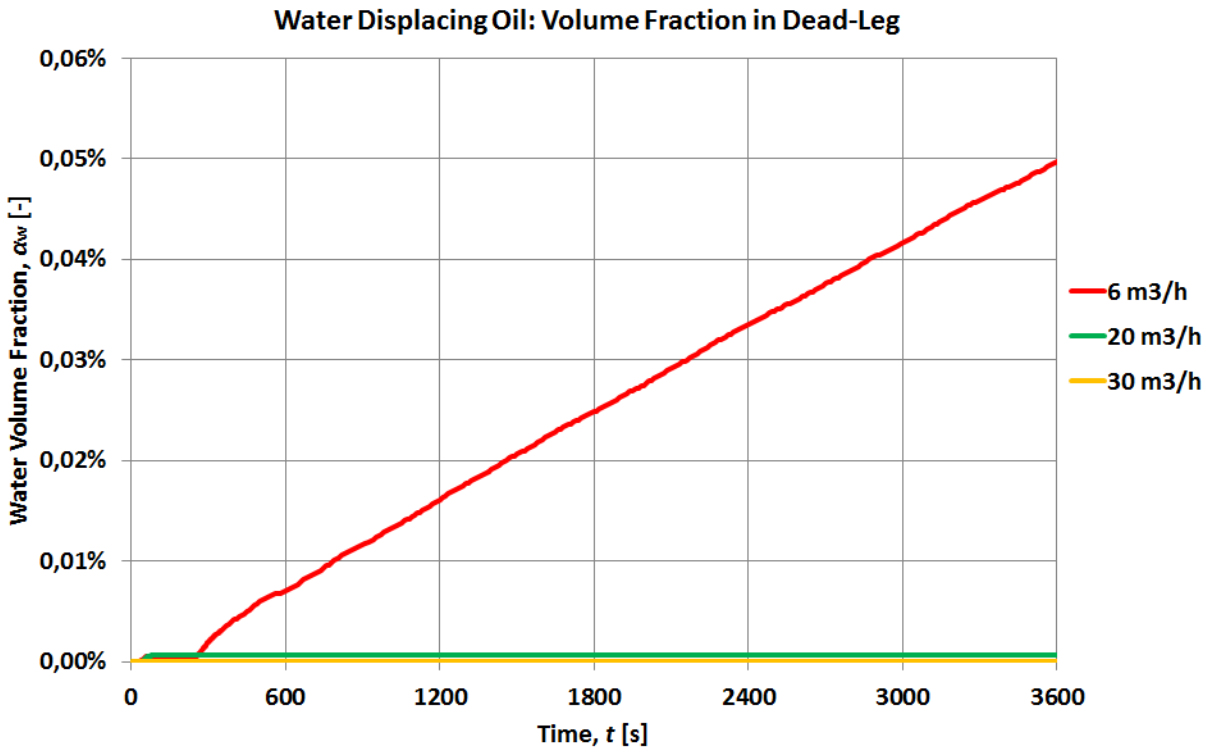

Figure 5.30: Water volume fraction in the dead-leg versus time for water displacing oil

When looking at the plot in Figure 5.30 one can see the same trend as observed for oil displacing water. Only the lowest flow rate of 6 m^3/h gives a visible change in the volume fraction of the displacing fluid. It should be noticed that the range of the volume fraction is from 0.00 % to 0.06 %, which is higher than in Figure 5.29.

It seems like the 1D model in LedaFlow, is not able to capture and simulate changes in the dead-leg connected to the pipe system. An alternative would be to use CFD for the analysis, as presented in the work by Reave and Rolland (2016) on temperature and insulation of dead-legs in connection with manifolds.

6 Conclusion

Based on the experiments and simulations performed in this thesis, the following conclusions have been made:

- For both oil displacing water and water displacing oil, a quick and almost linear increase in the volume fraction of the displacing fluid was seen until approximately one jumper volume was displaced. This is assumed to be due to piston-like displacement until the front is reaching the end of the domain. After one volume displaced, a more curved behavior of the volume fraction is observed. This is most likely due to that the displacing fluid starts to penetrate the other fluid. When 2 to 3 volumes have been displaced, the changes seen in the volume fractions are very small, and it seems like the displacement is stabilizing.
- An increase in the flow rate of the displacing fluid led to an increase in the displacement efficiency, where displacement efficiency is defined as the volume fraction of the displacing fluid.
- The same frequencies were used for both the oil pump and the water pump, but resulted in higher flow rates when water was pumped.
- For oil displacing water, the flow rate 28.16 $m^3/h \pm 1.03$ m^3/h was sufficient for reaching the criterion of a volume fraction of the displacing fluid above 95 %. It resulted in an oil volume fraction of 98.0 % ± 0.1 %, after 2.0 volumes displaced. For water displacing oil the rate 20.77 $m^3/h \pm 0.67$ m^3/h was needed, and resulted in a water volume fraction of 98.6 % ± 0.1 %, after 2.2 volumes displaced.
- The two first volume fraction meters calibrated and tested did not present good results. The third volume fraction meter was tested qualitatively. Electrode pair 1 showed a difference in the average impedance values of approximately 1700 Ω when the pipe was either water filled or oil filled. Electrode pair 2 resulted in water and oil impedance values with a small difference of 0.3 %.
- The model from LedaFlow is in good agreement with the experimentally obtained data. For oil displacing water the average error was 5.5 %, and for water displacing oil it was 5.7 %.

- A comparison of the animation in LedaFlow with pictures from experiments shows similar behaviors in the displacement processes for the real case and the simulation case.
- The models from ANSYS CFX were better at predicting the displacement in the jumper than the model from LedaFlow. For oil displacing water, the inhomogeneous model had an error of 11.2 %, while the model from LedaFlow had 14.3 %. For water displacing oil, the homogeneous model had an error of 3.1 % compared to 11.0 % for LedaFlow. The errors between the results from LedaFlow and the experimental data of Opstvedt (2016) are higher than for the experimental data of present thesis.
- The sensitivity analysis for oil displacing water with varying PVT-properties showed:
    - For water densities higher than the density of the displacing oil, it was observed an exponential decrease in the volume fraction as the water density was increased.
    - No significant changes were seen in the oil volume fraction when neither water viscosity nor the oil viscosity was changed in an interval of ± 40 % of the original value. However, when increasing the oil viscosity 50 times an increase in the displacement efficiency of 5 % was seen.
    - Changes in the interfacial tension showed a linear relationship for the resulting oil volume fractions, with the displacement efficiency decreasing as the interfacial tension increases.
- When simulating methanol displacing oil, it was found that 13.0 m^3/h is an optimal displacing rate and that displacing for 1.5 volumes is an optimal time. More efficient displacements were seen when methanol displaces oil, compared to when oil displaces water, with obtained volume fractions of respectively 86.7 % and 82.6 %.
- From the simulations of oil displacing gas, water and oil, it appears to be critical to use high flow rates for the displacement when gas is included. The highest rate 40 m^3/h resulted in a volume fraction of 98.5 %, compared to 100.0 % for methanol displacing oil and 99.8 % for oil displacing water.
- It was observed that the 1D model in the LedaFlow transient multiphase flow simulator was not suitable for modelling flow in the dead-leg.

7 Recommendations and Further Work

The study of displacement in pipe systems is important for offshore systems and developments. Recommendations for further work are listed below.

- Run experiments using the bottom inlet, and insert a blind flange in the first riser.
- Run more experiments to obtain a larger database with high quality data. Additional tests should be conducted for water displacing oil, for the frequencies that were not tested during this semester.
- Run experiments by testing with other fluids. For example a more viscous oil.
- Continue to work with the volume fraction meter to make the measuring process of volume fractions more automatically. Introduce the conductive principle, by making holes in the experiment pipe for physical contact with the fluid.
- When the flow meter is back from testing, it should be connected to the computer so that the flow rates may be logged digitally while running experiments.
- Simulate flow in dead-leg using a CFD simulator.
- Try simulating the displacement processes using LedaFlow Q3D for simulations in 3D.
- Measure PVT-properties for the fluids that will be used during experiments.
- Change the left elbow of the U-Jumper setup as this part has a leakage. Also, there are some cracks in the main PVC-pipe in the jumper next to the bottom inlet, and this should be changed.

8 References

AntonPaar (2017) *Rheometer: MCR 102, 302, 502*. Available at: http://www.anton-paar.com/us-en/products/details/mcr-rheometer-series/ (Accessed: 31.01.17.

Brauner, N. (2003) 'Liquid-Liquid Two-Phase Flow Systems', in Bertola, V. (ed.) *Modelling and Experimentation in Two-Phase Flow*. Vienna: Springer Vienna, pp. 221-279.

Cagney, T. L., Hare, S. C. and Svedeman, S. J. 'Hydrate Inhibition of Subsea Jumpers During Shut-in', 2006/1/1/. SPE: Society of Petroleum Engineers.

Cai, J., Li, C., Tang, X., Ayello, F., Richter, S. and Nesic, S. (2012) 'Experimental study of water wetting in oil–water two phase flow—Horizontal flow of model oil', *Chemical Engineering Science,* 73, pp. 334-344.

Chen, X., Weibel, J. A. and Garimella, S. V. (2016) 'Continuous Oil–Water Separation Using Polydimethylsiloxane-Functionalized Melamine Sponge', *Industrial & Engineering Chemistry Research,* 55(12), pp. 3596-3602.

Coputational Fluid Dynamics blog (CFD) (2013) 'Tips & Trick: Convergence and Mesh Independence Study'.

Dellecase, E., Mele Solano, S., Lu, H. and Volk, M. 'Hydrate Inhibitor Displacement Experiments in Jumper-Like Pipe Configurations', 2013/6/12/. BHR: BHR Group.

Environment Canada, E. S. a. T. D. 'Diesel Fuel Oil (Canada)'.

ExxonMobil (2005) 'Performance Fluids - Exxsol D60'.

Falcone, G., Hewitt, G. F. and Almonti, C. (2009) *Multiphase Flow Metering.* Elsevier.

FMCTechnologies (2016) *Jumper Spools*. Available at: http://www.fmctechnologies.com/en/SubseaSystems/Technologies/SubseaProductionSystems/TieInAndFlowlines/JumperSpools.aspx (Accessed: 14.12.16.

Fossen, M. 2016. SINTEF. Trondheim.

GeneralElectricCompany (2014) *UNIK 5000 Pressure Sensing Platform*. Available at: https://www.gemeasurement.com/sites/gemc.dev/files/unik_5000_datasheet_english.pdf (Accessed: 18.12.16.

Giavarini, C. and Hester, K. (2011) *Gas Hydrates. Green Energy and Technology* Dordrecht: Springer, p. 97-136.

Kannan, A., Ray, S. and Das, G. (2016) 'Liquid-liquid flow patterns in reduced dimension based on energy minimization approach', *AIChE Journal,* 62(1), pp. 287-294.

Kazemihatami, M. 2013. Experimental study of displacement of viscous oil in pipes by water. Institutt for energi- og prosessteknikk.

Kjølaas, J. Prediction of high viscosity two-phase flows with LedaFlow. SINTEF.

Kolev, N. I. and SpringerLink (2007) *Multiphase Flow Dynamics, 3 : Turbulence, Gas Absorption and Release, Diesel Fuel Properties. Multiphase Flow Dynamics 3 : Turbulence, Gas Absorption and Release, Diesel Fuel Properties* 1st Edition. edn.: Springer Berlin Heidelberg, p. 271-272.

KONGSBERG 2015a. LedaFlow Advanced Transient Multiphase Flow Simulator.

KONGSBERG (2015b) *LedaFlow user manual*.

KONGSBERG 2016a. LedaFlow 2.0 - The Advanced Transient Multiphase Flow Simulator.

KONGSBERG (2016b) 'LedaFlow Getting Started'.

Kvenvolden, K. A. (1988) 'Methane hydrate — A major reservoir of carbon in the shallow geosphere?', *Chemical Geology,* 71(1), pp. 41-51.

Liu, Y., Jiao, W. and Qi, G. (2011) 'Preparation and properties of methanol–diesel oil emulsified fuel under high-gravity environment', *Renewable Energy,* 36(5), pp. 1463-1468.

MaritimConsultants (2017) *Hva er dieseldyr?* Available at: http://maritim.as/norway/hva_er_dieseldyr_/ (Accessed: 30.01.17.

Max, M. D., Johnson, A. H. and Dillon, W. P. (2006) *Economic Geology of Natural Gas Hydrate. Coastal Systems and Continental Margins* Dordrecht: Springer, p. 34, 45.

Merilo, M., Dechene, R. L. and Cichowlas, W. M. (1977) 'Void Fraction Measurement With a Rotating Electric Field Conductance Gauge', *Journal of Heat Transfer,* 99(2), pp. 330-332.

MethanolInstitute (2017) *Physical Properties of Pure Methanol*. Available at: http://www.methanol.org/wp-content/uploads/2016/06/Physical-Properties-of-Pure-Methanol.pdf (Accessed: 19.03.17.

Miljødirektoratet (2015) 'Tillatelse til forbruk og utslipp av kjemikalier i forbindelse med installasjon av havbunnskompressorstasjon på Gullfaksfeltet'.

Miljødirektoratet (2017a) *Olje*. Available at: http://www.norskeutslipp.no/no/Komponenter/Utslipp/Olje/?ComponentType=utslipp&ComponentPageID=78&SectorID=700# (Accessed: 31.05.17.

Miljødirektoratet (2017b) *Oljeholdig vann*. Available at: http://www.norskeutslipp.no/no/Komponenter/Utslipp/Oljeholdig-vann/?ComponentType=utslipp&ComponentPageID=1154&SectorID=700 (Accessed: 31.05.17.

NorwegianEnvironmentAgency (2017) *About us*. Available at: http://www.miljodirektoratet.no/en/About-us/.

Offshore (2016) *Subsea Production Systems Collection*. Tulsa: PennWell Corporation. Available at: http://www.offshore-mag.com/learning-center/subsea/subsea-production-systems/subsea-connectors.html (Accessed: 31.05.17

Opstvedt, J. A. K. 2016. Experiments and Numeric Simulation on Displacement and Flushing of Hydrocarbon Fluid in Subsea Systems. NTNU.

PubChem_Compound_Database (2017) *Methanol*: National Centre for Bitotechnology Information. Available at: https://pubchem.ncbi.nlm.nih.gov/compound/methanol#section=Top (Accessed: 19.03.17.

Reave, K. D. and Rolland, J. 'Temperature prediction in dead-legs of subsea manifolds', *Underwater Technology Conference*, Bergen.

Sain, K. (2008) 'Seismic Methods for Recognition and Evaluation of Gas-Hydrates', *The 12th International Conference of International Association for Computer Methods and Advances in Geomechanics*

Sandstad, J. 2015. impedans - fysikk. *Store Norske Leksikon.*

Schumann, H., Kazemihatemi, M., Yang, Z., Diaz, M. and Nydal, O. J. 'Liquid-Liquid Displacement in a Horizontal and Inclined Pipe Section', 2014/7/9/. BHR: BHR Group.

Sivertsen, Å. 2002. Kontakt-frie målinger av impedans og kapasitans i kjerner. Institutt for petroleumsteknologi og anvendt geofysikk, NTNU.

SulzerPumpesLtd Centrifugal Pump Handbook. Winterthur, Switzerland.

Technip (2014) *Glossary*. Available at: http://www.technip.com/en/media-center/glossary (Accessed: 14.12.16.

TheEngineeringToolbox (2016a) *Emissivity Coefficients of some common Materials*. Available at: http://www.engineeringtoolbox.com/emissivity-coefficients-d_447.html (Accessed: 07.12.16).

TheEngineeringToolbox (2016b) *Modulus of Elasticity or Young's Modulus - and Tensile Modulus for common Materials*. Available at: http://www.engineeringtoolbox.com/young-modulus-d_417.html (Accessed: 07.12.16).

TheEngineeringToolbox (2016c) *Specific Heat of some common Substances*. Available at: http://www.engineeringtoolbox.com/specific-heat-capacity-d_391.html (Accessed: 07.12.16).

TheEngineeringToolbox (2016d) *Thermal Conductivity of common Materials and Gases*. Available at: http://www.engineeringtoolbox.com/thermal-conductivity-d_429.html (Accessed: 07.12.16).

TheEngineeringToolbox (2016e) *Thermal Expansion of PVC, CPVC, Carbon Steel, Stainless Steel and Fiberglass Pipes*. Available at: http://www.engineeringtoolbox.com/thermal-expansion-pvc-d_782.html (Accessed: 07.12.16).

TheEngineeringToolbox (2016f) *Thermoplastics - Physical Properties*. Available at: http://www.engineeringtoolbox.com/physical-properties-thermoplastics-d_808.html (Accessed: 07.12.16).

TheEngineeringToolbox (2017a) *Water - Dynamic and Kinematic Viscosity*. Available at: http://www.engineeringtoolbox.com/water-dynamic-kinematic-viscosity-d_596.html (Accessed: 06.05.2017).

TheEngineeringToolbox (2017b) *Water - Thermodynamic Properties*. Available at: http://www.engineeringtoolbox.com/water-thermal-properties-d_162.html (Accessed: 06.05.17).

TheEngineeringToolbox_A (2017) *Methane*. Available at: http://www.engineeringtoolbox.com/methane-d_1420.html (Accessed: 18.03.17.

Thomas, M. (2010) 'Subsea Developments Key To Future Production', pp. 34-36.

Wischnewski, B. (2017a) *Calculation of thermodynamic state variables of methane*: PeaceSoftware. Available at: http://www.peacesoftware.de/einigewerte/calc_methan.php5 (Accessed: 19.03.17.

Wischnewski, B. (2017b) *Calculation of thermodynamic state variables of water*: Peace Software. Available at: http://www.peacesoftware.de/einigewerte/calc_dampf.php5 (Accessed: 19.03.17.

Xu, G.-L., Zhang, G.-Z., Liu, G., Ullmann, A. and Brauner, N. (2011) 'Trapped water displacement from low sections of oil pipelines', *International Journal of Multiphase Flow,* 37(1), pp. 1-11.

Zhai, L., Jin, N., Zong, Y., Wang, Z. and Gu, M. (2012) 'The development of a conductance method for measuring liquid holdup in horizontal oil–water two-phase flow'.

Øren, H. M. and Christensen, B. A. 2016. Vedtak om tillatelse til utslipp ved tømming av rørledning på Vigdis - Statoil Petroleum AS. Oslo: Miljødirektoratet.

Appendixes

Appendix A Measured Volumes during Experiments

Appendix A consists of tables showing measured volumes during experiments run in the lab. An excel file with the data is included in the digital appendix.

FREQUENCY	10,50	Hz			OIL DISPLACING WATER (~6 m3/h)					
Date	02.05.2017		02.05.2017		02.05.2017		02.05.2017		04.05.2017	
Experiment # this day	#1		#2		#3		#4		#2	
Time [s]	105		209		314		70		35	
Bucket#	V_w	V_o	V_w	V_o	V_w	V_o	V_w	V_o	V_w	V_o
1	9,9	0	10,15	0	10	0	9,95	0	11,55	0
2	9,6	0	9,9	0	9,8	0	9,6	0	9,9	0
3	10,3	0	9,2	0	9,8	0	9,2	0	10,3	0
4	10,2	0	9,75	0	10,15	0	10	0	10,4	0
5	10,25	0	10,1	0	10,5	0,1	9,9	0	9,9	0
6	10,5	0	5,2	4,2	2,05	7,95	10,25	0	10,25	0
7	4	5,1	0,7	9,5	0,1	9,7	9,9	0	10,2	0
8	0,4	9,4	0	10	0	10,05	10	0	10,4	0
9	0	10,1	0	9,95	0	9,6	6,9	3,25	10,85	0
10	0	9,75	0	9,9	0	9,9	0,45	9,85	9,9	0
11	0	10,1	0	10	0	10	0	10,4	10,45	0
12	0	9,7	0	9,75	0	9,2	0	9,7	10,05	0
13	0	10,3	0	9,85	0	10,05	0	10,2	1,05	9
14	0	10,25	0	9,3	0	9,6	0	9,7	0	10,3
15	0	9,9	0	9,65	0	9,6	0	10,15	0	10
16	0	10	0	9,95	0	10,15	0	9,5	0	10,95
17	0	6,1	0	8,6	0	7	0	6,2	0	0
Tot oil/water volume	65,15	100,7	55	110,65	52,4	112,9	86,15	78,95	125,2	40,25
Tot volum	165,85		165,65		165,3		165,1		165,45	
Volume Fraction	60,72 %		66,80 %		68,30 %		47,82 %		24,33 %	

Figure A.1: Measured volumes for oil displacing water at f = 10.50 Hz

FREQUENCY	13,50	Hz			OIL DISPLACING WATER (~10 m3/h)					
Date					27.04.2017		08.05.2017		08.05.2017	
Experiment # this day					#2		#1		#2	
Time [s]	63		125		188		23		45	
Bucket#	Vw	Vo	Vw	Vo	Vw	Vo	Vw	Vo	Vw	Vo
1	10,00	0,00	11,00	0,00	10,50	0,00	9,8	0	9,75	0
2	10,00	0,00	9,30	0,00	10,10	0,00	9,95	0,00	10,20	0
3	10,00	0,00	9,70	0,00	9,80	0,00	9,70	0,00	9,35	0
4	10,00	0,00	8,40	1,40	6,20	3,70	9,80	0,00	9,60	0
5	9,60	0,50	0,25	9,65	1,40	8,40	10,40	0,00	9,80	0
6	0,70	9,50	0,30	10,20	0,25	10,30	9,85	0,00	9,60	0
7	0,00	9,85	0,00	10,00	0,00	10,20	9,60	0,00	9,60	0
8	0,00	10,05	0,00	10,60	0,00	9,90	9,90	0,00	2,90	6,3
9	0,00	10,30	0,00	10,55	0,00	10,85	9,60	0,00	0,10	8,85
10	0,00	10,15	0,00	10,05	0,00	9,90	9,70	0,00	0,00	9,6
11	0,00	10,40	0,00	9,95	0,00	10,55	9,85	0,00	0,00	10,2
12	0,00	10,15	0,00	8,90	0,00	10,00	9,65	0,90	0,00	9,9
13	0,00	9,90	0,00	9,45	0,00	9,85	0,25	9,60	0,00	9,3
14	0,00	9,90	0,00	9,60	0,00	9,70	0,00	9,80	0,00	9,95
15	0,00	10,10	0,00	9,10	0,00	9,95	0,00	9,80	0,00	10,1
16	0,00	7,15	0,00	9,80	0,00	8,00	0,00	9,70	0,00	10,3
17	0,00	7,70	0,00	7,85	0,00	7,00	0	9,05	0	8,2
Tot oil/water volume	50,3	115,65	38,95	127,1	38,25	128,3	118,05	48,85	70,9	92,7
Tot volum	165,95		166,05		166,55		166,9		163,6	
Volume Fraction	69,69 %		76,54 %		77,03 %		29,27 %		56,66 %	

Figure A.2: Measured volumes for oil displacing water at f = 13.50 Hz

FREQUENCY	24,50	Hz			OIL DISPLACING WATER (~20 m3/h)					
Date	03.05.2017		03.05.2017		03.05.2017		03.05.2017		03.05.2017	
Experiment # this day	#1		#2		#3		#4		#5	
Time [s]	31		63		94		20		11	
Bucket#	Vw	Vo	Vw	Vo	Vw	Vo	Vw	Vo	Vw	Vo
1	9,4	0	10,3	0,4	9,7	1,2	9,6	0	9,4	0
2	10,2	0	2,8	7,25	2	7,9	9,7	0	10,2	0
3	6,8	2,1	0	10,05	0	9,75	9,7	0	9,55	0
4	0,8	8,9	0	10,25	0	10,1	10,2	0	9,9	0
5	0,25	9,95	0	10,15	0	10,5	10,7	0	10,55	0
6	0	10,3	0	10,9	0	10,25	3	7,15	10,2	0
7	0	10,4	0	10	0	9,65	0	10,6	10,15	0
8	0	10,45	0	10,35	0	9,6	0	10,15	10,2	0
9	0	11,15	0	9,5	0	10,4	0	10	10,3	0
10	0	10	0	10,3	0	10,2	0	9,5	8,85	1,85
11	0	9,9	0	10,05	0	10,3	0	9,75	0,2	9,8
12	0	10,45	0	9,75	0	9,45	0	9,25	0	9,55
13	0	9,8	0	9,95	0	10	0	9,8	0	10,25
14	0	9,2	0	9,9	0	9,95	0	10	0	10,5
15	0	10,2	0	9	0	9,05	0	9,9	0	10
16	0	9	0	8,15	0	10,35	0	9,45	0	9,5
17	0	6,3	0	6,8	0	5,7	0	6,55	0	4,2
Tot oil/water volume	27,45	138,1	13,1	152,75	11,7	154,35	52,9	112,1	99,5	65,65
Tot volum	165,55		165,85		166,05		165		165,15	
Volume Fraction	83,42 %		92,10 %		92,95 %		67,94 %		39,75 %	

Figure A.3: Measured volumes for oil displacing water at f = 24.50 Hz

FREQUENCY	34,00	Hz			OIL DISPLACING WATER	(~30 m3/h)				
Date	05.05.2017		05.05.2017		05.05.2017		05.05.2017		08.05.2017	
Experiment # this day	#4		#3		#2		#1		#3	
Time [s]	21		42		64		9		14	
Bucket#	Vw	Vo	Vw	Vo	Vw	Vo	Vw	Vo	Vw	Vo
1	9,9	0	3,35	6,85	1,55	8,9	9,7	0	9,5	0
2	5,95	4	0	9,85	0	10,15	10,3	0	9,75	0
3	0,75	9,3	0	10,5	0	9,85	9,75	0	9,4	0
4	0	10,3	0	10,2	0	9,45	10,1	0	9,15	0
5	0	9,8	0	10,75	0	10,05	10,05	0	9,4	0
6	0	10,1	0	10	0	9,7	9,3	0	6,05	4,15
7	0	10,2	0	9,75	0	10	9,1	0	0,9	8,5
8	0	10	0	9,7	0	9,6	9,65	0	0	9,9
9	0	10	0	10,4	0	10,3	9,7	0	0	9,95
10	0	10,1	0	10,05	0	10	8,75	0	0	9,8
11	0	9,55	0	10,1	0	10,15	3,4	7,2	0	9,9
12	0	9,3	0	10,9	0	10	0	10,2	0	9,9
13	0	9,75	0	10,25	0	9,75	0	9,95	0	9,1
14	0	9,9	0	9,6	0	10,1	0	10	0	9,25
15	0	9,2	0	10,15	0	10,35	0	10,15	0	9,7
16	0	9,5	0	10	0	10,3	0	10,05	0	10
17	0	5,9	0	2,9	0	5,7	0	6,7	0	10,3
Tot oil/water volume	16,6	146,9	3,35	161,95	1,55	164,35	99,8	64,25	54,15	110,45
Tot volum	163,5		165,3		165,9		164,05		164,6	
Volume Fraction	89,85 %		97,97 %		99,07 %		39,16 %		67,10 %	

Figure A.4: Measured volumes for oil displacing water at f = 34.00 Hz

FREQUENCY	44,40	Hz			OIL DISPLACING WATER	(~40 m3/h)				
Date	26.04.2017				04.05.2017		04.05.2017		04.05.2017	
Experiment # this day					#1		#3		#4	
Time [s]	16		31		48		6		13	
Bucket#	Vw	Vo	Vw	Vo	Vw	Vo	Vw	Vo	Vw	Vo
1	9,00	1,20	0,60	9,30	0,90	9,60	9,8	0	10	0
2	1,30	9,00	0,00	10,45	0,00	10,95	10,10	0	10,25	0,00
3	0,00	10,30	0,00	10,45	0,00	10,20	9,70	0	10,50	0,00
4	0,00	9,90	0,00	10,10	0,00	10,40	10,40	0	10,00	0,00
5	0,00	10,00	0,00	10,45	0,00	10,30	10,20	0	4,00	6,30
6	0,00	10,45	0,00	10,00	0,00	10,30	10,15	0	0,40	9,50
7	0,00	10,25	0,00	10,10	0,00	10,15	10,60	0	0,00	10,20
8	0,00	10,40	0,00	10,10	0,00	10,45	9,65	0	0,00	10,00
9	0,00	10,00	0,00	9,90	0,00	10,30	8,65	0	0,00	10,40
10	0,00	10,40	0,00	10,40	0,00	10,30	4,10	6,3	0,00	9,85
11	0,00	10,45	0,00	10,60	0,00	9,85	0,00	10,35	0,00	10,10
12	0,00	10,80	0,00	9,90	0,00	10,65	0,00	10,7	0,00	10,15
13	0,00	10,35	0,00	10,15	0,00	10,10	0,00	9,75	0,00	9,20
14	0,00	10,40	0,00	10,15	0,00	11,00	0,00	9,5	0,00	9,40
15	0,00	10,90	0,00	10,25	0,00	9,70	0,00	9,9	0,00	9,20
16	0,00	11,20	0,00	9,50	0,00	8,55	0,00	9,45	0,00	9,70
17	0,00	0,00	0,00	0,00	0,00	2,10	0	5	0	4,85
Tot oil/water volume	10,3	156	0,6	161,8	0,9	164,9	93,35	70,95	45,15	118,85
Tot volum	166,3		162,4		165,8		164,3		164	
Volume Fraction	93,81 %		99,63 %		99,46 %		43,18 %		72,47 %	

Figure A.5: Measured volumes for oil displacing water at f = 44.40 Hz

FREQUENCY	10,50	Hz			WATER DISPLACING OIL	(~6 m3/h)				
Date	10.05.2017		10.05.2017		10.05.2017		09.05.2017		08.05.2017	
Experiment # this day	#4		#3		#1		#2		#5	
Time [s]	37		72		106		209		314	
Bucket#	V_w	V_o	V_w	V_o	V_w	V_o	V_w	V_o	V_w	V_o
1	9,7	0	9,95	0	10,4	0	9,9	0	10,1	0
2	9,8	0	9,9	0	10,05	0	9,85	0	9,75	0
3	9,6	0	9,5	0	9,8	0	10,1	0	9,75	0
4	9,4	0	9,2	0	9,65	0	9,9	0	10,25	0
5	9,6	0	9,5	0	9,75	0	10,5	0	9,8	0
6	9,1	0,9	9,1	0	10	0	10	0	10,1	0
7	4,4	5,8	9,4	0	9,4	0	10,1	0	9,55	0
8	0	9,4	9,9	0	9,8	0	10,4	0	9,9	0
9	0	10,1	10,2	0	9,75	0	10,05	0	10,2	0
10	0	9,9	10,15	0	9,6	0	10,2	0	10	0
11	0	10,1	9,45	0	10,4	0	10	0	9,75	0
12	0	10,3	10,15	0	9,6	0	9,5	0	9,9	0
13	0	10,55	6	4	9,4	0	9,15	0	9,7	0
14	0	10,1	0	10	9,85	0	9,5	0	9,5	0
15	0	10,2	0	10,2	5,15	4,75	2,4	6,45	4,6	7,05
16	0	9,75	0	10,95	0	10,3	0	8,9	0	9,6
17	0	5,9	0	6,95	0	7,4	0	7,4	0	4,2
Tot oil/water volume	61,6	103	122,4	42,1	142,6	22,45	141,55	22,75	142,85	20,85
Tot volum	164,6		164,5		165,05		164,3		163,7	
Volume Fraction	37,42 %		74,41 %		86,40 %		86,15 %		87,26 %	

Figure A.6: Measured volumes for water displacing oil at f = 10.50 Hz

FREQUENCY	24,50	Hz			WATER DISPLACING OIL	(~20 m3/h)				
Date	09.05.2017		10.05.2017		08.05.2017		09.05.2017		09.05.2017	
Experiment # this day	#4		#2		#4		#3		#1	
Time [s]	11		21		32		63		95	
Bucket#	V_w	V_o	V_w	V_o	V_w	V_o	V_w	V_o	V_w	V_o
1	9,4	0	10	0	9,6	0	10	0	9,7	0
2	10,2	0	9,6	0	9,5	0	9,4	0	10,25	0
3	9,7	0	9,75	0	10,2	0	9,25	0	10,2	0
4	10,15	0	9,85	0	11,1	0	9,8	0	10,45	0
5	9,7	0	10	0	10,1	0	9,95	0	10,2	0
6	9,2	0	10	0	10,8	0	10	0	10	0
7	10,1	0,4	9,9	0	10,5	0	10,05	0	10,15	0
8	1,2	9,55	9,6	0	10,65	0	10	0	10,2	0
9	0	9,05	10,25	0	10	0	10,4	0	10,1	0
10	0	9,15	9,3	0	10,75	0	9,9	0	10,55	0
11	0	9,05	9,65	0	10,75	0	9,4	0	10,3	0
12	0	9,6	4	5,75	9,9	0	9,7	0	10,4	0
13	0	9,4	0	9,9	10,1	0	9,6	0	9,8	0
14	0	9,7	0	9,9	9,5	0	9,5	0	9,5	0
15	0	9,4	0	10	9,25	1,55	10,05	0	9,25	0
16	0	10,25	0	9,8	0	11,05	9,55	0	9,15	0
17	0	9,55	0	7,3	0	1,1	4,7	2,85	1,1	2,25
Tot oil/water volume	69,65	95,1	111,9	52,65	152,7	13,7	161,25	2,85	161,3	2,25
Tot volum	164,75		164,55		166,4		164,1		163,55	
Volume Fraction	42,28 %		68,00 %		91,77 %		98,26 %		98,62 %	

Figure A.7: Measured volumes for water displacing oil at f = 24.50 Hz

Appendix B Results from Volume Fraction Meters

Appendix B consists of the results from the tests of the volume fraction meters.

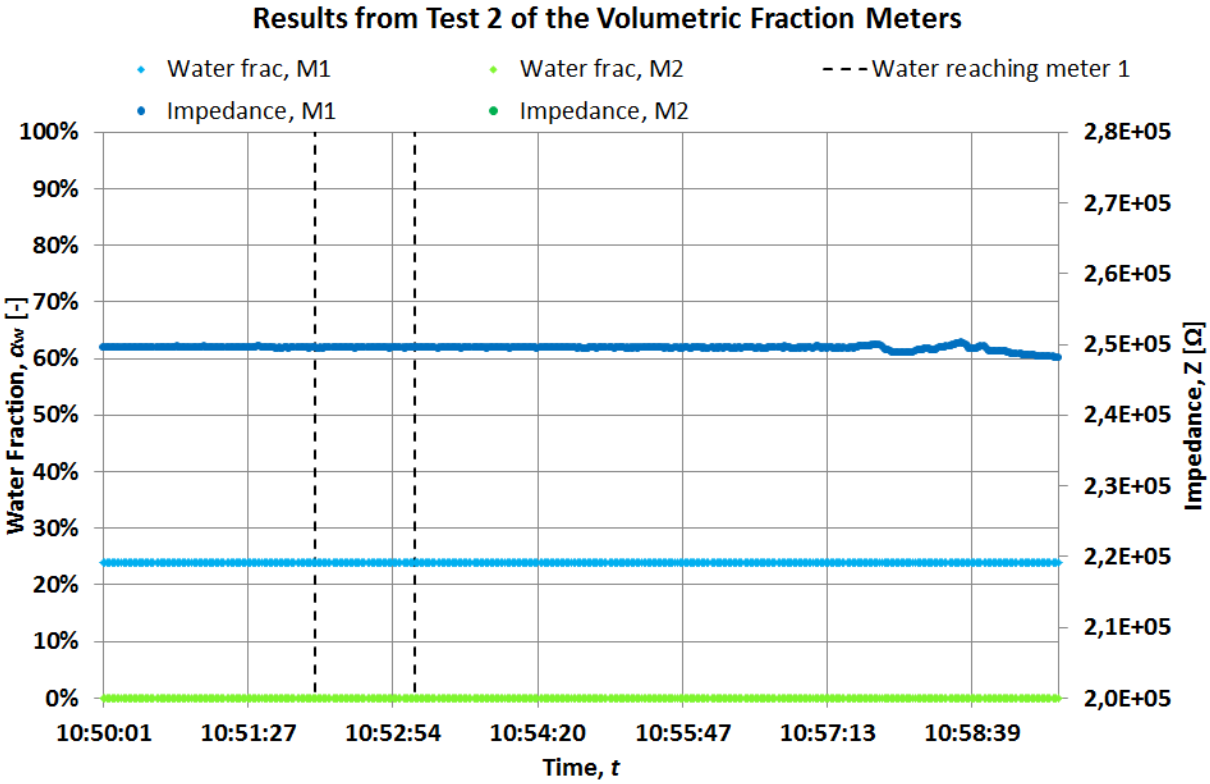

Figure B.1: Results from the volume fraction meters - test 2, 20 m3/h (21 s)

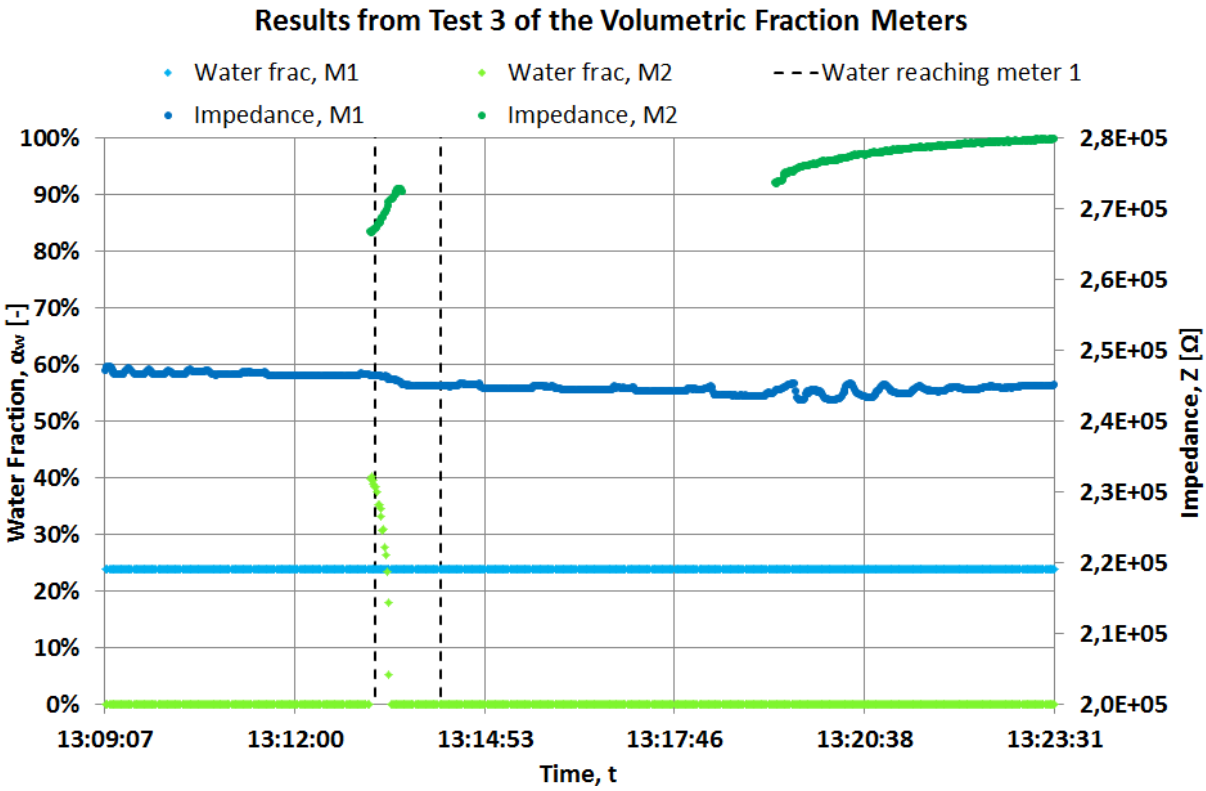

Figure B.2: Results from the volume fraction meters - test 3, 6 m3/h (72 s)

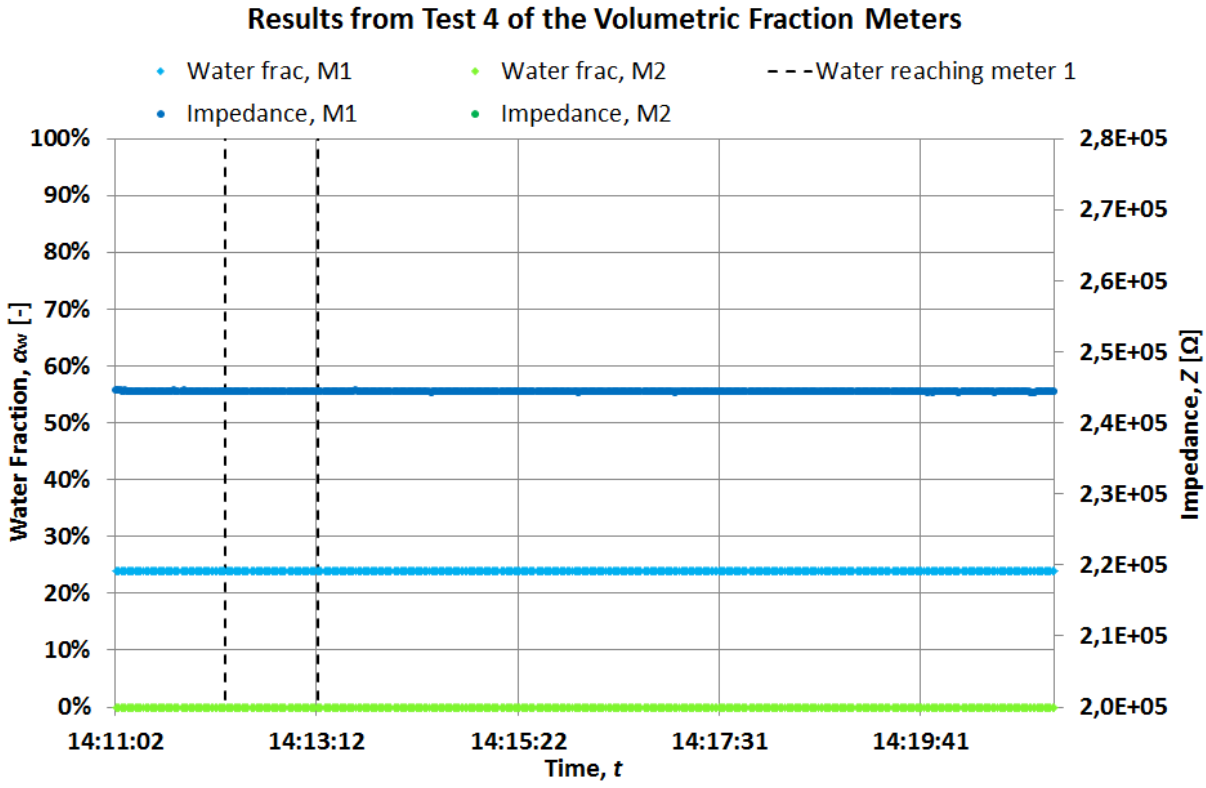

Figure B.3: Results from the volume fraction meters - test 4, 6 m3/h (37 s)

Appendix C Risk Assessment

Detaljert Risikorapport

ID	12339	**Status**	**Dato**
Risikoområde	Risikovurdering: Helse, miljø og sikkerhet (HMS)	Opprettet	09.09.2016
Opprettet av	Hanne Gjerstad Folde	Vurdering startet	09.09.2016
Ansvarlig	Hanne Gjerstad Folde	Tiltak besluttet	
		Avsluttet	01.06.2017

Risikovurdering:

Risk Assesment for Displacement Rig in the Laboratory Hall at the Department of Geoscience and Petroleum

Gyldig i perioden:

-

Sted:

4 - Sydområdet / 442 - PTS, hallbygg / 1010 - 1. etasje

Mål / hensikt

Målet med prosjektet er å se på fortrengning av hydrokarboner i rørsystemer.
Denne risikovurderingen er skrevet mtp å unngå farlige og uønskede situasjoner som kan være til skade for mennesker eller omgivelser. Prosjektet involverer store mengder Exxsol D60 og til dels store og tunge deler. Endringer i oppsettet av ustyr i hallen, gjør at deler av rig-en må ombygges.

Bakgrunn

Krav fra NTNU sier at en risikovurdering skal gjennomføres ved forsøk som kan innebære en risiko for helse, miljø og sikkerhet.

Beskrivelse og avgrensninger

Exxsol D60 er et brannfarlig stoff, og som kan være giftig ved inntak. Det er derfor nødvendig å planlegge HMS rundt håndtering av væsken under forsøkene, og dersom uventene situasjoner skulle oppstå. Siden deler av utstyret i hallen skal bygges om, inkludert denne rig-en, vil en del av arbeidet medføre løfting/håndtering av noen tyngre deler. Det er viktig å planlegge riktig verneustyr for dette arbeidet.
Denne risikovurderingen er avgrenset til håndtering av Exxsol D60 under forsøkene og til byging av en ny del til rig-en.

Forutsetninger, antakelser og forenklinger

Risikovurderingen er basert på tiltak og farer beskrevet i databladet til Exxsol D60. I tillegg er det vurdert mulige situasjoner som kan oppstå i frobindelse med bygging a nytt oppsett og tenkte scenarioer for Exxsol D60.

Vedlegg

[Ingen registreringer]

Referanser

[Ingen registreringer]

Oppsummering, resultat og endelig vurdering

I oppsummeringen presenteres en oversikt over farer og uønskede hendelser, samt resultat for det enkelte konsekvensområdet.

Farekilde: **ExxsolD60**

Uønsket hendelse: **Lekkasje av Exxsol D60**

Konsekvensområde:		
	Helse	Risiko før tiltak: Risiko etter tiltak:
	Ytre miljø	Risiko før tiltak: Risiko etter tiltak:
	Materielle verdier	Risiko før tiltak: Risiko etter tiltak:
	Omdømme	Risiko før tiltak: Risiko etter tiltak:

Uønsket hendelse: **Brann utløst av Exxsol D60**

Konsekvensområde:		
	Helse	Risiko før tiltak: Risiko etter tiltak:
	Ytre miljø	Risiko før tiltak: Risiko etter tiltak:
	Materielle verdier	Risiko før tiltak: Risiko etter tiltak:

Farekilde: **Tunge deler**

Uønsket hendelse: **Føtter klemstret av tunge deler.**

Konsekvensområde:		
	Helse	Risiko før tiltak: Risiko etter tiltak:
	Materielle verdier	Risiko før tiltak: Risiko etter tiltak:

Farekilde: **Tildekking av brannslange og brannslukkingsapprat**

Uønsket hendelse: **Uønsket hendelse: Vanskelig framkomst til brannslange og brannslukkingsapparat**

Konsekvensområde:		
	Helse	Risiko før tiltak: Risiko etter tiltak:
	Ytre miljø	Risiko før tiltak: Risiko etter tiltak:
	Materielle verdier	Risiko før tiltak: Risiko etter tiltak:
	Omdømme	Risiko før tiltak: Risiko etter tiltak:

Endelig vurdering

Vurderingen er av generell art, med tanke på fortrengningseksperimenter som gjøres i hallen. Personer bør sette seg inn i risikovurderingen og hvilke hensyn som skal tas før de begynner forsøkene.

Involverte enheter og personer

En risikovurdering kan gjelde for en, eller flere enheter i organisasjonen. Denne oversikten presenterer involverte enheter og personell for gjeldende risikovurdering.

Enhet /-er risikovurderingen omfatter

- Institutt for geovitenskap og petroleum

Deltakere

[Ingen registreringer]

Lesere

[Ingen registreringer]

Andre involverte/interessenter

[Ingen registreringer]

Følgende akseptkriterier er besluttet for risikoområdet Risikovurdering: Helse, miljø og sikkerhet (HMS):

Helse	Materielle verdier	Omdømme	Ytre miljø

Oversikt over eksisterende, relevante tiltak som er hensyntatt i risikovurderingen

I tabellen under presenteres eksisterende tiltak som er hensyntatt ved vurdering av sannsynlighet og konsekvens for aktuelle uønskede hendelser.

Farekilde	Uønsket hendelse	Tiltak hensyntatt ved vurdering
ExxsolD60	Lekkasje av Exxsol D60	Gassmaske
	Lekkasje av Exxsol D60	Verneustyr
	Lekkasje av Exxsol D60	Trykk-kontroll
	Lekkasje av Exxsol D60	Tette/unngå lekkasjer
	Brann utløst av Exxsol D60	Gassmaske
	Brann utløst av Exxsol D60	Verneustyr
	Brann utløst av Exxsol D60	Trykk-kontroll
	Brann utløst av Exxsol D60	Tette/unngå lekkasjer
Tunge deler	Føtter klemstret av tunge deler.	Verneustyr
Tildekking av brannslange og brannslukkingsapprat	Uønsket hendelse: Vanskelig framkomst til brannslange og brannslukkingsapparat	Tette/unngå lekkasjer

Eksisterende og relevante tiltak med beskrivelse:

Gassmaske

I forbindelse med liming av deler vil det brukes PVC-lim som ikke er anbefalt å puste inn. Heller ikke er det anbefalt å puste inn Exxsol D60 over lengre perioder. Som tiltak brukes derfor gassmaske, for å hindre innpusting av farlige gasser.

Verneustyr

For å unngå skader på mennesker skal det i forbindelse med både bygging av rig og under håndtering av forsøkene brukes passenede verneustyr. Dette innebærer bruk av vernesko, kjeledress, vernebriller og hjelm.

Trykk-kontroll

Da det er mulig for systemet å bygge opp en del trykk, er det installert ulike trykksensorer rundt om for å følge med på trykket. I tillegg er det lufteventiler slik at trykket kan slippes ut.

Tette/unngå lekkasjer

[Ingen registreringer]

Risikoanalyse med vurdering av sannsynlighet og konsekvens

I denne delen av rapporten presenteres detaljer dokumentasjon av de farer, uønskede hendelser og årsaker som er vurdert. Innledningsvis oppsummeres farer med tilhørende uønskede hendelser som er tatt med i vurderingen.

Følgende farer og uønskede hendelser er vurdert i denne risikovurderingen:

- **ExxsolD60**
  - Lekkasje av Exxsol D60
  - Brann utløst av Exxsol D60
- **Tunge deler**
  - Føtter klemstret av tunge deler.
- **Tildekking av brannslange og brannslukkingsapprat**
  - Uønsket hendelse: Vanskelig framkomst til brannslange og brannslukkingsapparat

Detaljert oversikt over farekilder og uønskede hendelser:

Farekilde: ExxsolD60

Kan utsettes for en del lukt for oljen som ikke er så bra over lengre tid.
I tillegg utgjør olje en stor brannkilde.

Uønsket hendelse: Lekkasje av Exxsol D60

Sannsynlighet for hendelsen (felles for alle konsekvensområder): **Lite sannsynlig (2)**

Kommentar:
[Ingen registreringer]

Konsekvensområde: Helse ***Risiko:***

Vurdert konsekvens: **Liten (1)**

Kommentar: [Ingen registreringer]

Konsekvensområde: Ytre miljø ***Risiko:***

Vurdert konsekvens: **Middels (2)**

Kommentar: [Ingen registreringer]

Konsekvensområde: Materielle verdier ***Risiko:***

Vurdert konsekvens: **Liten (1)**

Kommentar: [Ingen registreringer]

Konsekvensområde: Omdømme ***Risiko:***

Vurdert konsekvens: **Middels (2)**

Kommentar: [Ingen registreringer]

Uønsket hendelse: Brann utløst av Exxsol D60

Produktet kan akkumulere statisk elektrisitet som kan forårsake antennelse. Produktet kan avgi damper som lett kan danne brannfarlige blandinger. Dampansamlingen kan brenne eller eksplodere ved antennelse. Brennbart

Sannsynlighet for hendelsen (felles for alle konsekvensområder): **Svært lite sannsynlig (1)**

Kommentar:

[Ingen registreringer]

Konsekvensområde: Helse ***Risiko:***

Vurdert konsekvens: **Middels (2)**

Kommentar: [Ingen registreringer]

Konsekvensområde: Ytre miljø ***Risiko:***

Vurdert konsekvens: **Liten (1)**

Kommentar: [Ingen registreringer]

Konsekvensområde: Materielle verdier ***Risiko:***

Vurdert konsekvens: **Middels (2)**

Kommentar: [Ingen registreringer]

Farekilde: Tunge deler

Ventiler o.l. kan være ganske tunge.

Uønsket hendelse: Føtter klemstret av tunge deler.

Noen av delene er tyngre og bør håndteres med varmsomhet, slik at de ikke glippes og treffer uønskede punkter.

Sannsynlighet for hendelsen (felles for alle konsekvensområder): **Lite sannsynlig (2)**

Kommentar:
[Ingen registreringer]

Konsekvensområde: Helse ***Risiko:***

Vurdert konsekvens: **Middels (2)**

Kommentar: [Ingen registreringer]

Konsekvensområde: Materielle verdier ***Risiko:***

Vurdert konsekvens: **Liten (1)**

Kommentar: [Ingen registreringer]

Farekilde: Tildekking av brannslange og brannslukkingsapprat

Uønsket hendelse: Uønsket hendelse: Vanskelig framkomst til brannslange og brannslukkingsapparat

Det er mye utstyr nede i hallen, så viktig å passe på at ikke gjenstander (og spesielt store gjenstander) plasseres foran brannslange og brannslukkingspparat.

Sannsynlighet for hendelsen (felles for alle konsekvensområder): **Svært lite sannsynlig (1)**

Kommentar:

[Ingen registreringer]

Konsekvensområde: Helse ***Risiko:***

Vurdert konsekvens: **Middels (2)**

Kommentar: [Ingen registreringer]

Konsekvensområde: Ytre miljø ***Risiko:***

Vurdert konsekvens: **Liten (1)**

Kommentar: [Ingen registreringer]

Konsekvensområde: Materielle verdier ***Risiko:***

Vurdert konsekvens: **Middels (2)**

Kommentar: [Ingen registreringer]

Konsekvensområde: Omdømme ***Risiko:***

Vurdert konsekvens: **Liten (1)**

Kommentar: [Ingen registreringer]

Oversikt over besluttede risikoreduserende tiltak:

Under presenteres en oversikt over risikoreduserende tiltak som skal bidra til å reduseres sannsynlighet og/eller konsekvens for uønskede hendelser.

Detaljert oversikt over besluttede risikoreduserende tiltak med beskrivelse:

Detaljert oversikt over vurdert risiko for hver farekilde/uønsket hendelse før og etter besluttede tiltak

Appendix D Datasheets for Instrumentation

D-1 Pumps

F **50 Hz n= 2900 rpm**

Standardised "EN 733" centrifugal pumps

Clean water

Industrial use

PERFORMANCE RANGE

- Flow rate up to **6000 l/min** (360 m^3/h)
- Head up to **98 m**

APPLICATION LIMITS

- Manometric suction lift up to **7 m**
- Liquid temperature between **-10 °C** and **+90 °C**
- Ambient temperature between **-10 °C** and **+40 °C**
- Max. pressure in pump body **10 bar** (PN10)
- Continuous service **S1**

CONSTRUCTION AND SAFETY STANDARDS

EN 60335-1
IEC 60335-1
CEI 61-150

EN 60034-1
IEC 60034-1
CEI 2-3

CE

Pump body dimensions in compliance with **EN 733**

EU REGULATION N. 547/2012

CERTIFICATIONS

Company with management system certified DNV
ISO 9001: QUALITY
ISO 14001: ENVIRONMENT

EAC

INSTALLATION AND USE

- Water supply
- Pressure boosting
- Irrigation
- Water circulation in air-conditioning units
- Cleaning sets
- Firefighting sets
- Industrial applications
- Agricultural applications

The pump should be installed in an enclosed environment or sheltered from inclement weather.

OPTIONS AVAILABLE ON REQUEST

- Counter flange KIT complete with bolts, nuts and washers
- Special mechanical seal
- Other voltages or 60 Hz frequency
- Compatibility with hotter or colder liquids
- Compatibility with hotter or colder environments

134

PERFORMANCE RANGE

50 Hz n= 2900 rpm

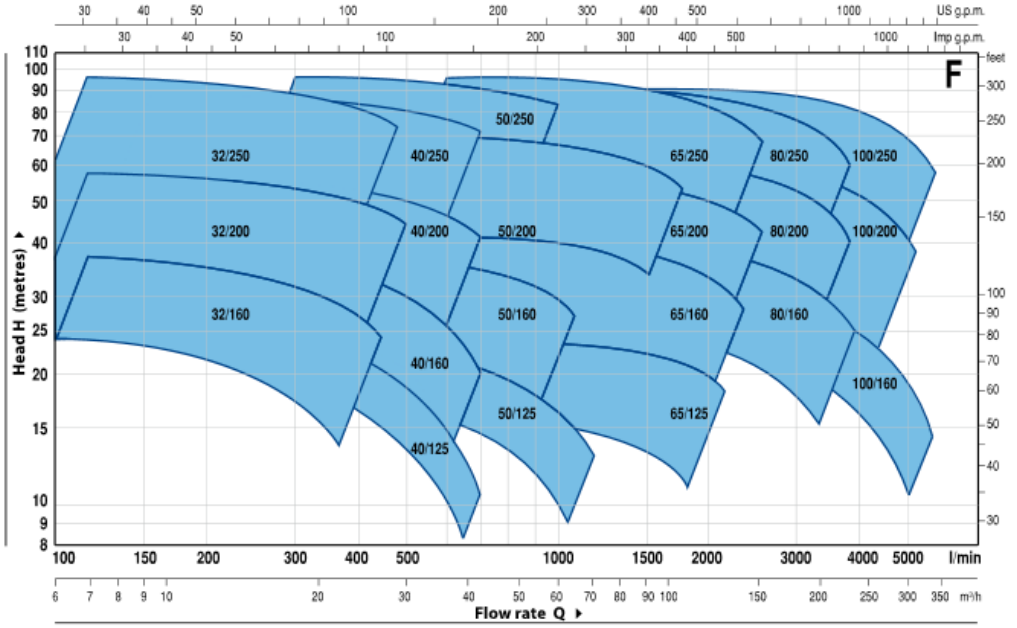

PERFORMANCE DATA

50 Hz n= 2900 rpm

MODEL	POWER (P2)			PERFORMANCE	
Three-phase	kW	HP	▲	Q l/min	H metres
F 32/160C	1.5	2		100 ÷ 350	24 ÷ 14
F 32/160B	2.2	3	IE3	100 ÷ 400	30 ÷ 17
F 32/160A	3	4		100 ÷ 450	37 ÷ 24
F 32/200C	4	5.5		100 ÷ 450	44 ÷ 31.5
F 32/200B	5.5	7.5	IE3	100 ÷ 500	51 ÷ 36
F 32/200A	7.5	10		100 ÷ 500	57 ÷ 44
F 32/200BH	3	4	IE3	100 ÷ 300	45 ÷ 37
F 32/200AH	4	5.5		100 ÷ 320	55 ÷ 44
F 32/250C	9.2	12.5		100 ÷ 400	75 ÷ 55
F 32/250B	11	15	IE3	100 ÷ 450	87 ÷ 62
F 32/250A	15	20		100 ÷ 480	97 ÷ 70
F 40/125C	1.1	1.5	IE2	100 ÷ 550	16 ÷ 6
F 40/125B	1.5	2	IE3	100 ÷ 600	20.5 ÷ 9
F 40/125A	2.2	3		100 ÷ 700	26 ÷ 10
F 40/160C	2.2	3		100 ÷ 600	27 ÷ 14
F 40/160B	3	4	IE3	100 ÷ 600	32 ÷ 20
F 40/160A	4	5.5		100 ÷ 700	38 ÷ 20
F 40/200B	5.5	7.5	IE3	100 ÷ 700	47 ÷ 28
F 40/200A	7.5	10		100 ÷ 700	55 ÷ 41
F 40/250C	9.2	12.5		100 ÷ 700	64 ÷ 47
F 40/250B	11	15	IE3	100 ÷ 700	71 ÷ 55
F 40/250A	15	20		100 ÷ 700	88 ÷ 72
F 50/125C	2.2	3		300 ÷ 1200	17.5 ÷ 6
F 50/125B	3	4	IE3	300 ÷ 1200	20.7 ÷ 9
F 50/125A	4	5.5		300 ÷ 1200	23.5 ÷ 13
F 50/160C	4	5.5		300 ÷ 1000	27 ÷ 16
F 50/160B	5.5	7.5	IE3	300 ÷ 1100	32 ÷ 21
F 50/160A	7.5	10		300 ÷ 1100	37 ÷ 27
F 50/200C	11	15	IE3	400 ÷ 1700	44 ÷ 30
F 50/200B	15	20		400 ÷ 1700	52 ÷ 38
F 50/200A	18.5	25		400 ÷ 1800	61 ÷ 45
F 50/200AR	22	30		400 ÷ 1800	69 ÷ 53
F 50/250D	9.2	12.5	IE3	300 ÷ 900	51 ÷ 32
F 50/250C	11	15		300 ÷ 900	59 ÷ 42
F 50/250B	15	20		300 ÷ 1000	72 ÷ 59
F 50/250A	18.5	25		300 ÷ 1000	85 ÷ 73
F 50/250AR	22	30		300 ÷ 1000	95 ÷ 83

MODEL	POWER (P2)			PERFORMANCE	
Three-phase	kW	HP	▲	Q l/min	H metres
F 65/125C	4	5.5		600 ÷ 1800	16 ÷ 11
F 65/125B	5.5	7.5	IE3	600 ÷ 2000	18 ÷ 13
F 65/125A	7.5	10		600 ÷ 2200	23 ÷ 18
F 65/160C	9.2	12.5		600 ÷ 2200	32 ÷ 22
F 65/160B	11	15	IE3	600 ÷ 2400	36.5 ÷ 23
F 65/160A	15	20		600 ÷ 2400	40.5 ÷ 28
F 65/200B	15	20		200 ÷ 2400	44 ÷ 30.5
F 65/200A	18.5	25	IE3	200 ÷ 2500	50 ÷ 36.5
F 65/200AR	22	30		200 ÷ 2600	57 ÷ 42
F 65/250C	30	40		400 ÷ 2350	76 ÷ 53
F 65/250B	37	50	IE3	400 ÷ 2500	87 ÷ 62
F 65/250A	45	60		400 ÷ 2600	95 ÷ 68
F 80/160D	11	15		500 ÷ 4000	25 ÷ 10
F 80/160C	15	20	IE3	500 ÷ 4000	30 ÷ 15
F 80/160B	18.5	25		500 ÷ 4000	35 ÷ 20
F 80/160A	22	30		500 ÷ 4000	40 ÷ 25
F 80/200B	30	40	IE3	500 ÷ 3650	56 ÷ 34.5
F 80/200A	37	50		500 ÷ 3900	62 ÷ 40
F 80/250B	45	60	IE3	600 ÷ 3600	77 ÷ 54
F 80/250A	55	75		600 ÷ 3900	88.5 ÷ 60
F 100/160C-N	15	20		1000 ÷ 5000	28.5 ÷ 11
F 100/160B-N	18.5	25	IE3	1000 ÷ 5500	32.5 ÷ 11
F 100/160A-N	22	30		1000 ÷ 6000	37 ÷ 13
F 100/200C	30	40		833 ÷ 4650	51 ÷ 28
F 100/200B	37	50	IE3	833 ÷ 4900	57 ÷ 33
F 100/200A	45	60		833 ÷ 5250	63 ÷ 38
F 100/250B	55	75	IE3	800 ÷ 5150	75 ÷ 48
F 100/250A	75	100		800 ÷ 5750	89 ÷ 58

Q = Flow rate

H = Total manometric head

Tolerance of characteristic curves in compliance with EN ISO 9906 Grade 3B.

▲ Performance class of the three-phase motor (IEC-60034-30)

F40/200

CHARACTERISTIC CURVES AND PERFORMANCE DATA

50 Hz n= 2900 rpm HS= 0 m

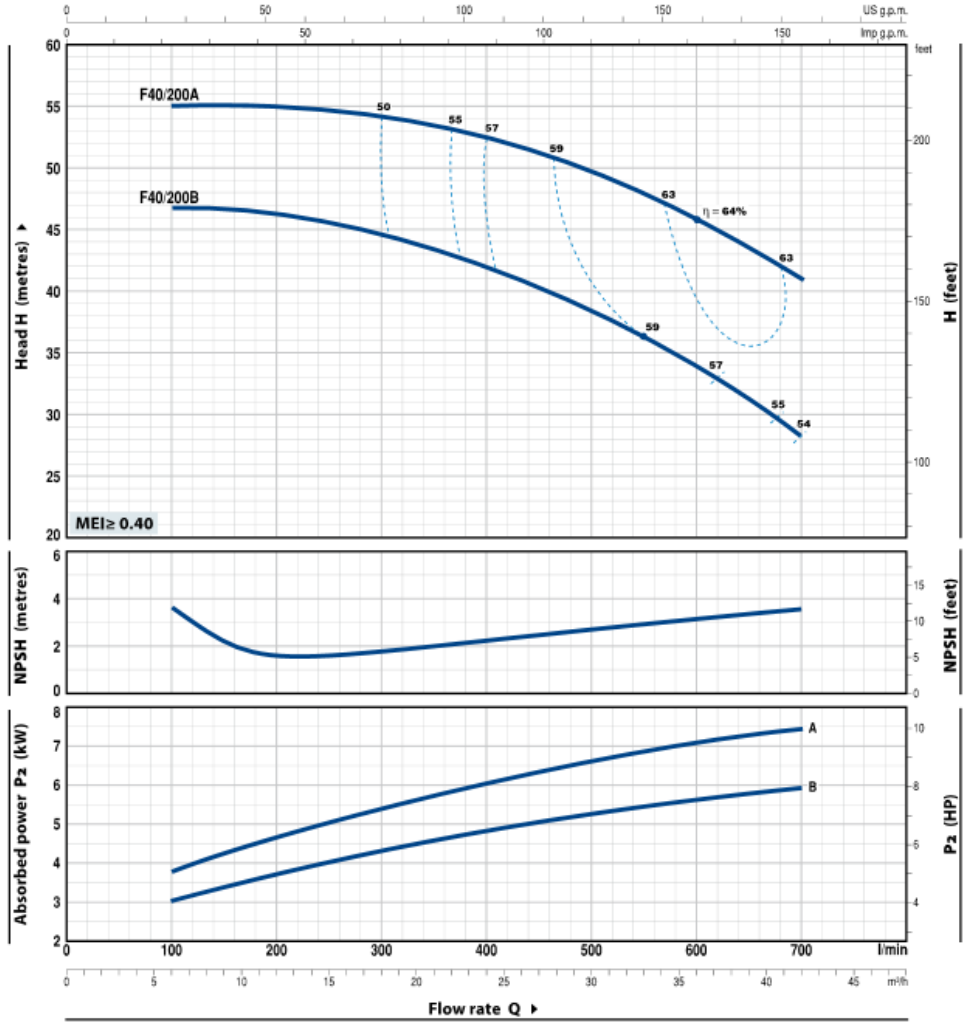

MODEL	POWER (P2)		Q										
Three-phase	kW	HP	m³/h	0	6	9	12	15	18	24	30	36	42
			l/min	**0**	**100**	**150**	**200**	**250**	**300**	**400**	**500**	**600**	**700**
F 40/200B	5.5	7.5	H metres	48	47	46.5	46	45.5	44.5	42	38	34	28
F 40/200A	7.5	10		56	55	55	55	54.5	54	52.5	49.5	46	41

Q = Flow rate **H** = Total manometric head **HS** = Suction height

Tolerance of characteristic curves in compliance with EN ISO 9906 Grade 3B.

F

POS.	COMPONENT	CONSTRUCTION CHARACTERISTICS
1	PUMP BODY	Cast iron complete with flanged suction and delivery ports
2a	BODY BACKPLATE	Cast iron for F32/160, F32/200, F40/125, F40/160, F40/200, F50/125, F50/160, F65/125
2b	MOTOR BRACKET	Cast iron for F32/250, F40/250, F50/200, F50/250, F65/160, F65/200, F65/250, F80/160, F80/200, F80/250, F100/160, F100/200, F100/250
3	IMPELLER	Brass for F32/160, F32/200, F40/125, F40/160, F40/200, F50/125, F50/160 Cast iron for F32/250, F40/250, F50/200, F50/250, F65/125, F65/160, F65/200, F65/250, F80/160, F80/200, F80/250, F100/160, F100/200, F100/250
4	MOTOR SHAFT	Stainless steel EN 10088-3 - 1.4104

5 MECHANICAL SEAL

Pump	*Seal*	*Shaft*	*Materials*		
Model	*Model*	*Diameter*	*Stationary ring*	*Rotational ring*	*Elastomer*
F32/160, F40/125, F40/160, 50/125	**FN-20**	**Ø 20** mm	Graphite	Ceramic	NBR
F32/200, F40/200, F50/160, F65/125	**FN-24**	**Ø 24** mm	Graphite	Ceramic	NBR
F50/200, F65/160, F65/200, F80/160, F100/160	**FN-32 NU**	**Ø 32** mm	Graphite	Ceramic	NBR
F32/250, F40/250, F50/250	**FN-38**	**Ø 38** mm	Graphite	Ceramic	NBR
F65/250, F80/200, F80/250B, F100/200	**FN-40 NU**	**Ø 40** mm	Graphite	Ceramic	NBR
F80/250A, F100/250	**FH-45 NU**	**Ø 45** mm	Graphite	Ceramic	NBR

6 BEARINGS

Pump	*Model*	*Pump*	*Model*
F32/160C F40/160C F32/160B F50/125C F40/125	**6206 ZZ-C3 / 6204 ZZ**	F32/250 F50/200 F40/250 F65/160 F50/250 F80/160 F65/200 F100/160	**6310 ZZ-C3 / 6308 ZZ-C3**
Fm32/160B F32/160A Fm40/160C F40/160B Fm50/125C F50/125B	**6206 ZZ-C3 / 6205 ZZ**	F65/250 F80/200 F80/250B F100/200	**6312 ZZ-C3 / 6212 ZZ-C3**
F40/160A F50/125A	**6306 ZZ-C3 / 6206 ZZ-C3**	F80/250A F100/250	**6314 ZZ-C3 / 6313 ZZ-C3**
F32/200 F40/200 F50/160 F65/125	**6307 ZZ-C3 / 6206 ZZ-C3**		

7 CAPACITOR

Pump	*Capacitance*
Single-phase	*(230 V or 240 V)*
Fm32/160C	**45** µF - 450 VL
Fm32/160B	**70** µF - 450 VL
Fm40/125C	**31.5** µF - 450 VL
Fm40/125B	**45** µF - 450 VL
Fm40/160C	**70** µF - 450 VL
Fm50/125C	**70** µF - 450 VL

8 ELECTRIC MOTOR

Fm: single-phase 230 V - 50 Hz with thermal overload protector incorporated into the winding (up to 1.5 kW)
F: three-phase 230/400 V - 50 Hz up to 4 kW
400/690 V - 50 Hz from 5.5 to 75 kW

➟ **The three-phase pumps are fitted with high performance motors up to P2=1.1kW in class IE2 and from P2=1.5kW in class IE3 (IEC 60034-30)**

– Insulation: class F – Protection: IP 55

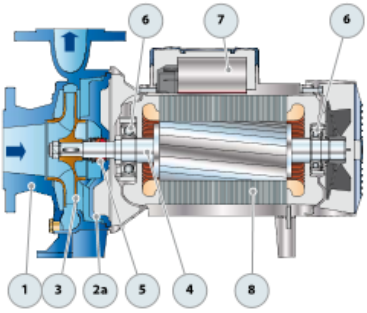

Single-phase version

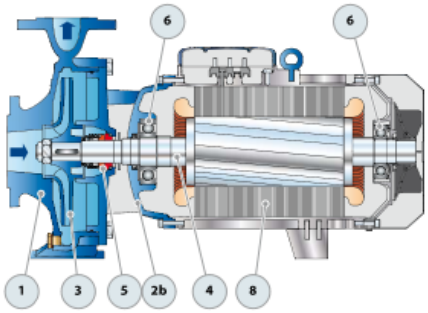

Three-phase version

158

ABSORPTION

MODEL	VOLTAGE	
Single-phase	230 V	240 V
Fm 32/160C	11.0 A	10.0 A
Fm 32/160B	15.0 A	13.8 A
Fm 40/125C	8.6 A	7.8 A
Fm 40/125B	15.0 A	13.8 A
Fm 40/160C	15.0 A	13.8 A
Fm 50/125C	15.0 A	13.8 A

MODEL	VOLTAGE		
Three-phase	230÷240 V	400÷415 V	690÷720 V
F 32/160C	7.5 A	4.3 A	2.5 A
F 32/160B	10.0 A	5.8 A	3.4 A
F 32/160A	12.0 A	7.3 A	4.2 A
F 32/200C	17.9 A	10.3 A	5.9 A
F 32/200B	–	11.7 A	6.7 A
F 32/200A	–	14.9 A	8.6 A
F 32/200BH	12.6 A	7.3 A	4.2 A
F 32/200AH	15.4 A	8.9 A	5.1 A
F 32/250C	–	17.2 A	9.9 A
F 32/250B	–	21.0 A	12.0 A
F 32/250A	–	27.0 A	15.6 A
F 40/125C	5.7 A	3.3 A	1.9 A
F 40/125B	7.5 A	4.3 A	2.5 A
F 40/125A	10.0 A	5.8 A	3.4 A
F 40/160C	9.9 A	5.7 A	3.3 A
F 40/160B	12.0 A	6.9 A	4.0 A
F 40/160A	17.2 A	9.9 A	5.7 A
F 40/200B	–	12.6 A	7.3 A
F 40/200A	–	15.6 A	9.0 A
F 40/250C	–	21.0 A	12.1 A
F 40/250B	–	23.5 A	13.6 A
F 40/250A	–	30.5 A	17.6 A
F 50/125C	9.4 A	5.4 A	3.1 A
F 50/125B	12.0 A	6.9 A	4.0 A
F 50/125A	16.3 A	9.4 A	5.4 A
F 50/160C	15.8 A	9.1 A	5.3 A
F 50/160B	–	12.3 A	7.1 A
F 50/160A	–	15.5 A	8.9 A
F 50/200C	–	23.0 A	13.3 A
F 50/200B	–	29.5 A	17.0 A
F 50/200A	–	34.5 A	20.0 A
F 50/200AR	–	41.5 A	24.0 A

MODEL	VOLTAGE		
Three-phase	230÷240 V	400÷415 V	690÷720 V
F 50/250D	–	17.2 A	9.9 A
F 50/250C	–	21.0 A	12.0 A
F 50/250B	–	27.0 A	15.6 A
F 50/250A	–	34.0 A	19.6 A
F 50/250AR	–	41.0 A	24.0 A
F 65/125C	17.5 A	10.0 A	5.8 A
F 65/125B	–	12.0 A	7.0 A
F 65/125A	–	16.5 A	9.5 A
F 65/160C	–	19.0 A	11.0 A
F 65/160B	–	23.0 A	13.5 A
F 65/160A	–	27.5 A	16.0 A
F 65/200B	–	31.0 A	18.0 A
F 65/200A	–	34.0 A	19.5 A
F 65/200AR	–	41.0 A	23.7 A
F 65/250C	–	53.0 A	31.0 A
F 65/250B	–	65.0 A	38.0 A
F 65/250A	–	79.0 A	46.0 A
F 80/160D	–	22.0 A	13.0 A
F 80/160C	–	29.0 A	17.0 A
F 80/160B	–	34.5 A	20.0 A
F 80/160A	–	39.0 A	22.5 A
F 80/200B	–	53.0 A	31.0 A
F 80/200A	–	65.0 A	38.0 A
F 80/250B	–	79.0 A	46.0 A
F 80/250A	–	98.0 A	57.0 A
F 100/160C-N	–	31.0 A	18.0 A
F 100/160B-N	–	36.0 A	21.0 A
F 100/160A-N	–	42.0 A	24.0 A
F 100/200C	–	53.0 A	31.0 A
F 100/200B	–	65.0 A	38.0 A
F 100/200A	–	79.0 A	46.0 A
F 100/250B	–	98.0 A	57.0 A
F 100/250A	–	126.0 A	73.0 A

DIMENSIONS AND WEIGHT

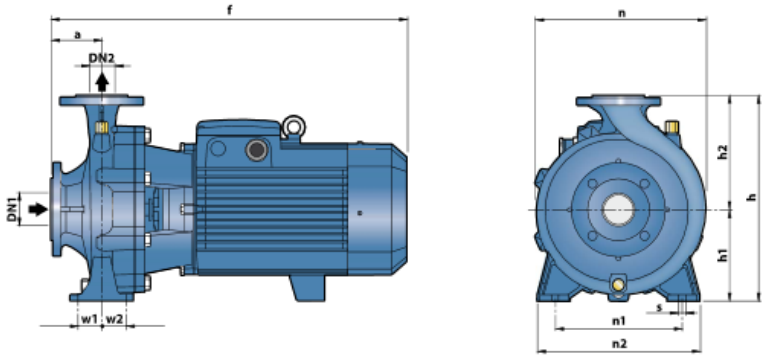

MODEL		DIMENSIONS mm												kg	
Single-phase	Three-phase	DN1	DN2	a	f	h	h1	h2	n	n1	n2	w1	w2	s	1~	3~
Fm 32/160C	F 32/160C	50	32	80	412	292	132	160	242	190	240	35	35	14	32.7	32.1
Fm 32/160B	F 32/160B				448/412										37.5	33.4
–	F 32/160A				448										–	37.4
–	F 32/200C				469	340	160	180	270						–	46.4
–	F 32/200B				515										–	48.4
–	F 32/200A														–	56.9
–	F 32/200BH				469										–	42.4
–	F 32/200AH														–	46.4
–	F 32/250C			100	606	405	180	225	330	250	320	47.5	47.5		–	100.0
–	F 32/250B														–	102.0
–	F 32/250A				701										–	119.8
Fm 40/125C	F 40/125C	65	40	80	421	252	112	140	244	160	210	35	35		31.5	29.5
Fm 40/125B	F 40/125B														33.0	31.5
–	F 40/125A														–	33.0
Fm 40/160C	F 40/160C				448/412	292	132	160	240	190	240				37.6	33.5
–	F 40/160B				448										–	37.5
–	F 40/160A				465										–	43.6
–	F 40/200B			100	535	340	160	180	275	212	265				–	54.0
–	F 40/200A														–	60.0
–	F 40/250C				606	405	180	225	328	250	320	47.5	47.5		–	100.0
–	F 40/250B														–	102.0
–	F 40/250A				701										–	119.8
Fm 50/125C	F 50/125C	65	50		465/431	292	132	160	242	190	240	35	35		37.3	33.2
–	F 50/125B				465										–	37.2
–	F 50/125A				484										–	43.3
–	F 50/160C				489	340	160	180	269	212	265				–	48.0
–	F 50/160B				535										–	52.5
–	F 50/160A														–	56.4
–	F 50/200C				616	360		200	316						–	97.7
–	F 50/200B				711										–	114.0
–	F 50/200A														–	126.5
–	F 50/200AR			100	743										–	140.3
–	F 50/250D				606	405	180	225	337	250	320	47.5	47.5		–	101.3
–	F 50/250C														–	103.3
–	F 50/250B				701										–	120.4
–	F 50/250A														–	134.3
–	F 50/250AR				733										–	147.4
–	F 65/125C	80	65		511	340	160	180	291	212	280				–	53.5
–	F 65/125B				557										–	56.8
–	F 65/125A														–	63.3
–	F 65/160C				621	360		200	300						–	98.3
–	F 65/160B														–	99.3
–	F 65/160A				716										–	114.3
–	F 65/200B				719	405	180	225	340	250	320				–	120.3
–	F 65/200A														–	132.9
–	F 65/200AR				751										–	144.4
–	F 80/160D	100	80	125	652				330						–	103.8
–	F 80/160C				747										–	115.6
–	F 80/160B														–	133.1
–	F 80/160A				779										–	144.6
–	F 100/160C-N	125	100		758	480	200	280	362	280	360	60	60	18	–	126.3
–	F 100/160B-N														–	136.3
–	F 100/160A-N				790										–	151.3

160

DIMENSIONS AND WEIGHT

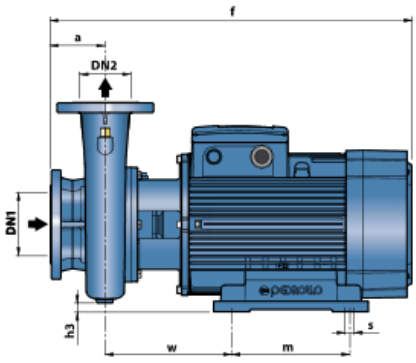

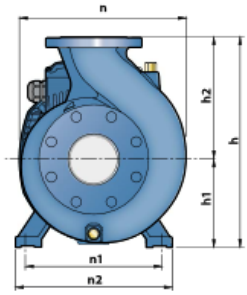

MODEL	DIMENSIONS mm														kg
Three-phase	DN1	DN2	a	f	h	h1	h2	h3	n	n1	n2	w	m	s	3~
F 65/250C	80	65	100	796	450	200	250	15	369	318	360	269.5	305	18.5	201.3
F 65/250B				847											201.3
F 65/250A				847											219.3
F 80/200B	100	80	125	824	430			25	360						201.6
F 80/200A				875											201.6
F 80/250B				872	480		280	12	380						234.5
F 80/250A				1015	620	250		55	490	400	490	294	350	24	539.0
F 100/200C	125	100		824	480	200	280	0	391	318	360	269.5	305	18.5	225.3
F 100/200B				875											225.3
F 100/200A				875											233.3
F 100/250B			140	1036	620	250	280	45	490	400	490	300	350	24	539.3
F 100/250A															539.3

FLANGED PORTS

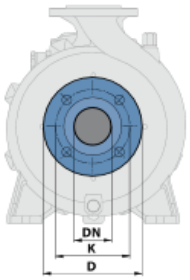

DN FLANGES	D	K	HOLES	
mm	mm	mm	N.	Ø (mm)
32	140	100	4	18
40	150	110		
50	165	125		
65	185	145		
80	200	160	8	
100	220	180		
125	250	210		

COUNTER FLANGES

(CAN BE ORDERED SEPARATELY)

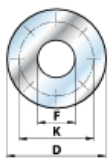

DN FLANGES	F	D	K	HOLES	
mm	COUNTER FLANGES	mm	mm	N.	Ø (mm)
32	1¼"	140	100	4	18
40	1½"	150	110		
50	2"	165	125		
65	2½"	185	145		
80	3"	200	160	8	
100	4"	220	180		
125	5"	250	210		

D-2 Temperature Sensors

Motstandselementer (RTD)

Generelt
RTD elementet (Resistance Temperature Detector) er foruten termoelementet det mest benyttede elementet i industrien for temperaturmåling. Måleområde er definert av The International Scale (ITS-90) fra -259 til +962 °C .
Dette kan være anvendelig i laboratoriesammenheng, men industrien har satt snevrere grenser. ASME definerer -200 til + 650 °C som akseptabelt område. Dette har også blitt industristandard selv om "International Electrotechnical Commission" (IEC) tillater opp til 850 °C.

Det mest benyttede RTD er PT100 elementet. Andre varianter som også anvendes er PT1000, PT500, PT250, PT50, og PT25. Platinaelementet har vist seg å være det beste både ut fra målenøyaktighet og langtidsstabilitet.

Motstandselementene har den egenskap at de har en motstand som varierer med temperaturen. På PT100 kan vi måle en motstand på 100 ohm ved 0 °C. Tilsvarende vil PT1000 måle 1000 ohm ved 0 °C etc.
Ved 100 °C vil et PT100 element måle 138,5 ohm og et PT1000 1385 ohm. Et PT1000 vil altså ha en mye større motstandsendring pr. grad C.
PT100 elementet som benyttes i våre sensorer baserer seg på følgende standarder:
BS 1904-1984 , DIN 43760-1980, IEC 751-1983.

PT100 element typer
PT100 elementet var tidligere en glasssylinder med innekapslet en spunnet platina tråd som var trimmet til 100 ohm ved 0°C. Dette var et tungt element med lang tidsrespons. Derfor ble gjerne termoelementer tidligere foretrukket på målepunkter som idag har klare fordeler med PT100.
Dagens PT100 elementer er delt i to hovedgrupper:

Keramisk
Disse består av platinatråd viklet opp om en keramisk kjerne. De kan leveres i alle nøyaktighetsklasser og regnes som de mest nøyaktige elementene. Ved anvendelse over 600 °C må spesielle hensyn taes ved produksjonen. Ulempen er at keramikken gjør de mer ømfintlig for vibrasjoner og trykkstøt.

Flatfilm
Flatfilmsensoren er basert på samme teknologi som ved produksjon av integrerte kretser. En tynn platinafilm er nedsmeltet på en bane og kapslet inn. Denne sensoren er lett og liten med meget rask tidsrespons. Den lages i flere mekaniske utførelser for maksimal følsomhet i enden eller på sidene.
Flatfilmsensorene leveres kun i klasse B eller A nøyaktighet og de bør ikke anvendes over 250 °C uten å ta spesielle hensyn ved produksjonen, maks (400°C).

Nøyaktighet
Nøyaktigheten på et PT100 element deles opp i nøyaktighetsklasser. IEC-751 eller DIN definerer klasser som vist i tabellen nedenfor. Den mest anvendte PT100 sensoren er i nøyaktighetsklasse B (1/1 DIN.)

Innen hver klasse er det også mulig å levere to eller flere sensorer som er spesielt plukket ut for å være like hverandre. På energimåling er det viktig å benytte slike "matched pair".

I henhold til DIN/IEC 751er:
Nøyaktighetsklasse B: (1/1- DIN): (0,3 +0,005 * t) °C
Altså ved t =100°C blir nøyaktigheten +0,3+0,005*100=±0,8°C
Nøyaktighetsklasse A: (1/2- DIN): (0,15 +0,002 * t) °C

Repeterbarhet / Stabilitet
DIN/IEC 751 krever at elementene skal holde seg innenfor nøyaktighetsklassen under drift i 250 timer ved maks. og 250 timer ved min. temperatur. Det samme kravet stilles også opprettholdt under 10 maks. og min. svingninger. Det vil si (250 + 250)*10 timer = 208 dager.
PT100 elementet er meget langtidsstabilt mens termoelementet er kjent for å tape seg (aldres) så det trenger stadig kalibrering og med tiden utbytting.

Vibrasjon
PT100 elementer er mer ømfindtlige for vibrasjon enn termoelementer, men det kan taes spesielle hensyn under produksjonen slik at PT100 sensorer også er godt egnet til store vibrasjoner.

Respons tid
Selv om termoelementer er raskest har PT100 elementer i dag en responstid som stort sett er akseptabel. Når man ser på en komplett installasjon med sensorinnsats og termolomme er det ikke lenger sensorelementet som er det utslagsgivende på responstiden.

Sensitivitet
PT100 elementet har en motstandsendring fra 100 til 138,5 ohm ved en temperaturendring fra 0...100°C. Dette gir en differanse på 38,5 ohm. Hvis vi benyttet en strømkrets på 1mA ville dette gitt en spenningsforandring på V=RI = 38,5*1mA=38,5millivolt. Tilsvarende ved termolelement type E som er det mest følsomme er 6,317 mV. Det har altså bare 1/6 av PT100 elementets følsomhet. Enda større følsomhet kan oppnåes ved å benytte PT1000 element som har en tilsvarende motstandsendring på 385 ohm over samme temperatur forandring.

Tilpasning av PT100 motstandssignal til transmitter
Motstanden i et PT100 element endres ikke lineært med temperaturen så det må benyttes temperatur transmittere som tar hensyn til disse ulineæritetene. Forholdet mellom temperatur og motstand er beskrevet i flere formler. Den mest anvendte i henhold til IEC 751 er "Callendar-van Dusen ligningen"
Rt = R0 [1 + At + Bt2 + C t3(t- 100)]
Konstantene R0, A, B, C er spesifikke for hver RTD type.
For PT100 i området 0....850 °C er:
R_0 =100, A =3,9083*10^{-3}, B = -5,775*10^{-7}, og C=0
For PT100 i området -200....0°C er:
R_0=100, A=3,9083*10^{-3}, B= -5,775*10^{-7}, og C= -4,18301*10^{-12}

Legg merke til at PT100 elementer i henhold til IEC 751, DIN43760 og BS1904 alle har en α =0,003850
Amerikanske og japanske alfa verdi α =0,003916

$$\alpha = \frac{R\ 100 - Ro}{100 \times Ro}$$

Alle våre temperatur transmittere tar hensyn til disse ulineæritetene så det er kun under helt ekstreme krav til nøyaktighet som dette bør taes opp til vurdering.

Tabell over forholdet motstand / temperatur for PT100 side 44.

Egenoppvarming.
PT100 elementet produserer ikke selv sin egen spenning slik som termo-elementet. Derfor må vi tilføre en strøm for å kunne måle motstandsendringen. Dersom denne strømmen blir for stor vil PT100 elementet bli opphetet og dermed gi en målefeil. Alle temperaturtransmittere som vi leverer har en målestrøm som er mindre enn 1 mA for å sikre seg mot oppvarmings-problemer. Hvis PT100 elementet skal kontrolleres med ohmmeter bør det sjekkes at ikke målestrømmen er så stor at den gir egenoppvarming av PT100 elementet.

Kabling

2-leder
2-leder kabling benyttes sjelden ettersom kablenes motstand vil komme i tillegg til PT100 elementet. Enkelte har benyttet seg av muligheten til å kalibrere dette bort, men det må bemerkes at kabelmotstanden varierer også med omgivelses-temperaturen slik at målefeilen ikke er stabil.

3-leder
3-leder kabling er den som blir mest benyttet innen industrien. Det måles da motstand over PT100 elementet samtidig med at det måles motstand i en sløyfe med den tredje lederen. På denne måten eliminerer vi både den motstand som er avhen-gig av kabellengden og kabelmotstanden som varierer med omgivelsestemperaturen.
Det forutsettes at alle tre ledere er helt identiske og blir likt påvirket av omgivelsene.

4-leder
4-leder kabling benyttes kun der ekstreme nøyaktigheter kreves. Her benyttes to ledere til måling av PT100 motstan-den, mens de to andre er til for å kompensere for kabel-motstanden i begge måleledere individuelt.

Alle våre temperatur transmittere har innebygget muligheter for automatisk ledningskompensering.

TOLERANSE FOR PT 100

DIN 43760-1980, IEC 751 1983, BS 1904-1984

Temperatur C	Klasse B 1/1 DIN +OHM	+C	Klasse A 1/2 DIN +OHM	+C	1/3 DIN +OHM	+C	1/10 DIN +OHM	+C
-200	0,56	1,30	0,24	0,55	0,18	0,43	0,06	0,13
-100	0,32	0,80	0,14	0,35	0,11	0,26	0,03	0,08
+0	0,12	0,30	0,06	0,15	0,04	0,10	0,01	0,03
+100	0,30	0,80	0,13	0,35	0,10	0,26	0,03	0,08
+200	0,48	1,30	0,20	0,55	0,16	0,43	0,05	0,13
+300	0,64	1,80	0,27	0,75	0,21	0,60	0,06	0,18
+400	0,79	2,30	0,33	0,95	0,26	0,76	0,08	0,23
+500	0,93	2,80	0,38	1,15	0,31	0,93	0,09	0,28
+600	1,06	3,30	0,43	1,35	0,35	1,1	0,11	0,33

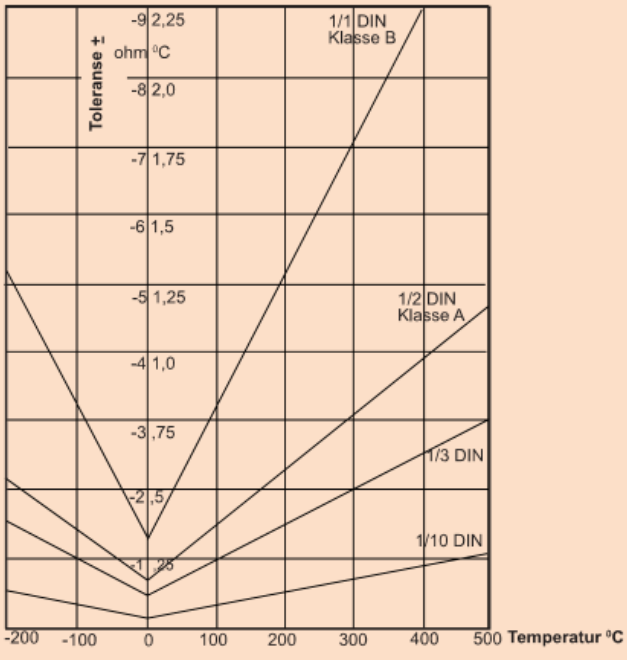

Eksempel:
Ved 100°C vil et klasse B element ha en toleranse på ± 0,8 °C eller ± 0,32 ohm. Legg også merke til at det med høyere temperaturer er viktig å ha en stabil α-verdi ettersom det er denne som her vil påvirke toleransen mer enn R_o verdien.

Koblingsskjema PT 100

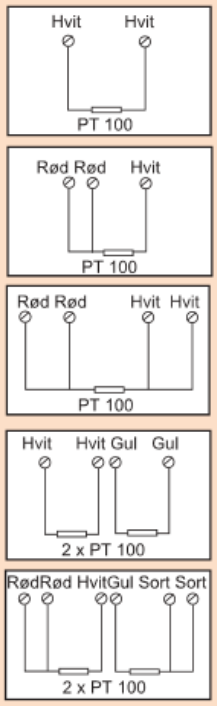

GE
Measurement & Control

UNIK 5000

Pressure Sensing Platform

The new UNIK 5000 is a high performance configurable solution to pressure measurement. The use of micromachined silicon technology and analogue circuitry enables best in class performance for stability, low power and frequency response. The new platform enables you to easily build up your own sensor to match your own precise needs. This high performance, configurable solution to pressure measurement employs modular design and lean manufacturing techniques to offer:

High Quality

The combination of a high technology sensor, together with advanced signal conditioning and packaging techniques, provides an ideal long term solution for reliable, accurate and economical measurements

Bespoke as Standard

Custom-built from standard components, manufacturing sensors to your requirement is fast and simple; each UNIK 5000 is a "bespoke" pressure sensing solution, but with the short lead times and competitive pricing you would expect from standard products.

Expertise

We have the people and the knowledge to support your needs for accurate and reliable product performance; our team of experts can help you make the right sensor selection, guiding you and providing the help and tools you need. It is important to ensure that the sensor material and performance selected are suitable for your application.

GE imagination at work

Features

- Ranges from 70 mbar (1 psi) to 700 bar (10000 psi)
- Accuracy to ±0.04% Full Scale (FS) Best Straight Line (BSL)
- Stainless Steel construction
- Frequency response to 3.5 kHz
- High over pressure capability
- Hazardous Area certifications
- mV, mA, voltage and configurable voltage outputs
- Multiple electrical & pressure connector options
- Operating temperature ranges from -55 to 125°C (-67 to 257°F)

5000 Specifications

Measurement

Operating Pressure Ranges

Gauge ranges

Any zero based range 70 mbar to 70 bar
(1 to 1000 psi) (values in psi are approximate)

Sealed Gauge Ranges

Any zero based range 10 to 700 bar
(145 to 10000 psi)

Absolute Ranges

Any zero based range 100 mbar to 700 bar
(1.5 to 10000 psi)

Differential Ranges

Wet/Dry

Uni-directional or bi-directional 70 mbar to 35 bar
(1 to 500 psi)

Wet/Wet

Uni-directional or bi-directional 350 mbar to 35 bar
(5 to 500 psi)

Line pressure: 70 bar max (1000 psi)

Barometric Ranges

Barometric ranges are available with a minimum span of 350 mbar (5.1 psi)

Non Zero Based Ranges

Non zero based ranges are available. For non zero based gauge ranges, please contact GE Measurement & Control to discuss your requirements.

Over Pressure

- 10 × FS for ranges up to 150 mbar (2 psi)
- 6 × FS for ranges up to 700 mbar (10 psi)
- 2 × FS for barometric ranges
- 4 × FS for all other ranges (up to 200 bar for ranges ≤70 bar and up to 1200 bar for ranges >70 bar)

For differential versions the negative side must not exceed the positive side by more than:

- 6 × FS for ranges up to 150 mbar (2 psi)
- 4 × FS for ranges up to 700 mbar (10 psi)
- 2 × FS for all other ranges up to a maximum of 15 bar (200 psi)

Containment Pressure

Ranges up to 150 mbar (2 psi) gauge 10 × FS
Ranges up to 70 bar (1000 psi) gauge 6 × FS
(200 bar (2900 psi) max)
Ranges up to 70 bar (1000 psi) absolute
200 bar (2900 psi)
Ranges above 70 bar (1000 psi)
1200 bar (17400 psi)

Differential (-ve port) must not exceed positive port by more than 6 × FS (15 bar (200 psi) maximum)

Supply and Outputs

Electronics Option	Description	Supply voltage (V)	Output	Current Consumption (mA)
0	mV Passive	2.5 to 12	10 mV/V^	<2 at 10 V
1	mV Linearised	7 to 12	10 mV/V^	<3
2	mA	7 to 28**	4-20 mA	<30
3	0 to 5 V 4-wire	7 to 16**	0 to 5 V	<3
4	0 to 5 V 3-wire	7 to 16**	0 to 5 V*	<3
5	Basic Configurable (3-wire)	See below~	See below	<3
6	0 to 10 V 4-wire	12 to 16**	0 to 10 V	<3
7	0.5 V to 4.5 V Ratiometric	5.0 ± 0.5	0.5 to 4.5 V	<3
8	Configurable (4-wire)	7 to 36	See below	See below
9	Configurable (3-wire)	7 to 36	See below	See below

^ with a 10 V supply mV output sensors give 100 mV over the full scale pressure.
• Output is ratiometric to the supply voltage
• Output reduces pro-rata for pressure ranges below 350 mbar (5 psi)
**0 to 5 V 3-wire output is non true zero. At pressures below 1% of span the output will be fixed at approximately 50 mV*
***32 V in non-hazardous area operation*
~ Supply voltage is between [Maximum Output + 1 V] (7 V minimum) to 16 V (32 V in non-hazardous area operation)

Basic Configurable (Option 5), Configurable 4-Wire (Option 8), Configurable 3-Wire (Option 9)

Any pressure signal output configurations will be available, subject to the following limitations:

Output specification	Basic Configurable (Option 5)	Configurable (Options 8, 9)
Minimum span:	4 V	2 V
Maximum span:	10 V	20 V
Maximum output limit:	11 V	±10 V
Maximum zero offset:	Span / 2	±Span
Current consumption:	< 3 mA	< 20 mA @ 7 Vdc decreasing to < 5 mA @ 32 Vdc
Reverse output response:	No	Yes
Maximum operating temperature:	+125˚C	+80˚C

Output voltage range can be specified to a resolution of 0.1 V.
The output will continue to respond to 110% FS. i.e. if a 0 to 10 V output is specified, the output will continue to increase proportionally to applied pressure until at least 11 V.
Option 5: Not true zero, the output will saturate at < 50 mV.
Options 8, 9: On startup <100 mA drawn for 10 ms typically.
Options 8, 9: Shunt calibration: not available with reverse output.

Examples

Configuration	Allowed	Not Allowed
Basic Configurable (Option 5)	0 to 5 V	1 to 4 V (span too small)
	0.5 to 4.5 V	4 to 11 V (offset too big)
	1 to 6 V	
	1 to 11 V	
Configurable (Options 8, 9)	-10 to 0 V	0 to 12 V (outside ±10 V limits)
	0 to 5 V	6 to 10 V (offset too big)
	-5 to 5 V	0 to 0.5 V (span too small)
	-2 to 10 V	
	1 to 6 V	
	10 to 0 V	

Power-Up Time
- mV, Voltage and current versions: 10 ms
- Configurable 3-wire and 4-wire versions: 500 ms

Insulation
- 500 Vdc: 100 MΩ
- 500 Vac: ≤ 5 mA leakage current (mV and mA versions only).

Shunt Calibration
Shunt Calibration provides a customer accessible connection which, when applied, causes a shift in output of 80% FS in order to simulate applied pressure.
It is fitted to the mV, Configurable 4-wire and Configurable 3-wire versions as standard. It is not available with DIN, M12 x 1 or M20 x 1.5 electrical connectors (options 7, D, G and R)

Shunt calibration is activated in different ways depending on the electrical connector and version:
- mV versions: connect Shunt Cal to -ve Supply or, where available, connect both Shunt Cal connections together.
- Configurable 4-wire and Configurable 3-wire versions: connect Shunt Cal to -ve Output or, where available, connect both Shunt Cal connections together.

Note: Not available with reverse output.

Performance Specifications

There are three grades of performance specification: Industrial, Improved and Premium.

Accuracy
Voltage, Current and mV Linearised
Combined effects of non-linearity, hysteresis and repeatability:

Industrial:	±0.2% FS BSL
Improved:	±0.1% FS BSL
Premium:	±0.04% FS BSL

mV Passive

≤ 70 bar	
Industrial/Improved:	±0.25% FS BSL
Premium not available	
> 70 bar	
Industrial/Improved:	±0.5% FS BSL
Premium not available	

Note: For the barometric pressure range, accuracy is of span, not full scale.

Zero Offset and Span Setting
Demountable electrical connector options allow access to potentiometers that give at least ±5% FS adjustment (see Electrical Connector section)

Factory set to:

Product Description	Industrial	Improved and Premium
Current and Voltage Versions (Demountable Electrical Connections and Cable Gland)	±0.5% FS	±0.2% FS
Current and Voltage Versions (All Other Electrical Connections)	±1.0% FS	±1.0% FS
mV Versions	±3.0 mV	±3.0 mV

Long Term Stability
±0.05% FS typical (±0.1% FS maximum) per year increasing pro-rata for pressure ranges below 350 mbar

Temperature Effects
Four compensated temperature ranges can be chosen.
Industrial Accuracy performance:

-10 to +50°C (14 to +122°F):	±0.75% FS Temperature error band (TEB)
-20 to +80°C (-4 to +176°F):	±1.5% FS TEB
-40 to +80 °C (-40 to +176°F):	±2.25% FS TEB
-40 to +125°C (-40 to +257°F):	±2.25% FS TEB
Improved and Premium Accuracy performance:	
-10 to +50°C (14 to +122°F):	±0.5% FS TEB
-20 to +80°C (-4 to +176°F):	±1.0% FS TEB
-40 to +80°C (-40 to +176°F):	±1.5% FS TEB
-40 to +125°C (-40 to +257°F):	±1.5% FS TEB

Temperature effects increase pro-rata for pressure ranges below 350 mbar (5 psi) and are doubled for barometric ranges.

Line Pressure Effects (Differential Version Only)
Zero shift: <±0.03% span/bar of line pressure
Span shift: <±0.03% span/bar of line pressure
Effects increase pro-rata for differential pressure ranges below 700 mbar (10 psi).

Physical Specifications

Environmental Protection
- See Electrical Connector section
- Hyperbaric Pressure: 20 bar (300 psi) maximum

Operating Temperature Range
See Electrical Connector section

Pressure Media
Fluids compatible with stainless steel 316L and Hastelloy C276.
For the wet/dry differential version, negative pressure port: fluids compatible with stainless steel 316L, stainless steel 304, Pyrex, silicon and structural adhesive.

Enclosure Materials

Stainless steel (body), nitrile- or silicone-rubber (o-rings, gaskets), EPDM (gaskets), PVDF (depth cone), PTFE (vent filter), Nickel plated brass (lock rings), glass filled nylon (electrical connector assemblies), delrin (depth cone). Cable sheaths as specified (see Electrical Connector).

Pressure Connector

Available options are

- G1/4 Female*
- G1/4 Male Flat
- G1/4 Male 60° Internal Cone
- G1/4 Male Flat Long
- G1/4 Male Flat with Snubber
- G1/4 Male Flat with Cross Bore Protection
- G1/4 Male with Nipple
- G1/4 Quick Connect
- G1/8 Male 60° Internal Cone
- G1/2 Male via Adaptor*
- 1/4 NPT Female*
- 1/4 NPT Male
- 1/8 NPT Male
- 1/2 NPT Male via Adaptor
- 7/16-20 UNF Female
- 7/16-20 UNF Male Short Flat
- 7/16 UNF Long 37° Flare Tip
- 7/16-20 UNJF Male 74° External Cone
- 3/8-24 UNJF
- 1/4 Swagelok Bulkhead
- M10 X 1 80° Internal Cone
- M12 X 1 60° Internal Cone
- M14 X 1.5 60° Internal Cone
- M20 X 1.5 Male
- Depth Cone (G1/4 Female Open Face)
- M12 x 1.0 74° External Cone
- Quick Release Male
- VCR Female*
- VCR Male*
- NW16 Flange
- R3/8 Male
- R1/4 Male

Choose connectors marked * for pressure ranges over 70 bar. Other pressure connectors may be available, contact GE to discuss your requirement.

General Certifications

RoHS 2002/95/EC
CRN Certified 0F13650.517890YTN ADD1/ REV1, 0F13828.2 (sensor types K and O) and CSA 0F13650.56 ADD1 for pressure ranges up to and including 350 bar (5000 psi)

Electrical Connector

Various electrical connector options are available offering different features:

Code Number	Description	Max Operating temp range °C	Max Operating temp range °F	IP rating	Zero span Adjust
0	No Connector	-55 to +125	-67 to +257	-	Y
1	Cable Gland	-40 to +80	-40 to +176	65	N
2	Raychem Cable	-55 to +125	-67 to +257	65	N
3	Polyurethane Depth	-40 to +80	-40 to +176	68	N
4	Hytrel Depth	-40 to +80	-40 to +176	68	N
6/E	Bayonet MIL-C-26482	-55 to +125	-67 to +257	67	N
7	DIN 43650 Form A Demountable	-40 to +80	-40 to +176	65	Y
A/F	Bayonet MIL-C-26482 Demountable	-55 to +125	-67 to +257	65	Y
C	1/2 NPT Conduit	-40 to +80	-40 to +176	65	N
D	Micro DIN (9.4 mm pitch)	-40 to +80	-40 to +176	65	N
G	M12x1 4pin	-55 to +125	-67 to +257	67	N
K	Zero Halogen Cable Demountable	-40 to +80	-40 to +176	65	Y
M	Tajimi R03-R6F	-25 to +85	-13 to +185	65	N
R	M20 x 1.5 Inline	-40 to +80	-40 to +176	65	Y

Note: Electronics output options 8 and 9 are restricted to a maximum operating temperature of 80°C (176°F).
Note: Hazardous area approved versions are restricted to a maximum operating temperature range of -40°C to 80°C (-40°F to 176°F).
Note: Electrical connector option R IP65 rating only with suitable conduit/cable fitting.

CE Conformity

Pressure Equipment Directive 97/23/EC: Sound Engineering Practice
ATEX 94/9/EC (Optional)
EMC Directive 2004/108/EC

BS EN 61000-6-1: 2007	Susceptibility - Light Industrial
BS EN 61000-6-2: 2005	Susceptibility - Heavy Industrial (except mV versions)
BS EN 61000-6-3: 2007	Emissions - Light Industrial
BS EN 61000-6-4: 2007	Emissions - Heavy Industrial
BS EN 61326-1: 2006	Electrical Equipment for Measurement, Control and Laboratory Use
BS EN 61326-2-3: 2006	Particular Requirements for Pressure Transducers

Hazardous Area Approvals (optional)

General applications

- IECEx/ATEX Intrinsically Safe 'ia' Group IIC
- INMETRO Intrinsically Safe 'ia' Group IIC
- NEPSI Intrinsically Safe 'ia' Group IIC
- FM Approved (Canada & US) Intrinsically Safe Exia Class I, Division 1, Groups A, B, C & D and Class I, Zone 0 AEx/Ex ia Group IIC; Single Seal

Mining applications

- IECEx/ATEX Intrinsically Safe 'ia' Group I
- INMETRO Intrinsically Safe 'ia' Group I

For full certification details, refer to the type-examination certificates (or approval listings) and supplied hazardous area installation instructions.

Electrical Connector

Connector Type	Option code		Electronics Option					
			4 to 20 mA	Voltage (3-wire) and Basic Configurable	Voltage (4-wire)	Configurable Voltage (4-Wire)	Configurable Voltage (3-Wire)	mV
Molex	0	1 Red	+ve Supply	+ve Supply	+ve Supply	+ve Supply	+ve Supply	+ve Supply
		2 Yellow	-	+ve Output	+ve Output	+ve Output	+ve Output	+ve Output
		3 Green	-	-	-ve Output	-ve Output	0V Common	-ve Output
		4 Blue	-ve Supply	0V Common	-ve Supply	-ve Supply	0V Common	-ve Supply
		5 Orange	-	-	-	Shunt Cal	Shunt Cal	Shunt Cal
		6 Black	Case	Case	Case	Case	Case	-
Cable (Not Raychem)	1, 3, 4, C	Red	+ve Supply	+ve Supply	+ve Supply	+ve Supply	+ve Supply	+ve Supply
		Yellow	-	+ve Output	+ve Output	+ve Output	+ve Output	+ve Output
		Blue	-	-	-ve Output	-ve Output	0V Common	-ve Output
		White	-ve Supply	0V Common	-ve Supply	-ve Supply	0V Common	-ve Supply
		Orange	-	-	-	Shunt Cal	Shunt Cal	Shunt Cal
		Black	-	-	-	-	-	-
		Screen	-	-	-	-	-	-
Raychem Cable	2	Red	+ve Supply	+ve Supply	+ve Supply	+ve Supply	+ve Supply	+ve Supply
		White	-	+ve Output	+ve Output	+ve Output	+ve Output	+ve Output
		Green	-	-	-ve Output	-ve Output	0V Common	-ve Output
		Blue	-ve Supply	0V Common	-ve Supply	-ve Supply	0V Common	-ve Supply
		Black	-	-	-	Shunt Cal	Shunt Cal	Shunt Cal
		Screen	-	-	-	-	-	-
Bayonet	6, A	A	+ve Supply	+ve Supply	+ve Supply	+ve Supply	+ve Supply	+ve Supply
		B	-ve Supply	+ve Output	+ve Output	+ve Output	+ve Output	+ve Output
		C	-	-	-ve Output	-ve Output	0V Common	-ve Output
		D	-	0V Common	-ve Supply	-ve Supply	0V Common	-ve Supply
		E	-	-	-	Shunt Cal	Shunt Cal	Shunt Cal
		F	-	-	-	-	-	Shunt Cal
DIN A Micro DIN	7 D	1	+ve Supply	+ve Supply	+ve Supply	+ve Supply	+ve Supply	+ve Supply
		2	-ve Supply	0V Common	-ve Supply	-ve Supply	0V Common	-ve Supply
		3	-	+ve Output	+ve Output	+ve Output	+ve Output	+ve Output
		E	Case	Case	-ve Output	-ve Output	0V Common	-ve Output
Bayonet Alternative Wiring Options	E, F	A	+ve Supply	+ve Supply	+ve Supply	+ve Supply	+ve Supply	+ve Supply
		B	-	0V Common	-ve Supply	-ve Supply	0V Common	-ve Supply
		C	-	+ve Output	+ve Output	+ve Output	+ve Output	+ve Output
		D	-ve Supply	-	-ve Output	-ve Output	0V Common	-ve Output
		E	-	-	-	Shunt Cal	Shunt Cal	Shunt Cal
		F	-	-	-	Shunt Cal	Shunt Cal	-
M12 X 1 4-Pin	G	1	+ve Supply	+ve Supply	+ve Supply	+ve Supply	+ve Supply	+ve Supply
		2		+ve Output	+ve Output	+ve Output	+ve Output	+ve Output
		3	-ve Supply	0V Common	-ve Supply	-ve Supply	0V Common	-ve Supply
		4	Case	Case	-ve Output	-ve Output	0V Common	-ve Output
Zero Halogen Cable (Demountable)	K	Pink	+ve Supply	+ve Supply	+ve Supply	+ve Supply	+ve Supply	+ve Supply
		White	-	+ve Output	+ve Output	+ve Output	+ve Output	+ve Output
		Green	-	-	-ve Output	-ve Output	0V Common	-ve Output
		Blue	-ve Supply	0V Common	-ve Supply	-ve Supply	0V Common	-ve Supply
		Grey	-	-	-	Shunt Cal	Shunt Cal	Shunt Cal
		Brown	-	-	-	-	-	-
		Yellow	-	-	-	-	-	-
		Screen	-	-	-	-	-	-
Tajimi R03-R6F	M	A	+ve Supply	+ve Supply	+ve Supply	+ve Supply	+ve Supply	+ve Supply
		B	-	0V Common	-ve Supply	-ve Supply	0V Common	-ve Supply
		C	-ve Supply	Case	Case	Case	Case	-
		D	-	-	-ve Output	-ve Output	0V Common	-ve Output
		E	Case	+ve Output	+ve Output	+ve Output	+ve Output	+ve Output
		F	-	-	Shunt cal	Shunt cal	Shunt Cal	Shunt cal
M20 x 1.5 Female Demountable	R	+ve	+ve Supply	-	-	-	-	-
		-ve	-ve Supply	-	-	-	-	-

Ordering Information

See the online configuration tool at www.unik5000.com

(1) Select model number

Main Product Variant

PMP Amplified Pressure Transducer
PDCR mV Pressure Transducer
PTX 4-20 mA Pressure Transmitter

Product Series

5 UNIK 5000

Diameter and Material

0 25mm Stainless Steel

Electrical Connector Note 6

0 No Electrical Connector **Note 7**
1 Cable Gland (Polyurethane Cable)
2 Raychem Cable
3 Polyurethane Cable (Depth)
4 Hytrel Cable (Depth)
6 MIL-C-26482 (6-pin Shell Size 10) (Mating connector not supplied)
7 DIN 43650 Form A Demountable (Mating connector supplied)
A Demountable MIL-C-26482 (6-pin Shell Size 10) (Mating connector not supplied)
C 1/2" NPT Conduit (Polyurethane cable)
D Micro DIN (9.4 mm Pitch) (Mating connector supplied)
E MIL-C-26482 (6 pin Shell Size 10) Alternative Wiring (Mating connector not supplied)
F Demountable MIL-C-26482 (6 pin Shell Size 10) Alternative Wiring (Mating connector not supplied)
G M12 x 1 4-pin male (Mating connector not supplied)
K Zero Halogen Cable Demountable
M Tajimi R03-R6F
R M20 x 1.5 Inline Female Conduit Demountable **Note 8**

Electronics Option

0 mV Passive 4-wire (PDCR) **Note 1**
1 mV Linearised 4-wire (PDCR)
2 4 to 20 mA 2-wire (PTX)
3 0 to 5 V 4-wire (PMP)
4 0 to 5 V 3-wire (PMP)
5 Basic Configurable 3-wire (PMP)
6 0 to 10 V 4-wire (PMP)
7 0.5 to 4.5 V Ratiometric 3-wire (PMP) **Note 5**
8 Configurable 4-wire (PMP) **Note 4, 5**
9 Configurable 3-wire (PMP) **Note 4, 5**

Compensated Temperature Range

TA -10 to +50 °C (14 to +122 °F)
TB -20 to +80 °C (-4 to +176 °F)
TC -40 to +80 °C (-40 to +176 °F)
TD -40 to +125 °C (-40 to +257 °F) **Note 2, 5**

Accuracy

A1 Industrial
A2 Improved
A3 Premium

Calibration

CA Zero/Span Data
CB Room Temperature
CC Full Thermal

Hazardous Area Approval Note 6

H0 None
H1 IECEx/ATEX Intrinsically Safe 'ia' Group IIC
H2 IECEx/ATEX Intrinsically Safe 'ia' Group I
H6 FM (C & US) Intrinsically Safe 'ia' Group IIC/ABCD
HA IECEx/ATEX Intrinsically Safe 'ia' Groups I/IIC (H1 + H2)
HS IECEx/ATEX/FM (C & US) Intrinsically Safe 'ia' Groups IIC/ABCD (H1 + H6)
J1 IECEx/ATEX/NEPSI Intrinsically Safe 'ia' Group IIC
JA INMETRO Intrinsically Safe 'ia' Group IIC
JB INMETRO Intrinsically Safe 'ia' Group I
JF INMETRO Intrinsically Safe 'ia' Group I/IIC (JA + JB)

Pressure Connector

PA	G1/4 Female **Note 3**	**PV**	7/16-20 UNF Female
PB	G1/4 Male Flat	**PW**	Depth Cone (G1/4 Female Open Face)
PC	G1/4 Male 60° Internal Cone	**PX**	7/16-20 UNF Male Short Flat
PD	G1/8 Male 60° Internal Cone	**PY**	3/8-24 UNJF
PE	1/4 NPT Female **Note 3**	**PZ**	M10 x 1 80° Internal Cone
PF	1/4 NPT Male	**RA**	VCR Female **Note 3, 9**
PG	1/8 NPT Male	**RB**	G1/4 Male Flat with Snubber
PH	M20x1.5	**RC**	G1/4 Male Flat with Cross Bore Protection
PJ	M14x1.5 60° Internal Cone	**RD**	M12 x 1.0 74° External Cone
PK	M12x1 Internal Cone	**RE**	Quick Release Mount
PL	7/16-20 UNJF Male 74° External Cone	**RF**	VCR Male **Note 3, 9**
PN	G1/2 Male via Adaptor **Note 3**	**RQ**	NW16 Flange
PQ	G1/4 Quick Connect	**RU**	R3/8 Male
PR	1/2 NPT Male via Adaptor **Note 3**	**RV**	R1/4 Male
PS	1/4 Swagelok Bulkhead	**RW**	G1/4 Male with Nipple
PT	G1/4 Male Flat Long		
PU	7/16-20 UNF Long 37° Flare Tip		

PTX	**5**	**0**	**7**	**2**	**-**	**TA**	**-**	**A2**	**-**	**CB**	**-**	**H0**	**-**	**PA**	**Typical Model Number**

Ordering Notes
Note 1 Premium Accuracy is not available on this version
Note 2 Please ensure that the electrical connector selected is option 0, 2, 6, A, E, F or G.
Note 3 Select one of these pressure connectors for pressure ranges over 70 bar
Note 4 Max operating temperature is 80°C (176°F)
Note 5 Hazardous area certifications not available
Note 6 Hazardous area certifications are restricted by electrical connector options in line with the following table:

	Connector													
Approval	0	1	2	3	4	6/E	7	A/F	C	D	G	K	M	R
H0	Y	Y	Y	Y	Y	Y	Y	Y	Y	Y	Y	Y	Y	Y
H1	Y	Y	Y	Y	Y	Y	Y	Y	Y	Y	Y	-	-	Y
H2	Y	-	Y	Y	Y	Y	-	-	Y	-	Y	-	-	-
H6	Y	Y	Y	Y	Y	Y	Y	Y	Y	Y	Y	-	-	-
HA	Y	-	Y	Y	Y	Y	-	-	Y	-	Y	-	-	-
HS	Y	Y	Y	Y	Y	Y	Y	Y	Y	Y	Y	-	-	-
J1	Y	Y	Y	Y	Y	Y	Y	Y	Y	Y	Y	-	-	Y
JA	Y	Y	Y	Y	Y	Y	Y	Y	Y	Y	Y	-	-	Y
JB	Y	-	Y	Y	Y	Y	-	-	Y	-	Y	-	-	-
JF	Y	-	Y	Y	Y	Y	-	-	Y	-	Y	-	-	-

Note 7 Available with component certification, use of which requires incorporation into certified apparatus with an IP rated enclosure appropriate to the certification type supplied.
Note 8 Electronics option 2 only.
Note 9 Pressure ranges less than 500 bar.

2) State pressure range and units: e.g. 0 to 10 bar, -5 to + 5 psi

Unit options are:

Symbol	Description
bar	bar
mbar	millibar
psi	pounds/sq. inch
Pa	Pascal
hPa	hectoPascal
kPa	kiloPascal
MPa	MegaPascal
mmH_2O	mm water
cmH_2O	cm water
mH_2O	metres water
inH_2O	inches water
ftH_2O	feet water
mmHg	mm mercury
inHg	inches mercury
kgf/cm^2	kg force/sq. cm
atm	atmosphere
Torr	torr

3) State Pressure reference: e.g. gauge

Reference options are:
gauge
absolute
barometric
sealed gauge
wet/dry differential
wet/wet differential

4) State cable lengths and units: Integer values only, e.g. 1m cable, 8 ft. Minimum length 1 m (3 ft) cable (only required on certain electrical connectors). Maximum cable length 100 m (300 ft) for approval options not H0; 200 m (600 ft) for approval option H0.

5) Output options 5, 8 and 9: State voltage output at minimum and maximum pressure: e.g. output -1 to 9 V

Typical order examples:

PTX5012-TB-A2-CA-H0-PA, 0 to 10 bar, gauge, 3 m cable
PMP5028-TD-A3-CC-H0-PE, -15 to 75 psi, gauge, 15ft cable, output voltage -1 to 5 volts
PDCR5071-TB-A1-CB-H0-PB, 0 to 100 bar, sealed gauge

Accessories

Mating connector for MIL-C-26482 (Electrical connector options 6, A, E and F) under part number S_163-009.

Note: Not considered suitable for use in hazardous areas due to light metals content and low ingress protection (IP) rating.

Mechanical Drawings

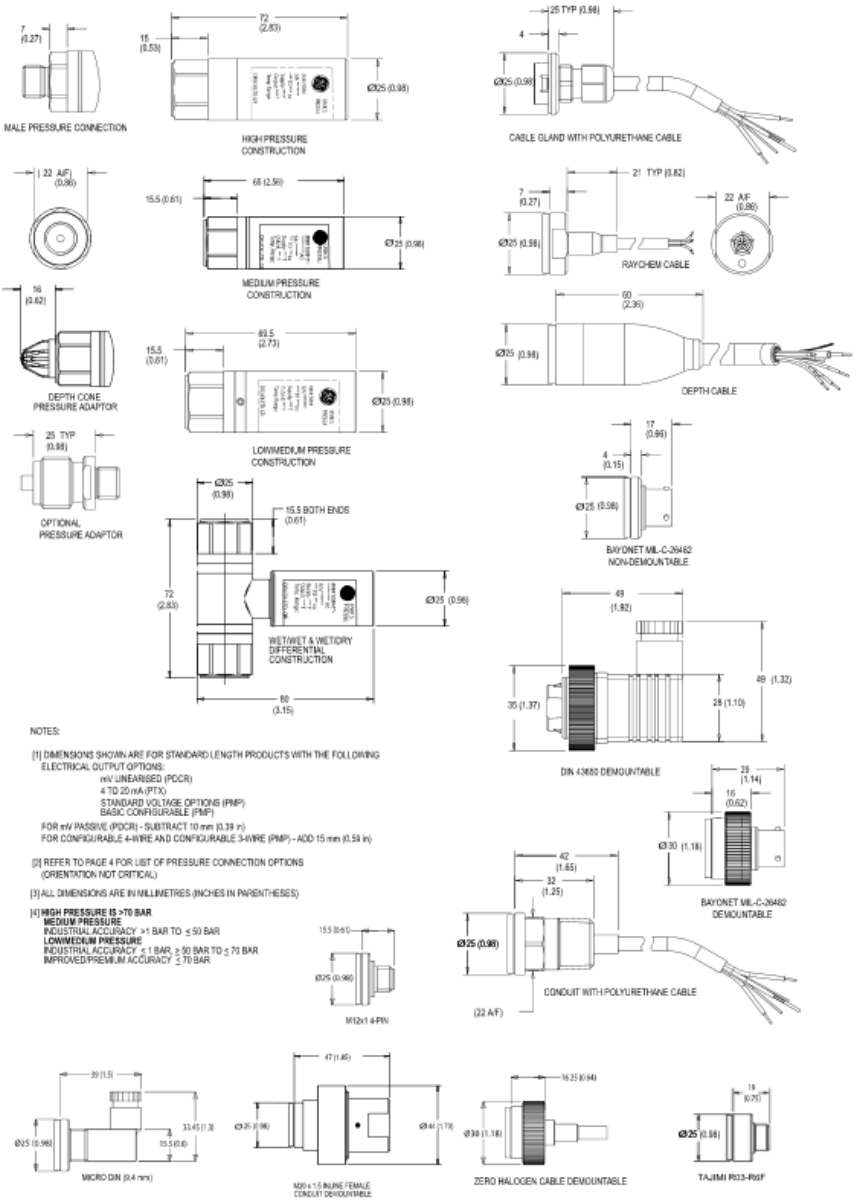

NOTES:

[1] DIMENSIONS SHOWN ARE FOR STANDARD LENGTH PRODUCTS WITH THE FOLLOWING ELECTRICAL OUTPUT OPTIONS:
- mV LINEARISED (PDCR)
- 4 TO 20 mA (PTX)
- STANDARD VOLTAGE OPTIONS (PMP)
- BASIC CONFIGURABLE (PMP)

FOR mV PASSIVE (PDCR) - SUBTRACT 10 mm (0.39 in)
FOR CONFIGURABLE 4-WIRE AND CONFIGURABLE 3-WIRE (PMP) - ADD 15 mm (0.59 in)

[2] REFER TO PAGE 4 FOR LIST OF PRESSURE CONNECTION OPTIONS (ORIENTATION NOT CRITICAL)

[3] ALL DIMENSIONS ARE IN MILLIMETRES (INCHES IN PARENTHESES)

[4] **HIGH PRESSURE IS >70 BAR**
MEDIUM PRESSURE
INDUSTRIAL ACCURACY >1 BAR TO ≤ 50 BAR
LOW/MEDIUM PRESSURE
INDUSTRIAL ACCURACY ≤ 1 BAR, ≥ 50 BAR TO ≤ 70 BAR
IMPROVED/PREMIUM ACCURACY ≤ 70 BAR

www.ge-mcs.com

920-483J

Appendix E Wiring Diagram for Volume Fraction Meter

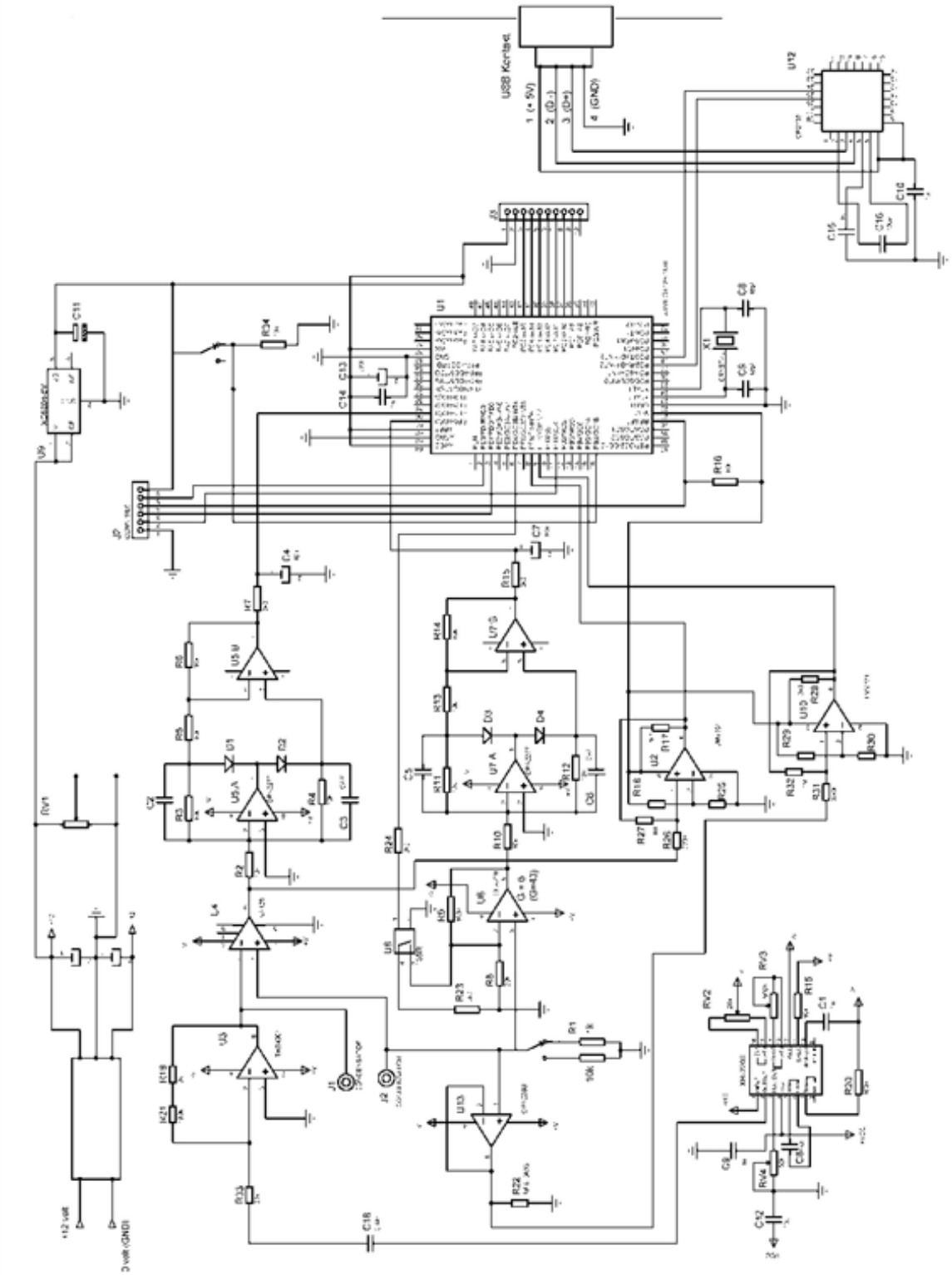

Figure D.1: Wiring diagram of the volume fraction meter developed by Sivertsen (2002)

A version of the wiring diagram with a higher resolution is included in the digital attachment.

Appendix F Pictures of Experiments and LedaFlow

8.925 m^3/h: Exxsol D60 displacing Water (f = 13.50 Hz)

23 s

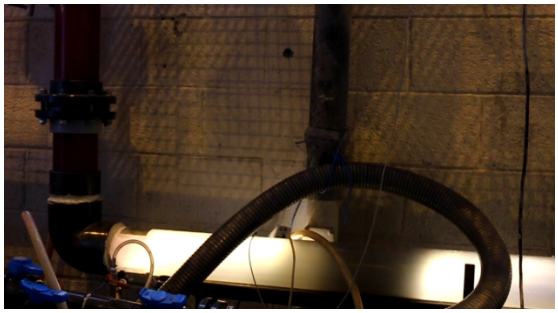

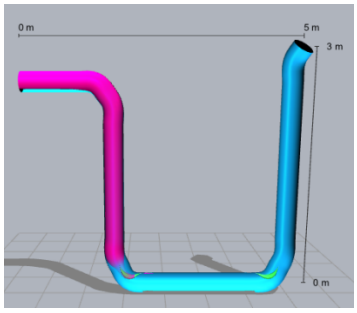

45 s

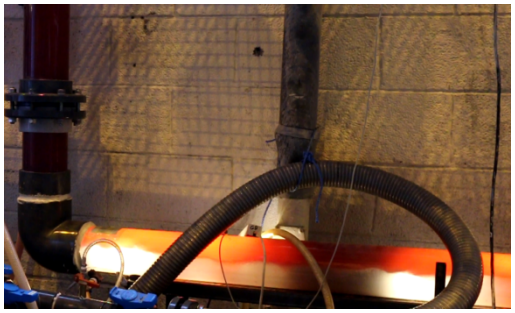

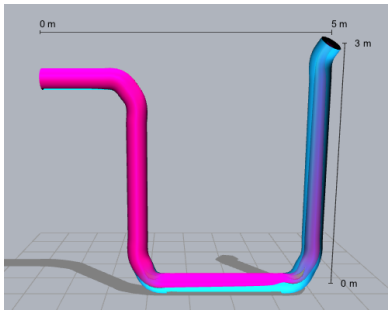

63 s

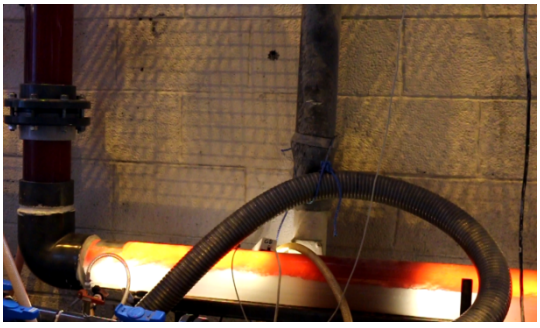

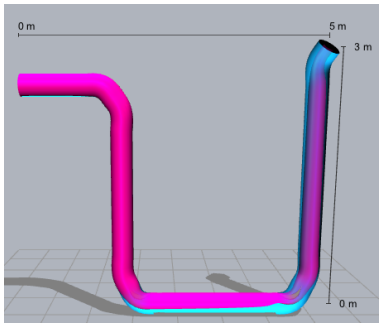

125 s

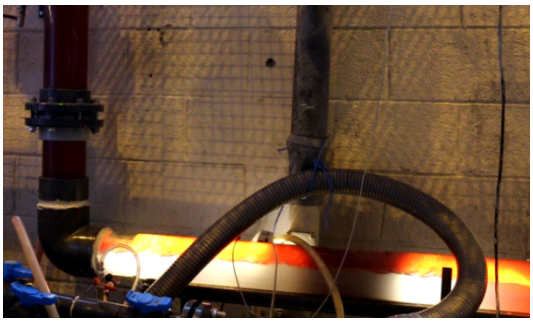

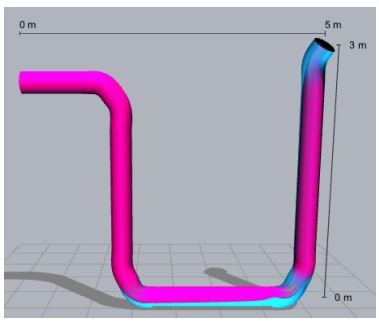

188 s

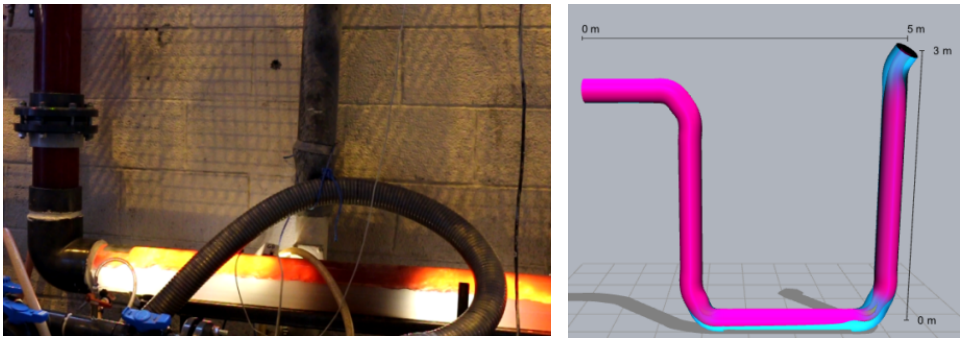

360 s

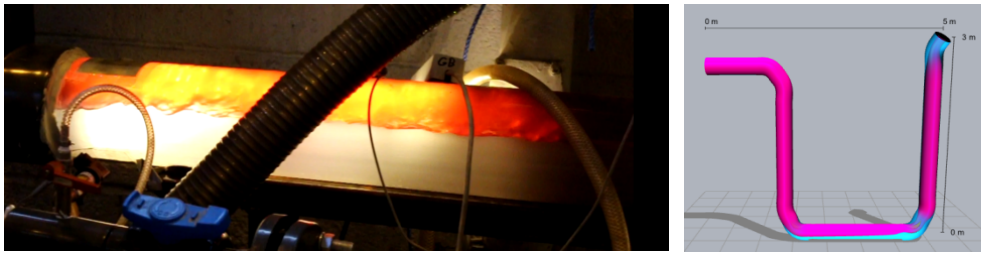

Figure F.1: Pictures of experiment and LedaFlow model at different times, for oil displacing water at 8.925 m3/h

19.730 m^3/h: Exxsol D60 displacing Water (f = 24.50 Hz)

11 s

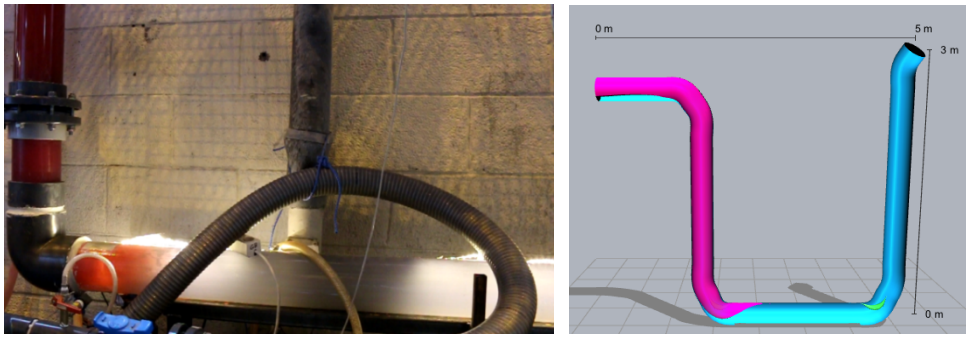

13 s

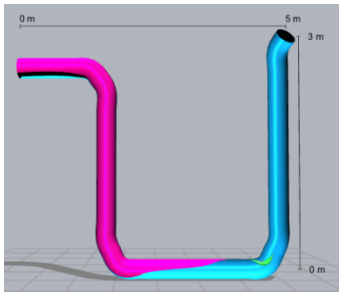

20 s

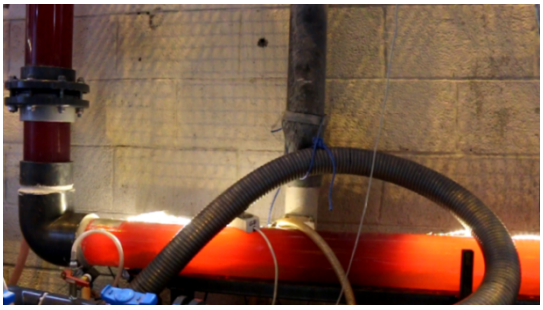

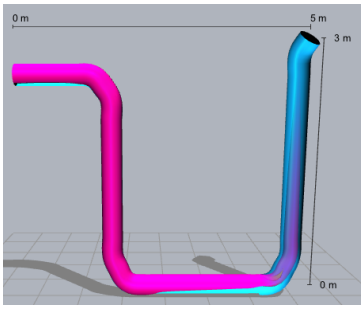

31 s

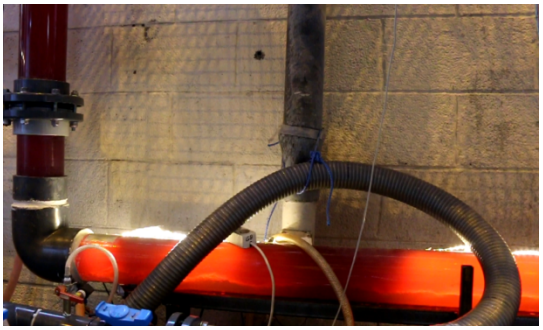

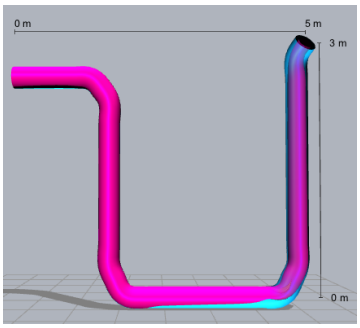

63 s

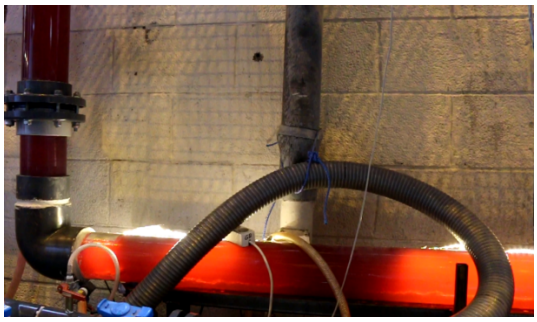

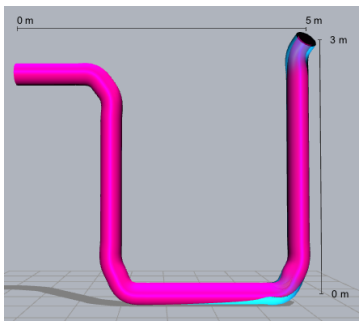

94 s

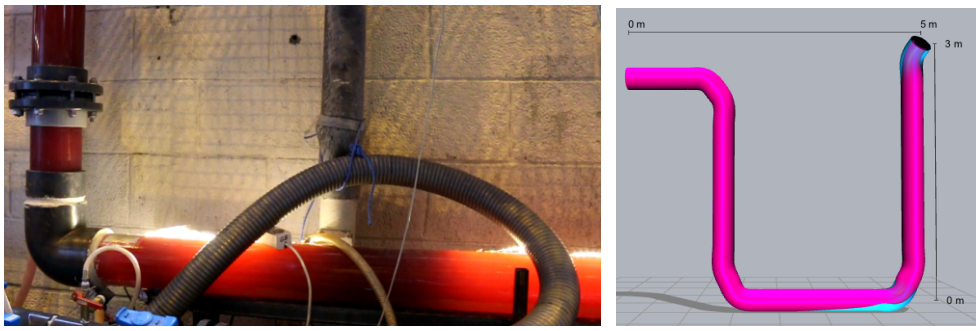

243 s

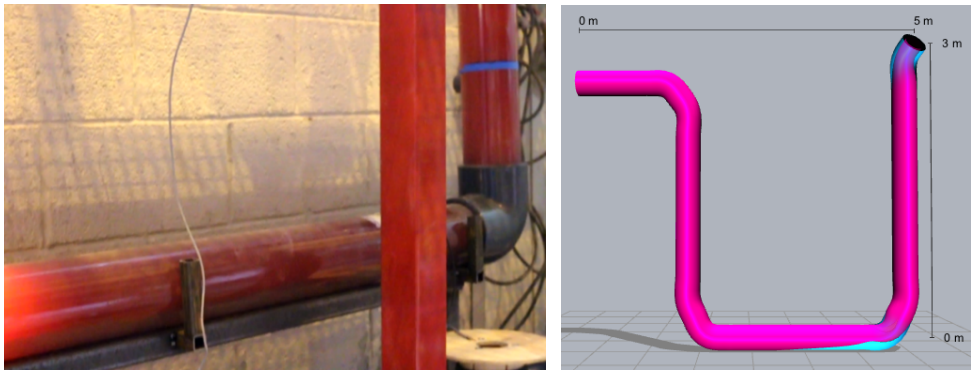

Figure F.2: Pictures of experiment and LedaFlow model at different times, for oil displacing water at 19.730 m3/h

28.164 m^3/h: Exxsol D60 displacing Water (f = 34.00 Hz)

9 s

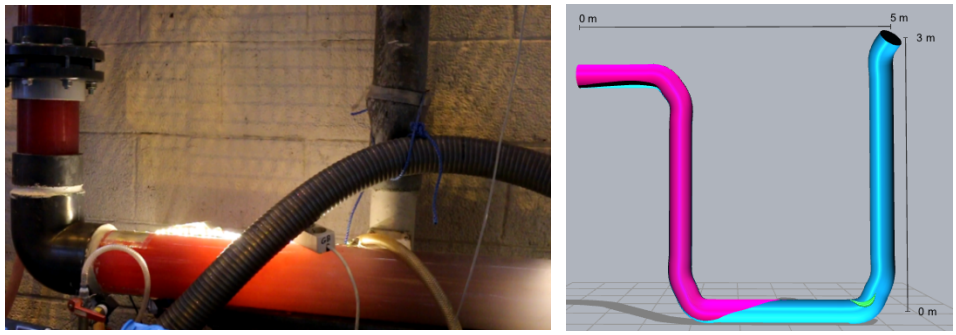

14 s

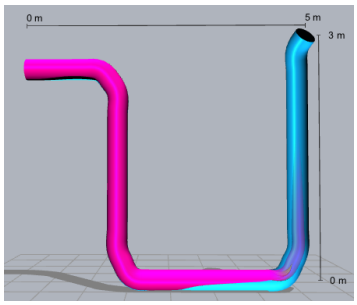

21 s

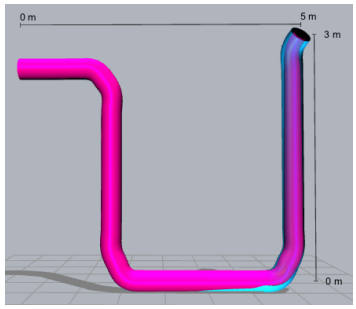

42 s

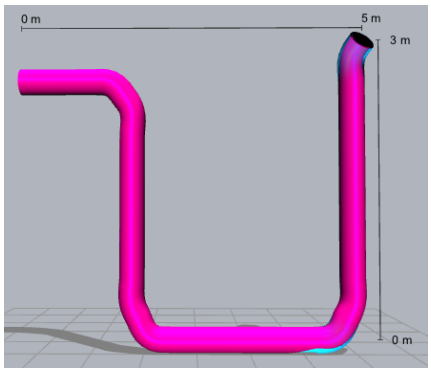

64 s

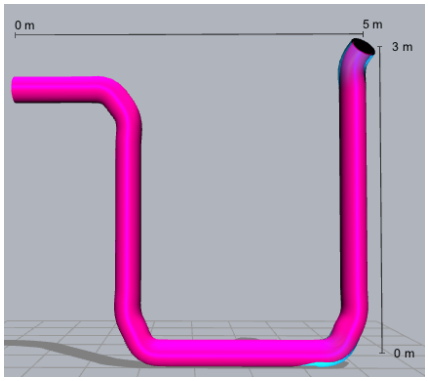

140 s

Figure F.3: Pictures of experiment and LedaFlow model at different times, for oil displacing water at 28.164 m3/h

37.743 m3/h: Exxsol D60 displacing Water (f = 44.40 Hz)

6 s

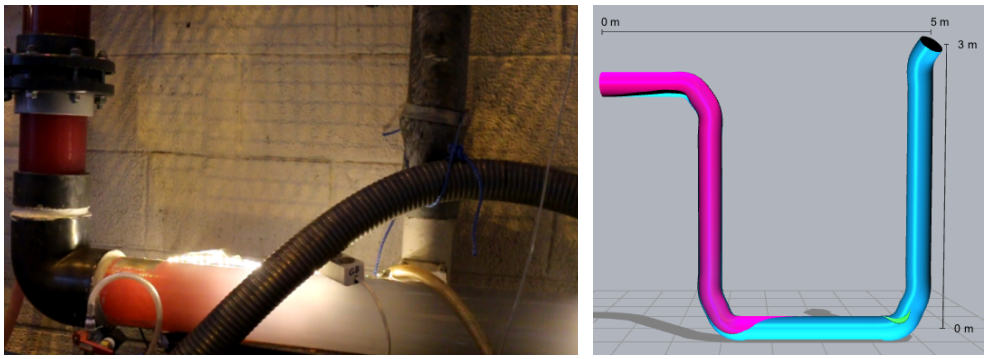

13 s

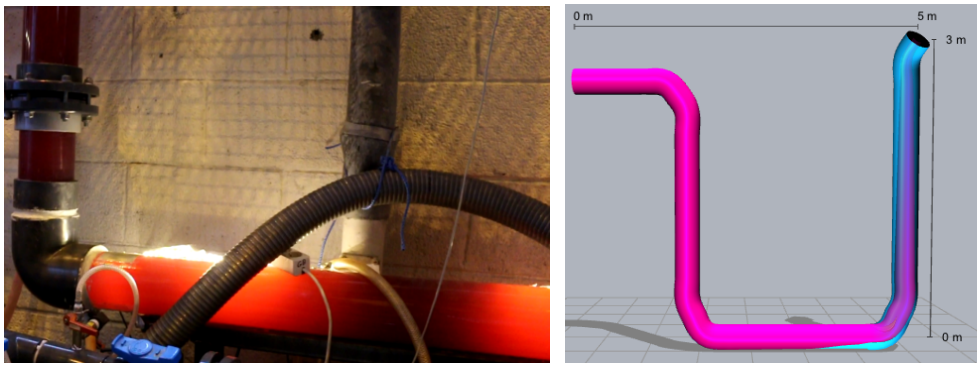

16 s

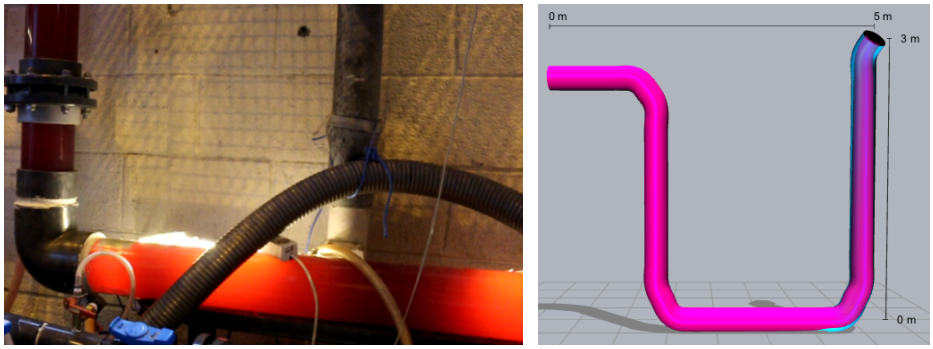

31 s

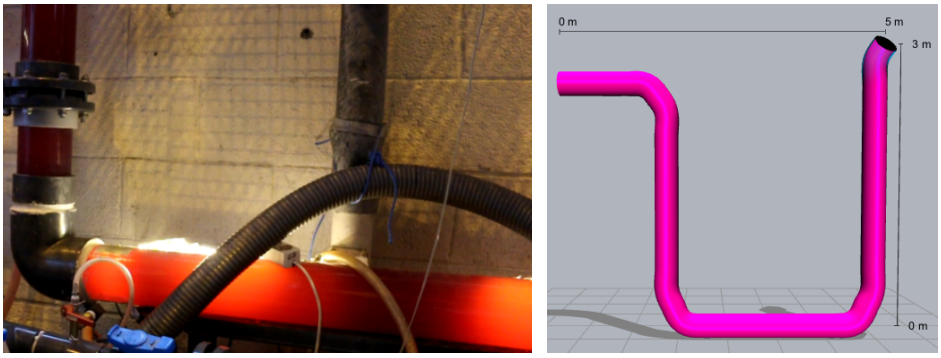

48 s

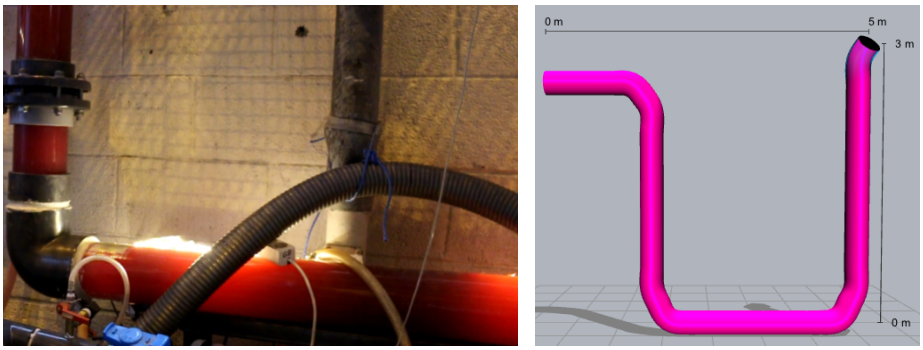

263 s

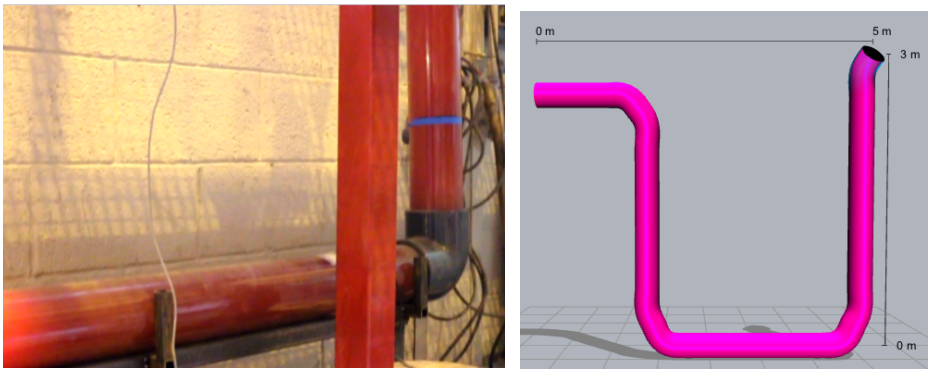

Figure F.4: Pictures of experiment and LedaFlow model at different times, for oil displacing water at 37.743 m3/h

6.190 m^3/h: Water displacing Exxsol D60 (f = 10.50 Hz)

37 s

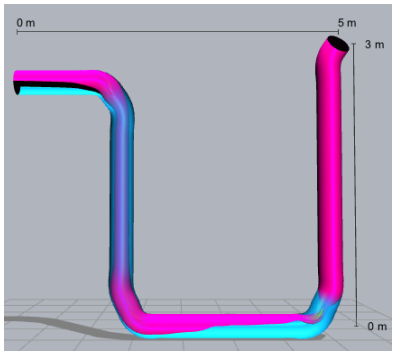

72 s

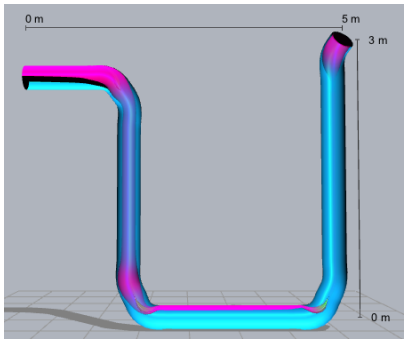

106 s

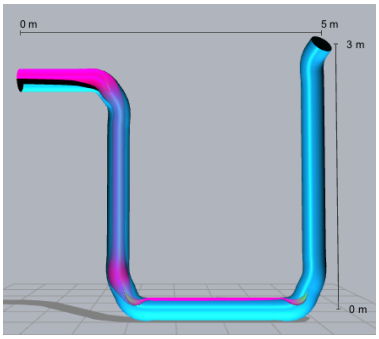

209 s

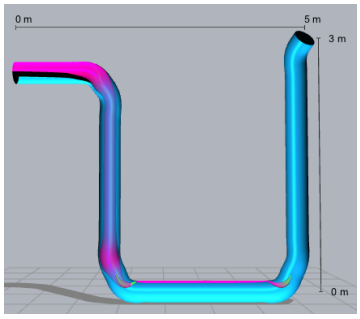

314 s

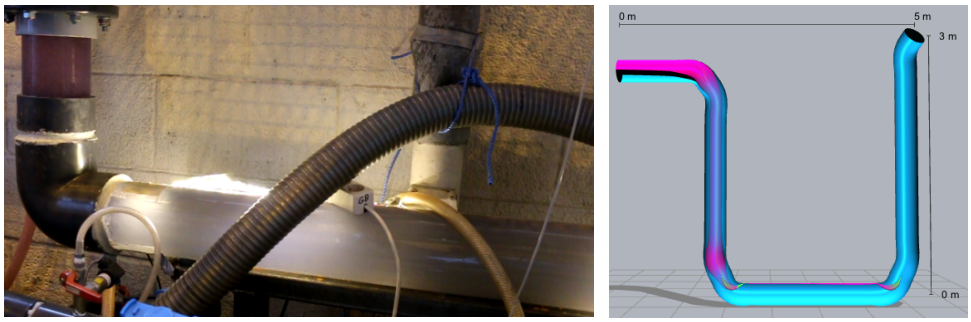

329 s

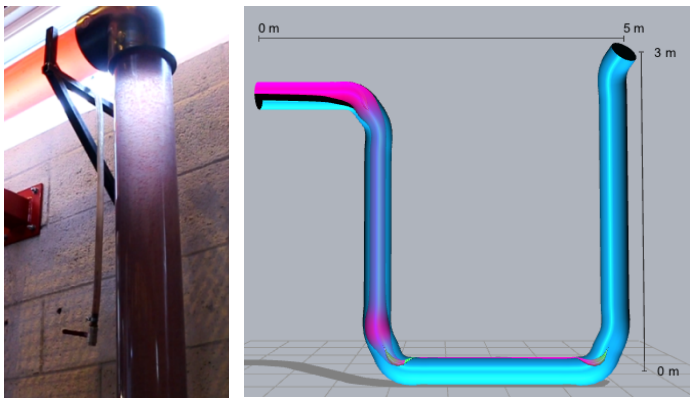

341 s

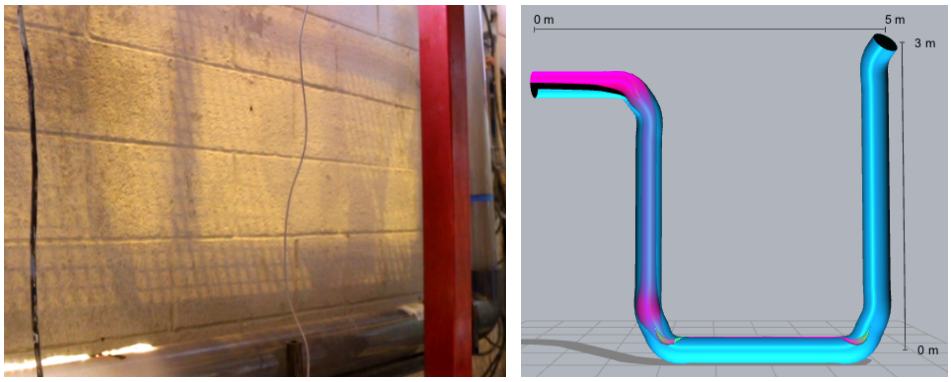

Figure F.5: Pictures of experiment and LedaFlow model at different times, for water displacing oil at 6.190 m3/h

20.769 m^3/h: Water displacing Exxsol D60 (f = 24.50 Hz)

11 s

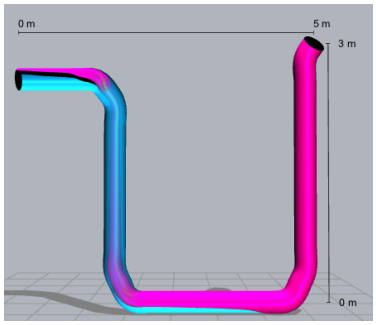

21 s

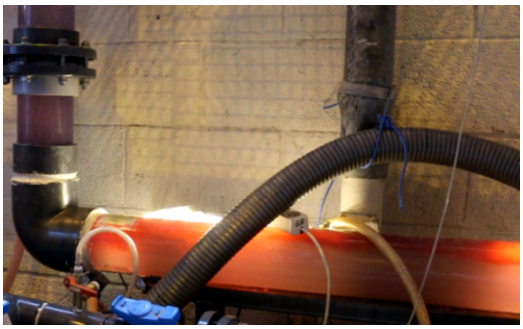

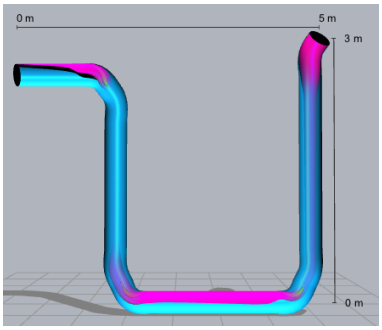

32 s

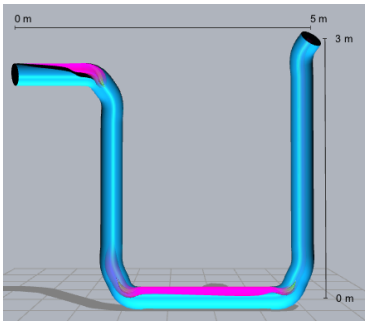

63 s

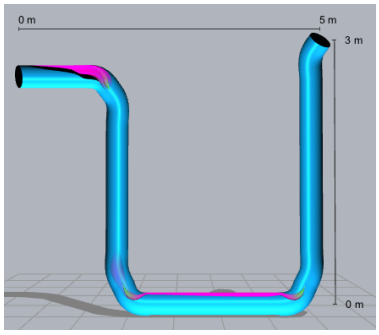

95 s

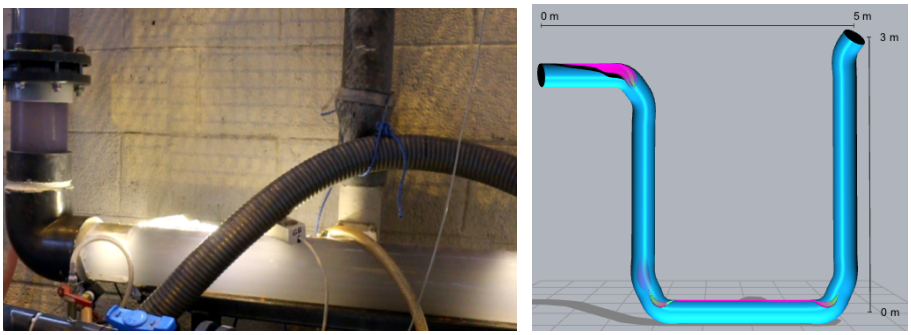

219 s

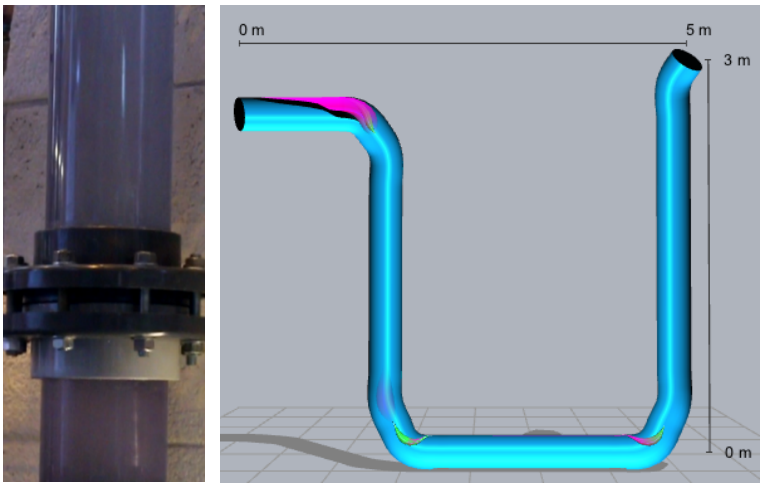

224 s

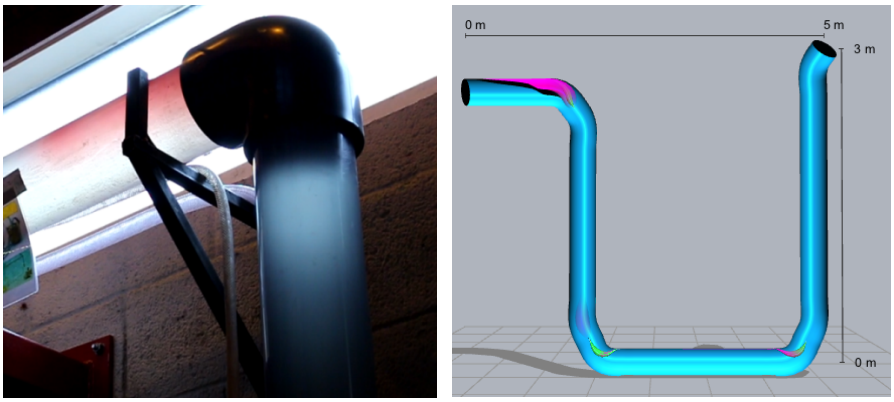

Figure F.6: Pictures of experiment and LedaFlow model at different times, for water displacing oil at 20.769 m3/h

Appendix G How to Build a Simple Model in LedaFlow

Appendix G contains a simple tutorial on how to build a model in LedaFlow.

STEP 1: Getting to know LedaFlow

The Graphical User Interface, GUI, for LedaFlow can be seen in Figure G.1. The window consists of a case browser where all the projects and their cases may be found, a status window showing the progress of the running simulations and a display area where the operators from the toolbox are shown. The toolbox on the left side has five different functions that are described in Table G.1.

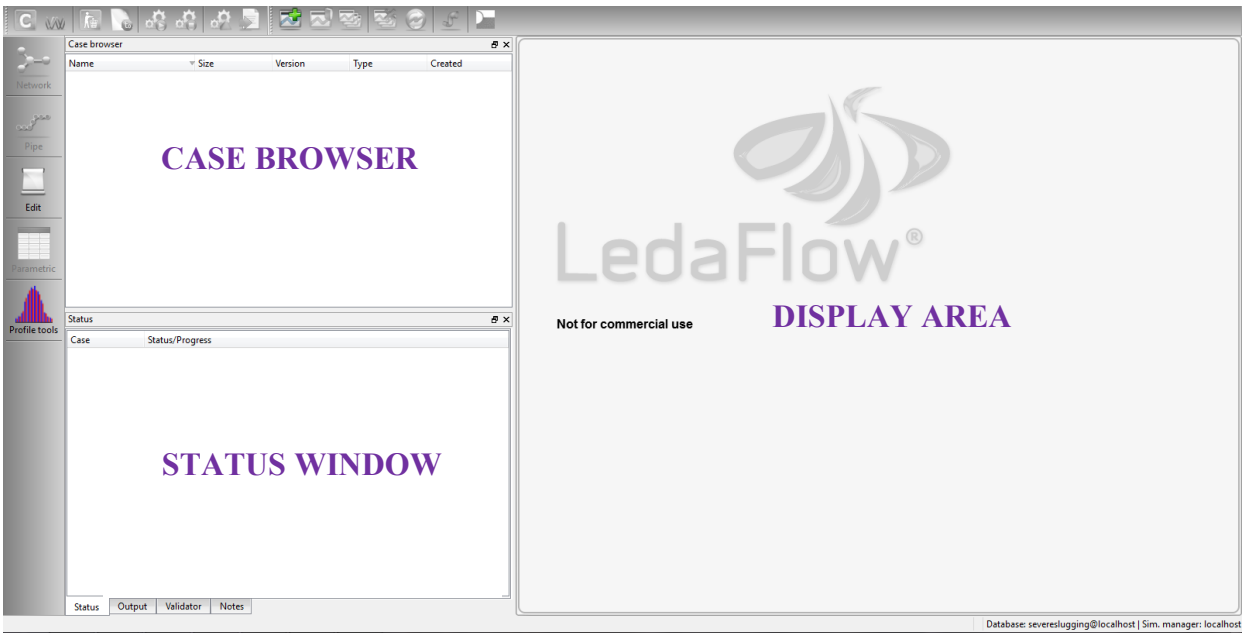

Figure G.1: LedaFlow GUI

Table G.1: Toolbox functions (KONGSBERG, 2016b)

FUNCTION	Purpose
NETWORK	Visualization and constructing/editing the global networks: Where one can add pipes and components to a system
PIPE	Setting the geometry of the pipelines, the meshing and defining the wall properties
EDIT	Script functionalities
PARAMETRIC STUDY	Parametric study functionality
PROFILE TOOLS	Profile generation, filtering and simplification toll

STEP 2: Building a model

1. Creating a case:

Right-click in the case browser window to create a case. The user has two choices

a. Default case with 2 phases (liquid-gas) or 3 phases (water-oil-gas) that is composed of a 300 meter horizontal line with default properties, giving the user the possibility to run it straight ahead

b. Sample case with different scenarios

2. Case settings:

Press the C-button marked by the red ring in the figure below.

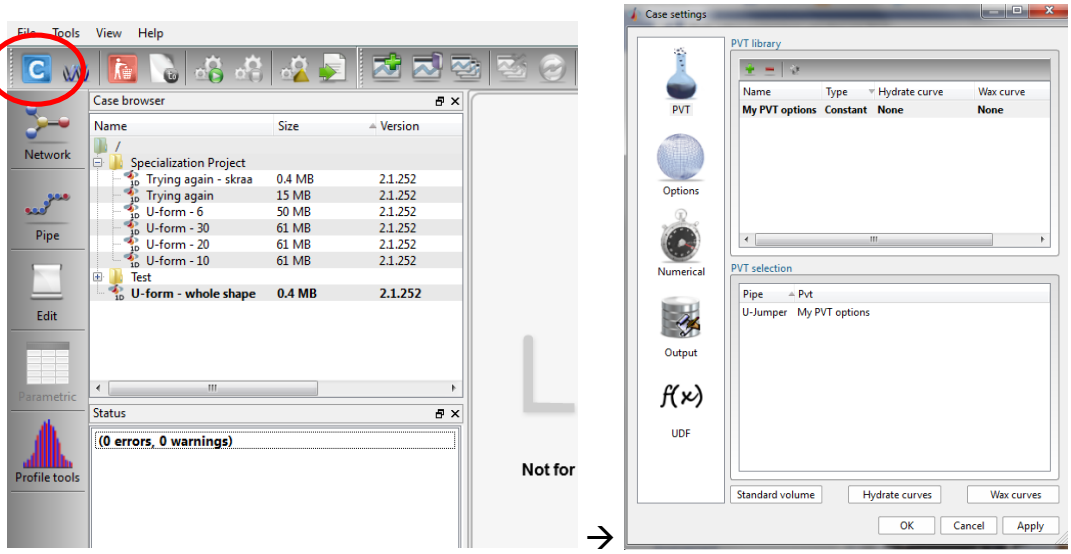

a. PVT-Properties

Insert the PVT-properties: constant, table or MultiFlash^{TM}.

b. Options

Here are the general options, the thermal options and the flow assurance (emulsion, pigging, hydrate etc.) settings specified.

c. Numerical

The numerical settings for the simulation are specified. **Simulation time:** The time the simulator will use to advance the solution. **Time step control:** LedaFlow is using dynamic time steps. The user may specify the maximum time step and the CFL number for a time period. The

CFL number is the Courant-Friedrichs-Lewy condition number, and is specified to ensure that the time step is low enough in relation to the grid cell length and the phase velocities (KONGSBERG, 2016b).

d. Output

e. UDF

3. Network:

Use the "Network"-button on the toolbar

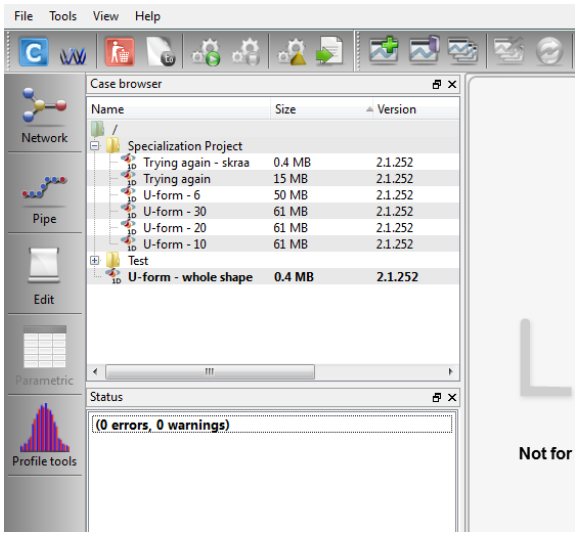

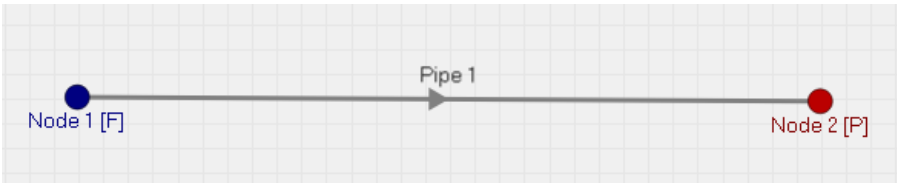

a. Pipelines

Extra pipelines can be added to the system by right-clicking in the window or at the node where one wants the pipe to start/stop.

b. Devices

Extra devices such as valves, pumps, separators, etc. may be added by right-clicking on the pipeline where one wants to add it.

c. Nodes

Boundary conditions → Choose between either mass-pressure boundaries or pressure-pressure boundaries. Different phase split options for the

boundaries are found in Table G.2 for the mass inlet boundaries and in Table G.3 for the pressure boundaries.

Table G.2: Phase Split Options for Mass Inlet Boundary (KONGSBERG, 2016b)

Phase Split Options for Mass Inlet Boundary	
Flash	The mass fractions are calculated from the PVT table. Mass flowrates and fluid temperature need to be specified.
Flash hydrocarbons only	The mass fraction of gas and oil are calculated from PVT table but the mass fraction of water is specified by the user.
Mass fractions	The mass fractions of gas, oil and water have to be defined in addition to the total mass flow rate and the temperature of the fluid.
Standard volumes	The standard volume flowrate of gas or oil (optionally water too) and the fluid temperature need to be specified to calculate the mass flowrates of the phases based on flash calculations.

Table G.3: Phase Split Options for Pressure Boundary (KONGSBERG, 2016b)

Phase Split Options for Pressure Boundary	
Flash	The volume fractions are calculated from PVT table. Pressure and fluid temperature need to be specified.
Flash hydrocarbons only	The mass fractions of gas and oil are calculated from PVT table but the mass fraction of water is specified by the user together with the pressure and fluid temperature.
Mass fractions Volume fractions	The mass or volume fractions of gas, oil and water should be specified. This option will be selected to account for back flow; for example if gas fraction is equal to 1, only gas will flow back.
Standard volume fractions	The user may provide 1 or 2 standard volume fractions. Instead of standard volume fractions, the user may provide GOR, GLR and WC but need to provide only 1 or 2 of them. The others are calculated automatically.

4. Pipe:

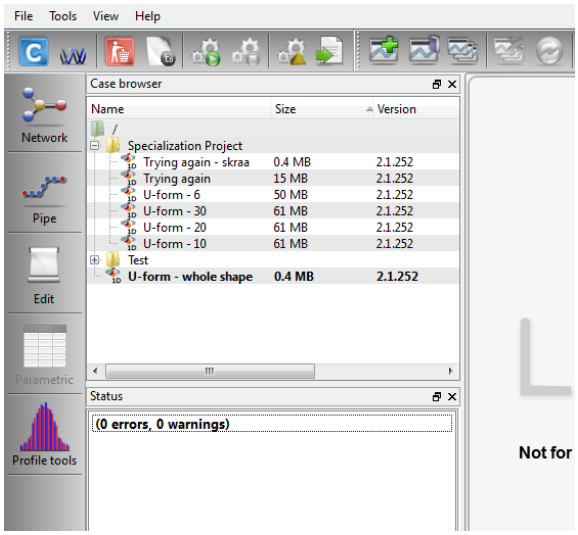

→

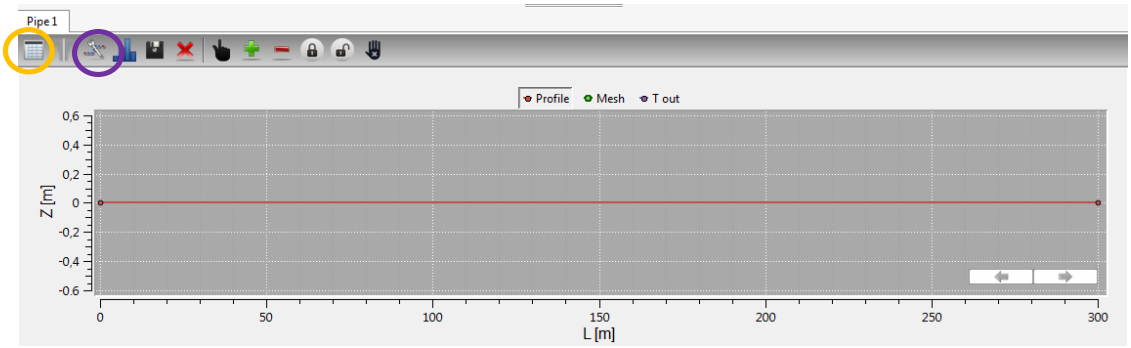

a. Pipe editor (orange circle)

Possibilities to add/change properties of the pipelines.

Profile → Add the desired profile of the pipeline

Ambient → Add properties for thermal calculations

Geometry → Add geometry (diameter, roughness, wall type) of the pipeline

Burial

Slug capturing

b. Mesh editor (purple circle)

Possibilities to add/change the mesh properties of the pipeline including adding/removing mesh points. The mesh is a discretization of the geometry used for numerical computation (KONGSBERG, 2016b).

Mesh Method → Choose between 4 types

Horizontal/Vertical

Least squares

Uniform

DeltaX/D

STEP 3: Running simulations

1. **Run simulation (red circle)**

By initializing the case the user has the options of running the case with a

Steady-state pre-processor:

User-defined initial conditions/gas-filled-pipe mode:

Restart file:

The box for "run dynamic" should be ticked off if one wants to run a transient solution.

The status window is showing the progress of the simulation process for the case and when it is completed

2. **Purge results (yellow circle)**

If the user wish to do modifications to the model it is necessary to "purge" the result. By purging the result one has the ability to delete parts or all of the stored data in the database. By choosing "initializing" when running a model, the case is automatically purged.

STEP 4: Extracting results

There are two types of loggers that can be used in the LedaFlow software; profile loggers and trend loggers.

Profile loggers: Used for capturing results for the whole profile of the pipeline.

Trend loggers: Used for capturing results of high frequency for devices or special points of interest along the pipe (KONGSBERG, 2016b).

One has the ability to create plots of the results in LedaFlow using the "Create new plot"-button (purple circle).

Or to extract the data as a .csv file to use for another program using the "Output files generator" (blue circle).

Appendix H Lengths of Mesh Cells for LedaFlow

Appendix H contains the lengths of the mesh cells used in the LedaFlow model.

Table H.1: Lengths of the mesh cells for simulating performed experiments

Cell Number (from horizontal inlet)	Length [m]	End locked
1-9	0.170667	(end of 9 locked)
10-11	0.0943398	(end of 11 locked)
12-20	0.172222	(end of 20 locked)
21-22	0.113137	(end of 22 locked)
23-39	0.176471	(end of 39 locked)
40-41	0.113137	(end of 41 locked)
42-53	0.166667	(end of 53 locked)
54	0.147567	(end of 54 locked)

Table H.2: Lengths of mesh cells for simulating changes in PVT-properties

Cell Number	Length [m]	End locked
From inlet of horizontal inlet pipe		
1-9	0.170667	(end of 9 locked)
From inlet of U-jumper		
1-8	0.16375	0
9-25	0.176471	0
26-35	0.18	(end of 35 locked)
From inlet of horizontal outlet pipe		
1-2	0.15	(end of 1 locked)

Table H.3: Length of the mesh cells for simulating dead-leg

Cell Number	Length [m]	End locked
From inlet of U-jumper_a		
1-9	0.170667	(end of 9 locked)
10-17	0.16375	(end of 17 locked)
18-25	0.175	(end of 25 locked)
From inlet of dead-leg		
1-6	0.166667	(end of 3 and 6 locked)
From inlet of U-jumper_b		
1-9	0.0.177778	(end of 9 locked)
10-19	0.18	(end of 19 locked)
20-21	0.15	(end of 21 locked)

Appendix I Constituents of Diesel

Table I.1: Constituents of diesel (Kolev and SpringerLink, 2007, pp. 271-272)

Groups	Mass %
Paraffin	45.6
Naphthalene	25.6
- Monocyclic	17.4
- Dicyclic	6.3
- Tricyclic	1.9
Aromates	28.6
- Alkylbenzole	9.6
- indane/tetralie	5.6
- indene	1.3
- monoaromats	16.5
- naphtaline	0.1
- alkylnaphthaline	6.9
- acenapthene/diphenyle	2.3
- acenapthene/fluorine	1.6
- diaromats	10.9
- triaromats	0.5